Sheffield Hallam University

A Sheffield Hallam University thesis

THE DETECTION OF HYDRAZINE AND RELATED MATERIALS BY ION MOBILITY SPECTROMETRY

HILARY ROBERTA BOLLAN
M.Phil., C.Chem., MRSC

A thesis submitted in partial fulfilment of the requirements of Sheffield Hallam University for the degree of Doctor of Philosophy
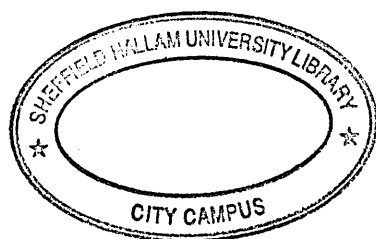
March 1998

ABSTRACT

A technique known as ion mobility spectrometry (IMS), which has been under development for about thirty years, has been shown to be capable of detecting hydrazines at low concentrations but with interference from ammonia. Ammonia is usually present in hydrazine environments, as a breakdown product or a by-product of the human metabolism.

This project was undertaken to investigate mechanical and chemical parameters for improved detection of these hydrazines in the presence of ammonia, and for the detection of nitrogen dioxide, by IMS. The subject areas investigated were compatibility of detector cell construction materials with the analytes, detector temperature, comparison of membrane versus direct inlet systems under their optimum conditions, pneumatics configurations for the spectrometer, and the investigation into the effects of different ion molecule chemistry regimes for the improvement of selectivity, sensitivity, and response and recovery times.

The optimum spectrometer operating conditions, for the detection of hydrazine, methylhydrazine, and 1,1-dimethylhydrazine in the presence of ammonia, and for the detection of nitrogen dioxide, were incorporated into a hand portable instrument (linked to a computer) capable of near real-time detection. Ammonia is still an interferent in the ion mobility spectrometry detection of the parent hydrazine.

The use of ketones as dopant chemicals has been shown to be effective in the ion mobility spectrometric determination of the hydrazines. However, the mobility of the ion-molecule clusters formed from these hydrazines are in the reverse order to that expected. In order to gain insight to the ion-molecule chemistry of the hydrazines/ketones systems molecular modelling and IMS coupled with tandem mass spectrometry studies were undertaken to investigate ion cluster formations of the hydrazines with an homologous series of symmetrical ketones. A fluorinated ketone was also studied by IMS-MS-MS to determine the effect of electron withdrawing groups upon ion cluster formation. The ion-molecule clusters formed were shown to be concentration dependent, with gas phase reaction recorded between the dopants and analytes at low ketone concentration.

CONTENTS

LIST OF ILLUSTRATIONS

Figures 1.1 to 1.7 inclusive and Figure 1.10 have been reproduced with the permission of Graseby Dynamics Limited, Figures 1.8 and 1.9 have been reproduced with the permission of Johnson Space Centre, NASA. Figures 2.1, 3.16, and 3.17 were produced by J L Brokenshire and G Crouch of Graseby Dynamics Limited.

Plates	Title	Following Page No.

Acknowledgements

Author's declaration

The practical work for this project was performed at the Defence Evaluation and Research Agency Environmental Sciences Department Laboratories at Bridgwater, and the Department of Chemistry at the New Mexico State University, Las Cruces. A preliminary screening of chemical materials for possible use as dopant compounds was carried out by staff at Graseby Dynamics Limited. Assistance in the design of the ion mobility spectrometer breadboard was provided by Dr. John Brokenshire of Graseby Dynamics Limited. Technical support for the maintenance and refurbishment of the ion mobility spectrometer was provided by Graseby Dynamics Limited, and was financed mainly by the Defence Evaluation and Research Agency.

Jaime Rodriguez, at NMSU, assisted with the IMS-MS-MS practical, and with maintaining the instrumentation in working order.

Due to the time the molecular modelling calculations required for completion of the geometric optimisations, Dr John Brokenshire provided assistance by programming the calculation parameters into a computer on a remote site and performing some of the calculations.

This work has been carried out with the support of the Defence Evaluation and Research Agency. The experimental work for optimisation of the ion mobility spectrometer was also supported by Ministry of Defence and the ion mobility spectrometry - tandem mass spectrometry was supported by the Chemistry Department of the New Mexico State University. The molecular modelling software was provided by DERA; all calculations, and preparation of this thesis, were carried out in the author's personal time.

GLOSSARY OF ABBREVIATIONS, SYMBOLS AND FORMULAE

Symbols and units of measurement

A	area; analyte
Å	angström, unit of length equivalent to 0.1 nm
amu	atomic mass units
β^-	beta radiation
c	concentration
c.	circa [about]
°C	degrees Celsius
cm	centimetre(s)
cm^2	square centimetre(s)
$cm^2.V^{-1}.s^{-1}$	units of ion mobility
D	diffusion coefficient
Δ	correction term for higher approximations
E	electric field; electrophilic sample
e	electronic charge
e^-	electron
E_D	energy of diffusion
eV	electronvolt(s)
ΔH_S	enthalpy of solution
”	inch(es)
$ions.s^{-1}.cm^{-3}$	number of ions produced per second per cubic centimetre
K	constant of proportionality for ion mobility
K_0	reduced mobility, ion mobility normalised for temperature and pressure
k	Boltzmann's constant, 1.38×10^{-23} $J.K^{-1}$ (Joules per Kelvin)
$kcal.Å^{-1}mol^{-1}$	kilocalories per angström per mole
keV	kiloelectronvolt(s)
kg	kilogram(s)
$kJ.mol^{-1}$	kiloJoules per mole [unit of energy]
l	thickness of membrane
l_d	drift length

l.min^{-1}	litres per minute
M	molecular mass of the neutral species in the drift tube, or, molar solution
m	ionic mass; metre(s)
mBar	millibar(s)
mCi	millicurie(s), units of radioactivity equivalent to 3 x 10^7 disintegrations per second
mg	milligram(s)
μg	microgram(s)
μg.l^{-1}	microgram(s) per litre
μl	microlitre(s)
μs	microsecond(s)
ml.min^{-1}	millilitres per minute
mm	millimetre(s)
mV	millivolt(s)
m/z	mass to charge ratio [with respect to mass spectrum]
N	molecular number density
ng	nanogram(s)
ng.l^{-1}	nanogram(s) per litre
nm	nanometre(s)
Ω	collision cross section
$\Omega^{(1.1)}$	first order collision integral
P	pressure; nucleophilic sample e g an amine
p	partial pressure
P_e	permeability
pcb	printed circuit board
%	percent(age)
pH	measure of acidity / alkalinity on a scale of 1 to 14
π	pi
psi	pounds per square inch; unit of pressure
q	rate of permeation
q_i	ionic charge
q_{an}	flow rate of contaminant 'a' at stage n

q_{Dn}	flow rate of diluent gas at stage n
R	molar gas constant
r_m	position of minimum potential for interaction
S	solubility coefficient
s	second(s)
T	temperature
t_d	drift time
V	volt(s)
v_d	drift velocity
$V.cm^{-1}$	volts per centimetre

Standard abbreviations

ACADA	Advanced Chemical Agent Detector and Alarm
ACGIH	American Conference of Governmental Industrial Hygienists
ADA	anthracene-2,3-dicarbaldehyde
AVM™	Airborne Vapour Monitor
ASP™	Advanced Signal Processor
CAM™	Chemical Agent Monitor
CID	collision induced dissociation
C-18	solid sorbent medium
DIMP	diisopropyl methane phosphonate
DNA	dioxyribonucleic acid
DNT	dinitrotoluene
EGDN	ethylene glycol dinitrate
EVM™	Environmental Vapour Monitor
FID	flame ionisation detector
Gas Chrom R	solid support for chromatographic stationary phase
GC	gas chromatography
3,5-HD	3,5-heptanedione
HTIMS	high temperature ion mobility spectrometer
HMX	octahydro-1,3,5,7-tetranitro-1,3,5,7-tetraazine, octogen
HPLC	high performance liquid chromatography
HSE	Health and Safety Executive (UK)
HZ	hydrazine

IBM-AT	type of computer configuration
IMS	ion mobility spectrometry (also referred to as Plasma chromatography); ion mobility spectrometer
IMS-MS-MS	ion mobility spectrometry coupled to tandem mass spectrometry
LC	liquid chromatographic
LOTIMS	low temperature ion mobility spectrometer
LSD	lysergic acid dimethylamide
LTEL	long term exposure limit
MIBK	methyl isobutyl ketone; 4-methyl-2-pentanone
MMH	methylhydrazine, monomethylhydrazine
NASA	National Aeronautics and Space Administration
NDA	2,3-naphthalene dicarboxaldehyde
NG	nitroglycerine
^{63}Ni	nickel 63
NIOSH	National Institute of Occupational Safety and Health (USA)
NMSU	New Mexico State University
NOAEL	no-observed-adverse-effect level
o.d.	outside diameter
OFM$^{\text{TM}}$	Otto Fuel Monitor
OPA	o-phthalaldehyde
OSHA	Occupational Safety and Health Administration (USA)
PEL	permissible exposure limit
PETN	pentaerythritol tetranitrate
ptfe	polytetrafluoroethylene
RDX	hexahydro-1,3,5-trinitro-1,3,5-triazine, hexogen
REL	recommended exposure limit
RH	relative humidity
RIP	reactant ion peak
RSD	relative standard deviation
SFC	supercritical fluid chromatography
Tetryl	N-methyl-N,2,4,6-tetranitroaniline
TMH	tetramethylhydrazine
TMHD	2,2,6,6-tetramethyl-3,5-heptanedione

TLV	threshold limit value
TNT	trinitrotoluene
UDMH	unsymmetrical dimethylhydrazine; 1,1-dimethylhydrazine
UHF	unrestricted Hartree Fock
USA	United States of America
vpb	parts per billion by volume
vpm	parts per million by volume
WASP™	waveform analysis software package
X	mole fraction (contaminant purity)

Note: Items marked ™ in the above list are the trade names of products marketed by Graseby Dynamics Limited.

Empirical formulae

C_3H_6O	acetone
$C_3H_8N_2$	acetone hydrazone
$C_5H_{10}O$	3-pentanone
$C_5H_{12}N_2$	3-pentanone hydrazone
$C_6H_{12}N_2$	acetone azine
$C_7H_{14}O$	4-heptanone
$C_7H_{16}N_2$	4-heptanone hydrazone
$C_9H_{18}O$	5-nonanone
$C_9H_{20}N_2$	5-nonanone hydrazone
$C_{10}H_{20}N_2$	3-pentanone azine
$C_{14}H_{28}N_2$	4-heptanone azine
$C_{18}H_{36}N_2$	5-nonanone azine
H_2O	water
H_2SO_4	sulphuric acid
$Na_3[Fe^{III}(CN)_5NH.$ $N(CH_3)_2]$	red complex formed from reaction of trisodium pentacyanoaminoferrate with 1,1-dimethylhydrazine
$Na_3[Fe^{III}(CN)_5NH_2]$	trisodium pentacyanoaminoferrate
NH_3	ammonia
$(NH_3)_2SO_4$	ammonium sulphate
NH_4^+	ammonium ion
N_2H_4	hydrazine

$N_2H_3CH_3$	methylhydrazine
$N_2(CH_3)_2H_2$	1,1-dimethylhydrazine
$N_2(CH_3)_4$	tetramethylhydrazine
NO_2	nitrogen dioxide

Chapter 1

INTRODUCTION

1.1 Background

Possibly the most well known use of hydrazine (HZ) is as a rocket propellant utilised, for example, in the German rocket-powered ME-163 fighter plane[1], but it is also used extensively in other areas. In addition to fuel cells and general utilisation in the aerospace industry, hydrazine is also used as a dissolved oxygen scavenger in boiler waters, a corrosion inhibitor and anti-oxidant, and in the manufacture of agricultural pesticides and plant-growth regulators, polymers, dyes, explosives, and pharmaceuticals (including hydrazine salts[2]). More recently hydrazine has been investigated for the anisotropic etching of silicon[3]. Monomethylhydrazine (MMH, methylhydrazine) and 1,1-dimethylhydrazine (UDMH, unsymmetrical dimethylhydrazine) are also used as fuels and propellants. HZ and MMH have been mixed together during their evaluation as a bipropellant in a regeneratively cooled engine[4]. Nitrogen dioxide is sometimes used in conjunction with hydrazines fuel systems, as an oxidant.

These hydrazines are hazardous by virtue of their flammability and toxicity. The genotoxic[5], mutagenic[6], and hepatotoxic[7-9] effects of HZ have been investigated in rats. Both HZ and MMH have been shown to be bacterial mutagens[10] and the teratogenicity of HZ has also been called into question[11]. The adverse effects of these hydrazines on the human body are well documented[12-17]. The vapours are irritating to the upper respiratory tract and can cause dizziness and nausea; itching, burning, and swelling of the eyes may develop over a period of hours, severe exposure causing temporary blindness lasting for about 24 hours[17]. Problems have also been recorded in

the nervous, lymphoreticular, haemepoietic, cardiovascular, genitourinary, integumentary, and musculoskeletal systems of humans following exposure to hydrazines[11]. In 1993 acute intoxication by a hydrazine-like gas, of workers in a garbage dump, was reported[18]; the main complaints of those affected were dyspnoea, nausea and eye burning. Following occupational exposure to HZ at concentrations of one to ten parts per million by volume (vpm) during production at a factory between 1945 and 1971, a subsequent report[19] suggested that there was insufficient evidence for the carcinogenicity of HZ in humans, however, all three hydrazines are now listed as human carcinogens. One publication[20] has stated that *"agents with a hydrazine functionality are metabolised to toxic intermediates capable of damaging cellular macromolecules and stimulating proteolysis.... Hydrazines and the substituted alkyl and aryl hydrazines undergo oxidation by oxyhaemoglobin or cytochrome 450 to yield highly reactive oxygen and organic free radical species. These highly reactive electrophiles are capable of damaging cellular DNA and protein."* The report also suggested that the hydrazines damage protein in human red blood cells and stimulate the rate of protein degradation; their toxicity ranges from autoimmune tissue injury to carcinogenesis and leukemogenesis. A newspaper article[21] reported the death of a cancer research doctor who died following work with UDMH.

Due to their hazardous nature there is a need to monitor for the presence of these hydrazines wherever there is a possibility that people will be exposed to their vapours. There are various exposure limits, cited in literature[22-29], ranging from 10 to 1000 parts per billion by volume (vpb), depending on the governing body and the hydrazine of interest. Ten years ago it was not possible to estimate a no-observed-adverse-effect level (NOAEL) from the available human data on HZ[28]. In 1990 the Occupational Safety and Health Administration (OSHA) [of the United States of America (USA)] permissible

exposure limits (PELs)[22,23] were 100[12], 200[26] and 500[27] vpb for HZ, MMH, and UDMH respectively. In 1992 a legal ruling declared the OSHA limit of 100 vpb for HZ as unlawful, following a law suit by a US company contesting the exposure limit. OSHA was forced to revert to the previous exposure PEL of one vpm. The American Conference of Governmental Industrial Hygienists (ACGIH) threshold limit values (TLVs)[13] corresponded to the OSHA PELs. The National Institute of Occupational Safety and Health (NIOSH) [also of the USA] recommended exposure limits (RELs)[24-27] were 30, 40, and 60 vpb respectively. As recently as 1996 the Health and Safety Executive (HSE) [United Kingdom] listed the long term exposure limit (LTEL) for HZ, for an eight hour time-weighted average reference period[29], as 100 vpb, but this limit was also under review and is now 20 vpb[30]. Although not a legislative body, ACGIH has recommended to the OSHA that the level for all three hydrazines be lowered to 10 vpb[31,32].

The author's main areas of consideration for monitoring are for hydrazines used in the aerospace and energy industries. Ideally, a hand-portable monitoring system, capable of detecting down to one tenth of the exposure limit, would be required to be of use for the purposes of occupational hygiene and propellant leakage, and should be capable of responding in near real-time. Ammonia, which is a breakdown product of hydrazines and is also emitted from humans as a natural product of metabolic processes, is usually present in hydrazines environments, so any monitoring equipment would have to be unaffected by the presence of ammonia. Typical levels of ammonia that are causing concern in the practical real-time determination of HZ are in the range of two to ten vpm. There is also a requirement to monitor for ammonia at a concentration of less than one vpm, possibly 0.3 vpm if the detection level is assumed to be one tenth of the current HSE long term exposure of 3 vpm[30]. At the outset of this work, commercial

bench instrumentation was capable of monitoring only down to one vpm of the hydrazines and nitrogen dioxide, with slow response. Below this level no suitable instrumentation was available with the necessary performance characteristics of selectivity, sensitivity, and response and recovery times, at the detection levels required.

1.2 Review of hydrazines monitoring techniques

1.2.1 Titrimetry

Quantification of HZ was reviewed by Audrieth and Ogg in 1951[33]. Various titrimetric methods detailed were wet chemical analyses, used typically for the determination of the purity of HZ, all of which have a low degree of sensitivity and are unsuitable for the determination of low concentrations of hydrazines in the atmosphere. Electrochemical titrations have been considered (section 1.2.4).

1.2.2 Spectrophotometric methods

Spectrophotometric analyses for the determination of hydrazines fall into two categories, colorimetric and fluorescence determinations. Colorimetric methods are used as wet chemical methods in the laboratory and also adapted for field use, employing paper tape technology and detector tubes.

Laboratory methods for HZ determination include reaction with picryl chloride in chloroform to produce bis-trinitrophenylhydrazine which, when buffered with borate, gives a red colour on the addition of alcoholic potassium acetate[34]. Pyridyl is also used for the detection of HZ but has insufficient sensitivity for the detection of UDMH. The reduction of phosphomolybdic acid to molybdenum blue has been used for the determination of UDMH[27] and MMH[26]. A kinetic method, based on the measurement of the rate of reaction between HZ and Mo(IV) in the presence of hydrochloric acid, monitors the redox reaction spectrophotometrically at 710 nm. This method[35] is quoted

as being sensitive to 10^{-4} M. The reduction of phosphomolybdic acid is unsuitable in the presence of other reducing agents[36]. Due to the non-specificity of this reaction, Pinkerton *et al.*[36] developed a method which reacted UDMH with trisodium pentacyanoaminoferrate to give a red complex:

$$Na_3[Fe^{III}(CN)_5NH_2] + H_2NN(CH_3)_2 \rightarrow Na_3[Fe^{III}(CN)_5NH.N(CH_3)_2] + NH_3 \qquad \textbf{1.}$$

Pesez and Petit[37] recorded that HZ reacted with 4-dimethylaminobenzaldehyde to give a characteristic yellow to orange-red colour, in hydrochloric acid solution, which could be used for photometric determination. Further work by Pilz and Stelzl[38] cited 8% sulphuric acid as a more efficient collecting medium than hydrochloric acid, which was only 78% effective. The dehydration reaction forms an azine from HZ:
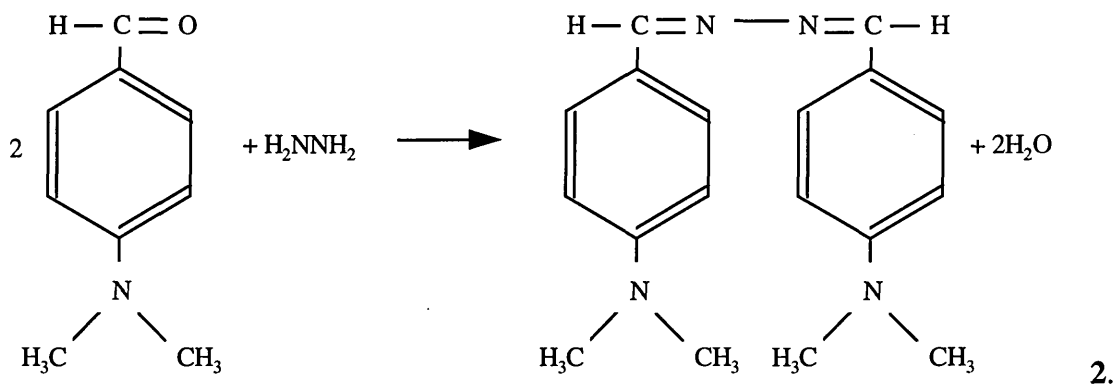
This method of determination has also been used for the detection of MMH, but due to the presence of only one primary amine group it can only react with one molecule of 4-dimethylaminobenzaldehyde. The product is a smaller molecule than the azine formed from reaction with HZ and has a lesser degree of conjugation. The method of measurement is visible spectrophotometry which depends upon the degree of conjugation and therefore the reaction is less sensitive for MMH than it is for the parent

HZ molecule. The measurement wavelength is 455 nm for both HZ and MMH reaction products. This method is unsuitable for the detection of UDMH. The process has been adapted for the determination of trace amounts of hydrazine in boiler feed water[39].

HZ has also been complexed with 4-dimethylaminobenzaldehyde in acetic acid[25] to form a quinoid derivative of 4-dimethylaminobenzaldazine. The reaction of HZ with 2,4-dimethylaminobenzaldehyde to form the hydrazone has been investigated for the continuous flow monitoring of HZ in water, using a flow gradient for calibration[40]. Reactions of HZ and its derivatives with various other aldehydes, including benzaldehyde and salicylaldehyde, are used for their quantification[33]. Another method[12] details the collection of HZ on sulphuric acid coated Gas Chrom R, desorption with water and analysis with colorimetric screening, again using 4-dimethylaminobenzaldehyde, or an HPLC procedure involving treatment with benzaldehyde solution and sodium borate, a method developed further by the HSE[41].

Another condensation reaction uses 3,4-dimethoxybenzaldehyde as the reagent[42], in acid medium. The product is again yellow, but the measurement wavelength is 410 nm.

Fluorescent detection of HZ through derivatization with 2,3-naphthalene dicarboxaldehyde (NDA)[43] has been shown to be selective against ammonia. The method is sensitive, at 500 nm, to 50 $ng.l^{-1}$ HZ at pH 2.5, and sensitive to 120 $ng.l^{-1}$ MMH and 40 $\mu g.l^{-1}$ UDMH. O-phthalaldehyde (OPA) and anthracene-2,3-dicarbaldehyde (ADA) produce fluorescence emission at 376 and 549 nm respectively[44]. By control of the pH and aromatic dicarbaldehyde chosen, it is possible to differentiate quantitatively between HZ, MMH, and UDMH in the same sample.

Field deployable methods have also included the reduction of phosphomolybdic acid to molybdenum blue, employed for determination using paper tape technology.

Detector tubes make use of colorimetric methods of determination for the monitoring of the hydrazines, including neutralisation of HZ by sulphuric acid, which turns pH indicator from pink to yellow[45]:

$$N_2H_4 + H_2SO_4 \rightarrow (NH_3)_2SO_4 \qquad\qquad 3.$$

Other amines and ammonia produce a similar stain by themselves and cause positive errors when co-existing. In a similar reaction, HZ reacts to give a hydrazinium salt which changes bromophenol blue indicator from yellow to blue[46]. This reaction is also non-selective. A more selective detector tube method involves the reaction of the hydrazines with a silver compound, producing a colloidal silver brownish-grey product on the originally white crystals[46]. The tubes were designed to react specifically with HZ but also react with MMH to ±50% accuracy. The indication with UDMH is diffused and is difficult to evaluate. Hydrogen sulphide produces a similar colour change and although sulphur dioxide is not indicated, its presence interferes with the detection of HZ and results in low readings.

1.2.3 Chromatographic methods

Gas chromatographic determination of HZ and MMH has been achieved at 0.1 to 50 ppm, in aqueous solution, following their reaction with 2,4-pentanedione to form substituted pyrazoles[47] prior to analysis. Separation of HZ mixtures and water has been effected using a stationary phase that is chemically similar to HZ[48]. Neither method is suitable for UDMH.

Another method[49] details detection of HZ and its methyl and phenyl derivatives by entrapment onto sulphuric acid coated silica gel, after which the sorbent is treated with water to desorb the hydrazines. Reagent, containing sodium acetate and 2-furaldehyde, is added and the resulting derivatives are extracted into ethyl acetate and

analysed by gas chromatography with flame ionisation detection. The method is most sensitive to HZ, with a lower limit of detection of 0.2 μg.

HZ in human plasma may be determined by HPLC using a reversed-phase (octadecylsilane) column and methanol-water (60:40) as the mobile phase[50]. Samples are denatured with trichloroacetic acid and derivatized with 4-hydroxybenzaldehyde to form an azine, which is determined by ultraviolet detection at 340 nm.

HPLC with electrochemical detection has been successful for the detection of selected HZ and hydrazide derivatives of 2,5-dihydroxybenzohydrazide[51] but it was not investigated for the hydrazines of interest in this research.

Prechromatographic derivatization of HZ with 2-nitrocinnamaldehyde[52] in combination with a preliminary solid-phase extraction (C-18 sorbent) has enabled sensitive and selective determination of HZ to be performed.

Gas chromatography is used for the simultaneous determination of all three of the hydrazines of interest, by separation of their acetone derivatives and subsequent detection using a nitrogen specific detector. The method[53] was developed to be sensitive to atmospheric, part per billion concentrations. This idea was pursued for the detection of HZ in boiler feed water, with the derivatization of the amine *in situ* and its subsequent recovery from the aqueous sample[54].

1.2.4 Electrochemical methods

Coulometric determination of HZ and substituted hydrazines in the 3 to 5 mg range has been achieved by reaction with bromine[55], and has been used for the continuous measurement of UDMH[56], in air, utilising a four electrode potentiostat with pH 8.0 buffer electrolyte. Coulometric oxidation / reduction titrations of HZ with electrogenerated lead(IV) acetate or manganese(III) acetate in acetic acid[57] have been reported, and another redox titration of HZ with p-carboxybenzenesulphone-

dichloroamide[58] has also been proposed. A coulometric method[59] employing galvanostatic titration, with bromine as the intermediate, and amperometric end-point detection is capable of detecting HZ and MMH to less than 25 ng per titration sample (equivalent to 2 ppb in air). Amperometric determination utilising potassium iodate as the titrant[60] has been used for the determination of HZ and its salts in the range 4×10^{-7} to 4×10^{-3} M; with manganese (III) pyrophosphate and use of a rotating platinum electrode[61] amperometric determination is sensitive to less than 1 mg of HZ in solution. Due to the similar oxidation potentials of HZ and UDMH on a platinum electrode in an aqueous sulphate medium, a method using their reaction products with 2-propanone was investigated for determination of their mixtures[62], again, using amperometric end-point detection.

Amperometric flow-injection analysis[50,63] has been applied to the determination of HZ in solution, by electrocatalytic oxidation of the HZ at a cobalt tetraphenylporphyrin, heat-treated, modified glassy carbon electrode; the method is sensitive to 0.1 ng. Similarly, glassy carbon electrodes have been treated with 3,4-dihydroxybenzaldehyde[64] where low picogram quantities of HZ have been determined and for remote monitoring using a 50 ft. long shielded cable[65], nafion / ruthenium oxide pyrochlore[66], polymeric cobalt phthalocyanine[67,68], and an electrode electrochemically pretreated with an alumina slurry[50] have been used for the determination of hydrazines separated by liquid chromatography. Following capillary electrophoresis, a platinum-modified carbon fibre electrode has been used for amperometric detection[69] of HZ, and a palladium-modified microdisk array electrode[70] has been used for the detection of both HZ and MMH.

Potentiometric / flow-injection determination of trace HZ in boiler water[71] was successful at 10 ppm in solution. Details of experimental work for the use of an

electrochemical cell for real time analysis of the hydrazines[72], but with interference from possible atmospheric contaminants, was published as early as 1979. A commercially available HZ monitor[73], for the detection of HZ concentrations in boiler waters, uses a polarographic redox electrode, and requires monthly refilling of the potassium chloride reagent. Solutions containing both HZ and ammonia have been quantified[74], by the use of potentiometric determination of the HZ reacted with bromine in acid medium, followed by amperometric determination of the ammonia reacted with BrO^- formed from hypobromite in alkaline medium.

Disposable screen-printed electrodes incorporating cobalt phthalocyanine or a mixed valent ruthenium cyanide coating have been evaluated for environmental and industrial monitoring of HZ compounds[68] and could be capable of on-site real-time environmental monitoring for hydrazine.

1.2.5   Miscellaneous methods of hydrazines detection

Chemiluminescence has been shown to be capable of detecting HZ in solution and in air. An automatic injection analysis method with chemiluminescence detection is sensitive to 20 $ng.ml^{-1}$. Colloidal platinum catalytically oxidises HZ to form an intermediate oxidising agent, which subsequently oxidises the luminol[31] in the system, thus generating a chemiluminescence signal which is proportional to the atmospheric HZ concentration, a process sensitive to sub ppm concentrations.

Modulated photoionization detection[75] has been reported to be successful for the determination of MMH at less than 100 vpb, even in the presence of ammonia, but because the measurement is differential any background signal drift must be eliminated from the system, and span drift would have to be overcome in the design of the modulator and the sample matrix considered.

A monoamine oxidase biosensor has also been considered for HZ monitoring[76] but, so far, specificity has been poor. A tyrosinase-based inhibition biosensor has been evaluated for the determination of hydrazines[77], and a double-stranded DNA biosensor has been demonstrated for HZ and MMH determinations[78], in water, and may be developed for atmospheric monitoring.

A passive sampling device was developed for the detection of MMH[79], but the badges were affected by tobacco smoke and strong sunlight. The MMH content of the samplers had to be determined by either coulometric or colorimetric analysis in the laboratory.

1.2.6   Summary of hydrazines detection

The methods of detection mentioned so far are based on laboratory techniques rather than portable instrumentation, and require relatively complex sample preparation or considerable technical support in the form of buffer or electrolytic solutions. In general they lack sensitivity and / or selectivity, and the instrumentation is not commercially available with the required performance characteristics necessary for the simultaneous detection of all three hydrazines of interest. Hence, an alternative technique which addresses these deficiencies is required.

Ion mobility spectrometry (IMS) is a technique concerned with the formation of ion-molecule clusters in air[80], or other gases[81,82] and their movement in an electric field at, or just below atmospheric pressure. Instrumentation used for this procedure has been shown to be capable of detecting the hydrazines (in the positive ion mode) at sub-vpm levels[83-85]. As a result of this earlier work, it seemed appropriate to further investigate IMS for application to the problem of monitoring hydrazines in the presence of ammonia, and for the detection of nitrogen dioxide (in the negative ion mode).

1.3   Basic theoretical principles of ion mobility spectrometry

1.3.1   Basic design of an ion mobility spectrometer

An ion mobility spectrometer cell consists of two sections[86-88]. Firstly there is a ion-molecule reaction chamber, incorporating the ionisation region. This is coupled via a shutter to the second major part of the assembly, the drift region, which contains a screen grid and an ion collector. A typical cell consists of metal guard rings, separated by insulators, connected to a resistance network with a high voltage attached to one end of the resistor chain, to produce a uniform electric field along the cell, usually 250 $V.cm^{-1}$, at atmospheric pressure[89]. In theory this can be altered to vary the drift time but, typically, commercially available cells do not have this facility.

Clean carrier gas is ionised, usually by irradiation with β^- rays from a ^{63}Ni radioactive source (corona discharge[90] photoemissive[91], and photo-ionisation[92,93] sources have also been used), and a number of stable long-lived positive and negative ions, known as reactant ions, are formed. (Ions of only one polarity are formed with a corona discharge source, depending on the polarity of the discharge[94].) Alternative ion-molecule chemistry can be achieved by the introduction of a dopant chemical, at a controlled rate of emission, from a temperature controlled chamber. If trace vapours are introduced into the carrier gas they may react with the parent (reactant) positive or negative ions to form product ions. The equilibrium concentrations of the product ions are governed by the proton affinity or electron affinity of the species and the concentration of the trace vapour in the carrier gas. If these ions are introduced into an electric field they will migrate according to their polarity and that of the applied field. For determining compounds with high proton affinity the source is held at high positive potential with the collector electrode at ground; for compounds with high electron affinity the polarity is reversed. Each individual ion has a component of acceleration in

the direction of the applied field between collisions. The bulk effect on all the ions appears as a constant ion drift velocity in the direction of the field[95]. In the ion-molecule reaction region the ion-molecules drift under the influence of the applied field until reaction has reached equilibrium. The ions are drawn by the electric field towards the shutter which is pulsed to allow a finite number of ions into the drift region.

The shutter is a Bradbury-Nielsen grid, made up of two planar grids of parallel wires, used to produce a transverse field by applying an offset voltage to one set of wires (the "moving" grid) and coupling the other set (the "fixed" grid) to the appropriate part of the resistor chain. Applying a voltage pulse to the moving grid removes the transverse field and allows ions to pass through for the duration of the pulse, under the influence of the continuously applied longitudinal field[96,97]. Operation of this shutter starts the timing sequence which measures the drift time. Ideally, in the drift region, ion-molecule reactions are quenched by a counterflow of clean drift gas. The screen grid shields the collector electrode from an approaching ion cloud, which would otherwise induce a charge on the electrode and consequently distort the shape of the current peak. The collector electrode is a Faraday plate[87], from which the current peak is amplified, and the drift time, from the opening of the shutter, measured. The complete mobility spectrum is generated by monitoring the collector electrode from the instant the voltage pulse is applied to the grid. By repetitively pulsing the grid the mobility spectrum can be continuously generated. Typically, twenty milliseconds is sufficient to allow all ions to drift from the grid to the collector electrode. Only small ion currents are involved, therefore the signal is relatively noisy. The signal to noise ratio may be improved by averaging the signal over several scans, the ratio increasing as the square root of the number of spectra averaged[98]. This process is sufficiently rapid that near real-time analysis[96] is achieved.

1.3.2 Sample acquisition

An ion mobility spectrometer detects materials in the gaseous or vapour phase, which may be introduced into the instrument either directly, as in an atmospheric sample, or by transfer to an alternative gaseous medium. A semi-permeable membrane is a means of achieving the latter and has the advantage of reducing the amount of interferent species taken into the system. For this process to be effective the membrane must have a higher permeability to the vapour than to potentially interfering species[99]. The use of a membrane may reduce the amount of sample taken into the detector, but it may also diminish the amount of possible interferents, including water vapour. Another advantage of a membrane based inlet, coupled with a recirculating system, is the ease with which alternative ion molecule chemistry can be established with stable vapour levels of dopant chemicals[100]. The permeability of a polydimethylsiloxane membrane, to the hydrazines, decreases with increase in temperature[101]. Direct inlet systems can allow more water into the spectrometer which may lead to larger ion clusters, loss of resolution, and reduced sensitivity[98].

1.3.3 Ion mobility

Average ion velocity, v_d, is related to the magnitude of the electric field, E, through which the ion is travelling[95] by the equation

$$v_d = KE \qquad\qquad 4.$$

The constant of proportionality, K, refers to the mobility of the ions, which is characteristic of a particular ion species in a specified drift gas, and may be calculated indirectly from drift time[102], t_d, which is related to drift velocity through the equation

$$t_d = l_d/v_d \qquad\qquad 5$$

where l_d is the drift length.

For the calculation of mobility the Mason-Schamp equation is[87,95,103,104]

$$K = (3e/16N)(1/m+1/M)^{\frac{1}{2}}(2\pi/kT)^{\frac{1}{2}}[(1+\Delta)/\pi r_m^2 \Omega^{(1.1)}]$$ 6

where,

e	= electronic charge
N	= molecular number density
m	= ionic mass
M	= molecular mass of the neutral species in the drift tube
k	= Boltzmann constant
T	= absolute temperature
Δ	= correction term for higher approximations
r_m	= position of minimum potential for interaction
$\Omega^{(1.1)}$	= first order collision integral

Values for r_m, $\Omega^{(1.1)}$, and Δ, are not readily available, so experimental work is required to give accurate values for mobility. Since the collision integral is proportional to the transport cross section, the mobility, and consequently ion drift velocity, is dependent upon[93] mass, size, shape, and polarizability. If drift gas, electric field gradient, temperature, pressure, and therefore molecular number density remain constant, mobility depends only on ion charge, q_i, reduced mass, and collision cross section, $\Omega^{(95,105)}$:

$$K \propto \{q_i/[mM/(m+M)]^{\frac{1}{2}}\Omega\}$$ 7.

Mobility is related to the diffusion coefficient by the Nernst-Townsend-Einstein[89] relationship, i.e.

$$K = q_i D/kT$$ 8

where,

k = Boltzmann's constant

D = diffusion coefficient

The collision processes undergone by the ions during their drift time are subject to normal gas laws and are affected by variations in temperature, T, and pressure, P, in the drift region. Ion cluster formation and fragmentation are governed by temperature[94]. Therefore, mobility of ions is normally recorded as the reduced mobility, K_0, where the mobility of the ions is normalised for temperature and pressure[89,95,102]:

$$K_0 = K \times (760/P)(T/273)$$ 9.

Note: In some texts K and K_0 are replaced by μ and μ_0 respectively. The units of mobility are $cm^2.V^{-1}.s^{-1}$[104].

In commercial ion mobility spectrometers, software programmes have been written for peak searching routines, designed to obviate the need to measure temperature and pressure, by taking the ratios of the reactant ion and product ion peak positions[106]. More recent instrumentation has integral temperature and pressure compensators for calculation of reduced mobilities.

1.3.4   Ion-molecule chemistry

A radioactive ^{63}Ni foil emits ß$^-$ rays, with maximum energy of 67 keV and an average energy of 20 keV[107], which produce secondary electrons on collision with gas molecules, e.g.:

$$ß^- + N_2 \rightarrow N_2^+ + e^- + ß^-$$ 10.
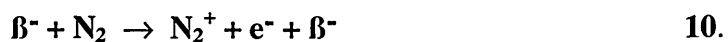
These electrons then react with other gas molecules and the process continues until low energy thermal electrons attach themselves to oxygen, resulting in

$$e^- + O_2 \rightarrow O_2^-$$ 11.

The initial distribution of positive and negative ions, a maximum of 8×10^{11} ions.s^{-1}.cm^{-3}, is modified by various chemical reactions. Positive ions are subject to proton transfer, nucleophilic attachment, hydride or hydroxide extraction, and oxidation; while negative ions are subject to electron capture, charge transfer, dissociative capture, proton abstraction, and electrophilic attachment; both positive and negative ions may undergo complex rearrangement[86,87].

The most abundant ion clusters[80,96,108] are $[H^+(H_2O)_x(N_2)_y]$ and $[(O_2)_z(N_2)_y(H_2O)_x]^-$. Molecules with greater proton or electron affinity than the reactant ions, react to form product ions thus[96]:

$$H^+(H_2O)_x(N_2)_y \quad + \quad P \quad \rightarrow \quad [PH^+(H_2O)_x(N_2)_y] \qquad 12$$
reactant   nucleophilic   monomer product
                 sample

$$[PH^+(H_2O)_x(N_2)_y] \quad + \quad P \quad \rightarrow \quad [P_2H^+(H_2O)_x(N_2)_y] \qquad 13$$
                                                dimer product
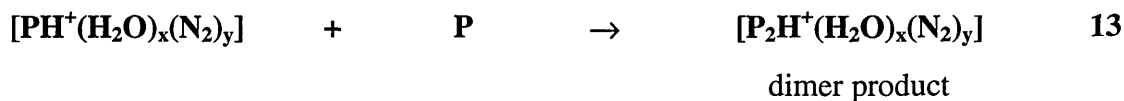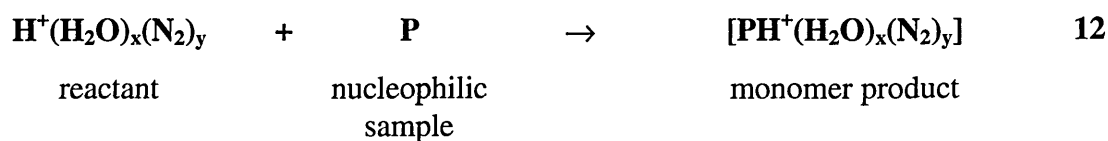
where $x = 2$ to $4^{(80,109)}$, and $y = 0$ to $3^{(80)}$

$$[(O_2)_z(N_2)_y(H_2O)_x]^- \quad + \quad E \quad \rightarrow \quad E[(O_2)_z(N_2)_y(H_2O)_x]^- \qquad 14$$
                                 electrophilic
                                 sample
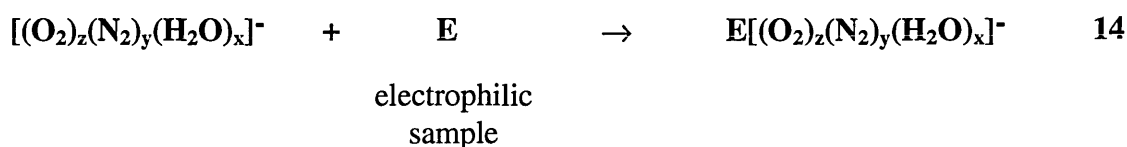
where[80] $z = 1$ to 3, $x = 0$ to 2, and $y = 0$ or 1.

Water plays an important part in ion-molecule chemistry, therefore the amount of water vapour must be controlled[96]. Better spectra are obtained with low vpm levels of water vapour, in which case the number of water molecules combined in an ion cluster is limited to two[97]. A greater number of water molecules gives rise to peak broadening; the greater the number of water molecules attached to an ion species, the slower the inter-ion reactions (due to a partially shielded ion) which also produces peak broadening. Low water vapour levels may be achieved by constantly recirculating the carrier gas through chemical filters, e.g. molecular sieve.

Specific chemicals may be added to the carrier gas, in trace quantities, in order to alter the ion-molecule chemistry so that an enhancement of the selectivity, resolution[87,95,110] and detection limits, may be achieved. Such chemicals are referred to as dopants. For example, addition of a small quantity of ammonia gas to the air, prior to ionisation, allows selective detection of amines in the presence of many other compounds, because the major reactant ion becomes $NH_4^+(H_2O)_x(N_2)_y$[111], and only compounds with a higher proton affinity than that of NH_4^+ cluster ions will react[95,108,111,112] as shown in the following equation, where P is an amine:

$$[NH_4^+(H_2O)_x(N_2)_y] \quad + \quad P \quad \rightarrow \quad [PH^+(H_2O)_x(N_2)_y] + NH_3 \qquad 15.$$

Lighter, more mobile ions, with a smaller collisional cross section, drift faster than heavier ions, and so separation occurs in the drift region. For chemically dissimilar materials the correlation between mass and mobility is weak[94]. Ions from closely related structural isomers can produce molecular ions of differing mobilities[89]. Ions of branched structure have a smaller cross sectional area for collision and, therefore, higher

mobility, as shown by the n-hexylamine, di-*n*-propylamine, triethylamine series[113].

Mobilities are inversely proportional to collision cross section, therefore separation is based on a size to charge ratio rather than a mass to charge ratio[86]. Almost all compounds yield positive ion mobility spectra, usually containing peaks of greater intensity than negative ion mobility spectra, which are obtainable only from compounds prone to electron capture. More accurate and reliable identification of analytes is achieved when both positive and negative ions are considered[111]. Sample overloading leads to disappearance of the reactant ion peak (RIP), multiple analyte peaks, and dimer product ions and cluster ions[95].

1.4   Historical development of ion mobility spectrometry

IMS was originally referred to as plasma chromatography[86,95]. It is a technique concerned with the formation of ion-molecule clusters in air, or other gases[80] and their movement in an electric field[89] at, or close to, atmospheric pressure[114]. The technique is extremely sensitive, so only small quantities of sample are necessary for detection.

The first instruments were developed, by the Franklin GNO Corporation in 1965, to generate information concerning negative ions produced from specific compounds in air under atmospheric pressure conditions. This early instrumentation soon found much wider application for the analysis of ultra-trace quantities of many organic molecules[88] forming either positive or negative ions. The first instrument patent[115] was issued in the USA in 1971. With improved understanding of the technique plasma chromatography became known by the more appropriate term, ion mobility spectrometry[86] (IMS). Much progress has been made in the development and application of IMS, progress which has occasionally been reviewed in publications.

These reviews, and the various components affecting the performance of ion mobility spectrometers, are discussed in the following sections.

1.4.1 Ion mobility spectrometry reviews

In 1984 a book edited by Carr[116] reviewed the fundamental theory, instrumentation, and applications of IMS, while in that same year Spangler *et al.*[87] reassessed developments in IMS. A year later Witkiewicz & Stryszak reconsidered the analytical applications of IMS[111]. Hill *et al.* have published numerous papers on IMS and hyphenated IMS techniques including their applications and, in 1990, published a paper which reviewed studies and applications up to 1990[95]. Later, a book by Eiceman and Karpas[118] re-evaluated the historical development of IMS, the theory behind the technique, and examined IMS applications. Chronologically the review started with fundamental research in the 1890s, which concerned studies of the ionisation of air, through the production of the first ion mobility spectrometers in the 1970s, the present applications of IMS and hyphenated IMS techniques and, finally, considered future trends of IMS and integrated topics. Karpas is preparing a review of the forensic applications of IMS[117].

1.4.2 Fundamental ion mobility spectrometry studies

Most ions encountered in the drift tube are clusters in local equilibrium. The cluster distribution is dependent upon temperature, pressure, composition and purity of the gas streams, and the applied drift voltage.

The temperature dependence of ion mobility spectra has been considered during experiments evaluating the reduced mobility of organic compounds. The majority of substances tested did not show temperature dependence, but benzene, toluene, and phenol did show a mild dependence[119] which produced less than 10% variation in all cases. The difference in mobility of small ions is independent of temperature effects

other than due to their different reaction rates. There have been studies involving the measurement of ion-molecule reaction rate constants at atmospheric pressure, using a kinetic ion mobility mass spectrometer[120].

Research into the effects of pressure has not been so well documented, but the effects of pressure differences due to the change in altitude have been considered. The decrease in the electric mobility ratio observed between measurements at ground level and altitudes of 3 to 5 km is mostly a consequence of the reduction of absolute humidity at low temperature[121].

The carrier gas used in IMS is generally air or nitrogen. The use of carbon dioxide[81] and helium[82] has been recorded for improved resolution for specialised techniques. The change in mobility recorded for a given species in different carrier gases is due to the alteration of ion-molecule chemistry and collisional cross sections of the different species. An alternative to changing the carrier gas, in order to improve species resolution, is the use of tandem ion mobility spectrometers[122]. The dependence of ion mobility on a size to charge basis, rather than a mass to charge ratio, has been revealed through the use of IMS coupled to tandem mass spectrometry (IMS-MS-MS) studies of two structurally different ions which had identical ion mass[123]. In a given carrier gas these two ions had different mobilities. In general terms, the lighter and more compact an ion is, the greater is its mobility[122].

Space charge effects in IMS[124] have also been considered and the relationship between the diffusion and mobility of gaseous ions in strong electric fields[125] has been studied. Peak broadening, due to the space charge field, increased proportionally with longer opening times of the shutter grid. The dependence of ion mobility on electric field intensity has been researched for an homologous series of tertiary amines, in conjunction with a radioactive β^- ionisation source and a surface ionisation source[126].

The conclusions were that the mobility spectra were discrete for each of the substances tested, the surface ionisation procedure improved the limit of detection, and the mobility of ions in nitrogen was independent of the intensity of the electric field but due instead to the polarisation interaction of the ion with the drift gas.

Karpas proposed 2,4-dimethylaniline as a standard reference material for the mobility scale in positive IMS studies[113] but because of these dependencies mentioned above an ion mobility standard has not been accepted[102]. However, a table of reduced mobility values has been produced for ambient pressure IMS[127].

1.4.3 Ionisation sources

An ionisation source is required to produce the electrons which react to establish the thermal electrons necessary for the formation of ion-molecules in the ionisation region of the mobility spectrometer. Tritium ionisation sources, which have lower radiation hazards than ^{63}Ni sources[128], have a high ionisation efficiency, which may improve the overall efficiency of ion mobility spectrometers. Alternative ion sources for IMS have been investigated in order to eliminate the reactant ion peak[129] and overcome the problems associated with radioactive sources[91], for example, laser produced ions[130], in which laser radiation at wavelengths greater than 200 nm will not ionise air at power levels required to ionise organic compounds.

Photoionization using a krypton lamp[129], with nitrogen carrier gas, has also been investigated. Photoionization in air, using a hydrogen discharge lamp[92], for IMS is problematic due to the oxygen quenching of photons, but has proved advantageous for an on-axis source. A photoemissive ionisation source based on ultraviolet irradiation of a thin gold layer has an energy of 4.5 eV[91] in which, in theory, the electron concentration can be controlled by changing the incident light intensity. The experimental work incorporated the use of a pulsed xenon light source eliminating the

shutter grid. The performance of the photoemissive source was constrained by mutual ion repulsion degrading the ion resolution, a problem which might be overcome by wider bore systems reducing the ion density. Photoionization sources have a larger volume than ^{63}Ni ionisation sources and are concentration dependent, therefore the larger cell volume reduces the sensitivity of the detector[129].

Electrospray IMS[131-134] and coronaspray nebulisation[135] with ionisation has been used for IMS detection of liquid samples of non-volatile and high molecular weight compounds, following separation of the analytes by microbore liquid chromatography, capillary zone electrophoresis, flow injection analysis, or field flow fractionation. Electrospray IMS has also been used for ionisation of samples eluting from gas chromatographs[136], prior to detection by IMS.

1.4.4 Reactant ion chemistry

As mentioned in section 1.3.4, dopant chemicals may be added to the carrier gas, in trace quantities, in order to enhance the selectivity, resolution and detection limits of an ion mobility spectrometer, through alteration of the ion-molecule chemistry. The dopant chemical must be capable of reducing the amount of interferent species whilst maintaining suitable ion-molecule chemistry for detection of the analyte. The chemicals are chosen for their respective proton or electron affinities, a higher value than the interferent species but lower affinity than that of the analyte is required, thus increasing selectively. Alteration of the ion-molecule chemistry can also effect selectivity through improved resolution and subsequent data manipulation. Cohen's patent for IMS detection of a trace substance[115] originally specified reaction of the sample with a different species of reactant ion [other than water], and identified halocarbon gases to be used as reagents to look for other halocarbons. Formation of chloride ions has also proven to be particularly beneficial for the detection of ethylene glycol dinitrate[110]. The

addition of ammonia to form ammonium reactant ions[112] has been successful for improved resolution and selectively for the detection of alkylamines.

Alternate reagent ion chemistry has also been investigated for GC-IMS, specifically for complex mixtures. The reagent chemicals evaluated[137] were acetone, dimethylsulphoxide (DMSO), and pyridine, which resulted in sequentially improved selectivity gained from the use of the first two chemicals but no advantage observed through use of the last.

1.4.5 Ion-molecule chemistry

The addition of dopant chemicals alters the ion-molecule chemistry with respect to the reactant ions. When sample ions enter into the system the ion-molecule chemistry is altered again with product ions resulting. Ion distribution profiles in the drift region of an ion mobility spectrometer[107] have been studied. The mobility and ion structure of protonated aminoazoles[138], protonated diamines and polyamines[139] have also been examined.

1.4.6 Resolution and peak identification

Resolution is defined[107] as $R = t/dt$, where t is the drift time of the ion and dt is the width of the peak at half the maximum height. Resolution has also been recorded as $R = t_d/t_w$[140] and $R = t_d/w$[141]. Resolution is governed by the shutter pulse, molecular diffusion, ion / molecule reactions in the drift region, electric field geometry particularly approaching the collector plate, ion-ion repulsion, induced charge on the collector electrode, and spectral processing.

A Gaussian deconvolution algorithm can be used to separate peaks where drift times differ by as little as 100 μs[142] for analysis of ion mobility spectra obtained for mixed vapours. Moisture content of the drift gas[143] is a dominant factor in determining peak shape and the success of deconvolution. Other factors involved in determining

resolution are relative proton affinities, concentrations, differences in drift times between the mobility peaks of the components and chemical interactions among them.

Research with neural networks[144-147] for analysis of ion mobility spectra indicated that peak location was the most important factor[147] in automated identification routines. Further work in this area[148] showed that algorithms used to identify compounds under conditions of low signal to noise ratio may overcome interference from incomplete resolution, but not from chemical interferences in the ion formation processes, however, detailed knowledge of the ion chemistry of the measured system is not required[148].

1.4.7 Concentration dependency and sample introduction

Studies of vapour concentration dependency of ion mobility spectra[149] with pulsed and steady state sampling showed the latter to yield time-stable improved resolution mobility spectra, with no evidence of bond breaking and recombination. Advanced IMS performance through combination with high-speed vapour sampling, preconcentration and separation techniques[150] (e.g. gas chromatography) for the detection of parts per trillion concentrations have been recorded.

1.4.8 Hyphenated ion mobility spectrometry techniques

Due to the need for improved selectivity of IMS instrumentation for monitoring compounds with similar mobilities, hyphenated IMS techniques, for example GC-IMS[151], have been employed to provide preseparation of the analytes before analysis by IMS. IMS is suitable for detection of compounds separated by GC[152] provided that solvent effects, matrix interferences, and column bleed are addressed, particularly in the positive mode as positive reactant ions react with almost all organic compounds. Elimination of a sample transfer line by using direct axial sample introduction from a GC column[109,153] has produced satisfactory ion mobility spectra. GC-IMS has been

evaluated for the detection of vinyl chloride[154], and with helium carrier gas has been investigated for the determination of C_1 to C_4 alkanes[82].

IMS has also been evaluated and deemed a successful detection technique when interfaced to other chromatographic techniques including supercritical fluid chromatography[81,105,155,156] (SFC), and high performance liquid chromatography (HPLC)[151]; the latter provided detection down to tens of picograms for halogenated compounds. These preseparation techniques can also act as preconcentration methods, improving the limits of detection of IMS and / or the associated technique. HPLC-IMS[157] has a lower limit of detection than HPLC combined with a UV detector. IMS has undergone some development towards being a unified detector[158] for capillary GC, SFC, and liquid chromatographic (LC) analyses. Laser desorption[159] has been used as a means of acquiring samples from solids in a form acceptable for analysis by IMS.

Another way to improve detection by IMS and hyphenated IMS techniques is data manipulation. Fourier transform-IMS[160] and the use of apodisation functions[161] have allowed collection of a complete mobility spectrum of a high-resolution chromatographic peak during its short residence time in an ion mobility spectrometer. Fourier transform coupled with electrospray IMS[162] enhanced the signal to noise ratio and the IMS resolving power.

1.4.9 Applications of ion mobility spectrometry as an analytical instrument

IMS has been applied to general and more specific environmental monitoring requirements and has also been used to address particular problems not normally associated with environmental issues. Since the applications of IMS are varied they have been divided into categories to assist with classification in this text. These categories have been selected in order to demonstrate the leading applications of IMS, namely,

environmental monitoring, detection of explosives, detection of illicit drugs, the determination of potential pollutants in liquid media, and a miscellaneous section.

Environmental monitoring. IMS has been investigated as a sensor for environmental analytical chemistry[163]. Environmental and industrial applications are directed toward monitoring for toxic chemicals, and chemicals considered to be hazardous to man or the environment. Amongst these are included acid and stack gases, amines, isocyanates, halogens, solvents, anaesthetics, fuels, and gases used in the semiconductor industry.

The major application of ion mobility spectrometers as environmental monitors is for chemical agent monitoring[80,164,165] by the military. A brief demonstration study of ion-molecule behaviour of selected agents and interferents has been made with the atmospheric IMS-MS[80]. Modifications of the hand-held CAM™ chemical agent monitor (Figure 1.1) led to the Otto fuel monitor (OFM™), used for detecting fuel leaks.

Figure 1.1: CAM chemical agent monitor; a hand-held ion mobility spectrometer

Figure 1.2 depicts an OFM kit complete with its protective carrying case and spare consumables. The CAM was also developed for fixed installation continuous monitoring of chemical warfare agents (Figure 1.3), on board surface ships, and some work has been carried out on development of a continuous monitor for Otto fuel.

Figure 1.2: OFM kit
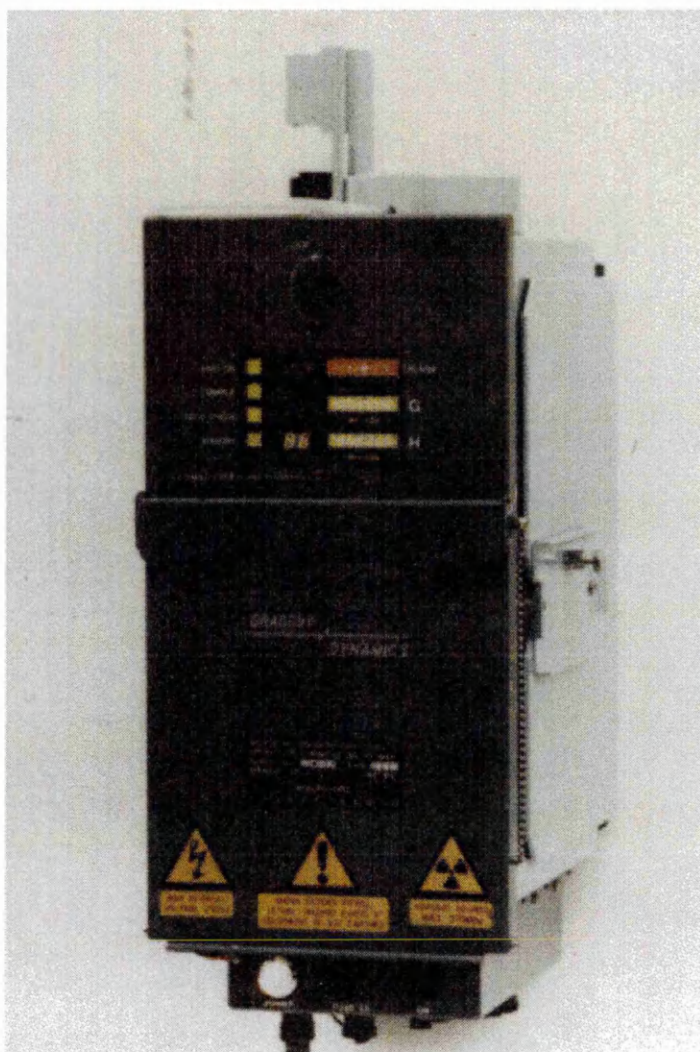
Figure 1.3: Ion mobility spectrometer for the continuous monitoring of chemical warfare agents

IMS has been evaluated for near real-time environmental monitoring of dimethyl sulphate[97] and toluene diisocyanate[96,97], cyanide[166], nicotine[167], polychlorinated biphenyls[168], organophosphorus compounds[104,169], benzene[170], hydrocarbons[171], hydrogen fluoride[172], perfluoroisobutene[173], aromatic ketones[174], aliphatic and aromatic amines[113,126], ethers[149], anaesthetics in air and respired gases[175], volatile organic compounds used in the semi-conductor industry[176], and a mixture of organic compounds[177]. Investigation of UDMH detection in the presence of ammonia[84] proved it worthy of further development, as did the determination of other amine fuels, HZ and MMH with ammonia present in air, using either acetone or 5-nonanone reagent gases[178]. An airborne vapour monitor (AVM™) based on IMS was found to be more sensitive to HZ than to MMH[32], with slow response and recovery giving rise to differences in the responses to repeat exposures of the analytes; ammonia interfered with the detection of HZ. Projected uses for IMS include screening for hazardous wastes and toxic chemicals.

Explosives. Ion mobility spectrometers are used qualitatively to detect contraband explosives, for example, at customs sites or potential terrorist targets, where the detection of explosives is critical. Some explosives have been detected by their vapours, others have very low vapour pressure at room temperature and require identification through the use of tagging agents (taggants), or preconcentration of the sample. Detection of trace explosives by IMS has been investigated for RDX[179,180], TNT[88,179-181], PETN[179,180], NG[179,180], ammonium nitrate[179], 2,4-DNT[88,180], EGDN[180], HMX[180], and tetryl[180], including identification of trace levels of explosives in the presence of complex matrices[180]. Commercially available instruments for the detection of explosives include the Plastec™ (Graseby Dynamics Ltd., Watford, UK).

Drugs. The detection of illicit drugs is important for forensic and law enforcement purposes. Heroin and cocaine were targeted first of all, and have been detected simultaneously. Target drugs have been detected in luggage and mail, on people, on books kept by drug dealers, and on paper money. Due to the low vapour pressures of contraband drugs, detection is based upon the entrapment of microparticles which may have drugs on them which are subsequently evaporated at an elevated temperature, in a furnace leading directly into the spectrometer.

Such instruments, for example the Ionscan™ (Barringer Research Ltd., Ottawa, Canada), and the Narcotec™ (Graseby Dynamics Ltd., Watford, UK) shown in Figure 1.4, are available commercially.

Figure 1.4: Illegal drugs detector, the Graseby Narcotec

Concentration and temperature studies have been performed for IMS used to detect drugs of abuse in customs scenarios[182]. Other classes of drugs detected by IMS include barbiturates, amphetamines and LSD. Further uses for drug identification have been for the characterisation of benzodiazepines[114] in blood and urine, and of tablets and containers.

Determination of analytes in liquid media. IMS has generally been associated with the detection of atmospheric pollutants because the technique involves analysis of samples in the gaseous or vapour phase. The need to detect pollutants in liquid media is becoming more desirable, and IMS is playing an increasingly important role in this area due to the ease of operation and low limits of detection obtainable. The application of

IMS to this problem requires a means of separation of the analyte from the liquid medium, usually in the form of a selectively permeable membrane. Analysis by IMS proceeds once the analyte has been transferred from the liquid to the vapour phase.

IMS has been developed as a continuous flow monitor for aniline in hexane and water[183], an important analysis due to the toxicity of this compound to aquatic life. Solid-phase enrichment followed by thermal desorption and IMS has been evaluated for field screening of organic pollutants in water[184], particularly alkyl phthalates. The IMS determination of aqueous ammonia[185] has also been achieved, providing information about water quality in rivers, waste water processing, and in drinking water treatment facilities. A complete sample handling and IMS detection system for on-site monitoring of ammonia is shown in Figure 1.5. Electrospray-IMS has been investigated for the determination of alkylamines in liquid waste streams, for the prevention of possible pollution.

IMS has also been investigated for the detection of bacteria in water and waste water sources[186], an application suitable for medical and clinical services. The biodetection potential of IMS has been extended to immunoassays[187].

With the addition of a specialised membrane inlet IMS has been used for on-line measurement of ethanol during yeast fermentation[188] for a potential market in the alcoholic beverages manufacturing industry. GC-IMS has been used to quantify mammalian lignans in biological fluids[189].

Miscellaneous. Other potential IMS applications are in the forestry industry, which requires the identification of different timbers before processing. Fast thermolysis-IMS proved successful for certain wood species[190]. This technique was also favourable for the detection of Northern Red Oak wetwood[191]. (Wetwood is an abnormal condition of wood from both deciduous and coniferous trees, caused by bacterial infection.)
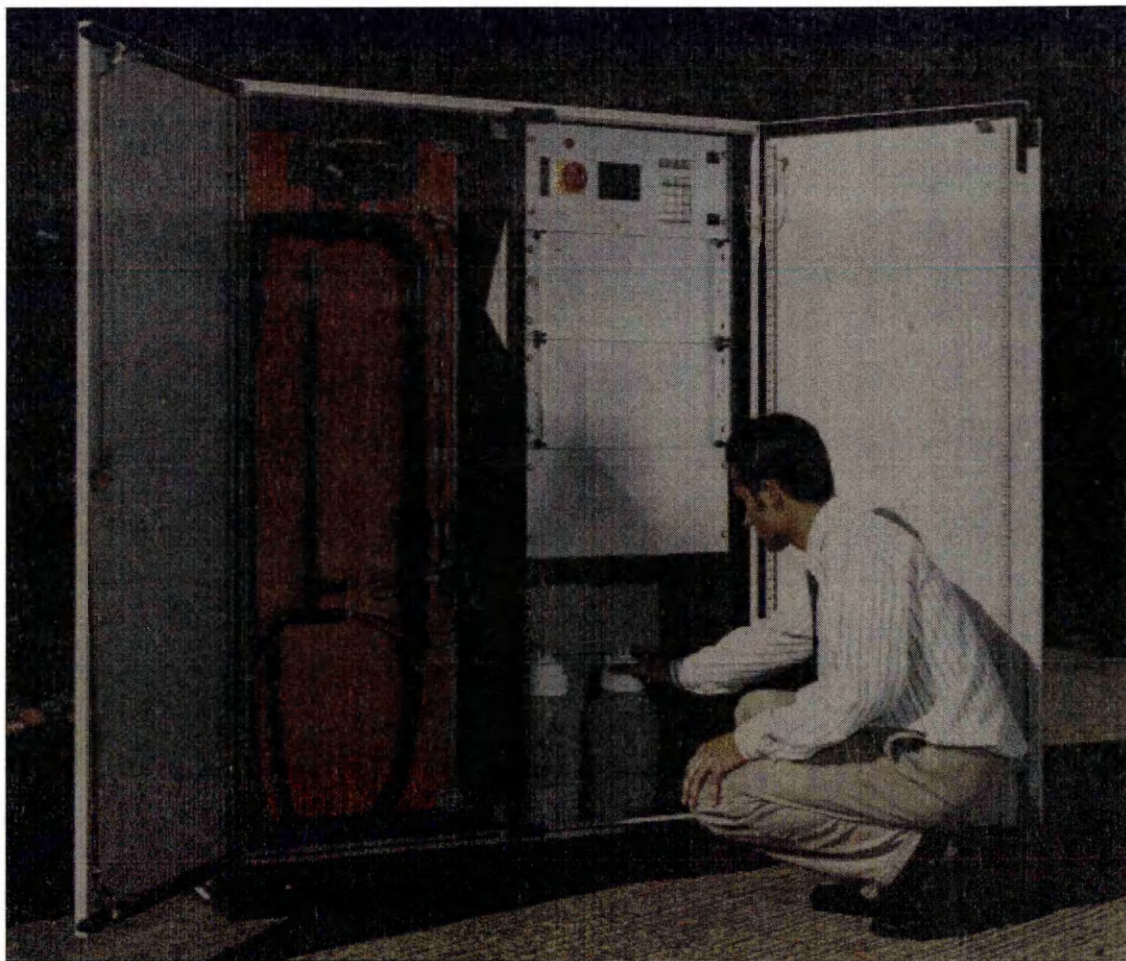
Figure 1.5: Ammonia in water monitor

IMS detection of coliforms is an important development for the food industry, indicating the microbiological quality and environmental contamination of processed foods[192], and automated bacterial identification and quantification[193] of headspace samples has been attempted.

Laser desorption-IMS has been investigated for the characterisation of polymers[159], with a view to sorting plastics for recycling.

1.4.10 Portable instrumentation

Originally, commercial ion mobility spectrometers actively tracked the reactant ion peak (RIP) so that product peak positions were always measured relative to an updated RIP. Therefore the reference to normalised peak positions provided a better understanding of the identification through the software programme, which enabled field portable instruments to be deployed under varying ambient conditions of temperature and pressure. More modern instrumentation includes temperature and pressure compensators, so that mobilities are corrected for varying ambient conditions, allowing absolute mobilities to be the defining criteria. Although some[194] have considered IMS to be a rather sophisticated technique more suitable for laboratory use than for portable monitors, hand-held instruments have been in use for a number of years, for example, the CAM and the OFM, both of which are commercially available. The advanced chemical agent detector and alarm, ACADA, is another portable instrument undergoing development for use by the US Department of Defence. Portable CAM-based instrumentation has also been used to demonstrate the effectiveness of IMS for the detection of nicotine in air[195], providing useful information on air quality and for determining patient compliance with non-smoking medical regimes.

In 1994, a futuristic approach ("the birth of the tricorder"[196]) depicted the qualifying requirements for field-portable hyphenated instrumentation. Hyphenated IMS techniques are already undergoing development. A portable hand-held GC-IMS[197] (Figure 1.6) has been evaluated for the determination of phosphates, phosphonates, alkyl ketones, and chlorophenols, and found to be feasible for most of the compounds investigated.
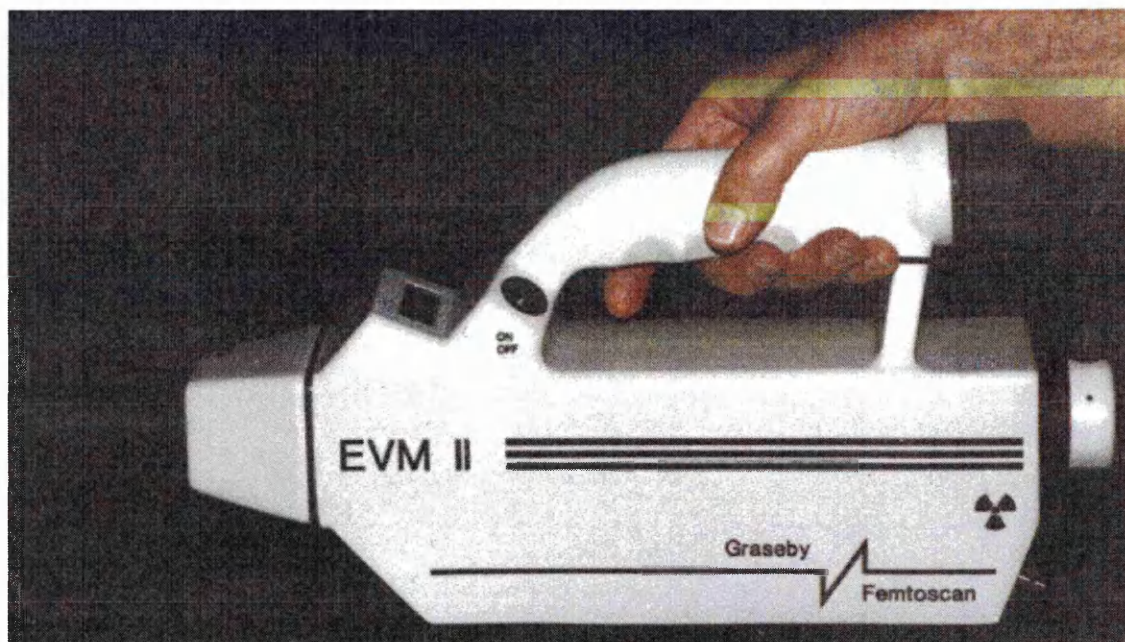
Figure 1.6: Hand-held GC-IMS

This instrument was developed from the EVM™ (environmental vapour monitor) shown in Figure 1.7, with recorded ion mobility spectra displayed on a connected computer terminal. GC-IMS has also been considered for environmental monitoring for solvent vapours, for example, a mixture of four isomeric butanol compounds[198], (poly)chlorophenols[197], alcohols[197], phosphate / phosphonate mixtures[197], ketone mixtures[197], drug synthesis / purification solvent mixture[197], amine mixtures[198], an illegal drug synthesis / purification solvent mixture, volatile carboxylic acids and their compounds[150], and explosives.
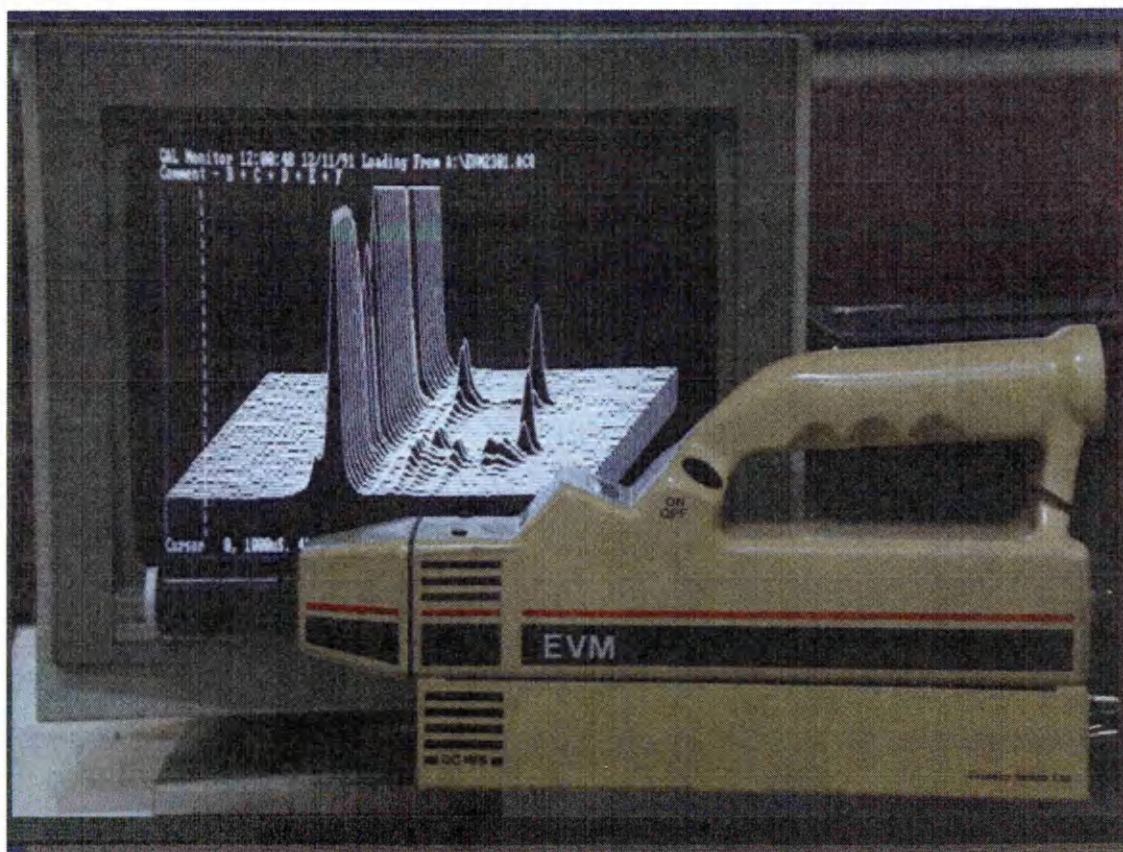
Figure 1.7: EVM with ion mobility spectra displayed on a connected computer terminal

GC-IMS has been investigated for cabin atmosphere monitoring of the Space Shuttle and International Space Station Alpha[200] and as a volatile organic analyser for Space Station Freedom[201], now designated International Space Station. A photograph of a volatile organic analyser, situated in a shuttle, is shown in Figure 1.8. Figure 1.9 shows the use of an IMS in an air lock on board a space shuttle.

S81E5514 1997:01:16 00:32:32

Figure 1.8: Volatile organic analyser (two units at centre top) on board a space shuttle

Figure 1.9: Use of an ion mobility spectrometer in an air lock on board a space shuttle

Miniaturisation of ion mobility spectrometers is being sought through decreased dimensions and integration of drift channel and signal acquisition in a silicon wafer[163] directly connected to a high speed portable computer.

Further miniaturisation of hyphenated IMS[199] instrumentation is being considered through the use of an absorption pumping system, eliminating the need for a pumped air flow, and a direct sample ingestion system, the combination of which reduces power consumption, size, and weight of the instrument. Such a miniature, palm-held ion mobility spectrometer is shown in Figure 1.10.

Figure 1.10: Miniature ion mobility spectrometer

Improved performance is also being sought through the use of microvolume preconcentrators / thermal desorption modules[150] to increase the limits of detection. A computer controlled variable sampling time technique[150], and automatic attenuation control, are also being investigated. Automation of responses would require a peak height detection algorithm to limit the RIP depletion.

1.5 Research considerations

1.5.1 Quantitative interpretation of ion mobility spectra

The sensitivity of ion mobility spectrometers, i.e. change in response with increase in concentration, depends on the compound being monitored. The results may be due, not only to the detector response, but also to the method and efficiency of sample ingress.

Little information regarding precision data has been recorded for ion mobility detection, but relative standard deviations (RSDs) for hexane, dialkylphthalates, and HZ vapour ranged from 3 to 11%, 6 to 27%, and 3 to 16% respectively[118], using hand-held instruments. The reproducibility of reduced mobilities has not been studied systematically, to date, but generally when measured under similar conditions of temperature and humidity, with respect to a standard reference, they are reproducible to within 1 to 2%[113].

The only documented evidence of stability refers to data concerning the long term stability of a hand-held IMS unit used on the space shuttle, which produced results of between 5 to 10% variation over a six week period[178].

A description of the quantitative response in IMS involves both the principles of the formation of ion-molecule clusters and their characterisation by mobility, under known conditions. In the formation of ion-molecule clusters, as outlined in section 1.3.4, the reactions are relatively slow. The population of reactant ions formed reaches a finite number, at equilibrium, which is dependent upon the rate of generation of the beta radiation. Because the number of reactant ions is limited by these processes, as the molecules collide with neutral analyte molecules, the RIP decreases in magnitude as the product ion peak increases proportionally. This phenomenon can also be observed in the apportioning of ions between monomer and dimer peaks. Only a negligible amount of ions or neutral molecules is lost in the drift process, enhancing the sensitivity of the

technique, for which only small volumes of sample are required for analysis at vpb concentrations, equivalent to low picogram levels. The detection limits are good because of the ion density in air at atmospheric pressure, which is governed by the radioactivity of the source. Eiceman *et al.*[178] have already detected HZ and MMH at low vpb concentrations.

The linear range of the detector is limited because the mobility spectrum comprises a constant total number of ions, regardless of proportion. Linear ranges of orders of magnitude of 10 to 100 have been reported for IMS[58], compared with values[202] of 50 and 500 for electron capture detectors with tritium and nickel 63 sources respectively, 10^3 for the alkali flame ionisation detector and gas density balance, 10^4 for the thermal conductivity detector, helium ionisation detector, and cross section detector, and 10^7 for the flame ionisation detector. Sample overloading in an ion mobility spectrometer leads to the disappearance of the RIP, multiple analyte peaks, and dimer product ions and cluster ions[95]. The linear range is satisfactory for targeting ions over a narrow concentration band providing that the working range is tailored to the desired level.

It has been assumed that provided that the beta radiation source maintains a constant concentration of ions, and the monitoring of the analytes is performed under reproducible conditions, the precision and stability of the spectrometer should be satisfactory. However, these parameters could be affected if the ion-molecule chemistry and construction materials are inappropriate and adversely alter the response and recovery characteristics.

In order to investigate this possibility, during investigation of the simultaneous monitoring of the hydrazines and nitrogen dioxide by IMS during this research project, an ion mobility spectrometer was designed and constructed and its optimum operating

conditions determined experimentally. The project also required the generation and quantification of dynamic atmospheres of the hydrazines and nitrogen dioxide at the appropriate concentrations. Ammonia is usually present in hydrazines' environments, as a breakdown product, and as a natural emission from human metabolic processes, and may interfere with the ion mobility detection of the hydrazines. Therefore, ammonia was generated at low vpm levels. The reagents, equipment, generation and determination of the required test atmospheres and the design features of the ion mobility spectrometer breadboard are detailed in chapter 2.

1.5.2 Response and recovery characteristics

Response and recovery characteristics are governed by the factors of surface adsorption, equilibration time of the membrane (if used), efficiency of removal of material from the ionisation region, and signal averaging effects[98]. Chemicals with low surface sorption will pass through the system relatively unhindered, although the equilibration time of the membrane will produce a time lag due to diffusion of the analyte in the membrane material, and will be affected by the thickness of the membrane.

Hydrazines have a high proton affinity and are subject to surface adsorption phenomena, which causes practical problems in their real time detection. The hardware and ion-molecule chemistry of the monitoring system needs to be tailored to minimising response and recovery times. In order to obtain information regarding the optimum conditions for satisfactory response and recovery characteristics, the experimental work for the project was designed to investigate the effects and compatibility of different detector cell construction materials, the most effective means of sample ingress through comparison of different sample inlet systems under optimum operating conditions, detector cell temperature, and pneumatics configurations for the detector cell. The response and recovery characteristics studied included response and recovery times,

selectivity, and sensitivity. The overall effects of these contributory factors have been defined in order to provide the most efficient combination of spectrometer parameters for the detection of the stated materials, in a hand-portable instrument (linked to a computer), as assigned in chapter 3. The experiments are detailed in chapter 2, with results and discussion following in chapter 3.

1.5.3 Ion-molecule regimes

Ion mobility spectrometers respond to a broad range of compounds with various functional groups, which, if present in the same sample, can compete for the reactant ions, if they have a greater proton or electron affinity than the reactant ions or the analyte of interest. These matrix effects are common in undoped systems i.e. with water based reagent gas chemistry. More accurate and reliable identification of analytes is achieved when ions of both polarities are considered[111]. Selectivity may be improved with the introduction of appropriate dopant chemicals into the detector carrier gas, in trace quantities, thereby altering the degree of affinity required for reaction, increasing resolution, sensitivity, and response and recovery times.

Cluster ions are formed when analyte molecules diffuse from the ionisation region into the drift region, followed by their consequent association reactions with the product ions. The reduced mobilities observed for these ions are weighted averages of the reduced mobilities of all the individual or cluster ions participating in a localised equilibrium between the ion swarm and the neutral molecules they encounter as they traverse the drift region[42].

None of the dopants previously examined[83,101,178] have given satisfactory resolution of the hydrazines, with sufficient sensitivity and overall selectivity from ammonia. Although it appeared that the three hydrazines and ammonia peaks were all resolved with an undoped system (i.e. water chemistry), previous experience has shown

that there are many chemical species present in air which have sufficient proton affinity to produce product ions. An ion mobility spectrometer using water chemistry was found to be unsuitable for quantifying the hydrazines at low concentration levels, because of the widely varying chemical composition of ambient air causing problems of interference by altering the hydrazines' product ions.

Since ammonia is present as a normal constituent of ambient air, it was previously considered as a dopant to overcome the problem of its probable interference in the detection of hydrazines[101]. With ammonia, all three hydrazines produced two peaks, the first of which, in each of the spectra, had similar mobilities, and if only this peak was present at low concentration then it would not be possible to determine which of the hydrazines was present. The possibility of loss of sensitivity to hydrazines with ammonia as dopant has not been investigated.

Ketones are known to be effective in the separation of HZ, MMH, and UDMH by IMS, when the ketones are present in large excess as vapour in the IMS drift tube. The drift times for product ions of these hydrazines are affected by vapour concentration of the ketone and the resolution of ammonia from these hydrazines is not effected under all conditions.

In an acetone doped system all three hydrazines produced two peaks. Ammonia produced a single peak close to both HZ and MMH, giving rise to uncertainty in identification and quantification. An acetone doped system was apparently more sensitive towards UDMH, and was dependent upon dopant concentration.

A publication by Eiceman et al.[178], regarding the ion-molecule chemistry of hydrazines with 5-nonanone as dopant, reported sufficient limit of detection of HZ and MMH in the presence of ammonia, and partial resolution of the HZ and ammonia product ion peaks.

During this work different chemicals, covering a variety of classes of chemical compounds, were evaluated for use as dopants in an ion mobility spectrometer breadboard (chapter 2). The ketones remained the most favourable class of compound for the determination of the hydrazines and ammonia; the detection of nitrogen dioxide did not prove problematic (chapter 4, part 1) and so further investigation of the ion-molecule chemistry of nitrogen dioxide systems was not considered.

A previous investigation into the detection of the hydrazines and ammonia with 5-nonanone reagent gas[178] highlighted the complex nature of ion-molecule reactions. The degree of resolution of peaks in a mobility spectrum was shown to be dependent upon the concentration of dopant within the system. The peaks were shown to comprise a combination of a protonated sample molecule, or a protonated sample molecule with either one or two molecules of dopant attached. A low concentration of dopant, a high proton affinity, or a high temperature favoured an equilibrium between the protonated sample molecule and the protonated molecule with one molecule of dopant. Increasing the amount of 5-nonanone, a low temperature, or a low proton affinity sample favoured an equilibrium between a protonated molecule with either one or two molecules of dopant attached. Partial resolution of HZ and ammonia was reported but prediction of a specific dopant for improved resolution has not been achieved.

These discoveries raised other questions. For example, why should 5-nonanone be any more effective than ketones lower down the homologous series in the separation of HZ and ammonia? Referring to equation 6, the inference was that mobility was due, in part, to the collisional cross section of the molecules. Empirical findings thus far have shown that the hydrazines traverse the drift tube of an ion mobility spectrometer in reverse order to that expected. The greater the degree of methyl substitution on the parent HZ molecule the higher was the mobility. The prediction would have been that

HZ should have the higher mobility due to the more compact nature of the molecule. So far, no explanation has been hypothesised for this anomaly. If the resolution achieved with 5-nonanone is concentration dependent, could the concentration control of other ketones render them as effective? What are the characteristics of these chemicals, e.g. their thermodynamic properties? Can the choice of dopant chemical become a predictable science through the use of molecular modelling?

Empirical findings suggest that resolution was dependent upon vapour concentrations of ketones in excess of 1 vpm[178]. In order to obtain knowledge with respect to the incomplete resolution of HZ and ammonia product ion peaks molecular modelling was undertaken to determine cross sectional diameters of ion-molecule clusters. Preliminary studies with molecular modelling using HyperChem (see chapter 4, part 2), of a series of symmetrical ketones with the hydrazines and ammonia individually, provided no obvious assistance in rationalising the observed trends in ion drift times and further studies in ion-molecule chemistry were deemed necessary. Therefore, IMS-MS-MS studies were performed (see chapter 4, part 3).

These further studies of ion-molecule chemistry of the hydrazines and ammonia, with the homologous series of ketones, were undertaken to investigate ion cluster formation, and any trends which might appear as a result of the differences in size of the ketones and the effect of methyl substitution of the hydrazines. For this reason, tetramethylhydrazine (TMH) was included in the research programme. The number of carbon atoms in the chains of the ketones in the series was limited to nine, due to the mass range of the spectrometer, but in keeping with the original work with 5-nonanone. A fluorinated ketone was also studied to determine the effect of electron withdrawing groups upon ion cluster formation. Acetone and other small ketones underwent ion-

molecule clustering and reactions with the ketone vapour to produce hydrazones and azines which in turn formed clusters with other ions.

A model proposed by Stone[203] suggested that the number of ketone molecules clustering with the sample ion-molecules generally decreased with the increase in methyl substitution from HZ through MMH to UDMH. Hence, protonated ammonia would be expected to have four molecules of dopant attached to its core, HZ would have three molecules, MMH and UDMH would have two and one molecule(s) respectively. An extension of this model, proposed by the author, relates to the symmetrical nature of the fully methyl subsistuted TMH. As with the symmetrical nature of the parent HZ molecule, there would also be protonation predominantly at one of the two core nitrogen sites. This would lead to the attachment of one molecule of the ketone. Within these restrictions, the higher the dopant concentration, the greater would be the number of ketone molecules attached to the protonated sample species, a phenomenon which may be predicted from the application of the principles of Le Chatelier:

$$H^+[A] \quad + [K] \quad \leftrightarrow \quad [A]H^+[K] \qquad 16$$

$$[A]H^+[K] \quad + [K] \quad \leftrightarrow \quad [A]H^+[K]_2 \qquad 17$$
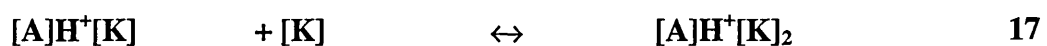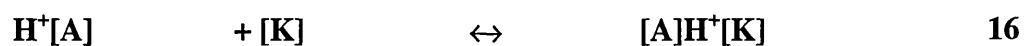
where,

[A] = analyte, H^+ = proton, and [K] = ketone.

The findings with these and other large molecular weight ketones suggested that the identity of cluster equilibria in the drift region were controlled by the number of protons on the core nitrogen and this provided the essential mechanism for

distinguishing the sample ions and controlling resolution in conjunction with vapour concentration.

In summary, the factors affecting the IMS detection of hydrazines and ammonia in the positive mode, and nitrogen dioxide in the negative mode of operation, have been investigated: namely, the comparison of sample inlet systems, detector cell construction materials, optimum detector operating temperature and flow configurations, and ion-molecule chemistry, through experimental trials, molecular modelling, and IMS-MS-MS studies.

Due to the number of parameters under investigation, the experimental areas overlapped so that a particular research topic may not always have been evaluated under optimum conditions. For this reason, some areas have been investigated under different regimes to try to ensure that the observed results were due to the parameter under test, and not coincidental.

Chapter 2

EXPERIMENTAL

2.1 Materiel

2.1.1 Reagents

All of the reagents acquired for the experiments were used as received, without further purification. For the purposes of calculations, used in the preparation of standards and general use in the IMS experimental trials, purity of the reagents was taken as the minimum assay value. The reagents were: [Shell Chemicals UK] acetone (2-propanone); [Aldrich Chemical Company] ammonium carbamate 99%, 2-butanone (methyl ethyl ketone) 99.5% HPLC grade, anhydrous HZ 98%, MMH (methylhydrazine) 99%, 4-methyl-2-pentanone (methyl isobutyl ketone) 99.5%, 5-nonanone (dibutyl ketone) 98%; [British Oxygen Company] ammonia gas 99.98%; [BDH] 0.880 concentrated ammonia (35%) GPR MMH 98%, 4-dimethylaminobenzaldehyde (specially prepared for HZ determinations) 99%, 2-methylpyridine (2-picoline) 98%; [Lancaster Chemicals] diisopropyl methane phosphonate 98%, 3,5-heptanedione, 2,2,6,6-tetramethyl-3,5-heptanedione; [Koch-Light Laboratories Ltd] UDMH "pure"; and de-ionised, distilled water.

The hydrazines used for IMS-MS-MS experimentation, at NMSU, were HZ, MMH, UDMH, and TMH, the first three of unspecified origin previously decanted and stored under nitrogen. Ammonia was produced by evaporation from ammonium hydroxide solution. The ketones used were acetone, 3-pentanone, 4-heptanone, 5-nonanone, and 1,1,1-trifluoroacetone. The chemicals were tested for identification and purity as specified in section 2.1.2.5. The only significant contamination of the

chemicals was found to be in the HZ, which contained approximately 4% aniline. The 3-pentanone contained several minor contaminant peaks which were too low in intensity to identify with any degree of certainty. Due to the production of low vpm concentrations of vapours of the chemicals involved, the levels and nature of these impurities were considered to be insignificant with respect to the IMS-MS-MS studies.

2.1.2 Equipment and test methods

2.1.2.1 Ion mobility spectrometer experimental breadboard

The ion mobility breadboard was designed and built to a customised specification, in order to facilitate the alteration of the operating conditions. The spectrometer comprised a number of features (see Figure 2.1 [page 50], and a photograph following on Plate 1).

A choice of sample inlet systems allowed transfer of sample across a semi-permeable membrane, or direct introduction to the spectrometer through a pinhole transfer line.

A dopant generation system was incorporated, consisting of a dopant chamber, which could be heated to increase the dopant vapour concentration output, and a split flow line which allowed the reabsorption of a portion of the dopant vapour.

Due to the reactive nature of hydrazines, and ammonia, two ion mobility detector cells were constructed with different insulation materials and were evaluated to determine their suitability for the detection of these compounds. The basic difference between the two cells was the use of either ptfe or ceramic insulators, used in conjunction with gold plated internal metal surfaces. The metal surfaces were gold plated in an effort to make the detectors as inert as possible. Their maximum operating temperatures were governed by their respective components. Included in these components were the insulating materials, and although these insulators alone did not dictate the maximum temperatures, reference to these temperatures provided an easy

method of differentiation between the two detectors. The maximum operating temperature of the cell with ceramic insulators was 225°C (HITIMS detector) compared with only 60°C for the cell with ptfe components (LOTIMS detector).

The ion mobility spectrometer breadboard was designed and constructed to allow one detector cell to be operational with doped carrier gas flowing through, while the other cell was maintained in a stand-by mode with undoped carrier flowing through. When experiments were to be conducted on the stand-by cell, the four flexible gas lines were disconnected from the operational cell at ptfe fittings close to the cell, and were reconnected at corresponding positions on the stand-by cell.

A pneumatic system provided flow through the inlet, ionisation and drift regions of the detector, and could be arranged to provide different flow patterns, either unidirectional or bi-directional. Using unidirectional flow, air entered the detector in the region of the collector electrode and flowed through the drift region to the ionisation region, from where it was exhausted. The sample stream was introduced at a much lower flow rate, and mixed with the carrier gas in the ionisation region. This configuration could only be used with a direct inlet system. The bi-directional system had a similar flow pattern, in which the air (the drift flow) flowed from the collector electrode, in the drift region, to the ionisation region, from where it was exhausted, but in addition a comparable and opposing flow (the source flow) was introduced into the ionisation region, where the two flows mixed. The source flow could be introduced directly from the detector side of a membrane inlet, or with the sample flow from a direct inlet system. All flows were controlled by fine metering valves (Nupro) and the flow rates indicated by integral flow meters (Platon). Both the flows and the operating pressure within the detector could be adjusted.
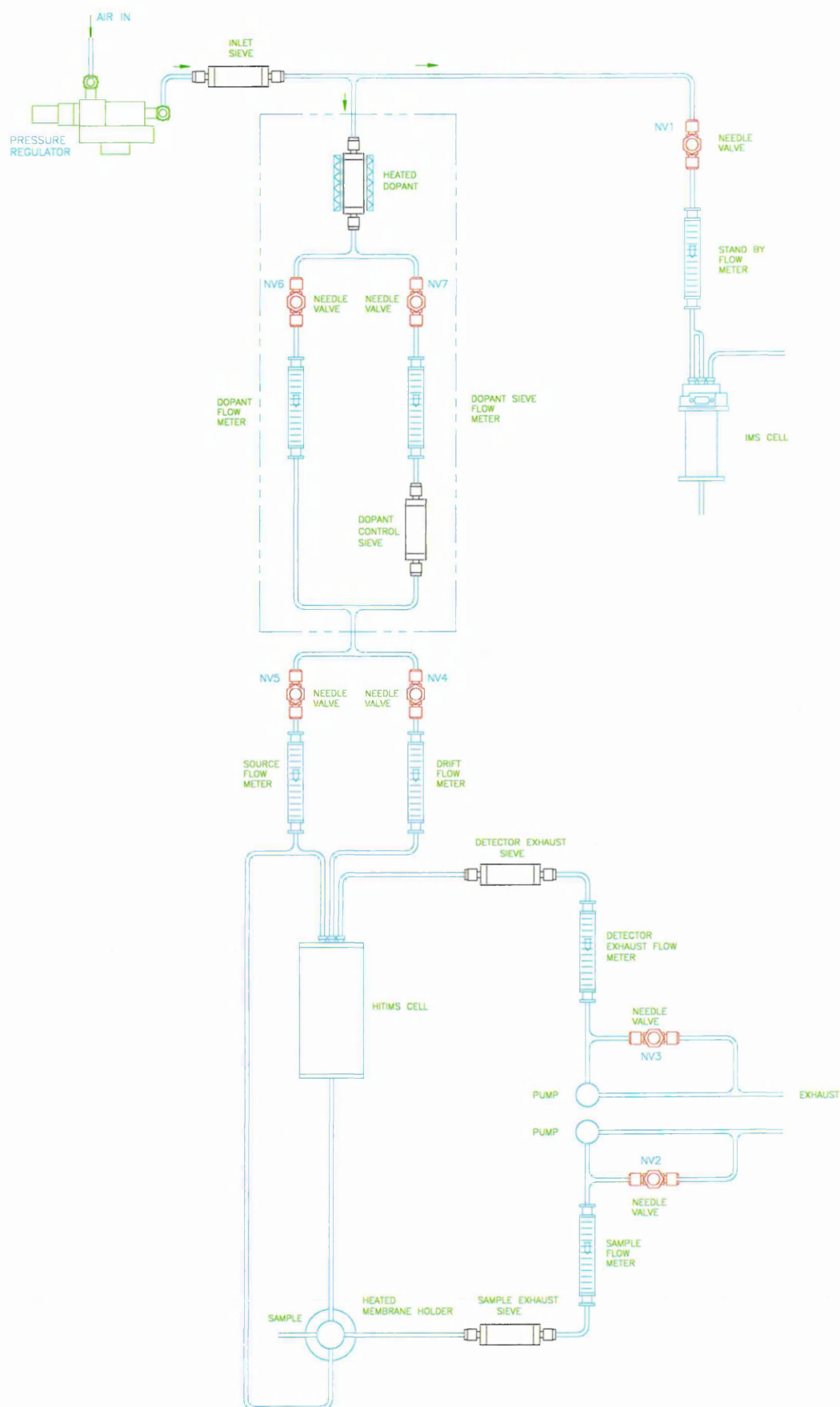
Figure 2.1: Schematic diagram of the ion mobility spectrometer breadboard pneumatic system, depicting bi-directional flow and membrane inlet systems
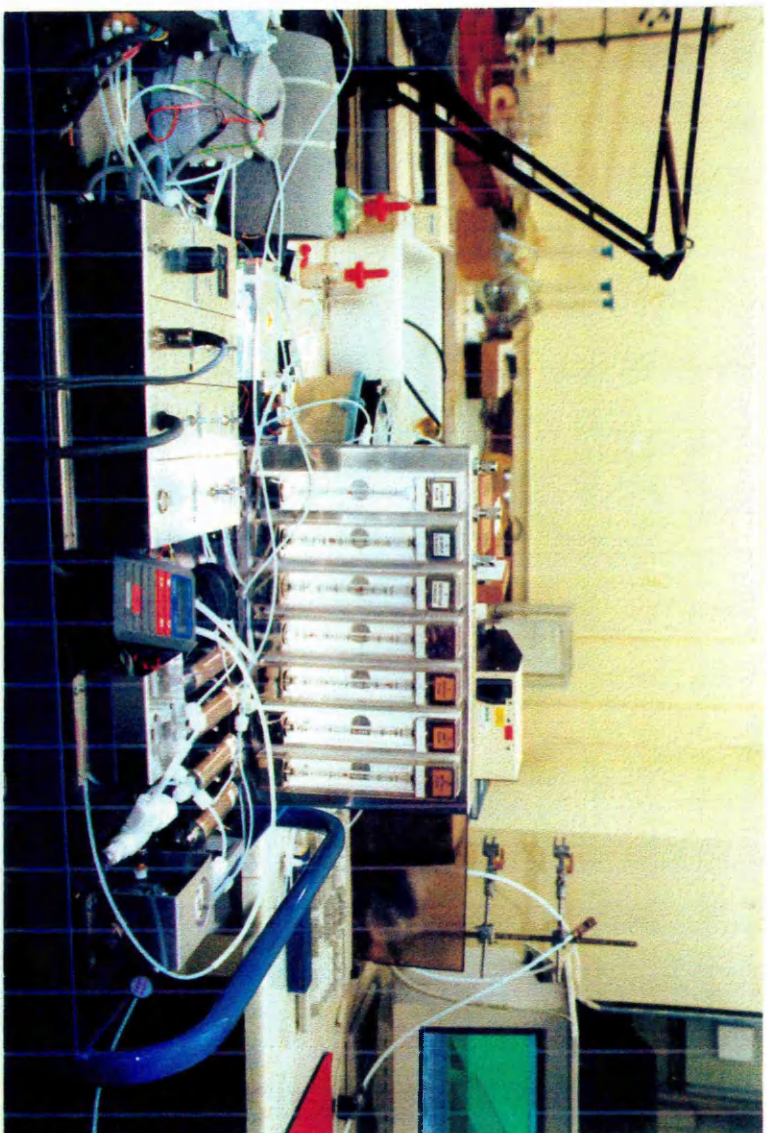
Plate 1: Ion mobility spectrometer breadboard

Electronic circuitry necessary for the control of various heaters, signal amplifiers, pumps, and the generation of electrical high tension and gating grid supplies was incorporated into a printed circuit board (pcb).

2.1.2.2 Generation of hydrazine, methylhydrazine, and 1,1-dimethylhydrazine vapours with varied percentage relative humidity levels

Standard Graseby Ionics vapour generators, model GI10, were used for the generation of the HZ, MMH, and UDMH atmospheres, however they were modified to incorporate nitrogen as the source gas.

Air used for the diluent gas was supplied from a compressor, at 100 psi, and passed through an air dryer unit (Balston model 75-20) for the provision of clean, dry compressed air to -70°C Pressure Dew Point. A humidifier assembly was connected into the generation system. This was constructed using a split air supply comprising dry and water saturated air lines, each with a needle valve control, which was recombined and connected to the diluent gas line of the vapour generators. Adjustment of the two air flows allowed the attainment of a range of relative humidity levels in the air used as the diluent gas. A flow-through humidity sensor cell, connected to a Protimeter Dew Point Meter Model DP383RK, was employed in line to enable a continuous check on humidity levels to be made.

Ptfe permeation tubes, containing the requisite materials, were used to generate low vpb concentrations of each of the hydrazines, individually.

2.1.2.3 The production of humidified ammonia and nitrogen dioxide gases

The production of vpm levels of ammonia and nitrogen dioxide was achieved with the use of sequential dilution apparatus. The dilution rigs were constructed using Chemcon flow meters with glass and ptfe components, including tubing, to connect the various flow meters. A humidifier system was incorporated into each of the dilution rigs, prior

to the final dilution stage, in order to provide humidified gas streams as required. The dilution was based on the principle of multiple dilution to the nth stage according to the equation$^{(204)}$:

$$c = 100X \ \{q_{a1}/(q_{a1}+q_{D1})\}\{q_{a2}/(q_{a2}+q_{D2})\}...\{q_{an}/(q_{an}+q_{Dn})\} \qquad 18$$

where,

c	= resultant concentration (per cent)
$q_{a1,2,...,n}$	= flow rate of contaminant 'a' at stage 1,2,...,n ($l.min^{-1}$)
$q_{D1,2,...,n}$	= flow rate of diluent gas at stage 1,2,...,n ($l.min^{-1}$)
X	= contaminant purity (mole fraction)

Ammonia was also generated from ammonium carbamate contained in a ptfe permeation tube, installed in a vapour generator, with the facility for humidified air, as described in section 2.1.3.

2.1.2.4 Ion mobility spectrometer breadboard dopant chemical vapour generation

Dopant chemicals were contained in small glass vials, either open for diffusion of the chemical (e.g. a mixed dopant and 5-nonanone), or closed with a polymeric membrane for vapour permeation of the chemical into the carrier gas. A silicone disc was also used on an additional 5-nonanone permeation source. All other sources had ptfe as the permeation membrane.

The dopant sources for each test material were installed into the dopant chemical chamber, to facilitate their introduction into the carrier gas.

The spectrometer breadboard components were cleaned and refurbished in order to produce a clean air RIP between each dopant trial. The following chemicals were evaluated for use as dopants: acetone, 5-nonanone, 4-methyl-2-pentanone, [ketones]; 3,5-heptanedione [a dione], 2,2,6,6-tetramethyl-3,5-heptanedione [a methyl substituted

dione]; 2,2,6,6-tetramethyl-3,5-heptanedione with 4-dimethylaminobenzaldehyde [a methyl substituted dione with an aromatic aldehyde as a mixed dopant]; and diisopropyl methane phosphonate [a phosphonate].

For the initial dopant trials, the instrument was configured with the high temperature detector cell (HITIMS), and a direct inlet system. A membrane inlet was utilised during the 3,5-heptanedione trials, and also during the acetone trial with ammonia. Unidirectional flow was employed for the trials involving acetone, 5-nonanone, 3,5-heptanedione, 2,2,6,6-tetramethyl-3,5-heptanedione, and the 2,2,6,6-tetramethyl-3,5-heptanedione / 4-dimethylaminobenzaldehyde mixed dopant. A bi-directional flow system was used when performing preliminary studies with acetone, 5-nonanone, and during a detailed study using 4-methyl-2-pentanone as the dopant.

2.1.2.5 Determination of hydrazine, methylhydrazine, and 1,1-dimethylhydrazine vapour concentrations

Sampling pumps capable of producing a stable through-put at a low flow rate were necessary to ensure precision in sampling, as low flow rates were involved. Sampling of individually generated atmospheres of the hydrazines was achieved using a single low flow adjustment holder connected to an SKC Universal Flow Sample Pump, Model PC224-EX7. The sampling medium of acetone containing 1 μl.ml^{-1} of acetic acid, and 0.5 μl.l^{-1} of 2-picoline as internal standard was contained in a standard micro-impinger (SKC Inc) submerged in a salt-water / ice bath, which was maintained at sub-zero temperatures by use of a cold plate (Aldrich Stirkool model SK12). The derivatized samples were analysed using a gas chromatograph (Perkin-Elmer AutoSystem) employing a nitrogen / phosphorus detector, and using helium carrier gas (at 15 psi inlet pressure) through a 25 metre, quartz coated capillary column with a 0.25 μm slightly polar stationary phase, designed for low bleed (SGE catalogue reference 25QC2/BPX5).

The injector and detector temperatures were 240 and 150°C respectively. The oven temperature was set at 40°C for the determination of UDMH, and 65°C for HZ and MMH. The expected accuracy and precision figures for the analytical method were ±10%.

The quantification of vapour source concentrations required information on the temperature and barometric pressure at the place and time of sampling. Temperatures were measured with a type K thermocouple connected to a digital thermometer (CP Instruments model PI 8013). Barometric pressures were measured with a digital barometer (Prosser Weathertrend).

2.1.2.6 Determination of ammonia and nitrogen dioxide gas concentrations

The concentration of ammonia gas was determined with the use of detector tubes, type Dräger 2/a, range 2 to 30 vpm. The reaction of ammonia with an acid to form an ammonium salt, was indicated by the colour change of bromophenol blue, from yellow to blue. This method was sufficiently accurate to determine the low vpm levels necessary for the initial qualitative work, involving ammonia as a potential interferent in the detection of hydrazines by IMS. The resultant concentrations from the dilution rig were typically twice the theoretical amounts, calculated from equation 18, probably due to memory effects, so the diluent flows were adjusted to provide the required vapour concentrations.

Detector tubes, type Dräger 0.5/c, range 0.5 to 25 vpm, were used to determine nitrogen dioxide levels, indicated by reaction of [pale grey] N,N-diphenylbenzidine to form a bluish grey product.

The manufacturer quoted the RSD for the detector tubes as 15% at the lower end of the range, and 10% at the higher range of each type of tube, and these statistics were accepted without verification.

The humidity of the two gas streams was measured with a humidity meter (Solexpress model 5065).

2.1.2.7 Experimentation using the ion mobility spectrometer breadboard

Once a stable RIP had formed, the ion mobility detector was exposed to generated vpb concentrations of the hydrazines, and vpm levels of ammonia and nitrogen dioxide, in turn, and the resultant spectra were recorded (see section 2.1.2.8).

2.1.2.8 Acquisition of ion mobility data

Ion mobility spectra were collected using digital signal averaging via an Advanced Signal Processor (ASP) interface board, installed into an IBM-AT compatible computer (Carrera 486 DX 33 MT), and processed using the corresponding Waveform Analysis Software Package (WASP). Parameters selected with the ASP software included the number of scans per spectrum, 256, and the number of sample data points per spectrum, 512.

2.1.2.9 Molecular modelling

Optimum geometric configurations of the molecular models of neutral molecules and ion-molecules, involving the hydrazines and ketones, were calculated using HyperChem™ release 4.5 software with the following set of parameters for semi-empirical calculations. PM3 calculations were performed using the Polak-Ribiere optimiser algorithm, in vacuo, with accelerated convergence and a convergence limit of 0.1, an RMS gradient of 0.01 $kcal.\text{Å}^{-1}.mol^{-1}$ and unrestricted Hartree Fock (UHF) calculations.

2.1.2.10 Determination of purity of ketones and hydrazines for IMS-MS-MS studies

All of the ketones and hydrazines were screened by GC-FID for qualitative purposes. The chromatographic conditions were: initial temperature 35°C; final temperature,

250°C; initial time, 5 minutes; temperature program rate, 8°C.min^{-1}; injection temperature, 250°C and FID temperature, 275°C. The conditions for the recording integrator were: peak width, 0.4; threshold, 5; area reject, 1x10^5; and attenuation, 2^6; quantitative determinations were made using integrated areas under peaks. 0.5 to 1 μl of neat liquid ketone was injected using split injection. The hydrazines were added to acetone prior to chromatographic analysis.

Principal and minor components of the reagents were also screened by GC-MS to confirm their identities and to determine the identity of impurities that might have caused inteference in the IMS-MS-MS studies. A Hewlett-Packard (HP) Model 5890 gas chromatograph was equipped with a 25 m capillary column with slightly polar phase (5% phenyl, 95% methylpolysiloxane). Conditions for analysis were: injector temperature, 250°C; column temperature, 35 to 250°C at 8°C.min^{-1}; an HP5971 mass selective detector was employed. The MS conditions were: start scan 3 minutes; stop scan 8 minutes; scan rate 1.5 scans.s^{-1}; threshold 150.

Two approaches to acquiring mass spectra were used in order to obtain high quality spectra both for major and minor components of the chemicals. In the first method, neat liquid was injected under split conditions; in order to avoid sample overload, the mass spectrometer filament was switched off during the elution of the principal component, always the ketone of interest. In a second screening, 6 to 10 μl of ketone was diluted into 200 μl of n-tetradecane, generally, or in the instance of 6-undecanone, n-hexadecane. Under these conditions, high intensity spectra were obtained for the principal components, without overloading the mass spectrometer.

2.1.2.11 IMS-MS-MS instrumentation

A TAGA 6000 tandem mass spectrometer (MS-MS) (Sciex Inc. Toronto, Ontario, Canada) was used in IMS-MS and collision induced dissociation (CID) studies to

determine the identity of ion clusters created in the IMS. The MS-MS was operated under standard conditions with the exception that the corona discharge source was replaced with a CAM drift tube. The end of the drift tube was an insulator which was placed against the plate used for corona discharges; the last conducting ring in the drift region was placed at 1400 V and was 1 cm from this plate (at + 650 V). A photograph of the equipment is shown on Plate 2. The ion mobility spectrometer was at ambient temperature, and the ion shutter was opened fully at all times during the experiment in order to provide an improved ion yield to the mass spectrometer. The latter was achieved by providing an electrical short to the one of the two sets of parallel wires, thereby maintaining a constant and equivalent voltage to both sets of wires, the gate open configuration. This process allowed the continually scanning triple quadrupole mass spectrometer to be used to collect data from the ion mobility spectrometer, which would not have been possible if the ion mobility spectrometer had been used in the normal pulsed mode. The IMS-MS-MS was used only for identification of ions created in the IMS under conditions similar to those in the hand-held units. In MS-MS studies, an ion was selected in the first quadrupole, injected into an argon gas curtain in a second quadrupole at 2×10^{-5} Torr, and the product ions were analysed in the third quadrupole. Mass axis calibration was nominally good for one mass but, because of the age of the quadrupoles (c. 1981), the mass calibration was only calibrated to within ± 3 amu. Consequently, MS-MS experiments were used extensively in assigning ion identities.

The IMS instruments employed in the laboratory had ketone vapours added intentionally to the gas flow before their return to either just the ion source region or both the ion source and the drift regions of the ion mobility spectrometer. Operating parameters for the IMS were established as a 10 mCi ^{63}Ni source; a 36 mm long drift region; drift gas flow, 200 ml.min^{-1}; field strength, 244 V.cm^{-1}; inlet sample flow, 0.5
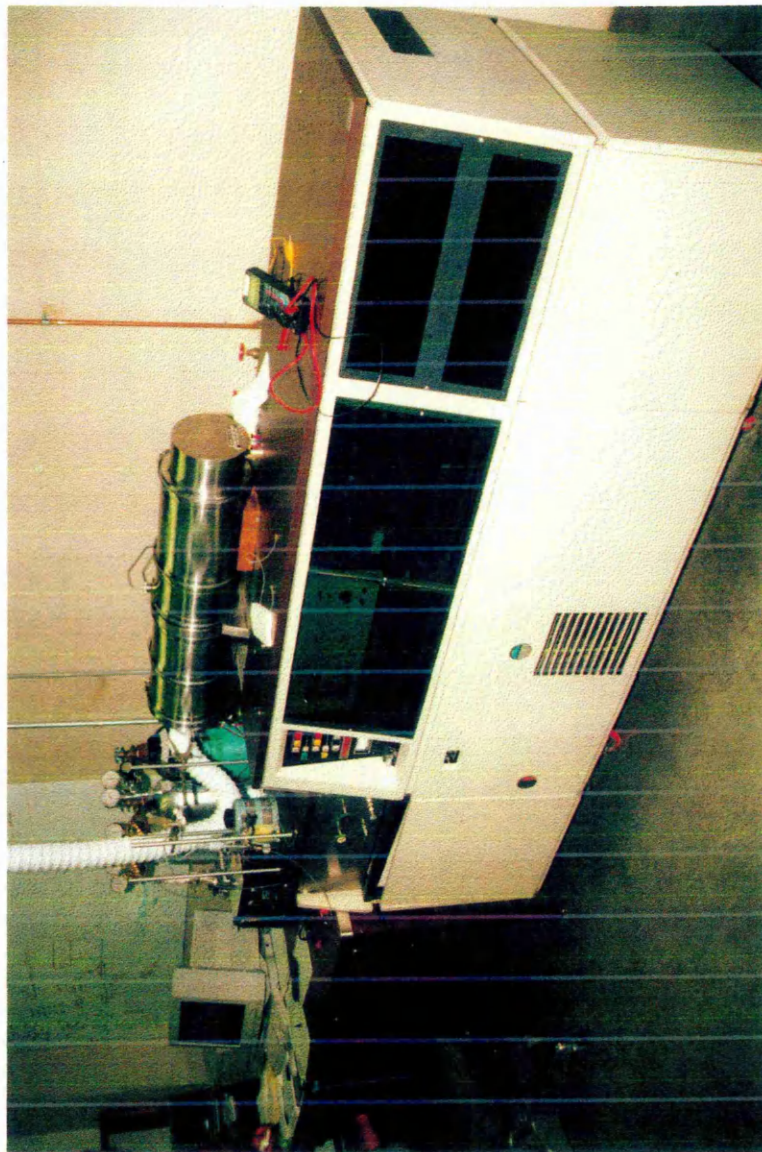
Plate: 2: TAGA 6000 IMS-MS-MS Instrumentation

l.min^{-1}; shutter pulse width, 180 μs; shutter repetition rate, 40 Hz; and drift tube temperature, ambient. The IMS was operated in positive polarity mode. The inlet nozzle allowed direct transfer of the analyte to the ion source region through a pinhole of diameter approaching 100 μm, and was maintained at approximately 40°C.

2.2   Experimentation

The following trials were performed in order to determine the most efficient combination of spectrometer operating parameters for the quantification of HZ, MMH, and UDMH without interference from ammonia, in the positive mode, simultaneously with nitrogen dioxide in the negative mode. Several factors affecting the IMS detection of these compounds were investigated. The experiments were designed for the comparison of sample inlet systems under their optimum conditions, detector cell construction materials, optimum detector operating temperature and pneumatic configurations, and ion-molecule chemistry. The effects of different ion-molecule chemistry regimes were investigated through experimental trials, molecular modelling, and IMS-MS-MS studies.

2.2.1   Detector cell construction material compatibility

The two cells were exposed to HZ, MMH, and UDMH, in turn. The nominal vapour concentrations were 15, 50, and 40 vpb respectively. The LOTIMS detector cell was also tested with ammonia, at about 10 vpm. (Ammonia was not available for testing when the high temperature detector was examined with the same dopant.) Each sample product ion peak amplitude was measured at its equilibrium response. Nitrogen dioxide was not tested.

In order to determine the suitability of the two basic cell construction materials, the two detectors were operated under comparable conditions to enable direct

comparison of their performance characteristics. The combination of low detector temperature and 5-nonanone dopant was used because previous research had shown that lower temperatures favoured a lower concentration limit of detection with the use of 5-nonanone[178] as dopant. The operating parameters are listed in Table 2.1.

Table 2.1 : Operating parameters for the ion mobility spectrometer breadboard

Operating parameter	Setting
Sample exhaust flow	190 ml.min^{-1}
Detector cell temperature	27°C
Detection mode	+ve
Source flow	85 ml.min^{-1}
Drift flow	105 ml.min^{-1}
Detector pneumatic configuration	Bi-directional
Dopant chemical	5-nonanone
Dopant carrier flow	100 ml.min^{-1}
Dopant flow split ratio	1:1
Dopant chamber temperature	23°C
Detector exhaust flow	400 ml.min^{-1}
Cell pressure differential	-16.4 mBar
Standby flow	115 ml.min^{-1}
Sample inlet system	Direct
Sample inlet flow rate	9.2 ml.min^{-1}
Sample relative humidity	50%

2.2.2 Detector operating temperature

The optimum operating temperature for an ion mobility detector should be high enough to prevent surface contamination from surface active chemicals but not high enough to cause decomposition of the analytes passing through the detector system. In order to determine the optimum detector cell temperature the high temperature detector was set

at different temperatures, over a given range (between 25°C and 170°C), in conjunction with individual dopants, as detailed in Table 2.2.

Table 2.2: Detector temperature test conditions

Detector temperature (°C)	Pneumatic configuration	Dopant chemical
105	Unidirectional	Acetone
87	Unidirectional	Acetone
66	Unidirectional	Acetone
178	Unidirectional	DIMP
152	Unidirectional	DIMP
102	Unidirectional	DIMP
58	Unidirectional	5-nonanone
57	Unidirectional	5-nonanone
35	Unidirectional	5-nonanone
31	Unidirectional	5-nonanone
51	Bi-directional	5-nonanone
38	Bi-directional	5-nonanone
25	Bi-directional	5-nonanone

DIMP = diisopropyl methane phosphonate

2.2.3 Pneumatics of a direct inlet system

The flow rate of a sample entering the detector cell has to be fast enough to provide sufficient sample for ionisation, and subsequent detection by the collector electrode. Flow rates through the direct inlet were set using a Chemcon RS1 Ruby flow meter, at roughly integer divisions from 1 to 4 scale units (approximately 5 to 20 ml.min^{-1}). The flow rate was optimised whilst employing an acetone doped ion mobility detector at a temperature of 66°C. The vapour sample streams were humidified to 45% relative humidity (RH), using distilled, de-ionised water. The effect of direct inlet flow rate upon sensitivity was investigated at different temperatures. Because direct inlet systems are more prone to the effects of humidity, c.f. *sample acquisition*, section 1.3.2, the

percentage RH was altered whilst observing the effect upon the spectra generated during experiments using UDMH at a set concentration.

2.2.4 Membrane operating temperature

The temperature of a semi-permeable membrane must be set to allow the maximum amount of sample through the membrane, without degradation of the sample through excessive heat, or condensation of the analyte on / in the membrane material through insufficient heat. The permeability of a membrane is affected by the properties of the membrane material, its thickness and surface area, solution and diffusion factors The optimum membrane temperature was determined during the assembly of the breadboard and commissioning with the membrane inlet system, by Graseby Dynamics Ltd.

2.2.5 Detector cell pneumatics configurations

The pneumatic configuration of an ion mobility detector can have considerable influence upon the sensitivity of the instrument. This is due to the efficiency of sample ingress through the ionisation region to the drift region, and the effectiveness of the counter flow of drift gas maintaining a relatively interferent-free environment. The measurement of all the analytes, the hydrazines and nitrogen dioxide, was investigated during a set of four tests, using combinations of 5-nonanone and 2,2,6,6-tetramethyl-3,5-heptanedione dopants, with the spectrometer breadboard configured for both unidirectional and bi-directional gas flows, as described in section 2.1.2.1.

2.2.6 Miniaturisation of the IMS breadboard for hand portable use

The optimum detector operating parameters were concluded from the results of the experimental work and were re-designed into a miniaturised, hand-portable ion mobility spectrometer.

2.2.7 Investigation into the effects of ion-molecule regimes

Following the test methods detailed in sections 2.2.3 and 2.2.4, in which the HZ, MMH, and UDMH concentrations were approximately 15, 50, and 40 vpb respectively, except for the 4-methyl-2-pentanone and diisopropyl methane phosphate trials, when the concentrations were roughly three to five times greater, the following parameters were measured from recorded spectra.

- **Detection levels.** Response was measured directly as the amplitude of the peak in mV.

- **Selectivity.** Due to the movement of peak times with change in temperature the RIP was assigned an arbitrary value of 100. The positions of sample (product ion) peaks were calculated as a ratio of measured peak times compared to the RIP (a normalisation process) in order to produce an indication of resolution comparative with 100.

- **Response and recovery characteristics.** The results of a visual examination of recorded contour spectra was listed for fast, medium, or slow response, and recovery times, in relative terms.

2.2.8 Molecular modelling

Models of the neutral molecules of HZ, MMH, UDMH, ammonia, and a series of symmetrical ketones were constructed. In order to examine the effects of steric hindrance straight chain and branched aliphatic ketones were considered. The ketones studied were acetone, 3-pentanone, 4-heptanone, 5-nonanone, 6-undecanone, 2,4-dimethyl-3-pentanone (diisopropyl ketone), 2,2,4,4-tetramethyl-3-pentanone (di-*t*-butyl ketone), 2,2,6,6-tetramethyl-4-heptanone (dineopentyl ketone), 2,6-dimethyl-4-heptanone (diisobutyl ketone), and 2,8-dimethyl-5-nonanone (diisopentyl ketone). Ion-molecules of the hydrazines and monomer and dimer ion-molecules of the ketones

were also constructed. The optimised molecules were used as building blocks to form protonated molecules of the hydrazines with either one or two molecules of each ketone in turn. These compiled ion-molecule clusters were also optimised. The longest diameter of each of the neutral molecules, ion-molecules, and ion-molecules clusters was measured, the total energy and the heat of formation of each optimised molecule / cluster were recorded.

2.2.9 IMS-MS-MS studies

Studies of the ion-molecule chemistry of an homologous series of ketones and the analytes, ammonia and the hydrazines (HZ, MMH, UDMH, and TMH), followed a common procedure. The analytes were introduced into a unidirectional flow IMS drift tube and ketone vapours were added either in the ionisation region only or at the detector end of the drift region (and thus throughout the drift tube). The vapours of the dopants and analytes were introduced into the gas stream by flowing air, at constant rates, across open vials containing the individual chemicals. Concentrations of the ketones were obtained from calculations based upon vapour pressures and gas flows. The IMS data were recorded as follows:

- A mass spectrometric scan of background ions i.e. those produced in clean air conditions, was recorded.

- A second scan was recorded when the analyte entered into the ion source of the IMS drift tube.

- A third scan was recorded when the analyte and one of the ketones was introduced to the ion source of the IMS drift tube, simultaneously. Ions with high intensity, created during these studies, were subjected to CID for MS-MS analysis. Product ion scans were recorded.

- A final scan of the analyte (introduced via the ion source region) with ketones introduced at the detector end of the drift region, was recorded. The high intensity ions created during these studies were also subjected to CID for MS-MS analysis. Again, product ion scans were recorded.

OPTIMISATION OF EQUIPMENT

3.1 Choice of detector cell

The choice between the detector cells was determined from consideration of the degree of sensitiveness and the response and recovery characteristics. The low temperature cell, with ptfe insulators, showed improved limits of detection for the detection of MMH and UDMH compared with the high temperature cell which had ceramic insulators. The recorded amplitudes for HZ detection were similar for both detector cells, at the concentration tested. Sample product ion peak amplitudes are recorded in Table 3.1; response and recovery characteristics are also recorded.

Table 3. 1: Results of sensitiveness, response and recovery, for two detector cells

Detector cell	Sample material	Product ion peak amplitude (mV)	Response time (s) (Initial, 90%, 100%)	Recovery time (s) (90%, 100%)	Normalised peak position (RIP = 100)
HITIMS	HZ	22	6, 44, 56	-	131
LOTIMS	HZ	17	12, 38, 100	12, 12	129
HITIMS	MMH	57	30, 42, 66	12, 12	108
LOTIMS	MMH	124	22, 86, 110	38, 70	107
HITIMS	UDMH	295	12, 18, 30	62, 62	84
LOTIMS	UDMH	825	20, 58, 126	74, 216	83
LOTIMS	Ammonia	373	24, 228, 282	>>4 hr.	129

The results indicated that the responses were generally slightly slower with the LOTIMS cell configuration, and the recovery times were significantly longer; the UDMH product peak took several minutes to clear down (see Figures 3.1 and 3.2).
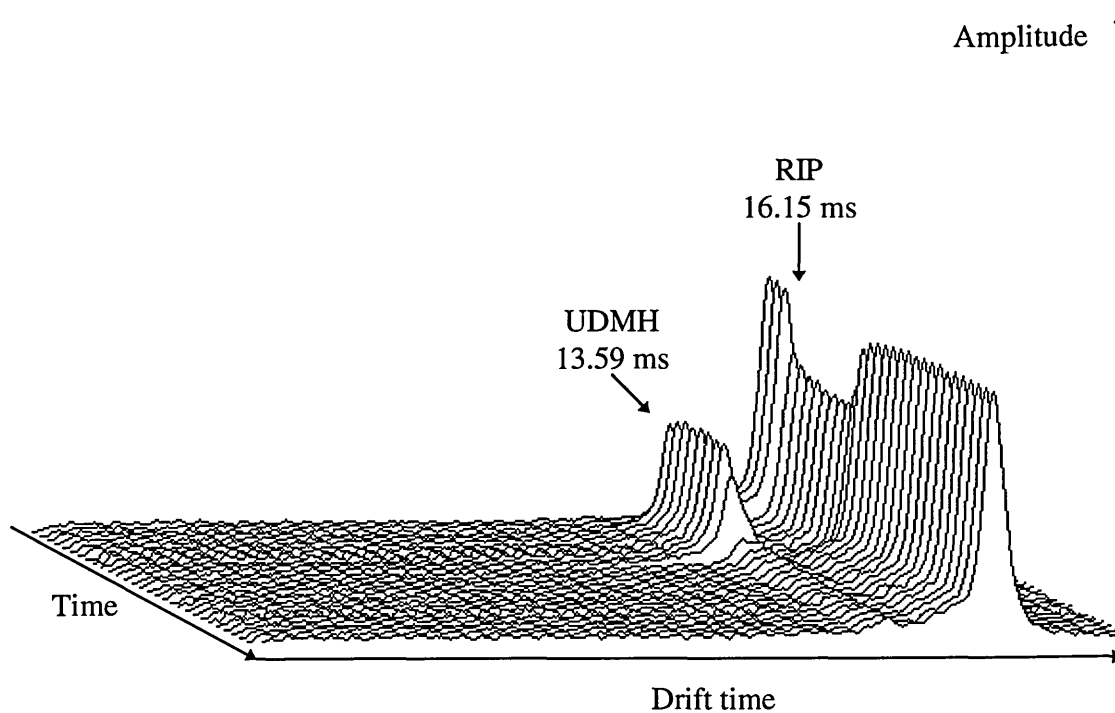
Figure 3.1: High temperature cell response and recovery characteristics to UDMH exposure, 25°C, 5-nonanone doped system
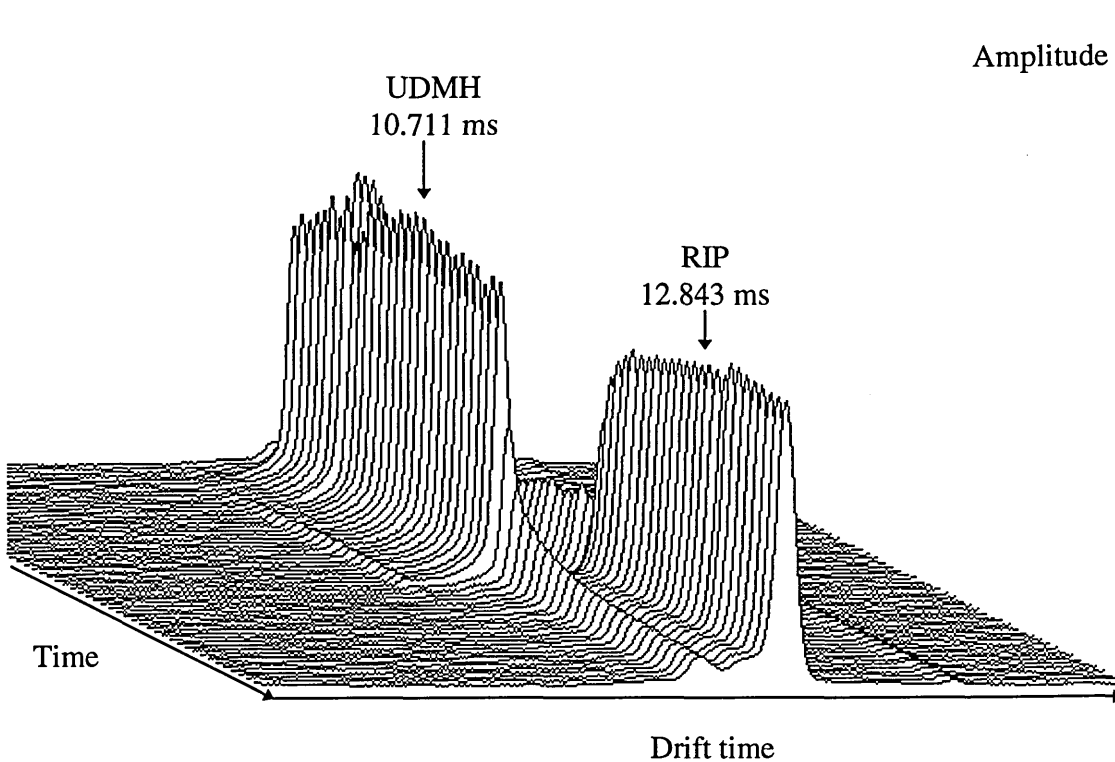
Figure 3.2: Low temperature cell response and recovery characteristics to UDMH exposure, 27°C, 5-nonanone doped system

The LOTIMS detector cell was also tested with ammonia, at about 10 vpm. The detector was very slow to respond to ammonia and even slower to recover; full recovery took several hours.

An indication of the slow recovery time can be perceived from the almost stable ammonia peak recorded during the recovery period, shown in Figure 3.3, when equated with the comparatively fast response and recovery times of the detectors as shown, for exposure to UDMH, in Figures 3.1 and 3.2.
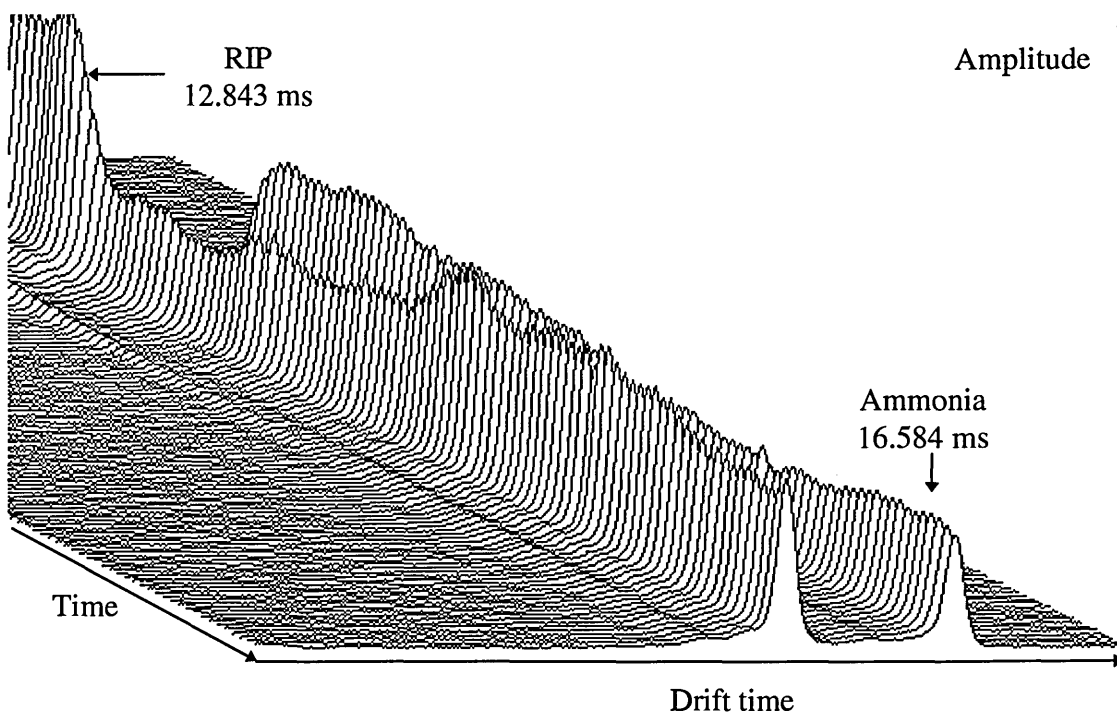
Figure 3.3: Low temperature cell recovery characteristics to ammonia exposure, 27°C, 5-nonanone doped system

At this point it was realised that there was a problem, not only with the detector materials, but also with the design of the cell, which allowed the mixing of the gas flows near the grid area where there were more metal surfaces. This appeared to cause problems with hang-up of the sample materials on the cell walls. As a result, the inlet system was redesigned.

For the low temperature detector cell, the slight increase in detection levels at low part per billion concentrations was offset against the increased response and recovery times. The time taken for the UDMH product ion peak to recover was relatively long. The time taken for the detector to recover from ammonia was unacceptably long, with several hours having elapsed before the detector was cleared of ammonia. The long recovery time meant that this detector could not be considered a viable proposition for near real-time analysis.

An overriding concern was a report issued by Graseby Ionics[205] which detailed the effect of long term storage of IMS detectors assembled for the detection of organic compounds. The report detailed degradation of the negative mode RIP, which was considered to be due to radiolysis of the cell's front end plastic components i.e. those in proximity to the radioactive source. The use of the lower temperature cell would not be advisable, in the long term, without design modifications with respect to the construction materials used.

Overall the high temperature cell appeared to be the more acceptable detector for the simultaneous detection of the hydrazines and ammonia.

3.2 Optimum detector temperature

The detector was heated to various temperatures and exposed to the hydrazines' vapours, ammonia, and nitrogen dioxide, to enable the optimum detector operating temperature to be determined. Assuming that the optimum temperature with one dopant in the system might not be the same as that observed with an alternative dopant, this trial was carried out with three different dopant chemicals in the gas streams, each tested during separate experiments.

Previous research[101] showed that the use of acetone as the dopant chemical in an ion mobility detection system produced insufficient resolution of the reactant and

product ion peaks of interest. However, an acetone based system provided a greater operational stability than water based ion-molecule chemistry, sufficient to enable a comparative evaluation of the two types of inlet system to be performed. Trends in sensitiveness were investigated at different temperatures combined with the use of a variety of dopants, namely, acetone, diisopropyl methane phosphonate, and 5-nonanone. The effect of temperature on mobility was also investigated, by comparing peak relative positions, with the RIP assigned an arbitrary value of 100.

The acetone doped system showed increased detectability of HZ and MMH as the temperature decreased (see Figure 3.4) i.e. the detector was more sensitive to HZ than to MMH. Figures 3.5 to 3.7 show the effect of temperature on the detection of HZ.

Response and recovery times were acceptable for the hydrazines. The nitrogen dioxide response decreased slightly with decrease in temperature, but the response and recovery times were rapid at all three temperatures tested (for an example, see Figure 3.8). UDMH and ammonia were not studied with the acetone doped system as they were not available at the time of this set of experiments.
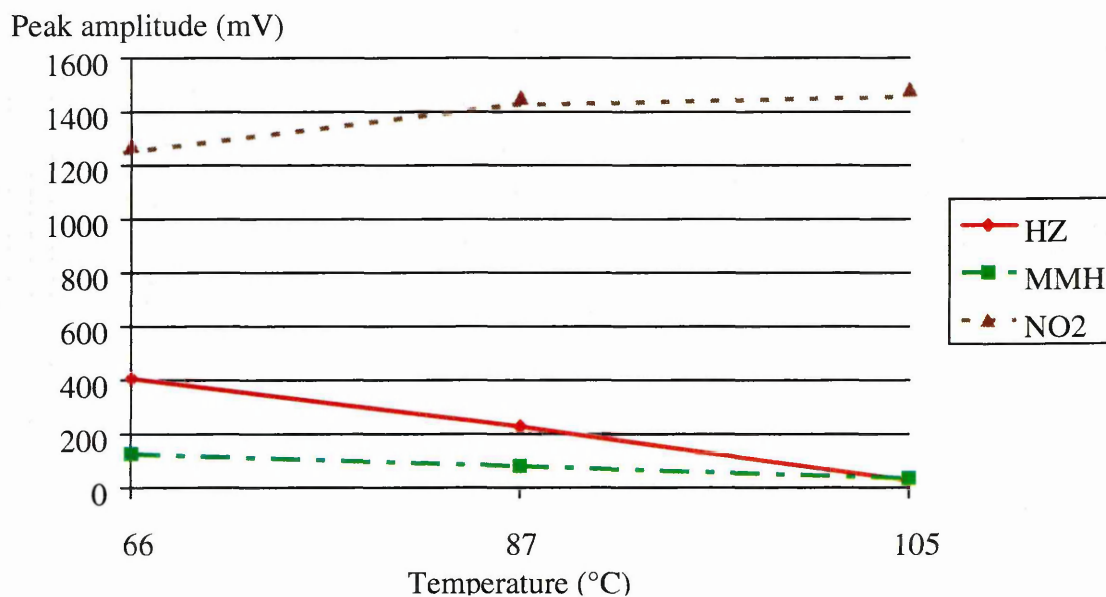
Peak amplitude (mV)

Figure 3.4: The effect of detector temperature on peak amplitude, acetone doped system
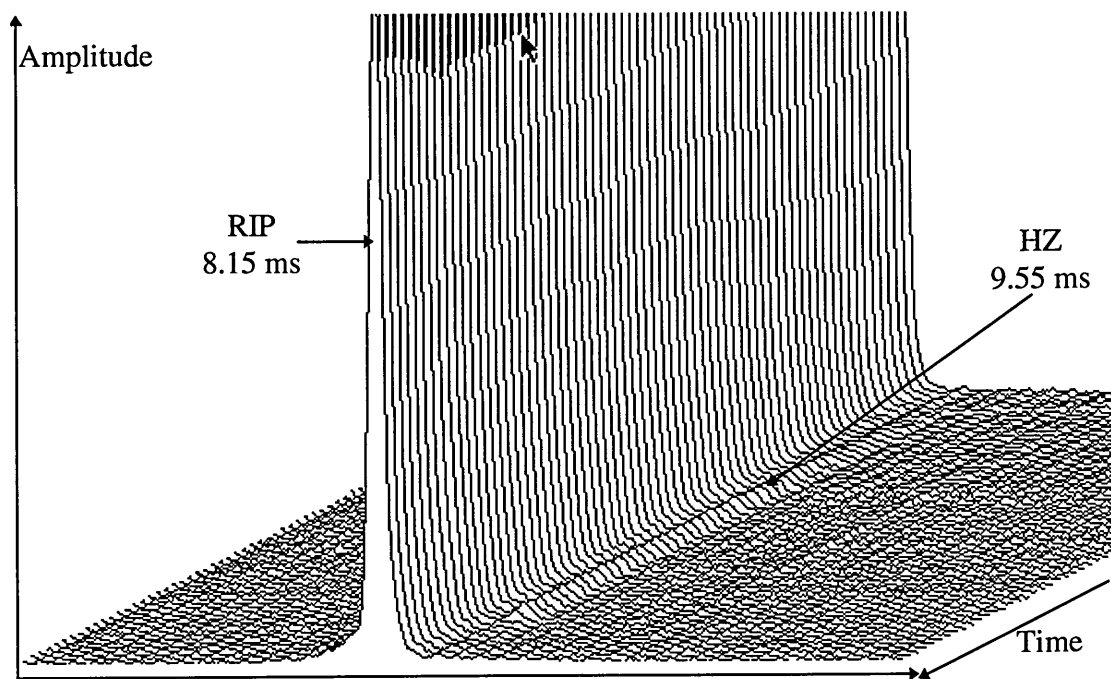
Figure 3.5: High temperature cell response and recovery characteristics to HZ exposure, at 105°C, acetone doped system
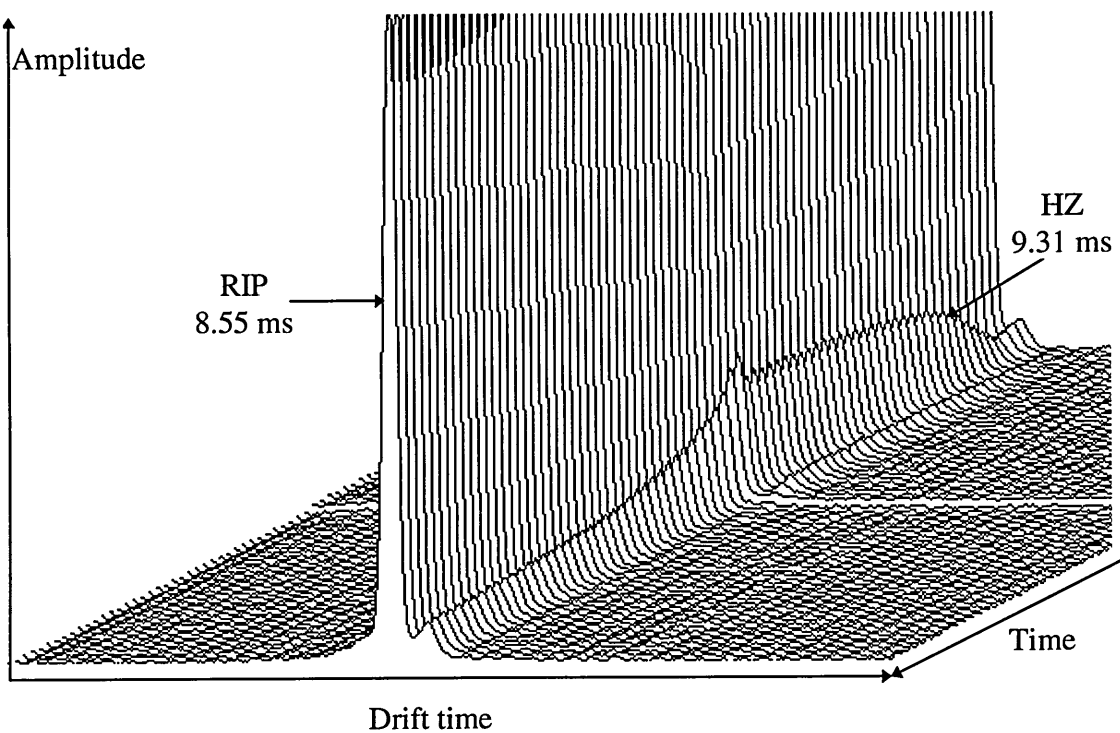
Figure 3.6: High temperature cell response and recovery characteristics to HZ exposure, at 87°C, acetone doped system
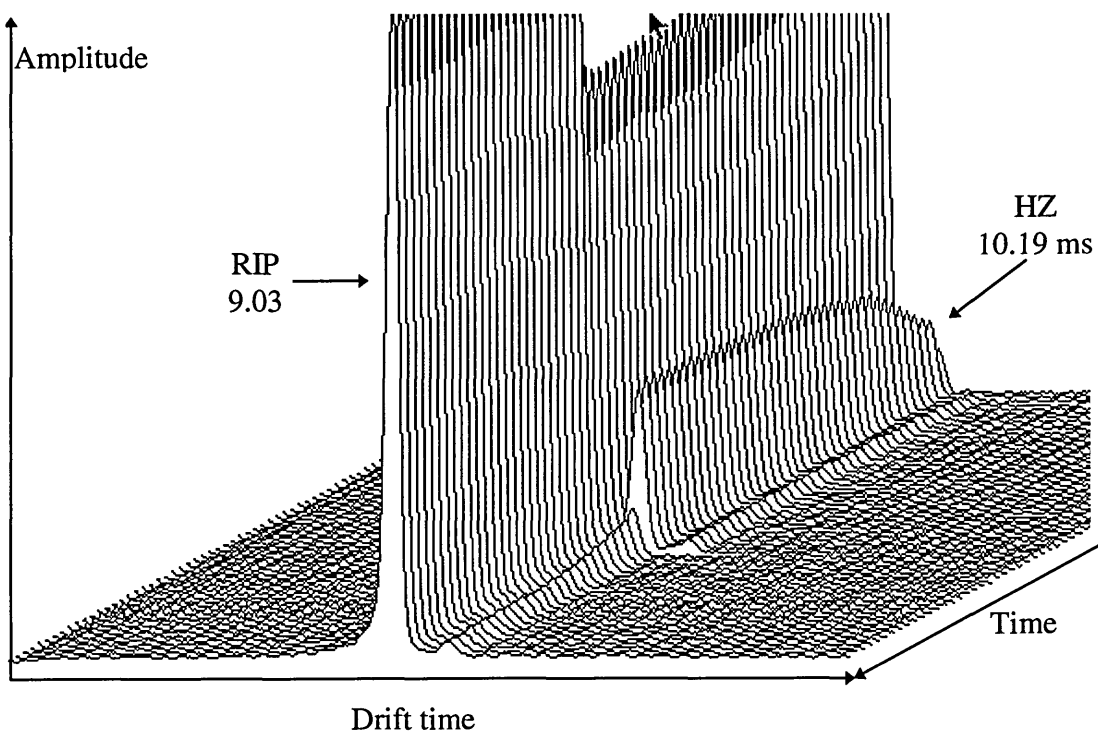
Figure 3.7: High temperature cell response and recovery characteristics to HZ exposure, at 66°C, acetone doped system
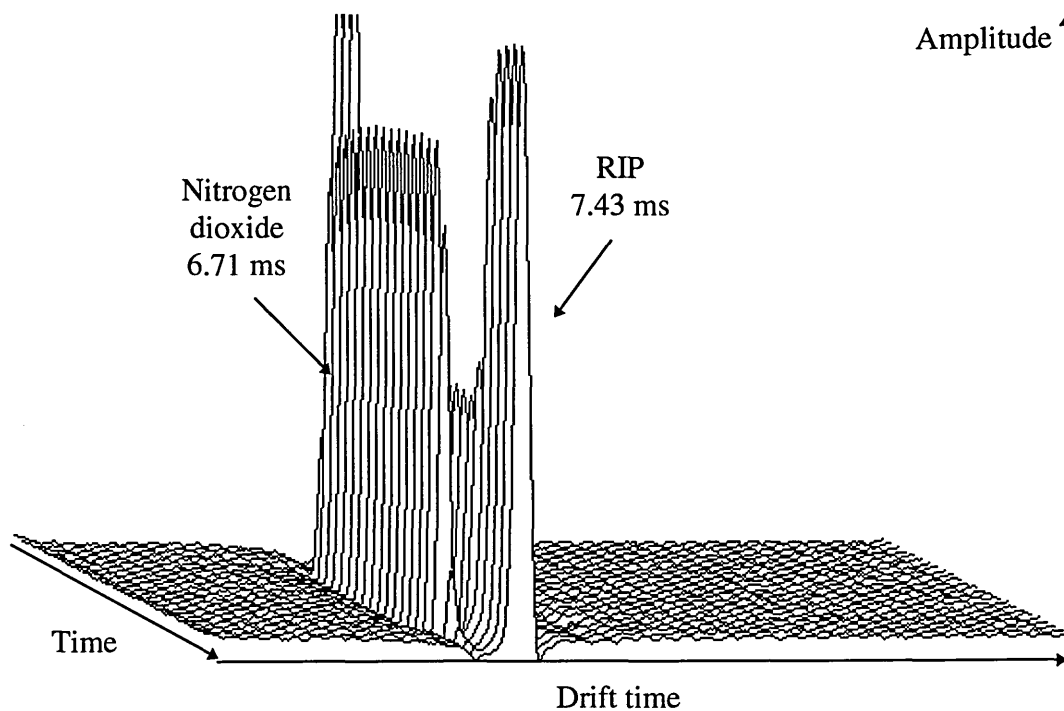
Figure 3.8: High temperature cell response and recovery characteristics to nitrogen dioxide exposure, at 65°C, acetone doped system

HZ produced two product ion peaks. Generally, mobility decreased with decrease in temperature i.e. the peaks shifted to the right. The results in Table 3.2 are based on normalised peak times, using 100 as the reference value for the RIP; the major product ion peak in each case is the peak used for the calculation of relative positions. The trend in results for MMH was as expected; the increase in temperature increased the speed of the samples to produce faster transportation times. However, an unexplained result was the lower mobility of HZ at 105°C, compared to 87°C, this result being atypical of the trends observed for the other analytes.

Table 3.2: The effect of detector temperature on peak resolution; acetone doped system

Detector temperature (°C)	Sample material	Sample RIP time (ms)	Sample peak time (ms)	Normalised peak position (RIP = 100)
105	HZ	8.15	9.55	117
87	HZ	8.55	9.31	109
66	HZ	9.03	10.19	113
105	MMH	8.15	6.83	84
87	MMH	8.47	9.15	108
66	MMH	9.03	10.15	112
105	Nitrogen dioxide	6.59	5.75	87
87	Nitrogen dioxide	6.91	6.07	88
66	Nitrogen dioxide	7.43	6.71	90

For the preliminary work using diisopropyl methane phosphonate dopant, while using a direct inlet system and unidirectional detector flow configuration, no response was obtained for the hydrazines at the temperatures investigated (see Table 3.3). The result for ammonia was increased peak amplitude with decrease in temperature. A single product ion peak was recorded at 102°C and two product ion peaks were visible in the spectrum recorded at 58°C (see Figures 3.9 and 3.10).

Table 3.3: The effect of detector temperature on peak amplitude; high temperature cell, diisopropyl methane phosphonate doped system

Detector temperature (°C)	Peak amplitude (mV)				
	HZ	MMH	UDMH	Ammonia	Nitrogen Dioxide
178	No response	No response	No response	No response	50
152	No response	No response	No response	No response	438
102	No response	No response	No response	54	1512
58	No response	No response	No response	180	1341
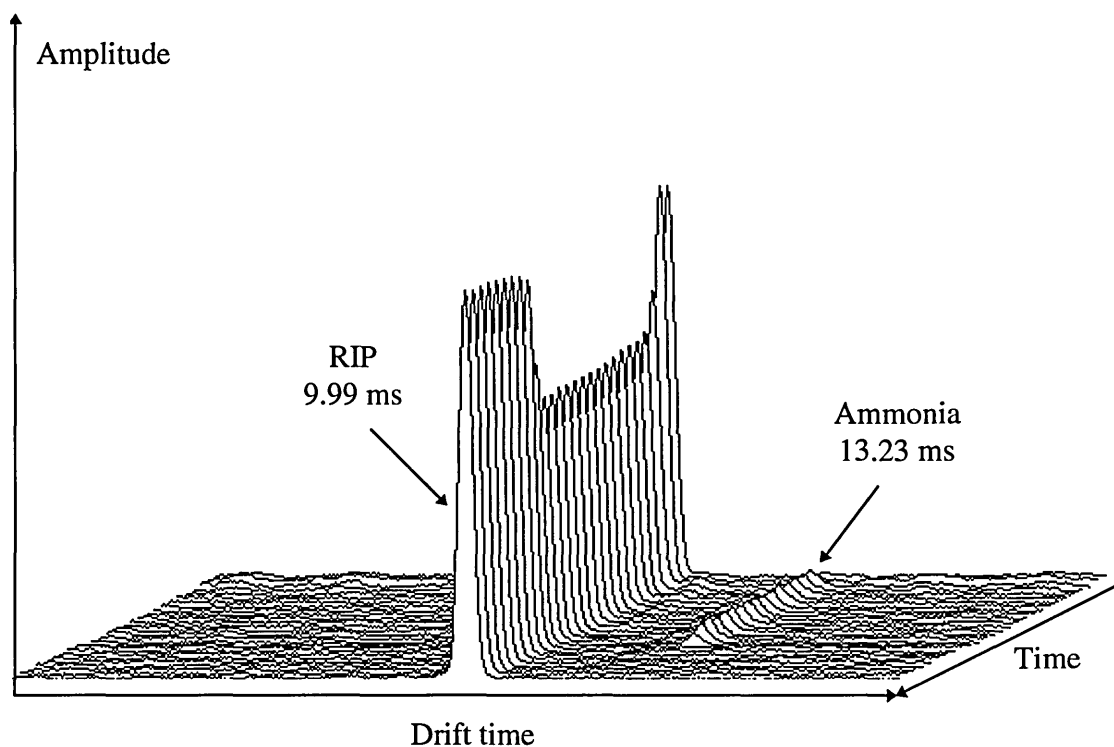
Figure 3.9: High temperature cell response and recovery characteristics to ammonia exposure, at 102°C, diisopropyl methane phosphonate doped system

For nitrogen dioxide detection the temperature went through an optimum stage at about 100°C (see Table 3.3). The difference in response obtained from that at 152°C was marked, but the decrease in peak amplitude from 102 to 58°C was less significant. At 58 °C the nitrogen dioxide product ion peak was resolved from the RIP. (See Table 3.4 for summary of results.)
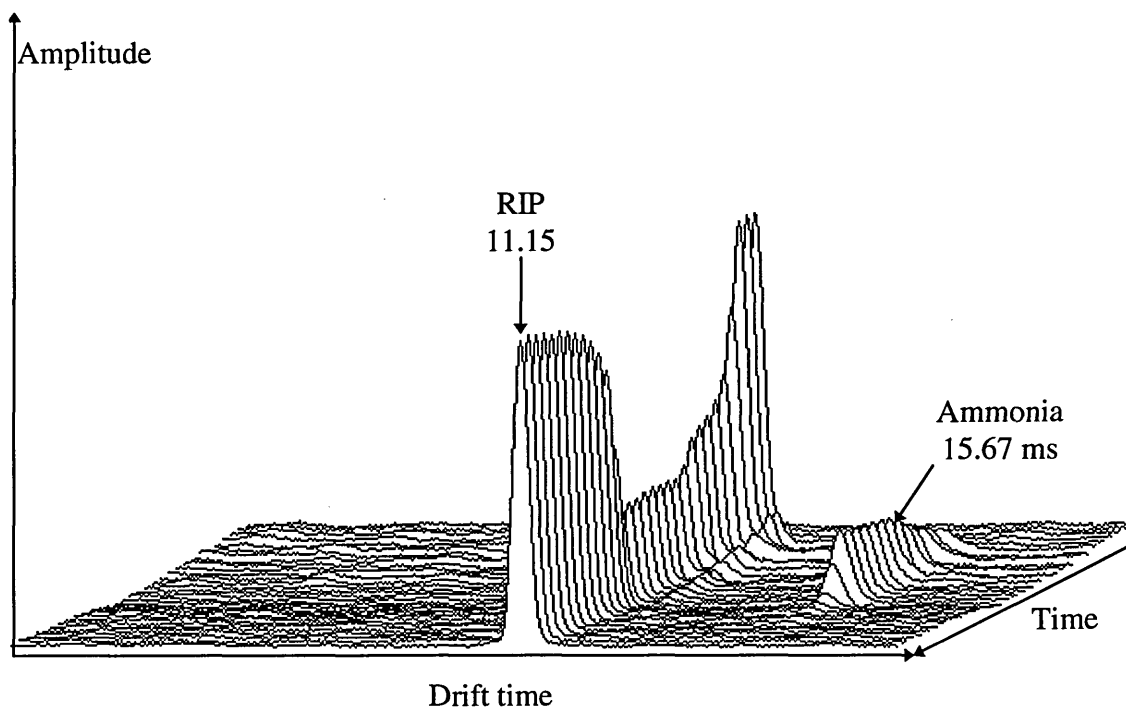
Figure 3.10: High temperature cell response and recovery characteristics to ammonia exposure, at 58°C, diisopropyl methane phosphonate doped system

Table 3.4: The effect of detector temperature on peak resolution; diisopropyl methane phosphonate doped system

Detector temperature (°C)	Sample material	Sample RIP time (ms)	Sample peak time (ms)	Normalised peak position (RIP = 100)
178	Ammonia	8.67	No response	-
152	Ammonia	9.07	No response	-
102	Ammonia	9.99	13.23	132
58	Ammonia	11.15	15.67	141
178	Nitrogen dioxide	5.51	3.43	62
152	Nitrogen dioxide	5.79	3.71	64
102	Nitrogen dioxide	6.47	4.83	75
58	Nitrogen dioxide	6.27*	5.71	91

* This normalised peak position for the nitrogen dioxide product ion peak was based upon the background RIP time, due to saturation of the detector with the sample.

The normalised peak position for the nitrogen dioxide product ion peak (Table 3.4), is based upon the background RIP time, due to saturation of the detector with the sample.

At 58°C an unresolved doublet RIP was evident in the negative mode, which was deemed to be impractical for peak searching routines.

Comparisons of the effects of temperature on peak amplitude, resolution, response and recovery, using 5-nonanone as the dopant chemical, were carried out using the ion mobility spectrometer breadboard in both the unidirectional and bi-directional flow configurations. Typically, with the spectrometer set for either pneumatic configuration, the detection ability of the high temperature detector to hydrazines increased with decrease in temperature (see Figure 3.11), although in the unidirectional configuration the response to UDMH appeared to improve with increased temperature. The results may have been affected by the formation of two product ion peaks (see Figure 3.12).
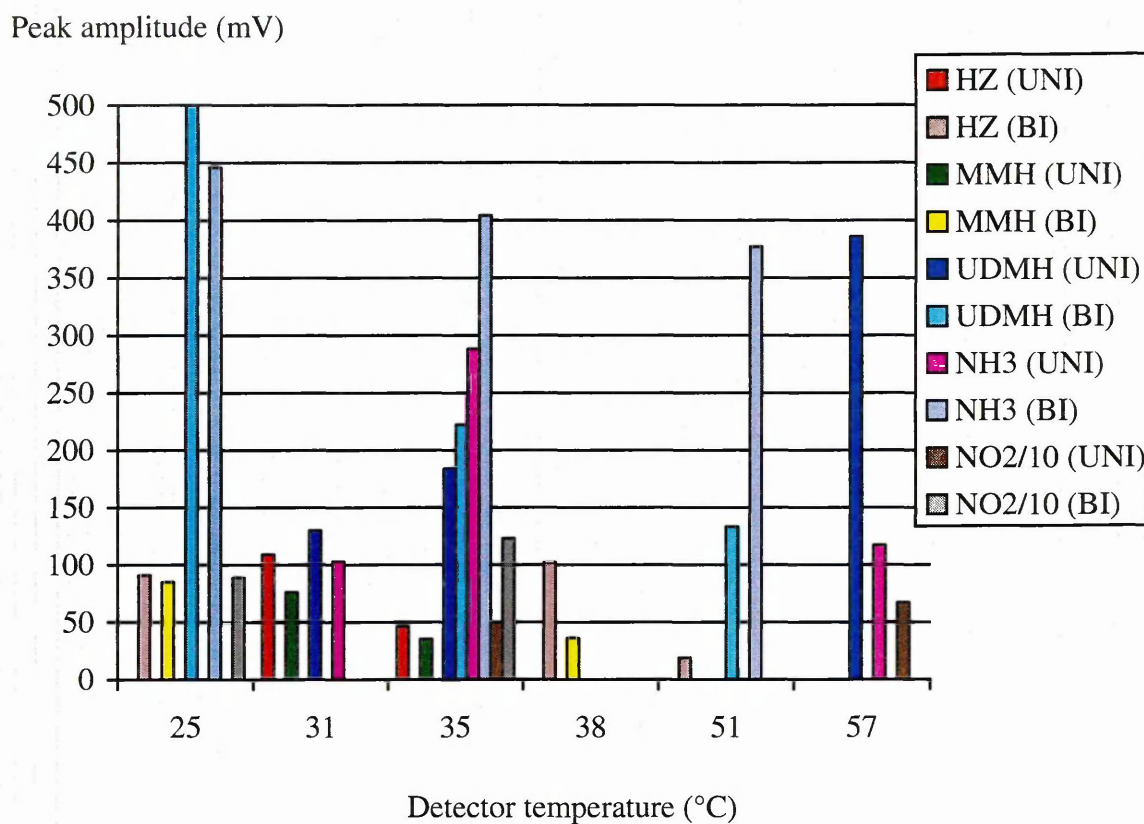
Figure 3.11: The effects of detector temperature on peak amplitude; 5-nonanone doped systems
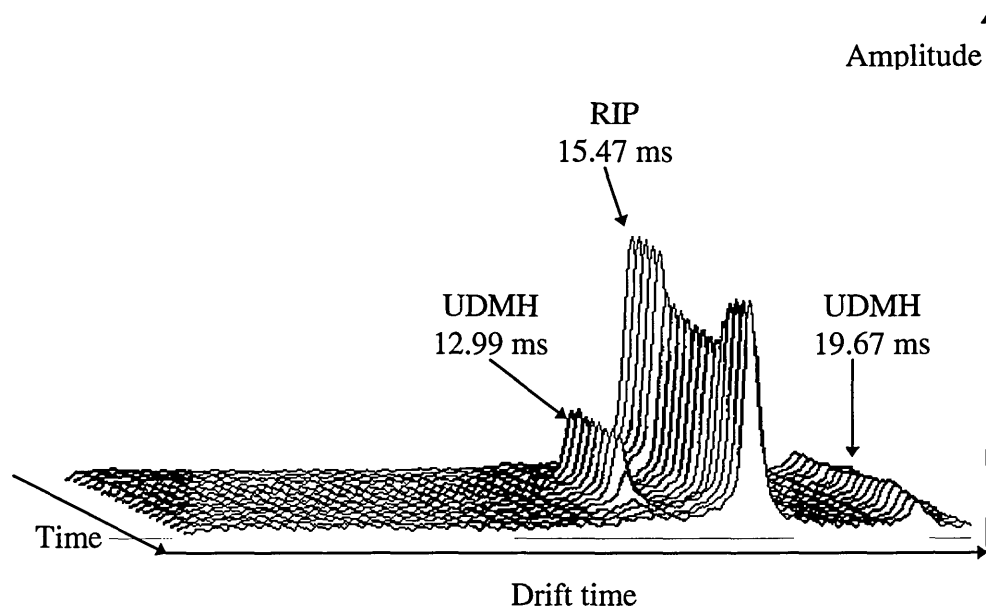
Figure 3.12: High temperature cell response and recovery characteristics to UDMH exposure, at 35°C, 5-nonanone doped system

However, two product ion peaks were formed for UDMH with the instrument configured for either of the pneumatic flow systems, for MMH in the bi-directional system and ammonia in the unidirectional system. The addition of the two peak amplitudes in the relevant spectra confirmed the observed trends; the detection of UDMH in the unidirectional flow configuration was the only result to show an increase in peak amplitude with increase in temperature. As stated previously, UDMH could not be tested with the ammonia doped system, at the same time as the temperature effects on the other analytes were tested. Also, none of the hydrazines were detected with the diisopropyl methane phosphate doped system. Therefore, it is unclear whether this observation would be repeated with alternative ion-molecule chemistry. The results for ammonia, with the instrument in the unidirectional configuration, were ambiguous due to the formation of multiple, unresolved peaks, but the indications were that ammonia detection increased with decrease in temperature for the bi-directional system.

The conclusions drawn from this set of experiments were that lower detector temperature favoured increased sensitivity to the hydrazines and ammonia, independent of both the dopant chemical used to effect ion-molecule regimes and, in general, detector flow configuration. For nitrogen dioxide, the peak amplitude increased slightly with increase in temperature below ~100°C. Above this temperature the detection level decreased rapidly.

Although for the detection of the hydrazines and ammonia, the lower operating temperature produced greater sensitivity, consideration must be given to the miniaturisation of the spectrometer. The limit on how low the temperature of the detector may be operated is dependent upon the ambient conditions. For effective operation in warmer temperatures e.g. ~30°C, maintaining the detector temperature would require the use of cooling circuitry, which is expensive, and might lead to increased weight and bulk; not acceptable for an instrument designed ultimately to be hand-held. The most convenient low temperature limit would be in the region of 50°C. This would allow a reasonable compromise for the simultaneous detection of the hydrazines, ammonia, and nitrogen dioxide without the need for bulky, heavy equipment.

3.3 Optimum flow for the direct inlet

The flow through the direct inlet system was altered by changing the detector exhaust flow setting. Allowing a faster or slower exhaust flow facilitated a respective change in the inlet flow rate. An increase in the inlet flow rate increased the amount of sample per unit time that entered the detector, and also the amount of water vapour. In theory, the former may lead to an increase in response but this may be offset by the humidity effect (i.e. increase in humidity may reduce detection capability). Very high flow rates may

affect the flow patterns around the grid area and might even lead to water vapour entering the drift region.

Although a direct inlet system would be easier to maintain, the increase in water vapour content of the sample stream leads to larger ion clusters, loss of resolution and reduced sensitivity. High concentrations of samples can produce both dimer and trimer ion peaks which can reduce the linear range and produce more complex ion mobility spectra[150]. The added complication of the effect of humidity can aggravate the situation further.

The flow rate of the direct inlet system was varied to determine the effect of inlet flow rate upon the detector sensitivity and peak resolution. Using an acetone doped ion mobility cell at 66°C, the optimum flow rate appeared to vary according to the contaminant being monitored (see Figure 3.13).

Peak amplitude (mV)

Direct inlet flow meter setting
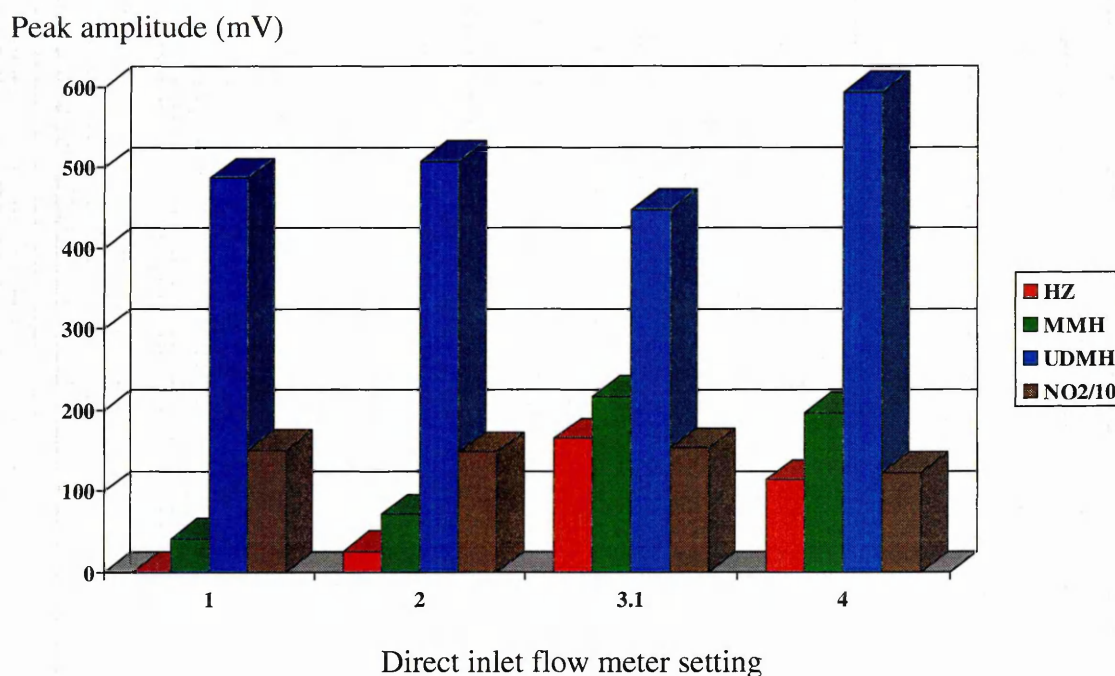
Figure 3.13: The effect of direct inlet flow rate on peak amplitude; acetone doped system

The fastest of the flow rates was required for UDMH, at 4 scale units, and the slowest for HZ, at 2 scale units (HZ was not detected whilst the inlet flow setting was at 1 scale unit). The optimum flow setting for both MMH and nitrogen dioxide was approximately 3 scale units. There were negative peaks (i.e. peaks which dipped below the baseline) observed in the negative mode spectra during the detection of nitrogen dioxide. These peaks were due to the signal processing electronic gain controls and the problem has since been rectified.

The effect upon UDMH and nitrogen dioxide appeared to be less significant than for HZ and MMH. The response and recovery times for all of the test vapours were fast, typically less than 12 seconds for both response and recovery. Ammonia was not available for testing at this time, due to delays from the supplier. Overall, the optimum setting was deemed to be 3 scale units, equivalent to approximately 15 ml.min^{-1}.

Table 3.5: Peak times and normalised peak position at various direct inlet flow settings, acetone doped high temperature cell, 66°C

Inlet flow setting	Material	Sample RIP time (ms)	Sample peak time (ms)	Normalised peak position (RIP = 100)
1	HZ	8.71	-	-
2	HZ	8.71	9.75	112
3.1	HZ	8.79	9.83	112
4	HZ	8.87	9.91	112
1	MMH	8.71	9.35	107
2	MMH	8.75	9.35	107
3.1	MMH	8.79	9.79	111
4	MMH	8.87	9.91	107
1	UDMH	8.71	9.15	105
2	UDMH	8.71	9.15	105
3.1	UDMH	8.75	9.19	105
4	UDMH	8.83	9.27	105
1	NO$_2$	6.99	6.35	91
2	NO$_2$	7.11	6.47	91
3.1	NO$_2$	7.07	6.43	91
4	NO$_2$	7.03	6.39	91

The results in Table 3.5 indicated that the internal flow patterns were disturbed by the alteration of the sample inlet flow rate; the faster inlet flow rates produced longer drift times. Although this result seemed contradictory initially, the increased amount of sample which entered the detector may have affected the drift time due to increased probability of collision. The slower flow rates produced better results for the detection of HZ, but the different flow rates required to achieve comparable peak amplitudes for different hydrazines' species, indicated that there was probably another factor to be accounted for, for example surface activity. However, the position of the product ion peaks, normalised against an RIP value of 100, remained constant for individual species. Thus, peak identification would not be a problem.

The results obtained from the work which used 5-nonanone dopant and bi-directional flow, combined with various direct inlet flow rates and different detector temperatures, are listed in Table 3.6.

Table 3.6: The effect of direct inlet flow rate on peak amplitude; 5-nonanone doped high temperature cell

Direct inlet flow rate (ml.min^{-1})	Detector temperature (°C)	Sample material	Peak amplitude (mV)
6.8	51	HZ	19
9.2	51	HZ	No response
13.0	51	HZ	No response
12.0	31	HZ	No response
9.2	27	HZ	109
6.8	51	MMH	No response
9.2	51	MMH	No response
13.0	51	MMH	No response
12.0	31	MMH	76
9.2	27	MMH	57
6.8	51	UDMH	133
9.2	51	UDMH	No response
13.0	51	UDMH	No response
9.2	31	UDMH	119
12.0	31	UDMH	130
9.2	27	UDMH	295

The general trend was for maximised peak amplitudes at an inlet flow rate of about 7 ml.min^{-1} for HZ at 51°C, with improved detection limits at the lower temperature of 27°C, even with a higher flow rate of 9 ml.min^{-1}. As 7 ml.min^{-1} was the lowest rate tested at the time, determined by the stability of the delivery system, it is not possible to estimate whether the HZ detection levels would have improved with an even lower inlet flow rate. For MMH a higher sample flow rate of about 12 ml.min^{-1}, as recorded at 31°C, produced a higher peak amplitude without improved detection at lower temperature. The results for the detection of UDMH were more complicated. At 51°C the slower flow rate of 7 ml.min^{-1} provided a greater amplitude, but at the lower temperature of 37°C the flow rate had to be increased to 12 ml.min^{-1} in order to achieve a comparable peak amplitude. At a flow rate of 9 ml.min^{-1} and a detector temperature of 27°C the UDMH peak amplitude more than doubled. The critical feature from this set of experiments was that response was affected by the combined effects of dopant, detector temperature and sample inlet flow rate. Further work indicated that the detector was more sensitive to the hydrazines at lower temperatures.

The diameter and length of a direct inlet system can be altered to produce the desired flow rate through that inlet, according to Poiseulle's equation

$$p_2 v = (p_1{}^2 - p_2{}^2)\, \pi\, a^4\, /\, 16\, \eta l \qquad\qquad \textbf{19}$$

where,

p_1 = inlet pressure absolute (Nm^{-2})

p_2 = outlet pressure absolute (Nm^{-2})

v = flow rate through inlet (l.min^{-1})

a = radius of inlet (cm)

η = viscosity of air (g.cm^{-1}.s^{-1})

l = length of inlet (cm)

3.4 The effect of humidity in conjunction with a direct inlet system

As stated in the section 3.3, direct inlet systems allow more water vapour into the spectrometer which may lead to larger ion clusters. The effect of the presence of variable concentration of water vapour was investigated by varying the degree of relative humidity entering the detector, with a constant concentration of the analyte species. UDMH vapour was selected for this study because it produced the highest peaks with the best resolution of the hydrazines at ppb levels, under the set conditions, including 5-nonanone as the dopant. Therefore, any changes in the peak amplitude of the UDMH product ion peak, as a result of changes in humidity levels, were easier to observe.

Changes in humidity produced only a negligible effect upon the detector sensitivity to UDMH. The maximum amplitudes recorded at equilibrium of the UDMH product ion peak at 5, 50, and 95% RH were 113, 121, 122 mV respectively. The equilibrium responses were monitored over a period of minutes and provided average peak amplitudes of 108, 115, and 113 mV respectively. The minimum values recorded were 101, 110, and 104 mV with 5, 50, and 95% RH respectively. The coefficient of variance for each set of humidity conditions was less than 5%, an acceptable level.

3.5 Optimum membrane temperature

3.5.1 Membrane permeability

Membranes are usually made of polymeric material, the desirable properties of which are high selectivity, high permeability, and mechanical and thermal stability. Polymers which have a high permeability usually have a low selectivity, and vice versa[206].

The polymer chosen for this work was polydimethylsiloxane which has a high permeability, is readily available, and has thermal properties characteristic of inorganic polymers.

The amount of solute which permeates through an homogeneous membrane is dependent upon solution and diffusion factors[206], which are determined mainly by permeability, concentration of the solute, and any forces acting on the solute, namely, chemical potential between the phases separated by the membrane.

Gradients in the chemical potential of a component in a membrane can be caused by a difference in temperature, pressure, or concentration, between the two phases either side of the membrane[99]. Figure 3.14 depicts part of a membrane with a solute, whose concentration is expressed in terms of partial pressures, p_1 and p_2, which permeates through the membrane at rate q.
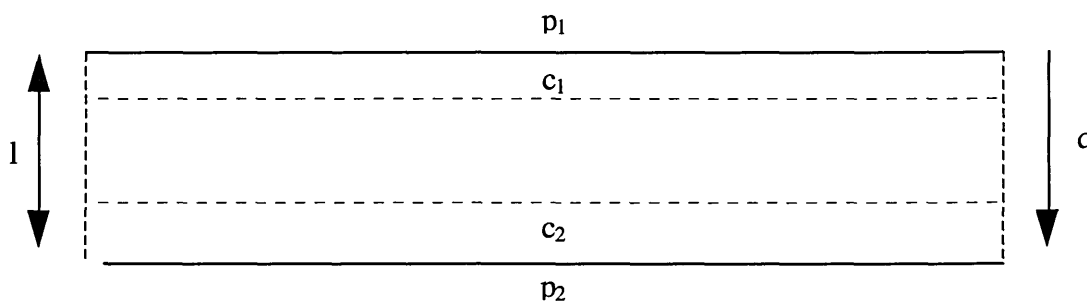
Figure 3.14: Factors affecting permeation of vapours through a membrane

The concentration in the boundary layer, c, is dependent upon the solubility coefficient, S, and the partial pressure of the solute on the feed side, i.e.:

$$c_1 = Sp_1 \qquad\qquad \textbf{20.}$$

The permeation rate, defined as the transfer of a mass of a solute through the membrane, per unit time, is determined by the permeability, P_e, of the membrane, and the difference in the partial pressures of the solute on either side of the semi-permeable

membrane. The permeation rate is also proportional to the area, and inversely proportional to the thickness of the membrane:

$$q = P_e(p_1 - p_2)A/l \qquad\qquad 21^{(207)}$$

but the permeation rate is also proportional to the diffusion coefficient and the difference in concentrations at the boundary layer, therefore,

$$q = D(c_1 - c_2)A/l \qquad\qquad 22$$

Combining equations 21 and 22,

$$P_e(p_1 - p_2) = D(c_1 - c_2) \qquad\qquad 23$$

and from equations 20 and 23,

$$P_e(p_1 - p_2) = DS(p_1 - p_2) \qquad\qquad 24$$

from which is derived,

$$P_e = DS \qquad\qquad 25.$$

Diffusive selectivity results from separation of components, through a polymer matrix, on the basis of size and shape. Solubility selectivity is determined by the chemical and physical interactions between the permeate and the polymer[206,208].

The products of diffusion coefficient and solubility, in terms of the Arrhenius equation, are:

$$D = k_1(exp\text{-}E_D/RT) \qquad\qquad 26$$

where E_D is the activation energy of diffusion and k_1 is a constant, and

$$S = k_2(exp\text{-}\Delta H_S/RT) \qquad\qquad 27$$

where k_2 is a constant and ΔH_S is the enthalpy of solution.

Combining equations 25, 26 & 27

$$P_e = k\{exp\text{-}(E_D+\Delta H_S)/RT\} \qquad\qquad 28$$

where $k = k_1 \times k_2$, and,

$$\ln P_e = \ln k - \{(E_D + \Delta H_S)/R\}(1/T) \qquad\qquad 29$$

Thus, assuming that over the experimental temperature range E_D and ΔH_S are constant, a plot of ln P_e against 1/T should produce a straight line graph of which the gradient is equal to $-(E_D + \Delta H_S)/R$, and the intercept equivalent to ln k. Although this assumption is frequently adopted it must be noted that E_D and ΔH_S can be functions of temperature, so that there may be circumstances where the foregoing assumption is not valid.

The diffusion coefficient increases with temperature, therefore higher temperatures favour a faster diffusion rate and more rapid equilibrium, but temperature also determines the solubility of the analyte in the membrane, which alters according to the heat of solution. An operating temperature must be selected which will allow the most acceptable combination of rate of equilibrium versus permeability[98]. The permeability of a polydimethylsiloxane membrane to the hydrazines was found, experimentally, to decrease with increase in temperature[101]. Membrane premeability varied for the different analytes, HZ > MMH > UDMH.

3.5.2 Experimentally determined optimum membrane temperature

Previous work[101] concerned with the membrane permeability to the hydrazines showed greater permeability with decrease in temperature towards ambient. However, during the assembly and commissioning of this experimental ion mobility spectrometer breadboard by the manufacturer (Graseby Dynamics Ltd.), the optimum membrane operating temperature was determined to be 108°C, due to improved performance at this higher membrane temperature (120°C was the highest practical operating temperature of the membrane). The higher temperature was assumed to be necessary because of different construction materials and configurations used in these experiments compared with the trials referred to in section 3.5.1. This operating temperature was not subjected to any further experimental evaluation, but was used for all research involving a membrane inlet.

3.6 Selection of the inlet system

With the optimum direct inlet flow rate determined, and the optimum membrane temperature known, the two inlet systems were compared, in order to determine the more efficient method of sample ingress, into the ion mobilirty spectrometer. The experimentation was performed whilst using acetone, 3,5-heptanedione, and 5-nonanone as the dopants.

The overall effects of the membrane at optimum temperature and the direct inlet at optimum flow rate were compared in terms of detection levels, resolution, response and recovery times. Summaries of peak amplitudes, response and recovery times, for the two inlet systems, employed in an acetone doped detector, have been compiled in Tables 3.7 and 3.8.

Table 3. 7: Comparative sensitiveness using the two inlet systems high temperature detector, 66°C, acetone doped system

Material	Peak amplitude (mV) at optimum setting	
	Membrane	Direct (flow setting)
HZ	410	300 (2)
MMH	126	217 (3)
UDMH	Not tested	670 (4)
Ammonia	873	Not tested
Nitrogen dioxide	1273	1528 (3.1)

Table 3.8 : Response and recovery times for the two inlet systems, high temperature detector, 66°C, acetone doped system

Material	Response time (s)						Recovery time (s)			
	Membrane inlet			Direct inlet			Membrane inlet		Direct inlet	
	Initial	>90 %	100 %	Initial	>90 %	100 %	>90 %	100 %	>90 %	100 %
HZ	7	115	223	42	42	42	34	265	62	62
MMH	6	62	310	50		418	28	>40	94	660
UDMH	-	-	-	14	14	14	-	-	-	-
NO₂	20	42	110	210	256	434	19	19	60	410

Ammonia was not tested.
NO_2 = nitrogen dioxide.

The direct inlet system at optimum flow rate for individual materials, provided generally comparable or better sensitivity than the membrane inlet, although the HZ peak amplitude was lower.

The initial response and recovery times recorded for the hydrazines were fast, typically less than one minute, while using either inlet system. For the detection of HZ, the direct inlet system was slower to produce an initial response, but immediately reached its maximum amplitude, a phenomenon also achieved for the detection of UDMH whilst employing a direct inlet system in the spectrometer (UDMH was not tested with the membrane inlet, acetone doped system). Initial recovery was faster when using a membrane inlet, but slower overall for complete recovery. The membrane inlet system allowed faster detection of nitrogen dioxide, and detector recovery was also quicker; however, sensitivity was impaired slightly, which probably accounted for the faster response times.

Comparable sensitivity, together with fast response and recovery times, suggested that there was no significant loss of sensitivity or degradation of resolution when comparing a direct inlet system with a membrane inlet system.

The spectra obtained with a membrane inlet appeared to be more stable than those collected when using a direct inlet. The membrane system took longer to reach equilibrium. The instability with the direct inlet could have been due to an unstable vapour source, varying acetone dopant concentration, or more probably the configuration of the inlet design. Due to the results obtained, the direct inlet system was improved to enhance performance. If a spectrometer, with a direct inlet, were to be used to detect more than one of the hydrazines, a compromise concerning optimum flow rate would have to be made, due to the variation in the optimum for each of the hydrazines tested.

Whilst using 3,5-heptanedione as the dopant chemical, with a membrane inlet, relatively good response, recovery, and sensitivity were achieved in the positive mode for the detection of UDMH, but not for HZ; acceptable sensitivity was obtained for nitrogen dioxide in the negative mode, but the response was unstable. The use of 3,5-heptanedione showed that sensitivity could be a function of the dopant chemical and not just the inlet system. The lack of sensitivity to HZ was due partly to insufficient peak resolution.
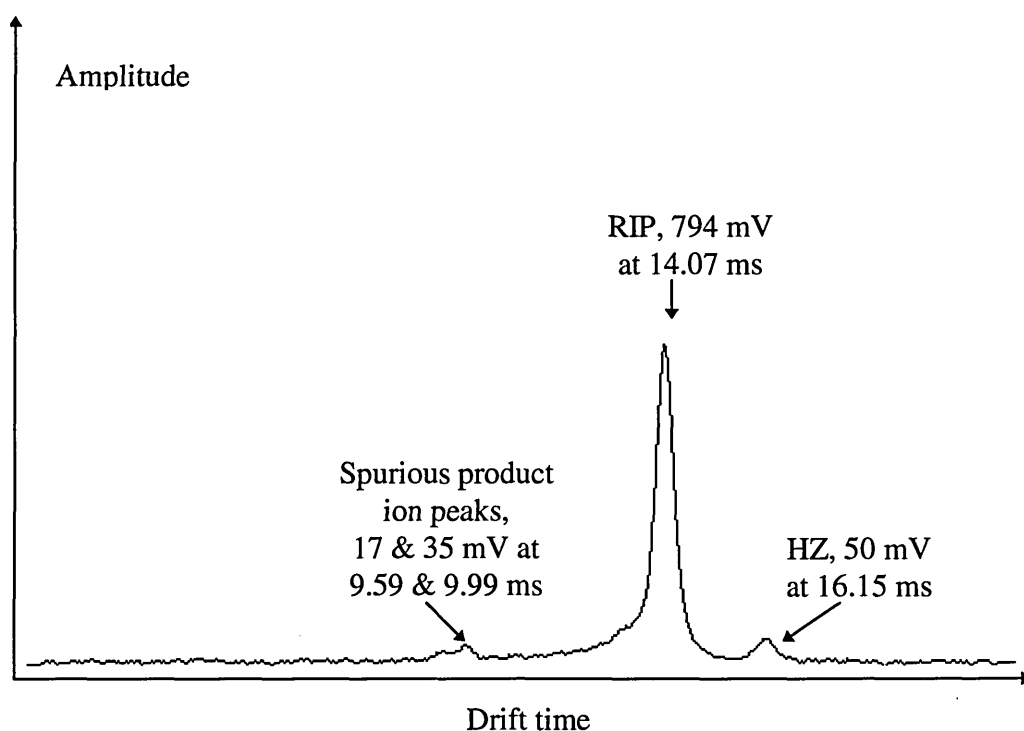
Figure 3.15: High temperature cell response and recovery characteristics to hydrazine exposure, at 65°C, 5-nonanone doped system. Spurious peaks recorded to the left of the RIP

During the period when 5-nonanone was being investigated for use as the dopant, with the membrane inlet incorporated into the system, spurious peaks were observed to the left hand side of the RIP (Figure 3.15). The unresolved doublet increased in amplitude over a period of days, and the dopant concentration appeared to

alter, being discernible from the RIP drift time and peak shape. After removing the membrane inlet from the detection system, and transferring to the direct inlet sampling mode, these spurious peaks disappeared. Examination of the permeation source revealed that the silicone membrane disc had also been affected, becoming more translucent and swollen.The spurious peaks observed with 5-nonanone dopant, in conjunction with a membrane inlet, underlined the importance of the chemical stability of membrane materials. The extraneous peaks were the result of interaction with, or degradation of, the membrane in the presence of 5-nonanone. Therefore, this chemical could not be used as the system dopant while a polydimethylsiloxane membrane was used. If a membrane was required for use with 5-nonanone as dopant, a different membrane material would be required. Polydimethylsiloxane membranes were chosen because of their relative permeability. An alternative material would probably have a different degree of permeability to the hydrazines and, therefore, any change of membrane material would require investigation into the effects upon sensitivity of the detection system as a whole.

The differences in the peak amplitudes measured at equilibrium were due, in part, to the positioning of the window cursors on the baseline. The measurements varied by, typically, ± 7 mV due to baseline noise. Therefore, the variation in peak amplitude, due to different % RH levels, was negligible. The various optimum flow settings, for maximum sensitivity of the detector to the analytes, meant that a compromise had to be made for the inlet flow. It was decided to set the intake flow between 10 and 15 ml.min^{-1}.

The indications are that there are no significant penalties involved in using a direct inlet system rather than a membrane inlet system (see Table 3.7). The direct inlet system would offer advantages in terms of ease of maintenance, and cost.

3.7 Optimum detector pneumatic configuration

The pneumatics incorporated into the ion mobility spectrometer breadboard allowed two different configurations to be effected, producing unidirectional or bi-directional flow patterns in the detector (see section 2.1.2.1). Both configurations were examined for their effect on sensitivity, resolution, response and recovery times. Resolution was examined in the tests because massive flow disturbances in the drift region might have led to peak broadening, thus reducing resolution.

A schematic diagram of the original IMS breadboard pneumatic circuit design, with bi-directional flow, is shown in Figure 2.1. Due to the sensitiveness of the detector, any background contamination, for example, from the components of the breadboard, sample tubing etc., had to be eliminated. Where possible, inert fittings and tubing were used for this purpose. Needle valves and flow meters containing elastomeric o-rings had to be replaced, due to lubricants that desorbed into the carrier gas. In the case of fine metering valves, which were necessary to regulate gas flows through the various sections of the spectrometer, sieve packs were inserted to absorb any leachates.

A conversion to version 2 of the spectrometer was carried out as follows: (1) a fine metering valve and sieve pack were inserted in-line prior to the heated dopant chamber. (2) The dopant and dopant sieve flow meters were removed. (3) The fine metering valves, positioned after the dopant chamber, were replaced with fixed restrictors. (4) The source and drift flow controls, and all sections in-line after this point, were removed from the dopant line outlet and connected to a tee leading directly from the air inlet line, and the output from the dopant section was attached to the inlet lines of the source and flows. The final configuration of version 2 of the breadboard is shown in Figure 3.16.
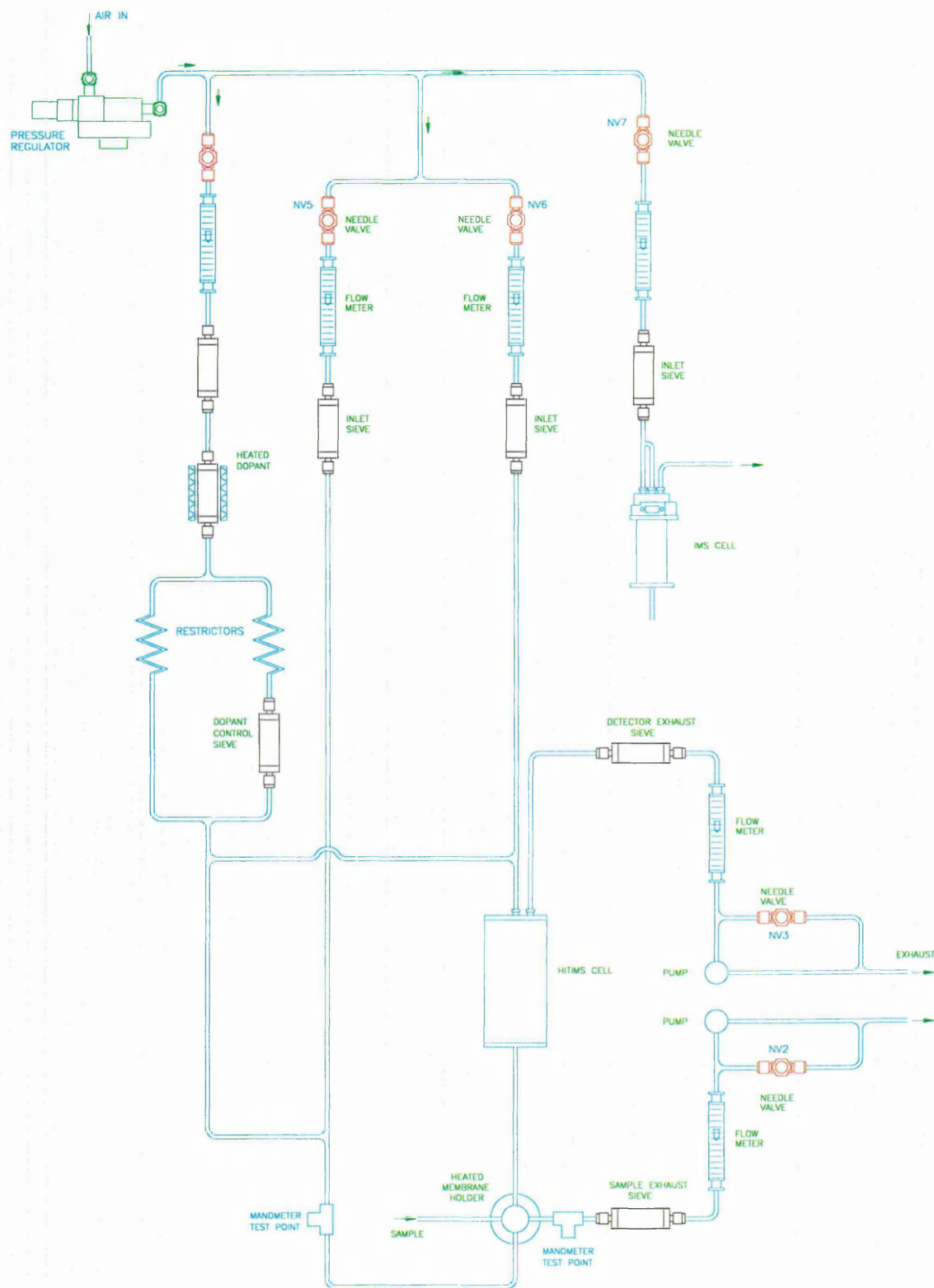
Figure 3.16: Schematic diagram of the ion mobility spectrometer breadboard pneumatic system, version 2, depicting bi-directional flow and membrane inlet systems

In order to gain final control of the dopant concentration, the restrictors were replaced with relatively inert ptfe fine metering valves, which did not contain o-rings.

The source and drift flows could be configured to enable the introduction of separate or combined flows into the detector cell. The 1/8" o.d. ptfe inlet tubing was wrapped in heating tape and insulated to facilitate heating of the sample tubing, with the aim of decreasing the amount of wall adsorption of the sample vapours.

Figure 3.17 schematically depicts version 3 of the breadboard, with the direct inlet configuration. The two systems were evaluated whilst using 5-nonanone and 2,2,6,6-tetramethyl-3,5-heptanedione dopants. The performance characteristics recorded for the two detector flow configurations, for version 3 of the spectrometer breadboard, with the detector set at various temperatures, are listed in Table 3.9. For convenience, 2,2,6,6-tetramethyl-3,5-heptanedione is referred to as TMHD in the table of results.

Overall, the flow configuration best suited for the analysis of hydrazines was the bi-directional system, although for MMH, with a 5-nonanone doped system the difference was less well defined. The sensitivity results were inconclusive; 5-nonanone produced better results for the detection of HZ but, although 2,2,6,6-tetramethyl-3,5-heptanedione produced higher peak amplitudes for both MMH and UDMH, no response was recorded during tests with HZ. The response times were also inconclusive. 5-nonanone was better for the detection of HZ, 2,2,6,6-tetramethyl-3,5-heptanedione was better for the detection of MMH, and either of the two dopants was acceptable for response times for UDMH determination. A similar pattern was followed for the recovery times, although 5-nonanone produced marginally improved recovery times during the monitoring of UDMH.

AIR IN

PRESSURE
REGULATOR

NEEDLE
VALVE

NEEDLE
VALVE

NEEDLE
VALVE

NEEDLE
VALVE

FLOW
METER

FLOW
METER

INLET
SIEVE

INLET
SIEVE

INLET
SIEVE

HEATED
DOPANT

IMS CELL

NEEDLE
VALVE

NEEDLE
VALVE

DOPANT
CONTROL
SIEVE

DETECTOR EXHAUST
SIEVE

MANOMETER
TEST
POINT

FLOW
METER

NEEDLE
VALVE

EXHAUST

HITIMS CELL

PUMP

DIRECT INLET

SAMPLE IN
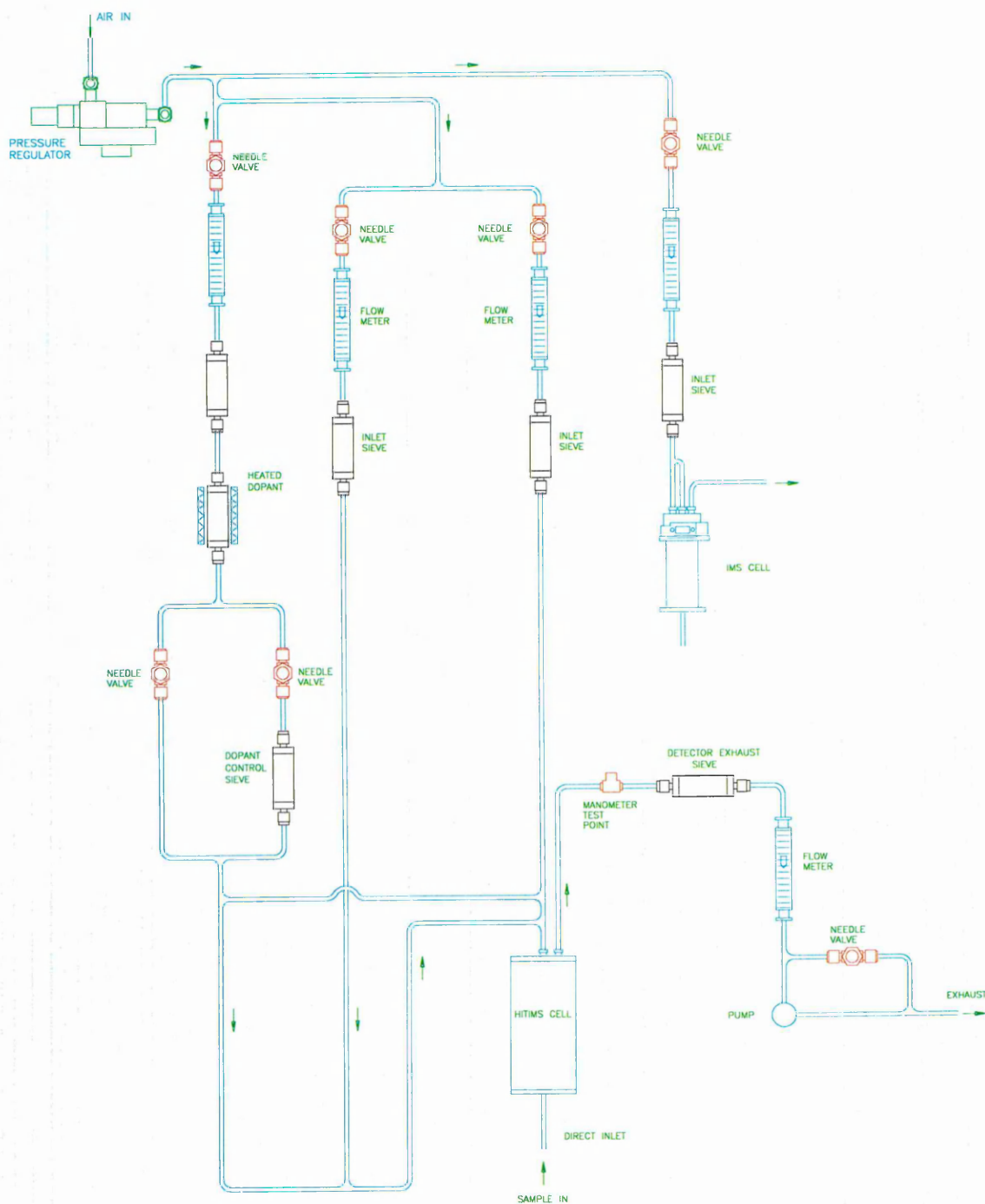
Figure 3.17: Schematic diagram of the ion mobility spectrometer breadboard pneumatic system, version 3, depicting unidirectional flow and direct inlet systems

Table 3.9: The effects of detector flow configuration on performance

Detector configuration	Dopant chemical	Detector temp. (°C)	Sample material	Peak amplitude (mV)	Peak resolution	Response and recovery
U	5-nonanone	35	HZ	46	Broad peak	
B	5-nonanone	35	HZ	102	Better than U	Slow response
U	TMHD	67	HZ	No response		
B	TMHD	67	HZ	No response		
U	5-nonanone	35	MMH	35	Poor	Slow response
B	5-nonanone	35	MMH	36	Slightly better	Better response
U	TMHD	67	MMH	172		Slower
B	TMHD	67	MMH	208		Fast
U	5-nonanone	35	UDMH	184	Multiple peaks	Fast R & R
B	5-nonanone	35	UDMH	222	Multiple peaks	Fast R & R
U	TMHD	67	UDMH	406		Fast response, slow recovery
B	TMHD	67	UDMH	539		Slightly better
U	5-nonanone	35	Ammonia	288	Broad peak	Slow recovery
B	5-nonanone	35	Ammonia	404	Multiple peaks	Very slow recovery
U	TMHD	67	Ammonia	98		Fast response, very slow recovery
B	TMHD	67	Ammonia	53		Slightly worse
U	5-nonanone	35	Nitrogen dioxide	500	Poor RIP	Fast R & R
B	5-nonanone	35	Nitrogen dioxide	1226	Poor resolution	Fast R & R
U	TMHD	67	Nitrogen dioxide	370	Multiple peaks	Fast R & R
B	TMHD	67	Nitrogen dioxide	No response	-	-

TMHD = 2,2,6,6-tetramethyl-3,5-heptanedione
R & R = response and recovery

For the detection of ammonia, the unidirectional system appeared to give better results with 2,2,6,6-tetramethyl,-3,5-heptanedione, but the 5-nonanone doped system produced improved limits of detection in the bi-directional pneumatic system. Despite the greater sensitivity to ammonia with a 5-nonanone doped bi-directional system, multiple peaks were formed and the recovery time was very long, however, the recovery time of the 2,2,6,6-tetramethyl,-3,5-heptanedione system was also very long. For the detection of nitrogen dioxide a 2,2,6,6-tetramethyl,-3,5-heptanedione doped system produced no response in the bi-directional mode.

The same system resulted in a better RIP and higher sensitivity with a 5-nonanone doped detector, compared with the unidirectional set-up. The overall results favoured the spectrometer configured with the bi-directional pneumatic system. However, it would be advisable to recheck the sensitivity of the final instrument configuration with the ultimate choice of dopant.

3.8 Summary of optimised spectrometer design features

Having determined the optimum operating conditions for the ion mobility spectrometer, it was found that much of the experimental breadboard could be reduced in size, with some parts becoming redundant. The bulky, heavy parts of the equipment required for flow control and measurement could be replaced with small fine control valves, pre-set to produce the required flow rates. Only one of the two detector cells was required; the membrane housing was no longer necessary; and the sieve packs were reduced in number, due to the improved design. Having decided upon these modifications a hand portable spectrometer was designed, in consultation with Graseby Dynamics Ltd.

3.8.1 Sample inlet system

The direct inlet system produced sensitivity, response, and recovery characteristics, comparable to the membrane inlet system, and appeared not to be affected to any significant degree by changes in humidity levels. If a membrane inlet system was used, the membrane material would have to be compatible with the chosen dopant chemical. A direct inlet system would be easier to maintain and more cost effective. A compromise on optimum direct inlet flow rate would have to be made if an ion mobility detector was to be used for simultaneous monitoring of more than one of the hydrazines' vapours. Hence, the direct inlet system was considered to be the better choice for sample ingress.

3.8.2 Spectrometer insulator material

The increase in sensitivity, apparent in the low temperature detector cell compared with the high temperature detector, was out-weighed by the excessive increase in response and recovery times, and the possibility of radiolysis degradation in the long term. The decision went in favour of the high temperature detector.

3.8.3 Detector operating temperature

The hydrazines had improved limits of detection with decrease in temperature, but to avoid the use of a cooling system in ambient conditions above 30°C, it was decided that the detector operating temperature should be set at 50°C.

3.8.4 Detector pneumatics configuration

A bi-directional flow system was considered to be the most suitable configuration for a combined HZ, MMH, UDMH, ammonia and nitrogen dioxide monitor, with a suitable choice of dopant chemical.

3.8.5 Dopant chemicals for the detection of the hydrazines, ammonia, and nitrogen dioxide

As dopant chemicals were required to enable the operating conditions of the ion mobility spectrometer to be optimised, a review of the dopants used so far seemed appropriate. The results were complicated due to the use of different dopant chemicals for the various trials, performed for the optimisation of the equipment. In order to evaluate the results fully, further study of the data was deemed necessary, and is described in chapter 4, part 1.

3.9 Miniaturised ion mobility spectrometer

The miniaturised breadboard comprised two sections, both hand portable. The detector module (see Figure 3.18) consisted of a direct inlet system coupled to a high temperature detector cell configured with a bi-directional pneumatic system, the requisite preamplifier and appropriate pcb for control of the detector, flow controls, operational mode switch, and umbilical gas line and electrical cable to the base unit. The base unit (Figure 3.19) contained the dopant chamber and control pcb, sieve packs, air pump, filters, air flow control valves, power supply and switch. The overall view of the combined pneumatic system is shown in Figure 3.20. The detector operating temperature was set at 50°C.

The hand unit was 380 x 240 x 160 mm; the base unit was 430 x 260 x 130 mm. The approximate weights were 3.1 and 6.6 kg respectively.

A photograph of the units is shown on Plate 3, following page 98.
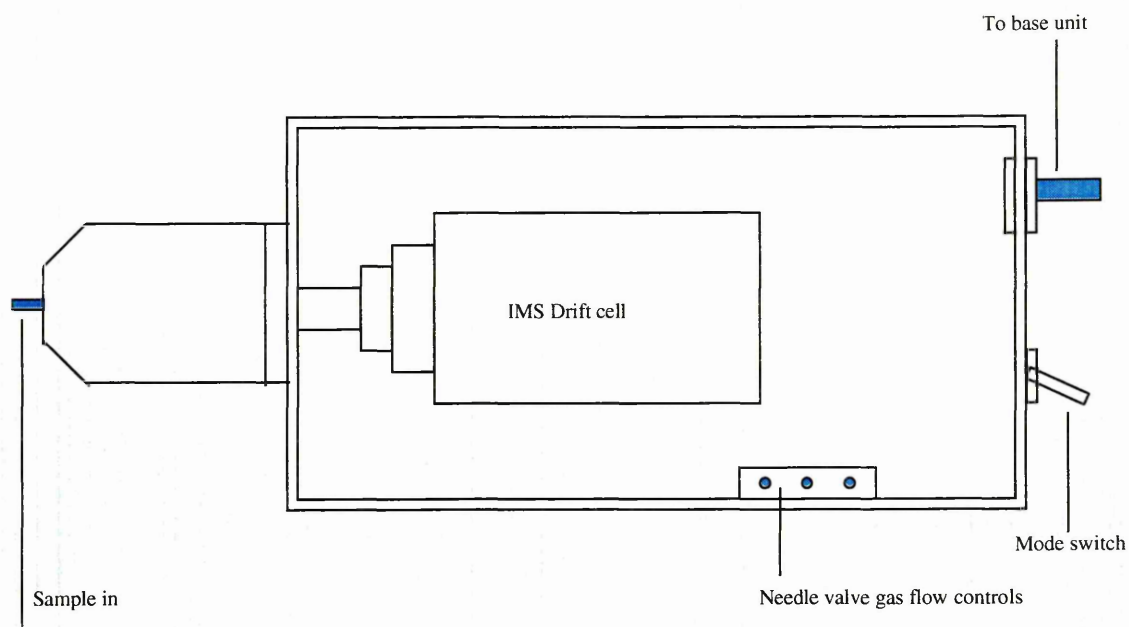
Figure 3.18: Schematic diagram of the miniaturised ion mobility spectrometer hand held unit (cover holding the pcb removed)
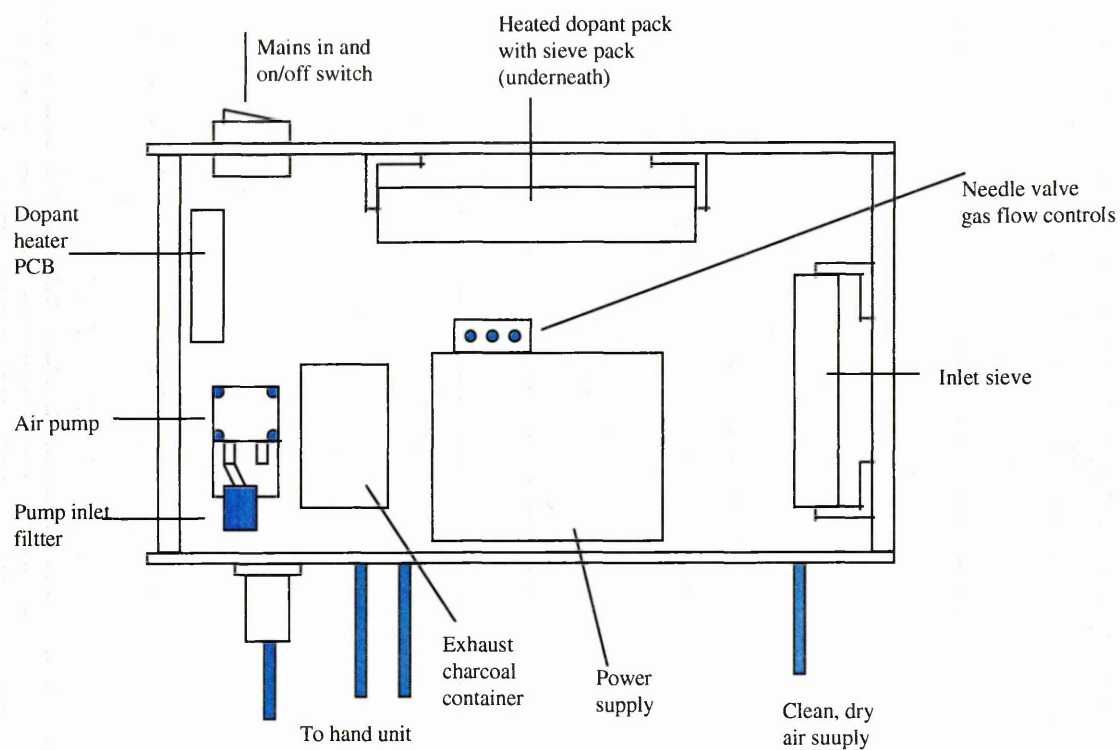
Figure 3.19: Schematic diagram of the miniaturised ion mobility spectrometer base unit (cover removed)
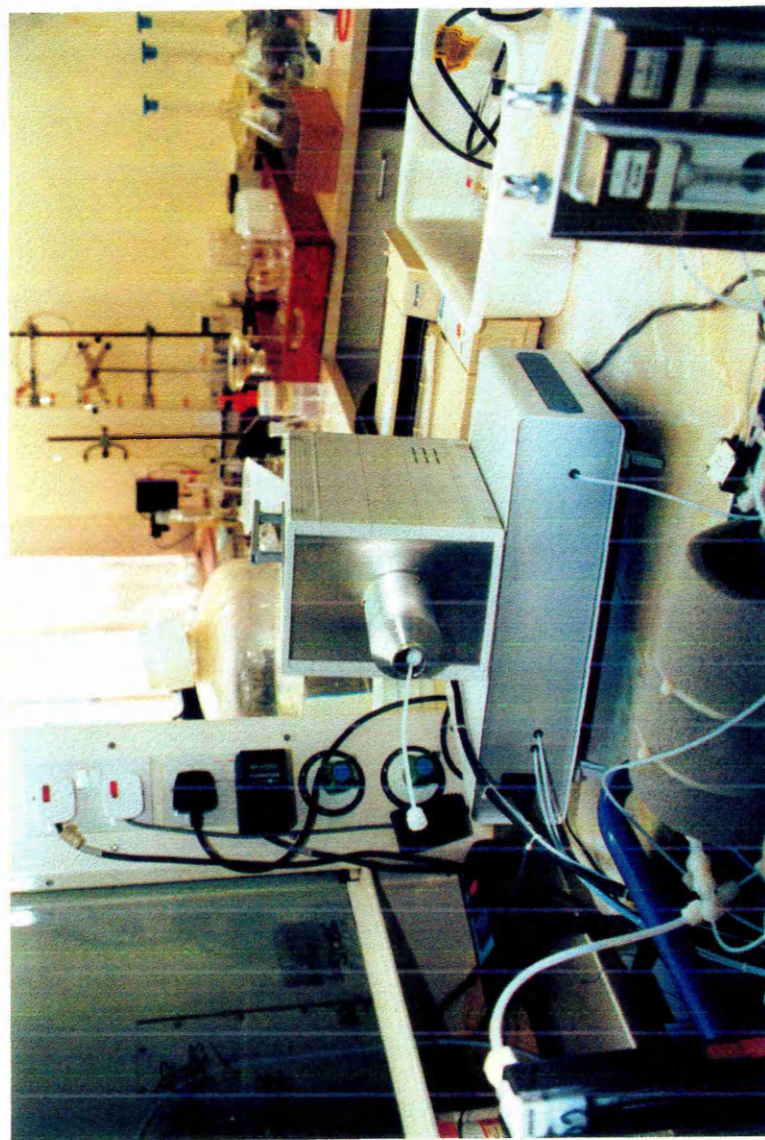
Plate 3: Miniaturised ion mobility spectrometer
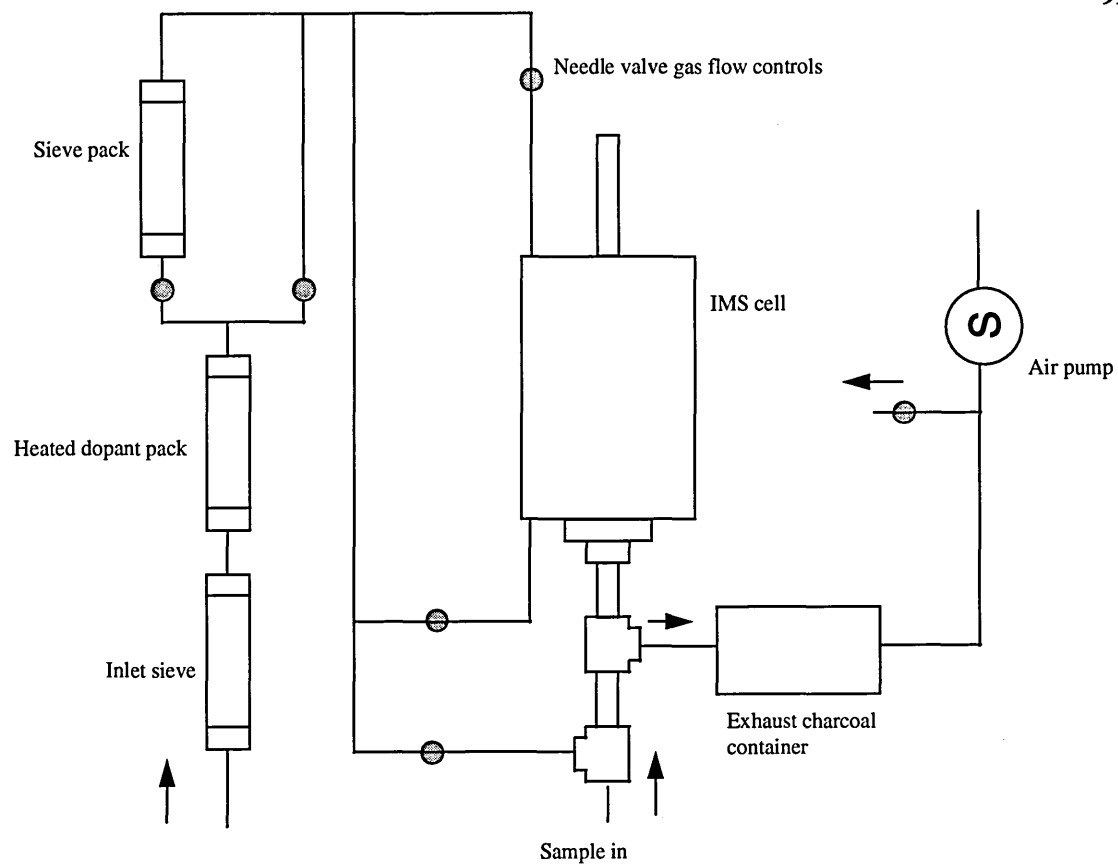
Figure 3.20: Schematic diagram of the miniaturised ion mobility spectrometer hand and base units' combined pneumatic system

ION-MOLECULE CHEMISTRY

Part 1

Evaluation of dopant chemicals with different functional groups

It was suspected that the use of different dopant chemicals, in the ion mobility detection system, might produce different effects with regard to resolution, response and recovery times, and possibly limits of detection. Therefore, some further studies, employing different ion-molecule chemistry, were carried out, using the ion mobility spectrometer breadboard configured with the direct inlet system. The tests involving the evaluation of different ion-molecule chemistry regimes were performed prior to and during the period when the miniaturised ion mobility spectrometer was being fabricated.

The chemicals used to produce alternative ion-molecule chemistry regimes were acetone, 3,5-heptanedione, 2,2,6,6-tetramethyl-3,5-heptanedione, a mixed dopant prepared from 4-dimethylaminobenzaldehyde with 2,2,6,6-tetramethyl-3,5-heptanedione, diisopropyl methane phosphonate, 4-methyl-2-pentanone, and 5-nonanone. These chemicals were evaluated as dopant chemicals because their use, by a commercial ion mobility spectrometer manufacturer, was under consideration. The dopant chemical vapours were generated as described in section 2.1.2.4, and once a stable RIP was established (section 2.1.2.7) spectra were recorded according to the details in section 2.1.2.8. The response characteristics, as described in section 2.2.7 were recorded. The results are listed in Tables 4.1 to 4.4, and are discussed below. For convenience, in the tables of results, the above list of chemicals is referred to as follows:

acetone 3,5-HD (3,5-heptanedione), TMHD (2,2,6,6-tetramethyl-3,5-heptanedione),

mixed (4-dimethylaminobenzaldehyde with 2,2,6,6-tetramethyl-3,5-heptanedione),

DIMP (diisopropyl methane phosphonate), MIBK (4-methyl-2-pentanone), and

5-nonanone, respectively.

Table 4.1: Normalised peak positions

	Ammonia	HZ	MMH	UDMH	Nitrogen dioxide
Acetone	113	113	111	105, 112	91
3,5-HD	Not tested	NR*	81	84, 92	70
TMHD	102	NR	78	79	73
Mixed	109	NR	NR	83	73
DIMP	111, 134	133	111, 131	110	94
MIBK	120	120	94, 113	92, 110, 117	96
5-Nonanone	124	126	104	84, 105	76

NR = no response
*Change in RIP only

Table 4.2: Peak amplitudes

	Ammonia (mV)	HZ (mV)	MMH (mV)	UDMH (mV)	Nitrogen dioxide (mV)
Acetone	873	165	217	446, 99	1528
3,5-HD	Not tested	NR	190	466, 18	300
TMHD	38	NR	172	447	370
Mixed	150	NR	NR	42	267
DIMP	15, 272	35	59, 52	57	263
MIBK	512	170	61, 204	65, 401, 21	1214
5-Nonanone	288	46	35	84, 20?	500

NR = no response

Table 4.3: Response times

%	Ammonia (s) 90	100	HZ (s) 90	100	MMH (s) 90	100	UDMH (s) 90	100	Nitrogen dioxide (s) 90	100
Acetone	S	S	150	150	468	500	60	60	256	792
3,5-HD	NT	NT	230	378	40	94	28	28	12	12
TMHD	54	80	NR	NR	244	362	54	68	34	34
Mixed	18	18	NR	NR	NR	NR	12	18	26	32
DIMP	18	24	24	30	66	96	96	126	18	24
MIBK	24	30	90	120	60	120	54	96	12	18
5-Nonanone	12	68	144	144	18	18	18	58	26	32

S = too slow to measure; NT = not tested; NR = no response

Table 4.4: Recovery times

%	Ammonia (s)		Hydrazine (s)		MMH (s)		UDMH (s)		Nitrogen dioxide (s)	
	90	100	90	100	90	100	90	100	90	100
Acetone	S	S	56	160	60	60	138	686	104	466
3,5-HD	NT	NT	14	176	28	112	28	54	12	12
TMHD	S	S	NR	NR	472	472	714	1020	34	20
Mixed	18	30	NR	NR	NR	NR	18	32	6	6
DIMP	66	126	18	30	66	72	66	72	6	12
MIBK	72	78	156	156	78	84	204	288	12	18
5-Nonanone	410	>25 min	32	38	*	*	44	88	32	88

S = too slow to measure; NT = not tested; NR = no response
*Unable to measure accurately as the peak was positioned on the tailing edge of the RIP

4.1 Detection of ammonia

Diisopropyl methane phosphonate, 4-methyl-2-pentanone, and 5-nonanone, were the only three dopants to produce well resolved peaks. The acetone doped system was the most sensitive to ammonia. The 5-nonanone system was the next most sensitive, followed by the 4-methyl-2-pentanone and mixed dopant systems, which produced sensitivity comparable with ammonia (with the results normalised approximately for concentration). The sensitivity of these systems was much higher than in the 2,2,6,6-tetramethyl-3,5-heptanedione system, which produced an unresolved doublet peak with the RIP (see Figure 4.1). The sensitivity of the diisopropyl methane phosphonate system was greater than that of the 2,2,6,6-tetramethyl-3,5-heptanedione system but not as good as the other systems. Ammonia was not available for testing with the 3,5-heptanedione system.

The mixed dopant produced the fastest response and recovery times for ammonia exposure. The 2,2,6,6-tetramethyl-3,5-heptanedione doped system produced a fast response but an unacceptably long recovery time; the acetone system was also slow to respond and recover. The product ion peaks formed from the 5-nonanone system were

broad, and the recovery time from exposure to ammonia rendered the 5-nonanone system unsatisfactory. The 4-methyl-2-pentanone, mixed dopant, and diisopropyl methane phosphonate systems produced acceptable response and recovery characteristics and satisfactory peak amplitudes, but as the resolution of both the 4-methyl-2-pentanone and diisopropyl methane phosphonate systems was higher than the mixed dopant system, either of these two dopants would be considered for the detection of ammonia.

Figure 4.1: High temperature detector response and recovery characteristics to ammonia exposure, 66°C, 2,2,6,6-tetramethyl-3,5-heptanedione doped system

4.2 Detection of hydrazine

Resolution for the four dopants which produced product ion peaks was satisfactory; acetone, diisopropyl methane phosphonate, 4-methyl-2-pentanone, and 5-nonanone doped systems produced product ion peaks resolved from the RIP. The diisopropyl methane phosphonate system provided the highest resolution.

For the detection of HZ, 2,2,6,6-tetramethyl-3,5-heptanedione and the mixed

dopant were unsatisfactory due to lack of response i.e. formation of an observed product

ion peak. 3,5-Heptanedione was unsuitable as the only indications of response were a

slight decrease in the RIP amplitude and broadening of the RIP at the tailing edge (see

Figure 4.2).

Figure 4.2: High temperature detector response and recovery characteristics to HZ
exposure, 67°C, 3,5-heptanedione

As stated in section 2.2.7 (page 61), tests with 4-methyl-2-pentanone and

diisopropyl methane phosphonate doped systems were performed using higher

concentrations of the hydrazines analytes. The peak amplitudes recorded in Table 4.2

were not corrected for concentration because the response characteristics of the

spectrometer were unknown. Therefore, the diisopropyl methane phosphonate and

4-methyl-2-pentanone doped systems required a higher concentration of HZ to produce

peak amplitudes comparable with alternatively doped systems. When the peak amplitudes for the 4-methyl-2-pentanone doped system were normalised using an estimated linear response this dopant still showed improved sensitivity over most of the 3,5-heptanedione, 2,2,6,6-tetramethyl-3,5-heptanedione, and mixed dopant systems which, as can be seen from Table 4.2, gave an essentially zero response. The acetone doped system was the most sensitive.

The response times for 90% and 100% peak amplitude were all less than four and seven minutes respectively. There was a general trend for increased sensitivity with increased response and recovery times. The 5-nonanone doped system required a longer equilibration time for the attainment of peak amplitudes comparable with that of the other ion-molecule systems of similar sensitivity. The choice of dopant chemical was narrowed down to acetone, 4-methyl-2-pentanone, diisopropyl methane phosphonate, and 5-nonanone. Acetone would be the preferred dopant because of sensitivity, response and recovery times and 4-methyl-2-pentanone would be the second choice.

4.3 Detection of methylhydrazine

The normalised MMH product peak amplitudes decreased from the acetone doped system through the 3,5-heptanedione, 2,2,6,6-tetramethyl-3,5-heptanedione, and 4-methyl-2-pentanone systems. The mixed dopant was unsatisfactory as no response was achieved for the detection of MMH. These results combined with the slower response and recovery times for the acetone and 2,2,6,6-tetramethyl-3,5-heptanedione systems eliminated these two chemicals from the list of possible dopants. 5-Nonanone was also eliminated because of insufficient resolution. The 3,5-heptanedione system produced greater sensitivity, and a single peak, compared with the diisopropyl methane phosphonate and 4-methyl-2-pentanone systems, which each produced two product ion peaks, and so 3,5-heptanedione was the chosen dopant.

4.4 Detection of 1,1-dimethylhydrazine

The UDMH product ion peaks were unresolved from the acetone RIP. 3,5-Heptanedione, 2,2,6,6-tetramethyl-3,5-heptanedione, diisopropyl methane phosphonate, and 5-nonanone all produced well resolved peaks. Although the normalised peak positions for one of the UDMH product ion peaks in each of the acetone and 5-nonanone systems corresponded, the peak amplitudes were higher in the acetone system and consequently overlapped with the RIP; baseline resolution was achieved with the lower peak amplitude of the 5-nonanone system. The waterfall spectra showing the response and recovery of the higher mobility UDMH product ion peak in the 3,5-heptanedione doped system have been reproduced in Figure 4.3.
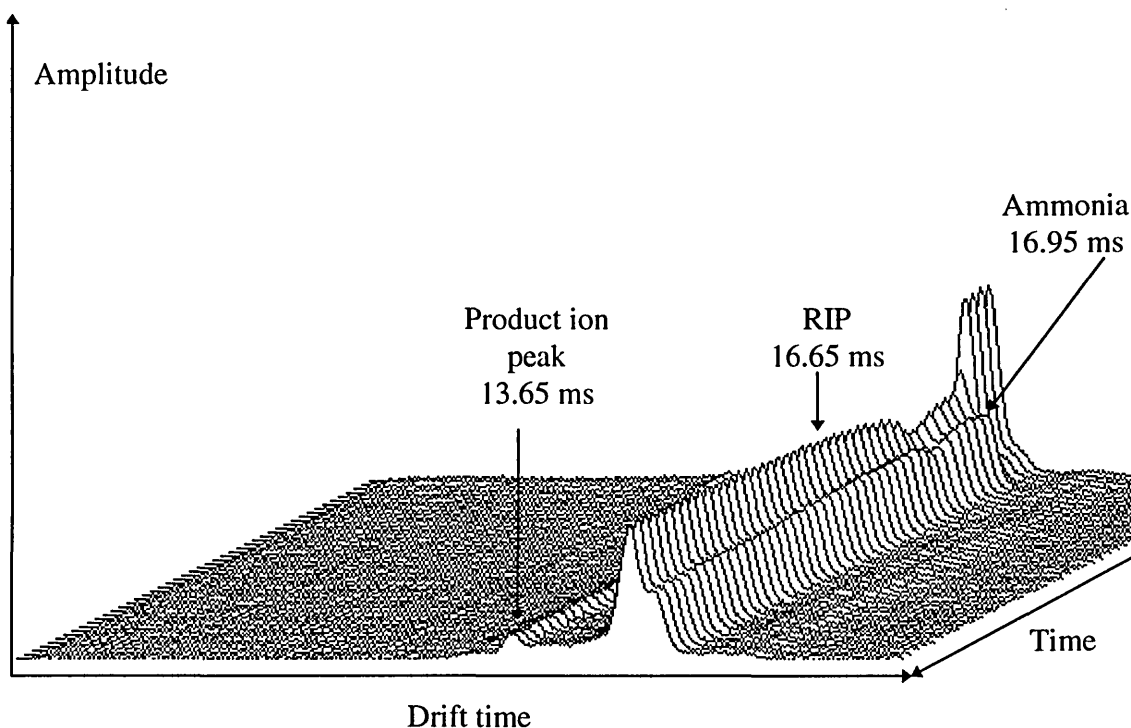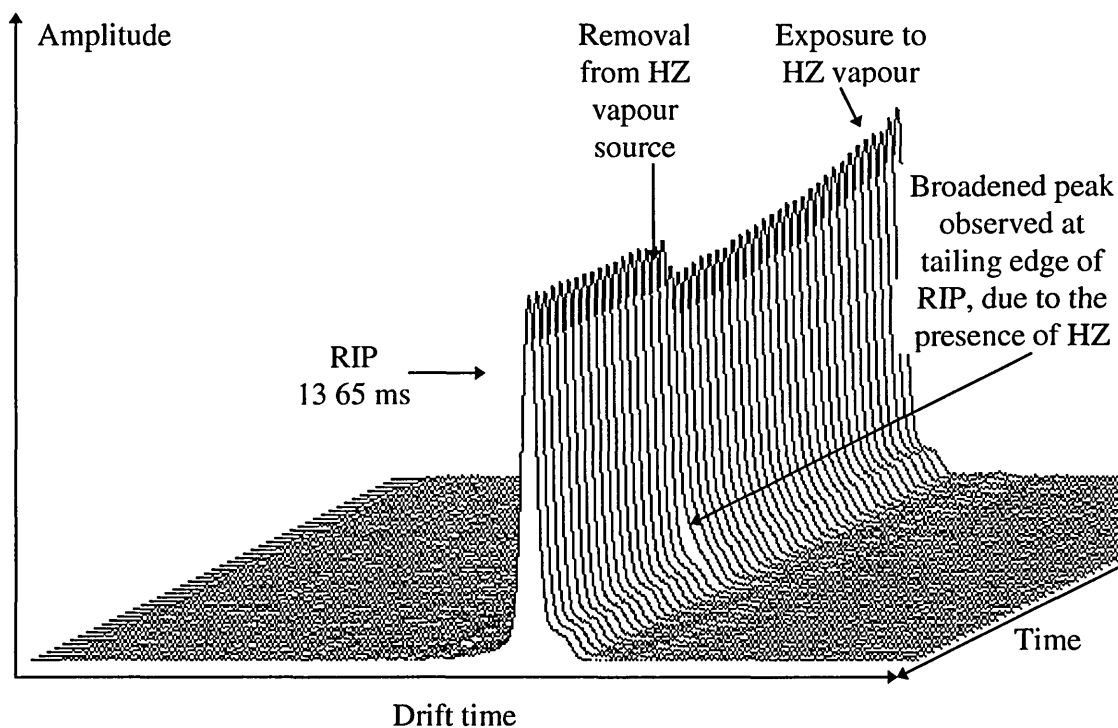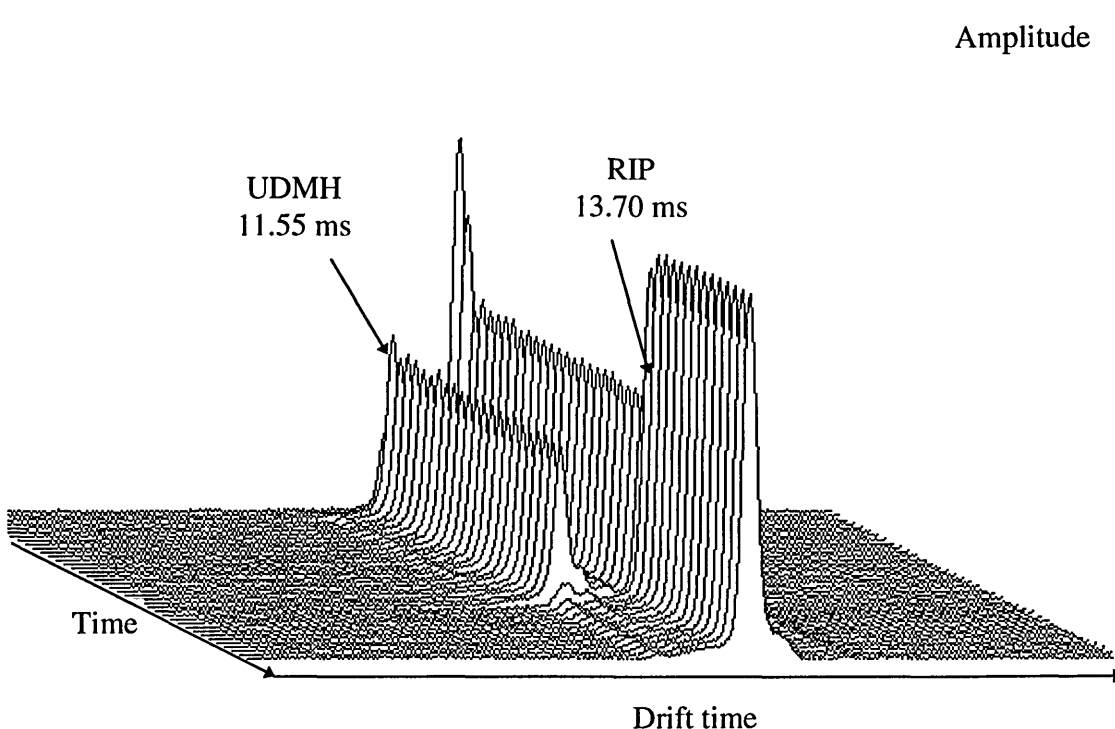

Figure 4.3: High temperature detector response and recovery characteristics to UDMH exposure, 67°C, 3,5-heptanedione doped system

The acetone, 3,5-heptanedione, and 2,2,6,6-tetramethyl-3,5-heptanedione systems produced comparable peak amplitudes for UDMH. Even taking into account the higher concentration of 4-methyl-2-pentanone, the peak amplitude was comparatively higher than that achieved for the 5-nonanone doped system. The diisopropyl methane phosphonate and mixed dopant systems had lowest sensitivity. The 4-methyl-2-pentanone system produced multiple peaks.

The system doped with diisopropyl methane phosphonate was relatively slower to respond; it took at least twice as long as the remaining doped systems to reach equilibrium response. The mixed dopant and 5-nonanone systems had fast response times for UDMH exposure. The acetone doped system was slow to recover fully, but still much faster than the 2,2,6,6-tetramethyl-3,5-heptanedione system. 4-Methyl-2-pentanone had a longer recovery time than the 3,5-heptanedione, mixed, diisopropyl methane phosphonate, and 5-nonanone. Due to the longer response and recovery times of the 4-methyl-2-pentanone and diisopropyl methane phosphonate systems, the other sensitive system with satisfactory resolution, 3,5-heptanedione, was considered the most satisfactory of the dopant chemicals evaluated. The second choice of dopant was 5-nonanone.

4.5 Detection of nitrogen dioxide

The acetone system produced the highest sensitivity, with a sharp peak in excess of 1500 mV partially resolved from the RIP. 3,5-Heptanedione, and the mixed dopant produced unstable nitrogen dioxide peaks; multiple peaks were formed with 3,5-heptanedione, one being a doublet with the RIP. 5-Nonanone produced a poor RIP (low amplitude and broad) but a sharp product ion peak. 2,2,6,6-Tetramethyl-3,5-heptanedione produced multiple unresolved peaks (see Figure 4.4). The mixed dopant produced a sharp product ion peak with a much smaller peak on the tailing edge.
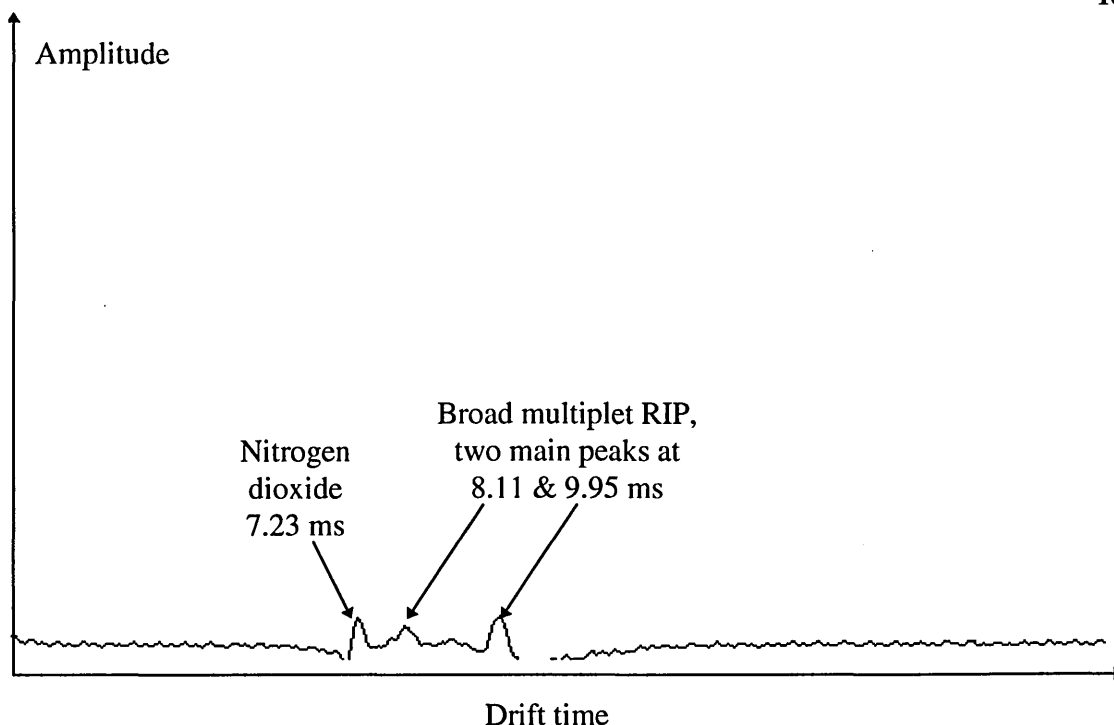
Figure 4.4: High temperature detector response to nitrogen dioxide exposure, 66°C, 2,2,6,6-tetramethyl-3,5-heptanedione doped system

Diisopropyl methane phosphonate produced a peak which was poorly resolved from multiple shallow RIPs. 4-Methyl-2-pentanone produced high sensitivity but an unresolved response to nitrogen dioxide. With peak amplitudes corrected for concentration, the diisopropyl methane phosphonate system showed poor sensitivity. The peak amplitudes increased in the following order of dopant systems: diisopropyl methane phosphonate < mixed < 3,5-heptanedione < 2,2,6,6-tetramethyl-3,5-heptanedione < 4-methyl-2-pentanone < 5-nonanone < acetone.

Apart from the relatively long response and recovery times observed for nitrogen dioxide detection in an acetone based system all response and recovery times were fast, within 35 seconds, except for recovery of the 5-nonanone system which took over a minute.

The choice of dopant for nitrogen dioxide detection was a difficult one because of the lack of resolution of the majority of the dopant systems. The 5-nonanone was discounted as a possible dopant because of impracticalities involved with the software programming aspects of broad low intensity RIPs. In the 2,2,6,6-tetramethyl-3,5-heptanedione system multiple peaks were formed; unstable peaks resulted in both the 3,5-heptanedione and mixed dopant systems. Therefore, despite the longer response and recovery times recorded for the acetone it was considered the most suitable choice of dopoant for the detection of nitrogen dioxide.

4.6 Simultaneous detection of the hydrazines and nitrogen dioxide

Of the dopant chemicals tested, acetone produced the greatest sensitivity but the peaks were not resolved, in the positive mode, so this system was unacceptable. The use of 3,5-heptanedione was satisfactory for the detection of MMH and UDMH. This dopant was not tested with ammonia, and it was discounted as unsatisfactory for the detection of HZ and nitrogen dioxide. 2,2,6,6-Tetramethyl-3,5-heptanedione was unacceptable for the detection of any of the analytes. The mixed dopant could only be considered for the detection of ammonia. Diisopropyl methane phosphonate was unsatisfactory for the detection of HZ, UDMH, and nitrogen dioxide. 4-Methyl-2-pentanone was satisfactory for the detection of ammonia, HZ, and MMH, and a minor possibility for the detection of UDMH. It was not acceptable for the detection of nitrogen dioxide. The broad peaks and long recovery times of the 5-nonanone system precluded its use as the dopant for simultaneous detection of the hydrazines and nitrogen dioxide.

It became obvious that the choice of dopant chemical would have to be a compromise of performance characteristics for detection of the different analytes, for example, between sensitivity, response and recovery times, and overall resolution. In order to assist with the final choice, a summary of the dopant systems was compiled and

has been reproduced in Table 4.5. The different dopant / analyte combinations have been rated for their performance characteristics, with seven points awarded for overall first choice of dopant for a given analyte (denoted by number in the table), six points for the second choice, down to zero points for a totally unsatisfactory dopant. The summed points awarded are listed in the rating column.

The key to the performance characteristics listed in the table are R_1 = response time, R_2 = recovery time, R_t = resolution, S = sensitivity, P = peak shape or unstable peaks, M = multiple peaks, and NT = not tested. Where these were not satisfactory, then no points were awarded below the third choice of dopant.

Table 4.5: Summary of the different dopant / analyte systems

	Ammonia	Hydrazine	MMH	UDMH	Nitrogen dioxide	Rating
Acetone	R_2	1	R_1	R_t, R_2	1	14
3,5-HD	NT	R_t	1	1	P, M	14
TMHD	S, R_2	S	R_1, R_2	R_2	M, R_t	0
Mixed	3	S	S	S	P, M	5
DIMP	2	S	M, 3	S, R_1	S, R_t	11
MIBK	1	2	M, 2	M, R_1, R_2, 3	R_t	24
5-Nonanone	P, R_2	R_2, 3	R_t	2	P	11

All of the dopants that produced usable responses to HZ also produced a response to ammonia, which would not have been resolved from the HZ peak if it had occurred simultaneously in the same [doped] spectrum. Ammonia remained an interferent in the ion mobility detection of HZ. Therefore, for the simultaneous detection of the hydrazines, 4-methyl-2-pentanone would require further investigation, or a completely different dopant chemical should be investigated. It is probable that a different detector cell, with alternative dopant chemistry, would be required for the detection of nitrogen

dioxide. However, it might be possible to incorporate the two detectors into one instrument, but this would mean a larger unit with additional hardware and software.

One instrument, for monitoring all of the compounds of interest, would be simpler for the operator in terms of convenience e.g. fewer pieces of equipment to use and maintain. This would also be more cost effective as fewer instruments would mean less initial cost and overall cheaper maintenance. From the research performed so far, optimum ion-molecule chemistry systems differ according to the analyte of interest. Therefore, a compromise would be necessary for the purpose of demonstrating the capabilities of a single monitor.

The product ion peaks produced for the hydrazines, in any of the doped systems, appeared in the mobility spectrum in reverse order to that expected. From the relative assumed diameters of the neutral species it would have been plausible for mobility to decrease in the order of ammonia > HZ > MMH > UDMH. However, empirical findings showed their mobilities decreased in the reverse order. This phenomenon, coupled with the ammonia and HZ product ion peaks having very similar ion mobilities, suggested that the ion clustering sequence of each analyte was different. Due to the results so far, it was decided that the detection of nitrogen dioxide should be segregated from the problems of separating HZ and ammonia in the mobility spectrum and that the remainder of the research should centre around the ion-molecule chemistry of the hydrazines. It was decided that further investigation of the thermodynamic properties and sizes of the ion-molecules formed should be undertaken through use of molecular modelling.

Chapter 4

Part 2

Molecular modelling

Of the dopant chemicals evaluated in this research project, the ketones and one of the diones had been shown to be more successful for the detection of the hydrazines. The acetone system had insufficient resolution of the hydrazines and ammonia, whereas 5-nonanone had lower sensitivity but greater resolution overall, although still only partial resolution of the ammonia and HZ peaks. It has been surmised that the increase in resolution of the HZ and ammonia product ion peaks, observed in changing from the acetone to the 5-nonanone doped system, was due to the greater difference in cross sectional diameter of the ammonia and HZ ion-molecule clusters formed in the 5-nonanone system. Previous work performed with 5-nonanone reagent gas[178] produced product ion peaks which were composed of the analyte clustered with either one or two molecules of the ketone. As it has been shown empirically from reduced mobility data that the increase in size of the dopant ketone molecule from acetone to 5-nonanone leads to the formation of bigger ion-molecule clusters, the improvement in resolution might be observed as a gradual progression through an homologous series of the ketones.

4.7 Chemical systems considered

In order to evaluate sizes and thermodynamic properties, which may have affected the apparent resolution and sensitivity, an homologous series of symmetrical ketones from acetone through to 6-undecanone (Figure 4.5) was studied through the use of the

HyperChem molecular modelling software package. The ketone series was terminated at 6-undecanone because it was thought that the changes in inductive effects due to increased carbon chain length would be negligible at this number of carbon atoms, and encompassed both acetone and 5-nonanone, which have been evaluated empirically.
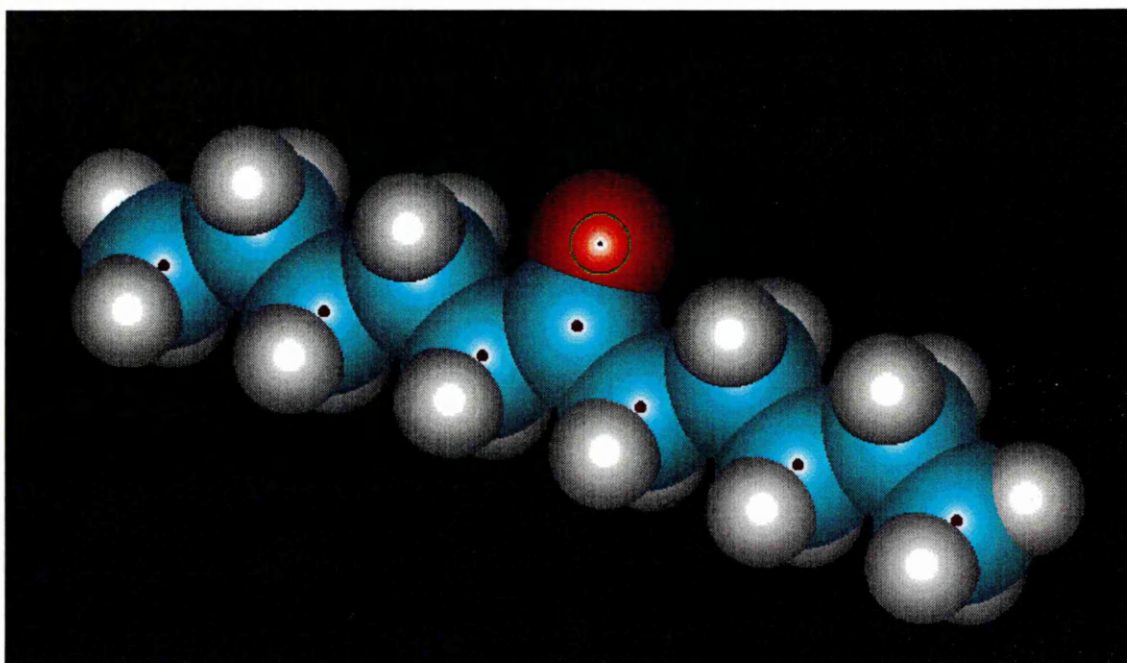
Figure 4.5: 6-Undecanone

Branched chain symmetrical ketones were also examined in order to investigate whether steric hindrance would affect ion-molecule cluster formation. The chemicals evaluated in this part of the study were 2,4-dimethyl-3-pentanone (diisopropyl ketone) (Figure 4.6), 2,2,4,4-tetramethyl-3-pentanone (di-*t*-butyl ketone) (Figure 4.7), 2,2,6,6-tetramethyl-4-heptanone (dineopentyl ketone) (Figure 4.8), 2,6-dimethyl-4-heptanone (diisobutyl ketone) (Figure 4.9), and 2,8-dimethyl-5-nonanone (diisopentyl ketone) (Figure 4.10).
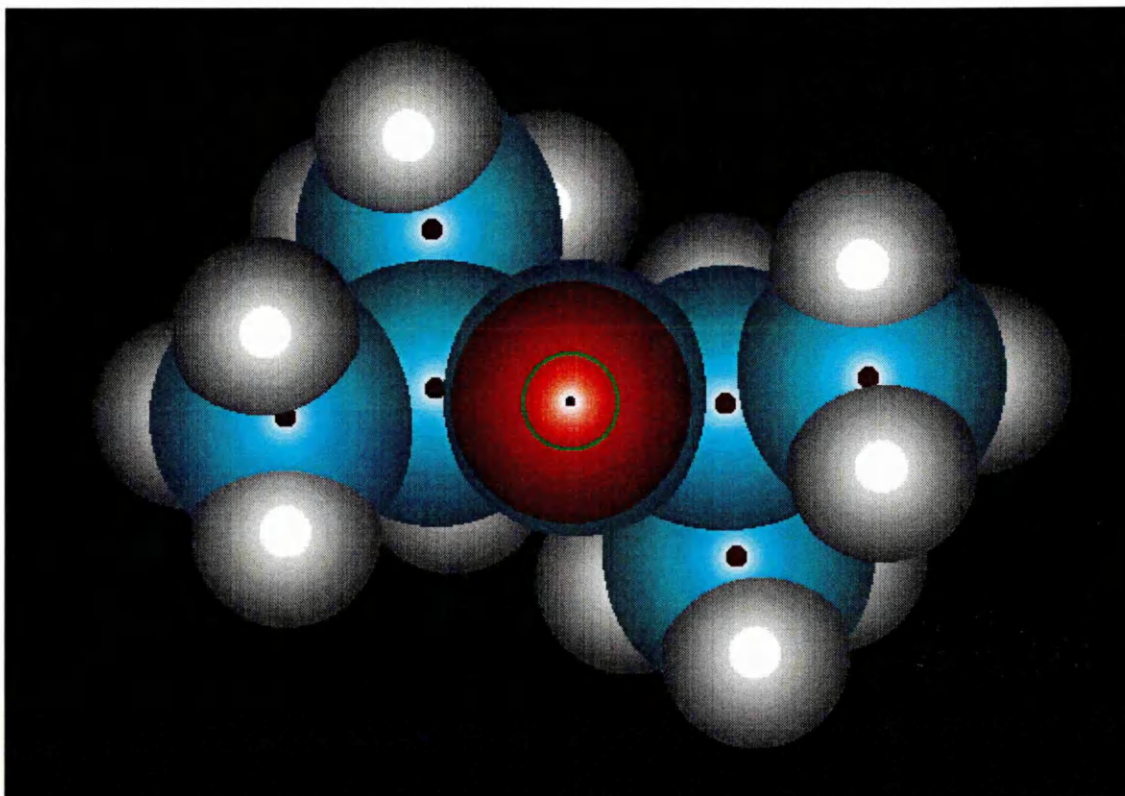
Figure 4.6: 2,4-Dimethyl-3-pentanone

These compounds were chosen for inclusion in the series of calculations in order to maintain the sequence of symmetrical ketones, determine the effect of methyl substitution close to the carbonyl group, and the effect of insertion of methylene groups between the methyl and carbonyl functional groups.
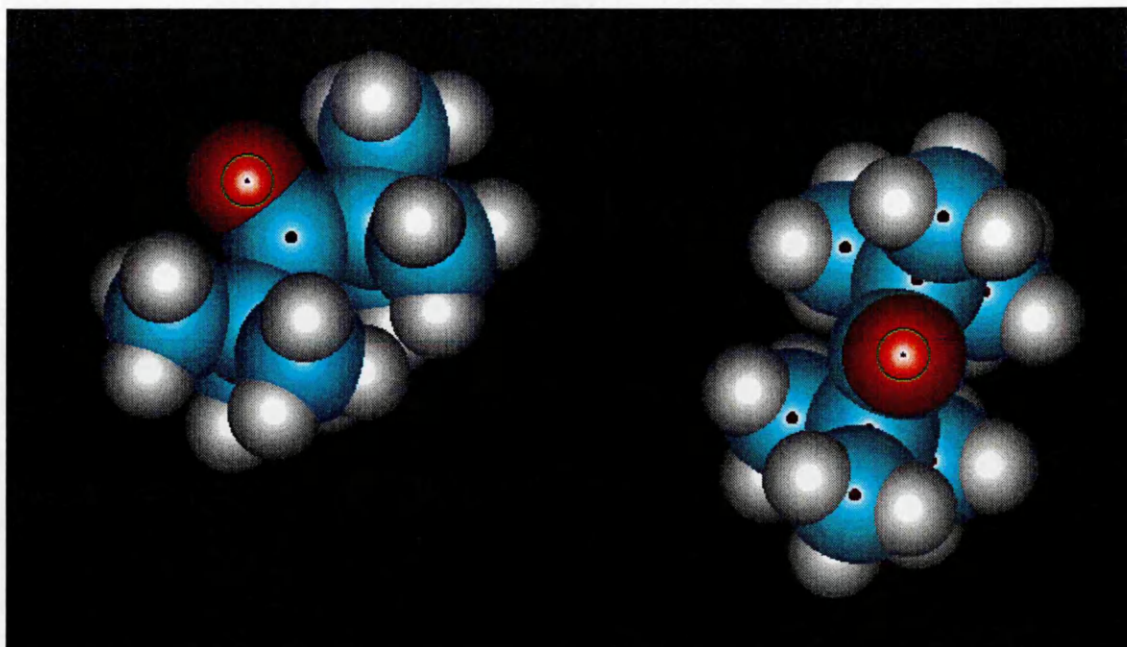
Figure 4.7: 2,2,4,4-Tetramethyl-3-pentanone, viewed from two different positions
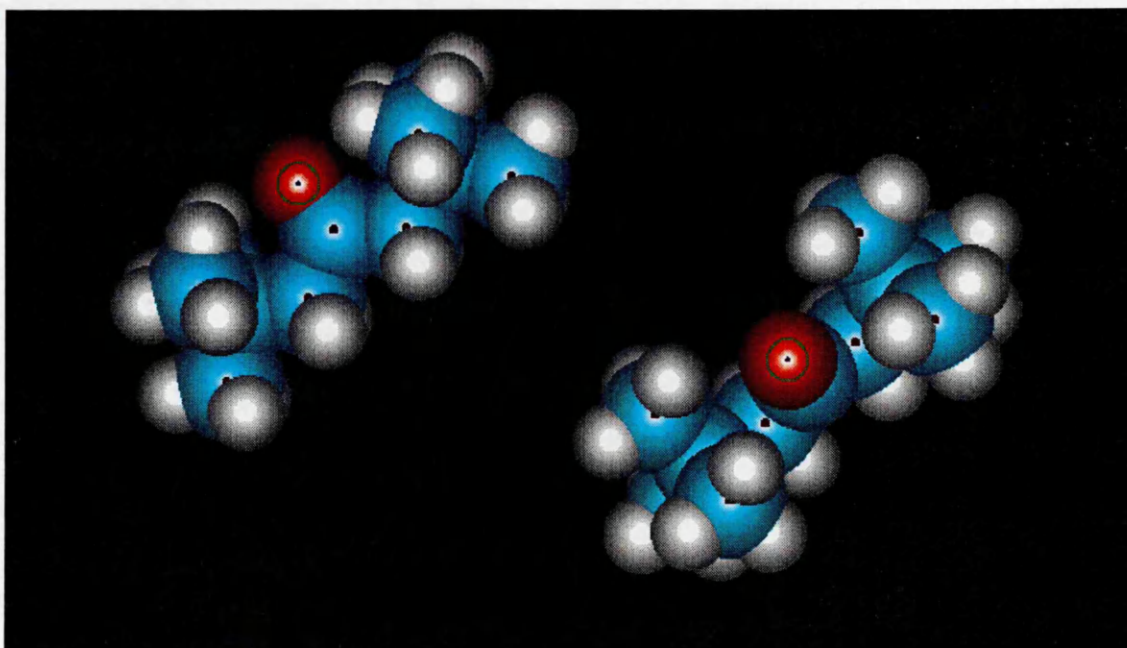
Figure 4.8: 2,2,6,6-Tetramethyl-4-heptanone, viewed from two different positions
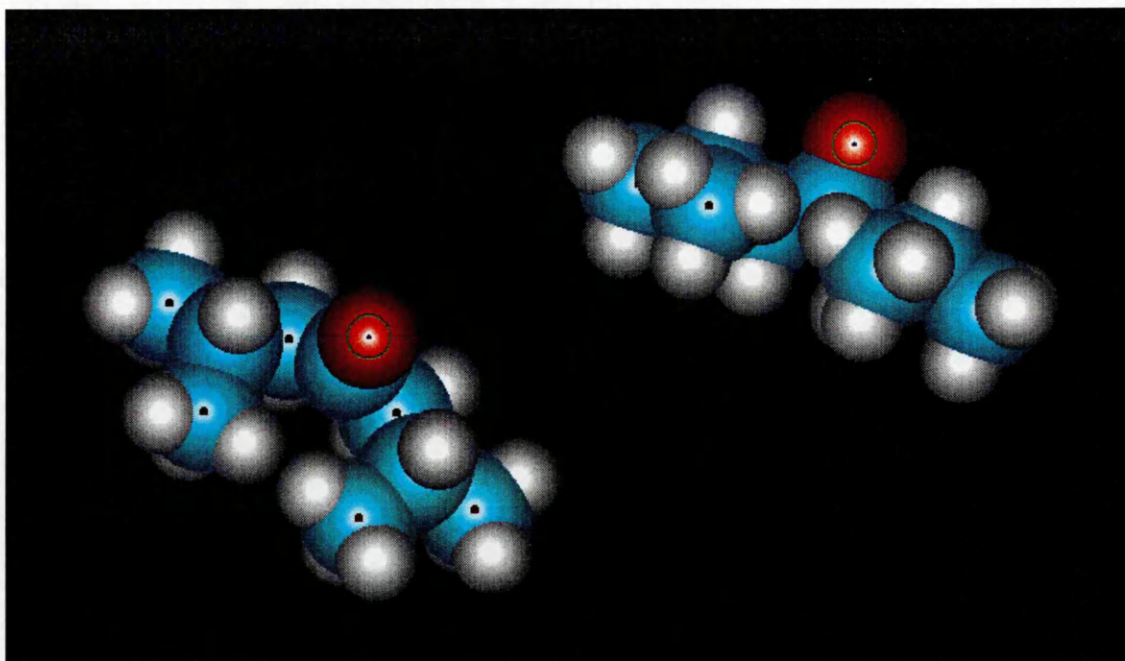
Figure 4.9: 2,6-Dimethyl-4-heptanone, viewed from two different positions
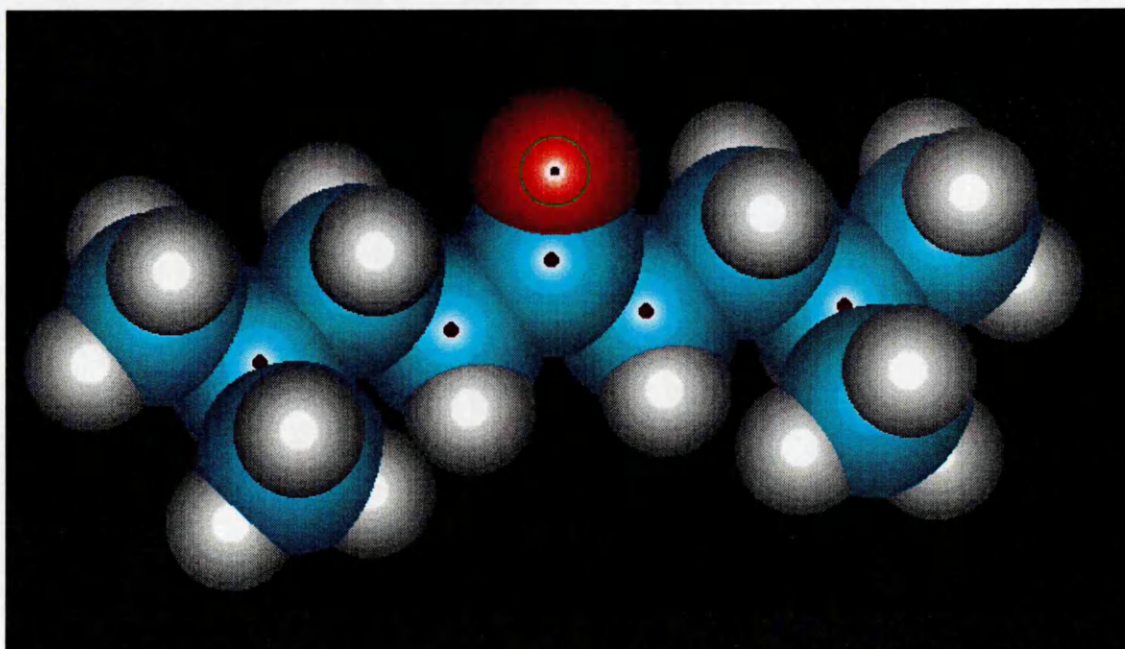
Figure 4.10: 2,8-Dimethyl-5-nonanone

In theory, the inductive effect should increase with an increased degree of methyl substitution close to the carbonyl group, for example, going from 2,4-dimethyl-3-pentanone to 2,2,4,4-tetramethyl-3-pentanone, or from 2,6-dimethyl-4-heptanone to 2,2,6,6-tetramethyl-4-heptanone. Also, the effect should decrease with increased distance of the methyl group from the carbonyl bond through the addition of the methylene groups, for example, going from 2,4-dimethyl-3-pentanone through 2,6-dimethyl-4-heptanone to 2,8-dimethyl-5-nonanone, or from 2,2,4,4-tetramethyl-3-pentanone to 2,2,6,6-tetramethyl-4-heptanone.

4.8 Computational chemistry considerations

Computational chemistry[209] can be used to characterise and predict the structure and stability of chemical systems, to estimate energy differences between different states, and to explain reaction pathways and mechanisms. The equilibrium geometry of a molecule describes the co-ordinates of a deep minimum on the potential energy surface, which may be very complicated even for relatively simple molecules. Geometry optimisation is a means of finding a set of co-ordinates corresponding to the minimum potential energy. In this research, the HyperChem software package was used to establish optimised geometry which represented a minimum on the potential energy curve, for each of the neutral molecules and ion-molecule clusters of interest.

Calculation parameters were as stipulated in section 2.1.2.9. An understanding of the complexity of the calculation considerations was required before the parameters could be programmed. The model building function was used to create a reasonable starting structure for individual molecules, but the initial structures of the ion-molecule clusters had to be constructed by employing knowledge of probable protonation sites, orientation of the ion and molecule(s) comprising the cluster, and possible repulsion / attraction interactions.

4.9 HyperChem computed data

Data obtained from the calculations were stored in log files, and subsequently accessed through "Write" software in the Microsoft Windows Accessories program. Information calculated included the total energy of each system, binding energy, isolated atomic energy, electronic energy, core-core interaction, heat of formation, gradient, eigenvalues, atomic orbital electron populations, net charges and co-ordinates, and dipoles. HyperChem calculates both heats of formation and binding energies, although the HyperChem literature recommended that the heats of formation were more useful, and that calculated molecular dipole moments varied from experimentally determined values. Distances between atoms in the cluster were measured through the selection of those atoms, whereby the interatomic distance was displayed in the "status" field.

Electrostatic potential, displayed as a contour plot, may be useful for finding probable sites of reaction in a molecule; for example, if the highest unoccupied molecular orbital (HOMO) of a system was plotted as a contour map, then the region of highest electron density would be the site of electrophilic attack .

4.10 Computation results and discussion

The numerical data calculated depends on the HyperChem program utilised and can only be used for comparison, for example, to determine trends with data obtained under identical conditions. The following information was recorded from the semi-empirical calculations performed as stated.

With respect to the neutral molecules, the charges on the nitrogen atoms of the ammonia and HZ molecules were 0.006, and -0.074 respectively. On the MMH and UDMH molecules the nitrogen atoms with two hydrogen atoms attached had charges of -0.063 and -0.048 respectively. The effect of sequential methyl substitution was to

increase the magnitude of the negative charge on the methylated nitrogen from -0.074 to

-0.103 and -0.121 respectively, forcing the electron density to be greater on the nitrogen

with the methyl groups attached, and thereby rendering that nitrogen more basic. Figure

4.11 shows the stick representations of the hydrazines labelled with the relative charge.

The net charges calculated for the neutral ketone molecules and the protonated

monomer and dimer species are documented in Table 4.6.
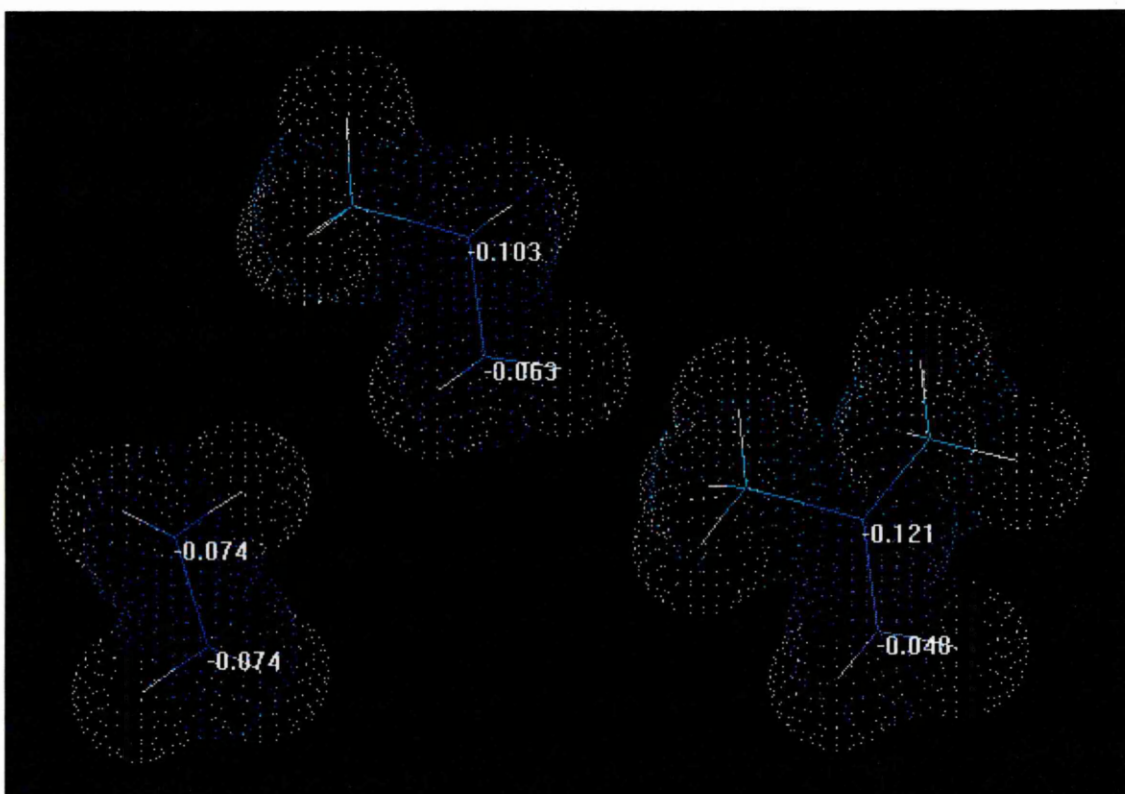
Figure 4.11: Relative charge distribution of the hydrazines' nitrogen atoms

As expected, the relative charges on the carbon and oxygen atoms of the

carbonyl group became more positive on protonation of the neutral molecule. The

charge on the carbon atoms decreased marginally on addition of the second ketone

molecule to the ion-molecule cluster (see Table 4.6), but the charge on the oxygen

atoms increased. With respect to the straight chain ketones, the average charge for the

carbonyl carbon atoms changed from 0.274 for the neutral molecule, to 0.398 for the

protonated monomer, and to 0.392 and 0.361 for the protonated dimer. The

corresponding oxygen atoms had charges of -0.310 (neutral), -0.076 (monomer), 0.128

and 0.427 (dimer).

Table 4.6: Net charges calculated for the carbon and oxygen atoms of the ketone carbonyl bonds

	Neutral molecule		Protonated monomer		Protonated dimer	
	C	O	C	O	C	O
Acetone	0.276	-0.314	0.422	-0.077	0.416	0.141
					0.372	0.437
3-pentanone	0.270	-0.307	0.384	-0.075	0.380	0.127
					0.356	0.423
4-heptanone	0.274	-0.310	0.396	-0.076	0.390	0.128
					0.360	0.426
5-nonanone	0.274	-0.309	0.395	-0.075	0.387	0.122
					0.358	0.423
6-undecanone	0.274	-0.310	0.395	-0.075	0.385	0.121
					0.358	0.426
2,4-Dimethyl-3-pentanone	0.274	-0.310	0.381	-0.064	0.376	0.110
					0.352	0.411
2,2,4,4-Tetramethyl-3-pentanone	0.281	-0.311	0.410	-0.081	0.392	0.105
					0.367	0.439
2,2,6,6-Tetramethyl-4-heptanone	0.288	-0.309	0.404	-0.089	0.376	0.084
					0.369	0.430
2,6-Dimethyl-4-heptanone	0.280	-0.315	0.412	-0.085	0.407	0.132
					0.368	0.435
2,8-Dimethyl-5-nonanone	0.279	-0.311	0.398	-0.084	0.392	0.133
					0.363	0.419

For the branched chain ketones, the corresponding net charges on the carbon

atoms were 0.280 (neutral), 0.401 (monomer), 0.389 and 0.364 (dimer); the net charges

on the corresponding oxygen atoms were -0.311 (neutral), -0.084 (monomer), 0.113 and

0.427 (dimer). The trend was for the carbonyl to become more positively charged in the

monomer and dimer, while the electron density of the oxygen atom decreased from the neutral ketone to the protonated monomer to the protonated dimer. (The trends are more significant than the absolute values.) One indication from these calculations was that the second ketone molecule in the dimer ion-molecule was not so strongly attracted as the first.

It was decided to continue the HyperChem geometry optimisation of ion-molecule clusters comprising the protonated ketones combined with the individual analytes. The maximum cross-sectional diameter of each of the previously optimised neutral molecules and these ion-molecule clusters was measured. These measurements were considered to be the effective size of the molecules and are recorded, for straight chain and branched chain species, in Table 4.7. The highlighted areas of the following tables indicate that HyperChem calculations were not performed for that particular ion-molecule cluster. These calculations were set up with neutral analyte molecules placed in the vicinity of a protonated ketone cluster.

The maximum diameters of the neutral molecules of ammonia and the three hydrazines of interest were also measured through use of the software. The empirical results obtained (see Chapter 4, part 1) showed these analytes to have mobilities in the reverse order to those predicted. The expected order would be ammonia > HZ > MMH > UDMH, based upon their respective cross sectional diameters of 1.6176 Å, 2.7781 Å, 4.0568 Å, and 4.2379 Å. The order of mobility was assumed to be affected by the characteristics of the ion-molecule clusters formed. The formation of ion-molecule clusters with equivalent numbers of ketone molecules should increase correspondingly and, therefore, should not affect the order of mobility. Thus, the assumption was that different numbers of ketone molecules were involved in the formation of the ion-molecule clusters for this series of analytes.

Table 4.7: Maximum diameters (Å) of neutral and protonated straight and branched chain ketones, and ion-molecule clusters comprising ammonia, and the hydrazines with ketones

	K	H⁺K	H⁺AK	H⁺HZK	H⁺MK	H⁺UK	H⁺K₂	H⁺AK₂	H⁺HZK₂	H⁺MK₂	H⁺UK₂	H⁺K₃
Acetone	4.3458	3.8859	6.3758	8.4583	7.7131	7.70520	8.5067	8.4077	8.3792	9.0156	8.4251	8.4130
3-Pentanone	6.8521	6.8628	7.0103	7.0520			10.0350	10.0322	11.0855			8.9536
4-Heptanone	9.3870	9.3934	9.3996	9.3945			11.7364	11.8845	11.7522			
5-Nonanone	11.8709	11.8674	11.8649	11.8594			12.7657	11.8600	12.7178			
6-Undecanone	14.4052	14.4110	14.4095	14.4099			14.3924	-	14.3817			
2,4-Dimethyl-3-pentanone	6.8527	6.8654	7.64016	7.4307			10.2256	10.2128	10.2107			8.4130
2,2,4,4-Tetramethyl-3-pentanone	6.9790	6.9504	7.8302	7.6255			9.8579	10.3987	10.5854			8.95363
2,2,6,6-Tetramethyl-4-heptanone	9.4190	9.4340	9.4199	9.3771			10.3604	10.7264	12.3417			
2,6-Dimethyl-4-heptanone	8.8247	8.7643	8.7705	8.7316			11.6499	12.2450	11.5963			
2,8-Dimethyl-5-nonanone	11.8786	11.8847	11.8524	11.8807			13.9698	14.5822	13.6771			

K = ketone; H⁺ = proton; A = ammonia; HZ = hydrazine, M = methylhydrazine; U = 1,1-dimethylhydrazine

A model hypothesised by Stone[203] suggested that, in the absence of gas phase reactions of the ketones and the hydrazines, the predicted number of ketone molecules per ion cluster would be four for the ammonia analyte, three for HZ, two for MMH, and one for UDMH.

Protonated ammonia has four hydrogen atoms attached to the nitrogen. These hydrogen atoms can attract the oxygen atom of a ketone carbonyl group through hydrogen bonding.

The HZ molecule is symmetrical, with an equivalent charge on each of the two nitrogen atoms. On protonation, the basicity of one of the nitrogen atoms increases with respect to the other. The three hydrogen atoms attached to this nitrogen can each attract the oxygen atom of a ketone carbonyl group.

In MMH, the presence of a methyl group increases the basicity of the methylated nitrogen atom, through the inductive effect, to which the proton would be attracted preferentially. Two ketone molecules would be attracted to the two hydrogens associated with the methylated nitrogen in protonated MMH.

In the UDMH molecule, the presence of two methyl groups on the same nitrogen further increases the basicity of the methylated nitrogen atom, compared with MMH. Protonation at this nitrogen permits the attraction of one molecule of ketone.

Additional computations were performed for the predicted clusters according to the Stone model. If the model holds then the effective diameter of the ion-molecule clusters is $H^+(ammonia)(K)_4 > H^+(HZ)(K)_3 > H^+(MMH)(K)_2 > H^+(UDMH)(K)$, where K is a ketone (see Table 4.8). These optimisations were performed by modelling the protonated analyte and placing neutral ketone molecules with the carbonyl group in close proximity to the protonated nitrogen atom. The measured diameters of the above series of computed ion-molecules, for an acetone doped system, were 10.5689 Å,

10.3399 Å, 9.6289 Å, and 7.7678 Å respectively. The consecutive differences between

the diameters were 0.229 Å, 0.711 Å, and 1.861 Å. The closer values of the ammonia

and HZ ion-molecules clusters, with four and three molecules of ketone respectively

might account for the insufficient resolution of the ammonia and HZ product ion peaks.

Table 4.8: Maximum diameters (Å) of ion-molecule clusters

	H^+AK_4	H^+HZK_3	H^+MK_2	H^+UK
Acetone	10.5689	10.3399	9.6289	7.7678
3-Pentanone	11.7665	11.9349	10.7395	8.3737
4-Heptanone	14.1747	13.5557	12.5791	9.3936
5-Nonanone	15.7262	14.7810	13.3410	11.8724
6-Undecanone	18.6819	16.3980	15.6212	14.4093
2,4-Dimethyl-3-pentanone	12.6728	12.5194	12.7773	8.8990
2,2,4,4-Tetramethyl-3-pentanone	13.6244	12.5223	12.9903	8.7559
2,2,6,6-Tetramethyl-4-heptanone	14.4496	13.3539	14.1374	9.4273
2,6-Dimethyl-4-heptanone	13.9506	13.7382	12.8044	9.3252
2,8-Dimethyl-5-nonanone	16.6692	14.9867	15.1096	11.8573

The UDMH product ion peak was found, empirically, in the acetone doped

system, to occur before the RIP i.e. it was of higher mobility. The RIP occurred before

the remainder of the product ion peaks. This would indicate that the RIP might consist

of either the protonated dimer of acetone (diameter 8.5067 Å) and / or the protonated

acetone trimer ion (diameter 8.4130 Å), each of which is larger than the computed

UDMH product ion cluster (7.7678 Å) (see Tables 4.7 and 4.8). Additionally to the

tabulated values, the diameter of the tetramer ion of acetone H^+K_4 (9.4587 Å) was

determined and indicates that it would occur after the trimer ketone / MMH ion-molecule cluster, $H^+(MMH)K_3$. This conflicts with the ion mobility data and further supports the assumption that the RIP consists of the protonated dimer and trimer ketone clusters.

The 5-nonanone dopant was shown empirically to be satisfactory for resolution of the analyte peaks from the RIP, and for resolution of the analyte peaks from each other, with the exception of the ammonia and HZ product ion peaks, which were only partially resolved. Examination of the computed cluster diameters has revealed that, as with the acetone doped system, there is little difference between the H^+AK_4 and $H^+(HZ)K_3$, 15.7262 Å and 14.7810 Å respectively. The close values of the corresponding ammonia and HZ product ion cluster molecules might account for the minimal resolution observed.

The ion-molecule clusters for the series $H^+(ammonia)(K)_4$, $H^+(HZ)(K)_3$, $H^+(MMH)(K)_2$, and $H^+(UDMH)(K)$, where K is 4-heptanone, are shown in Figure 4.12.

Applying the same principles to the ion-molecule clusters formed with the branched chain symmetrical ketones, in many cases the differences in effective diameters are more pronounced. It might be considered that the differences in diameter may be sufficient to effect resolution of the ammonia and HZ analytes, however steric hindrance could prove problematical. With reference to Table 4.8, the greatest difference in the relevant cluster diameters were those obtained for the 2,8-dimethyl-5-nonanone and 6-undecanone. Further examination of Table 4.8 indicates that with the branched chain ketones, there are only small differences in the diameters of the MMH and HZ clusters, suggesting that although HZ and ammonia might be resolved by mobility, MMH and HZ might not. 6-Undecanone gives the most uniform difference for

all the hydrazines and ammonia, but might be difficult to generate in sufficient concentrations to effect mobility separation.
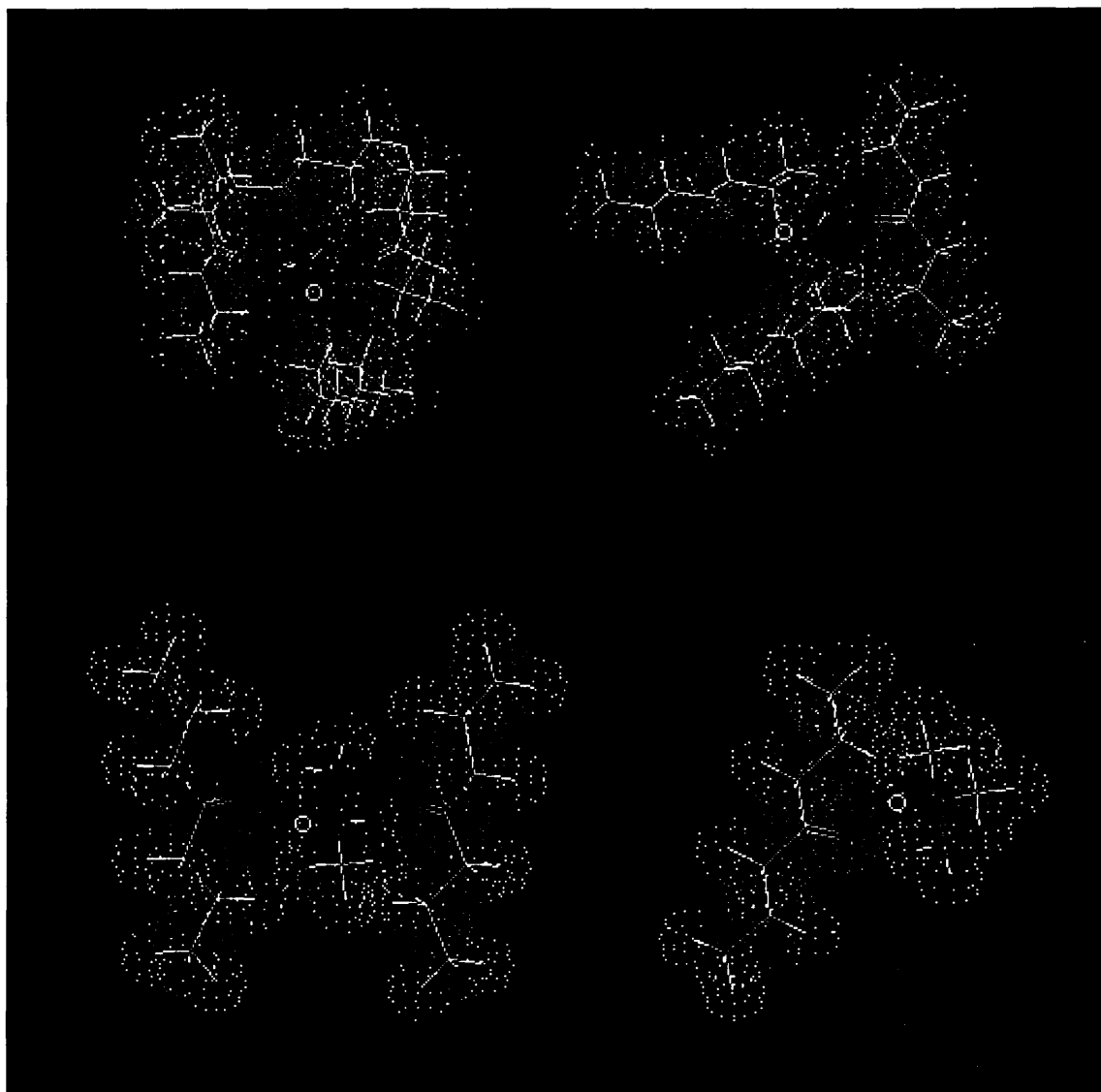
Figure 4.12: The ion-molecule clusters for the series H^+(ammonia)(K)$_4$, H^+(HZ)(K)$_3$, H^+(MMH)(K)$_2$, and H^+(UDMH)(K), where K is 4-heptanone

In order to evaluate the validity of these assumptions, derived from the computational chemistry, it was decided to investigate the composition of the ion-molecule clusters through the use of IMS-MS-MS.

Chapter 4

Part 3

Ion mobility spectrometry coupled with tandem mass spectrometry

- a study of ion-molecule chemistry

4.11 IMS-MS-MS

The IMS-MS-MS analysis was performed in order to determine the composition of the ion-molecule clusters formed in the ionisation and drift regions of the ion mobility spectrometer and which would normally be transported to the collector electrode of an ion mobility spectrometer (IMS). With the Faraday plate removed, the ion-molecules passed through the IMS into a tandem MS system, via a pinhole. The first of the two mass spectrometers was used to record the complete spectrum of ion-molecules of mass to charge ratio, m/z, in the range 1 to 500 atomic mass units (amu) although, generally, the range was limited to 450 amu. Peaks of sufficient intensity were subjected to MS-MS and targeted for analysis in the second mass spectrometer. The ion density of the sample species was important; the ion current reaching the mass spectrometer[121] had to be sufficient to enable identification of the ion clusters to be made through MS-MS analysis. The product ion spectrum recorded the ion-molecule cluster and the product ions as the cluster dissociated. From this data, and the knowledge of chemicals introduced into the system, the compositions of the ion-molecules clusters were determined.

The hydrazines of interest so far have been HZ, MMH, and UDMH. In order to test the Stone model more thoroughly, TMH was included with the other hydrazines and

ammonia as analytes for IMS-MS-MS analysis. The prior discussion (see section 4.10), concerning the probable protonation sites and numbers of ketone molecules attached, was extended to include TMH. This fully methyl substituted hydrazine is a symmetrical molecule and, as with HZ, either nitrogen atom would be susceptible to protonation, and so one ketone molecule would be attached to the single proton on TMH.

The ketones used in the study were those in the homologous series of symmetrical ketones C_3 to C_9 i.e. acetone to 5-nonanone. 5-Nonanone was set as the upper limit due to the range restrictions of the mass spectrometer. Additionally, it was decided to investigate the effects of an electron withdrawing group upon the formation of ion-molecule clusters. The chemical chosen for this part of the investigation was 1,1,1-trifluoroacetone.

The following results have been divided into separate sections for each analyte and further divided into sub-sections for each ketone and analyte system. For the first stage of the experiments only the source region of the ion mobility spectrometer was doped with ketone, whereas for the second stage both the source and drift regions were doped with the same ketone simultaneously. For ease of identification, these two configurations are subsequently referred to as source region doped and drift region doped.

Calibration of the MS-MS system showed that the recorded m/z values were accurate to ± 1 amu for the majority of the research, but sometimes drifted to ± 2 amu. Therefore, some values which appear on the following mass spectra appear to differ slightly from the tabulated results which have been corrected according to the relevant calibration. The tables of results list the peaks in order of intensity rather than numerical order. Precursor ions marked with an asterisk denote ion-molecule clusters for which product ion spectra could not be obtained due to insufficient peak intensity.

Since the dopant and analyte for each experiment were known, and Product ion

spectra provided proof of ion-molecule identity, cluster ions formed from analytes not

introduced in a given experiment were assumed to be residual from previous test runs.

The system was cleaned between experiments, however, the surface active hydrazines

proved problematical for complete removal from the ion mobility cell. All of the

experiments were repeated to ensure that the results were reproducible and to confirm

the presence of previously assigned, or expected, ion-molecule clusters. In order to

reduce the amount of residual contamination, two ion mobility cells were used in

sequence, one being cleaned whilst the other was in use. Steam cleaning was eventually

found necessary to clean the ion mobility cells. However, concurrent with the evolution

of this cleaning process there were some minor contaminants recorded during

experiments. Although mentioned in the text these contaminant peaks have not been

recorded in tabulated data in an effort to clarify the true constitution of the ion chemistry

for any given combination of analyte and dopant.

4.12 Proton bound clusters of ketones and ammonia

4.12.1 Acetone / ammonia ion chemistry

IMS-MS spectra of the undoped system showed major protonated water clusters at m/z

values of 37, 55, 73, and 91 corresponding to $H^+(H_2O)_n$, where n = 2 to 5 consecutively.

The addition of ammonia to the system produced clusters at m/z values of 18, 36, 54,

and 72, corresponding to $NH_4^+(H_2O)_n$ where n = 0 to 3. On the introduction of acetone

into the source region of the IMS, the observed major ions were those comprising

protonated combinations of acetone and ammonia, as recorded in Table 4.9. The

corresponding mass spectrum is shown in Figure 4.13.

Table 4.9: Summary of ammonia / acetone ion chemistry; source region doped

Precursor Ion		MS-MS Product Ions					
134	$NH_4^+(C_3H_6O)_2$	76	$NH_4^+(C_3H_6O)$	59	$H^+(C_3H_6O)$	18	NH_4^+
76	$NH_4^+(C_3H_6O)$	59	$H^+(C_3H_6O)$				
93	$H^+(NH_3)_2(C_3H_6O)$	76	$NH_4^+(C_3H_6O)$	35	$H^+(NH_3)_2$		
117	$H^+(C_3H_6O)_2$	59	$H^+(C_3H_6O)$				
59	$H^+(C_3H_6O)$						
18	NH_4^+						

+Profile Q1SCAN

run no 847

run no 847 - 6/10/96 - 1:53 PM
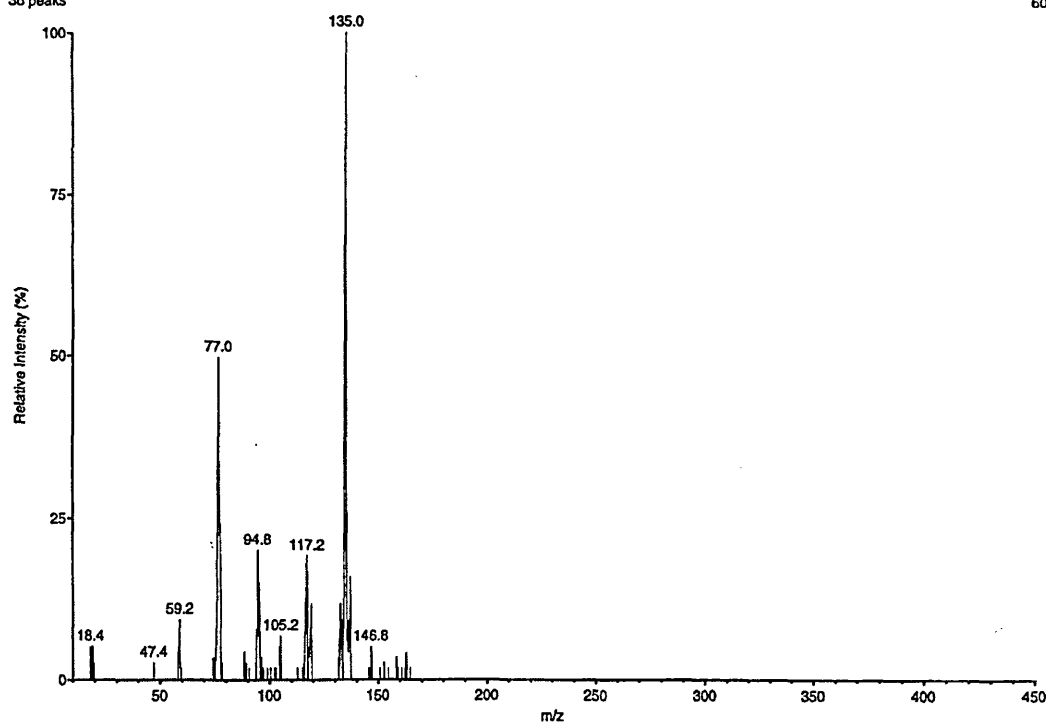No Title

36 peaks

60,500

Figure 4.13: Mass spectrum of the ion species produced from ammonia with an acetone doped source region

These results were consistent with acetone and ammonia having greater proton affinities than that of water, 812, 854, and 691 kJ.mol^{-1} respectively. The intensity of the peaks for the ion-molecule clusters comprising both ammonia and acetone indicated their

predominance. Ammonia with the highest proton affinity preferentially attracted protons and subsequently molecules of the ketone. The greater intensity of the dimer ion over the monomer ion of acetone indicated that the dimer would probably predominate over the monomer in the RIP, in the mobility spectrum.

Peaks at m/z values of 47, 105, and 147 were assigned formulae which involved contaminants, $H^+(N_2H_3CH_3)$, $H^+(N_2H_3CH_3)(C_3H_6O)$, and $H^+(N_2(CH_3)_4)(C_3H_6O)$ respectively.

With the IMS doped from the drift region the number of molecules per ion cluster increased. The predominant ions were the $H^+(C_3H_6O)_n$ series where n = 3 or 2, and the $NH_4^+(C_3H_6O)_n$ series where, again, n = 3 or 2. The $NH_4^+(C_3H_6O)_4$ ion, of m/z 250, was present at a low intensity. During the summation of spectra, ratios of peak intensities changed until an equilibrium was reached. In this experiment, a transient indication of the tetramer ion of acetone was also seen at the m/z value of 233. The results are listed in Table 4.10, and the product ion spectrum for the ion cluster at m/z 192 is shown in Figure 4.14. The MS-MS analysis indicated the higher proton affinity of ammonia; molecules of ketone dissociated from the ion-molecule cluster to leave the ammonium ion.

Table 4.10: Summary of ammonia / acetone ion chemistry; drift region doped

Precursor Ion		MS-MS Product Ions					
175	$H^+(C_3H_6O)_3$	117	$H^+(C_3H_6O)_2$	59	$H^+(C_3H_6O)$		
117	$H^+(C_3H_6O)_2$	59	$H^+(C_3H_6O)$				
192	$NH_4^+(C_3H_6O)_3$	134	$NH_4^+(C_3H_6O)_2$	76	$NH_4^+(C_3H_6O)$	18	NH_4^+
134	$NH_4^+(C_3H_6O)_2$	117	$H^+(C_3H_6O)_2$				
76	$NH_4^+(C_3H_6O)$	59	$H^+(C_3H_6O)$	18	NH_4^+		
59	$H^+(C_3H_6O)$						
250	$NH_4^+(C_3H_6O)_4$	192	$NH_4^+(C_3H_6O)_3$	134	$NH_4^+(C_3H_6O)_2$	76	$NH_4^+(C_3H_6O)$
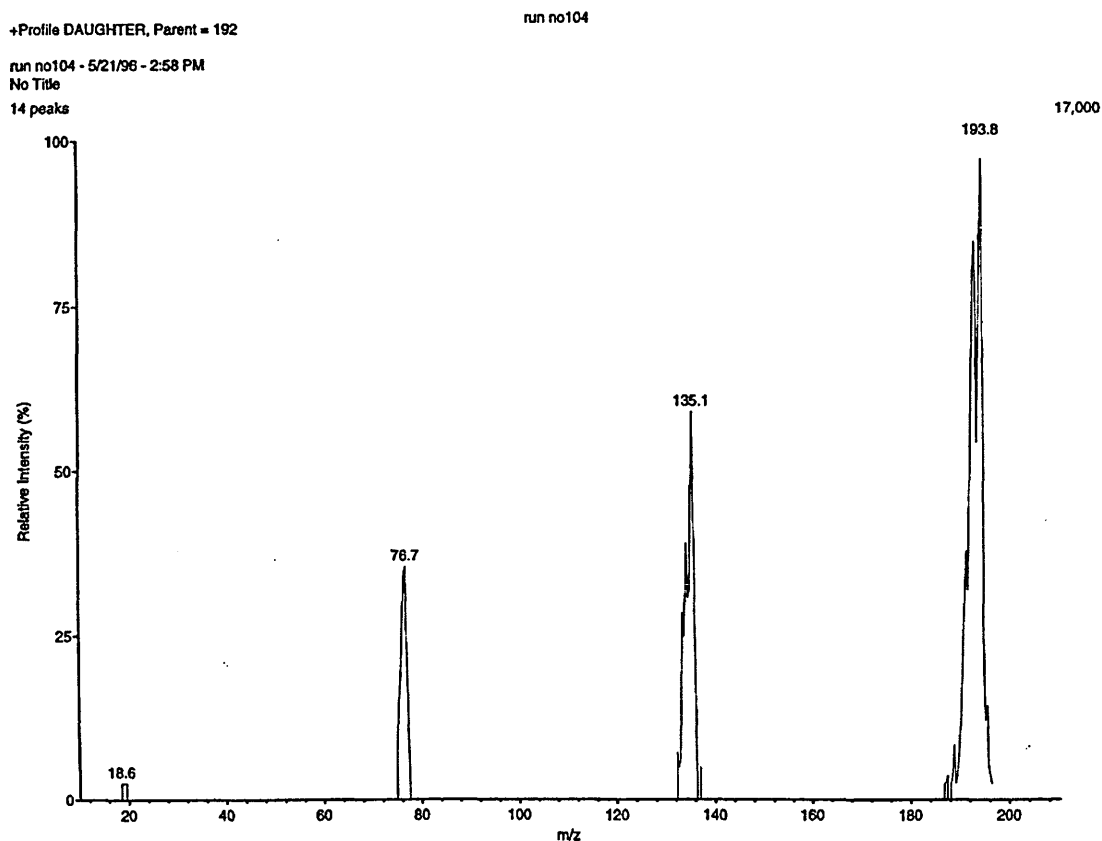
Figure 4.14: Product ion mass spectrum of the ammonia / acetone ion-molecule cluster at m/z 192

4.12.2 3-Pentanone / ammonia ion chemistry

In the presence of ammonia, the doping of the source region with 3-pentanone resulted

in the formation of the protonated monomer and dimer ions of the ketone. Ion-molecule

clusters were formed from the combination of an ammonium ion with either one or two

molecules of the 3-pentanone, and two molecules of ammonia combined with one

molecule of the ketone. A high intensity ion at m/z 133 was due to the presence of

MMH as a contaminant, combined with a molecule of 3-pentanone. An ion cluster at

m/z 161, which could not be identified at that time, was also observed. There was also

TMH contamination present, which led to further ion-molecule clusters. The results are

listed in order of peak intensity in Table 4.11.

Table 4.11: Summary of ammonia / 3-pentanone ion chemistry; source region doped

Precursor Ion		MS-MS Product Ions			
104	$NH_4^+(C_5H_{10}O)$	18	NH_4^+		
87	$H^+(C_5H_{10}O)$				
190	$NH_4^+(C_5H_{10}O)_2$	104	$NH_4^+(C_5H_{10}O)$	18	NH_4^+
173	$H^+(C_5H_{10}O)_2$	87	$H^+(C_5H_{10}O)$		
121	$H^+(NH_3)_2(C_5H_{10}O)$	35	$H^+(NH_3)_2$		
18	NH_4^+				
35	$H^+(NH_3)_2$	18	NH_4^+		

As the analyte and ketone, and therefore their relative masses, were known composition of the ion-molecule clusters could be estimated. An ion recorded at approximately m/z 190, in the original mass spectrum, was subjected to MS-MS analysis in order to determine whether the peak was due to the combination of ammonia with two molecules of 3-pentanone. It was also possible that the peak was due to carry over of the $NH_4^+(C_3H_6O)_3$ ion, m/z 192, from the previous experiment. Calibration of the mass spectrometers confirmed the true m/z values from which assigned identities were validated. The precursor and resultant product ions provided information about the mass differences caused by the dissociation of the ion ion-molecule cluster. The product ion spectrum (Figure 4.15) of the ion-molecule cluster confirmed the identity of the ion-molecule cluster as $NH_4^+(C_5H_{10}O)_2$. This emphasised the importance of the MS-MS analysis.

The doping of the drift region produced larger cluster ions, as shown in Figure 4.16 and detailed in Table 4.12, with the emergence of the trimer ketone ion (m/z 259). Again, the predominant ions were the ammonia / ketone clusters. There was a trace peak of the $NH_4^+(C_5H_{10}O)_4$ ion at m/z 362.
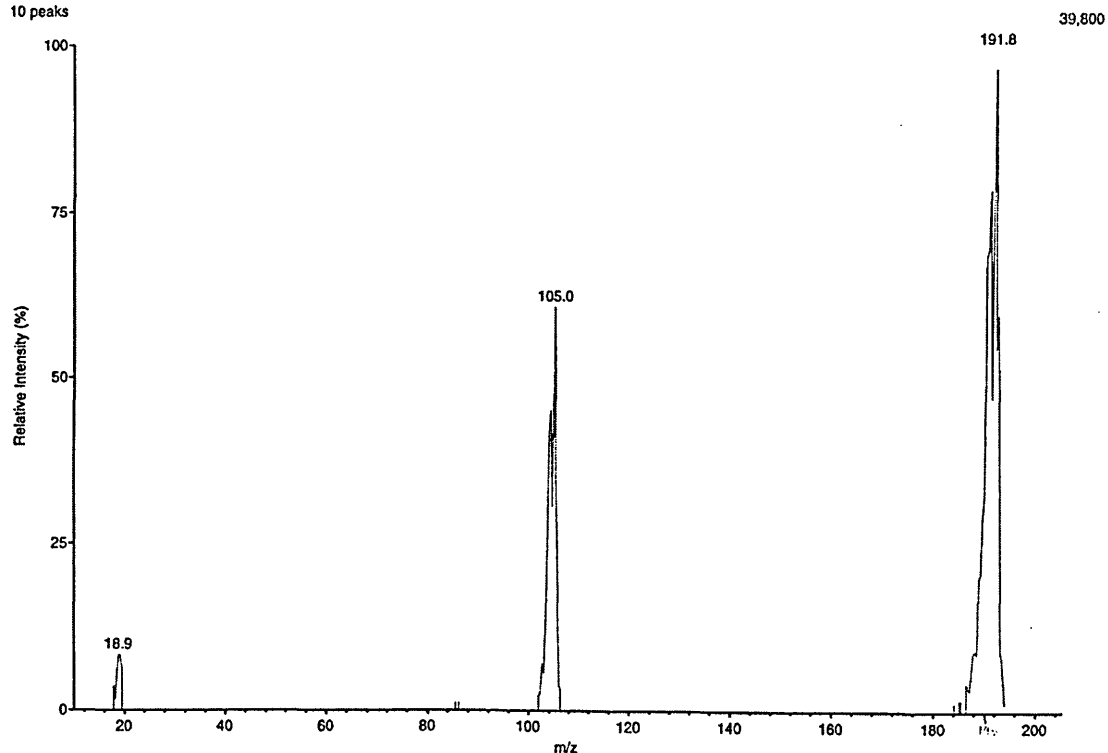
Figure 4.15: Product ion mass spectrum of the ammonia / 3-pentanone ion-molecule cluster at m/z 190
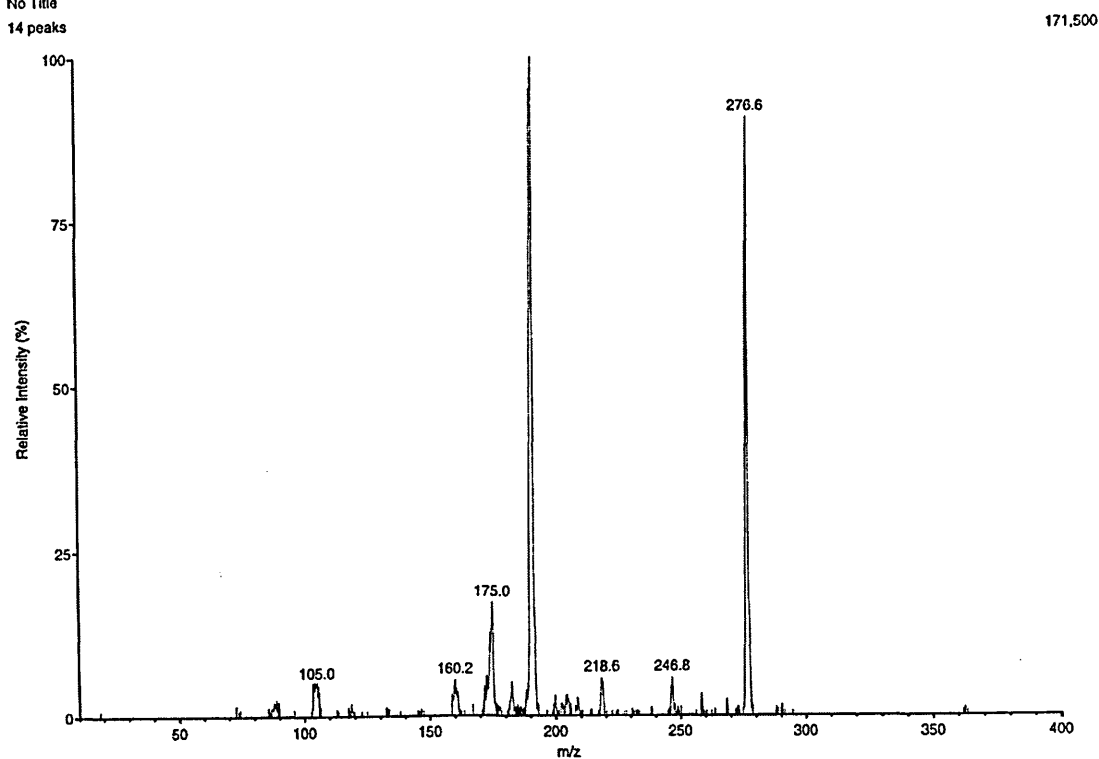
Figure 4.16: Mass spectrum of the ion clusters formed from ammonia with the 3-pentanone doped drift region

Table 4.12: Summary of ammonia / 3-pentanone ion chemistry; drift region doped

Precursor Ion		MS-MS Product Ions					
190	$NH_4^+(C_5H_{10}O)_2$	104	$NH_4^+(C_5H_{10}O)$	18	NH_4^+		
276	$NH_4^+(C_5H_{10}O)_3$	190	$NH_4^+(C_5H_{10}O)_2$	104	$NH_4^+(C_5H_{10}O)$	18	NH_4^+
173	$H^+(C_5H_{10}O)_2$	87	$H^+(C_5H_{10}O)$				
104	$NH_4^+(C_5H_{10}O)$	18	NH_4^+				
87	$H^+(C_5H_{10}O)$						
*259	$H^+(C_5H_{10}O)_3$						
*362	$NH_4^+(C_5H_{10}O)_4$						
18	NH_4^+						

*Confirmation of ion-molecule composition by MS-MS analysis was unavailable due to insufficient intensity of the precursor ion peak

A repeat experiment resulted in a change in the order of peak intensities to m/z 276 > 173 >190 > 362 > 259. This might have been due to a change in contamination levels which could have affected the ion-molecule chemistry and / or the difficulty in reproducing exactly the same dopant concentration in repeat experiments.

Peaks at m/z values of 161, 219, and 247 were also observed. Although it was stated previously that the ion at m/z 161 could not be identified, the first two of these ion-molecule clusters could be explained after experiments involving the hydrazines. The explanation of the reaction and ion-molecule clustering follows in subsequent section 4.13.1. These ion-molecule clusters were assigned the formulae $H^+(C_6H_{14}N_2)(N_2H_3CH_3)$, and $H^+(N_2H_3CH_3)(C_5H_{10}O)$. It was also possible that the third of these peaks might have represented an ion-molecule cluster such as $H^+(C_6H_{14}N_2)(N_2H_3CH_3)(C_5H_{10}O)$ but no other ion clusters of this complexity were recorded and the peak was too low in intensity for MS-MS analysis to provide an answer.

4.12.3 4-Heptanone / ammonia ion chemistry

The mass spectrum of ion-molecule clusters formed in the presence of ammonia in an

IMS with a 4-heptanone doped source region is shown in Figure 4.17. The identity of

the predominant ion, namely $H^+(NH_3)_2(C_7H_{14}O)$, was confirmed by the product ion

spectrum shown in Figure 4.18.

+Profile Q1SCAN

run no 868 - 6/10/98 - 6:50 PM
No Title
24 peaks

run no 868

143,000
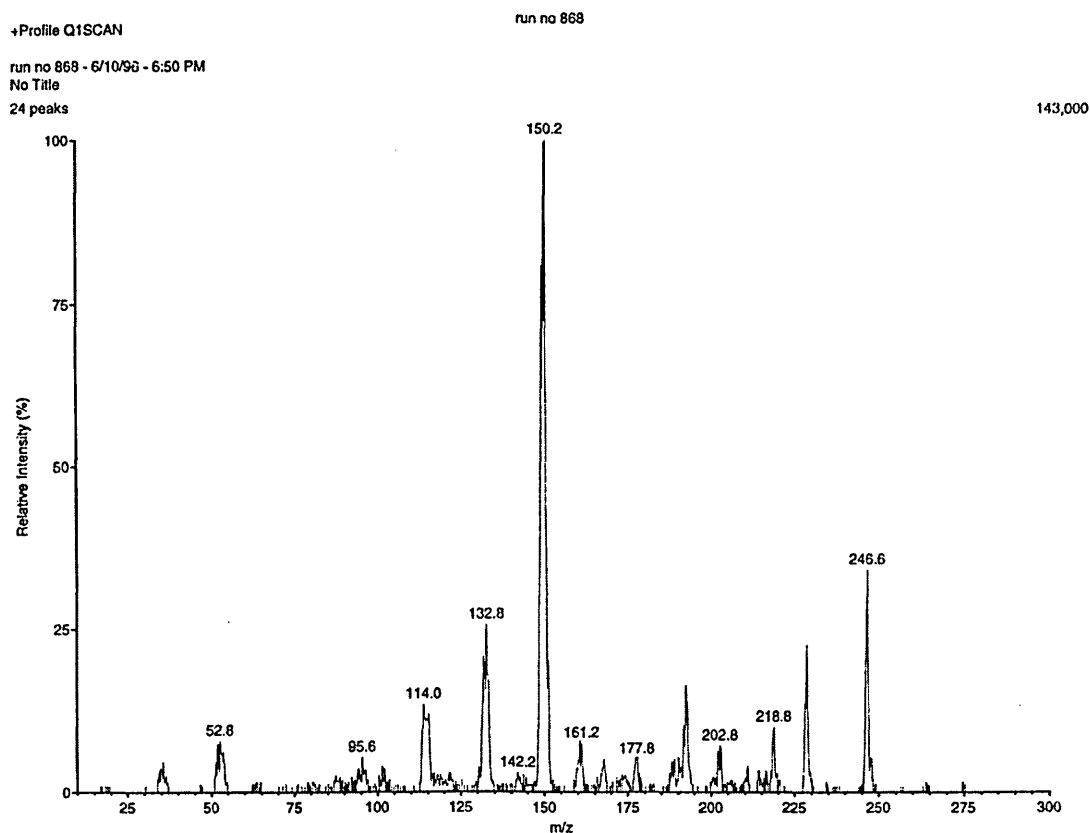
Figure 4.17: Mass spectrum of the ion clusters formed from ammonia with the
4-heptanone doped source region

Other peaks in the profile mass spectrum were attributed to $NH_4^+(C_7H_{14}O)_2$,

$NH_4^+(C_7H_{14}O)$, $H^+(C_7H_{14}O)_2$, $H^+(C_7H_{14}O)$, and either $NH_4^+(H_2O)_2$ and $NH_4^+(H_2O)$ or

$H^+(NH_3)_3$ and $H^+(NH_3)_2$ ion-molecule clusters, depending on the accuracy of the

calibration. The ion clusters were probably those consisting of protonated ammonia

clusters rather than ammonia / water clusters because of the greater proton affinity and

relatively high concentration of ammonia. The precursor and product ions are recorded in Table 4.13.

The difference of 17 amu from 149 to 132 corresponded to the loss of one ammonia molecule from the precursor $H^+(NH_3)_2(C_7H_{14}O)$ ion-molecule cluster. The decrease from 149 to 35 represented the loss of the ketone molecule from the precursor ion cluster. The ion recorded at m/z 18 was the ammonium ion. Thus, the precursor ion $H^+(NH_3)_2(C_7H_{14}O)$ dissociated into $NH_4^+(C_7H_{14}O)$, $H^+(NH_3)_2$, and NH_4^+ product ions.

+Profile DAUGHTER, Parent = 150

run no 871

run no 871 - 6/10/96 - 6:58 PM
No Title

19 peaks

8000
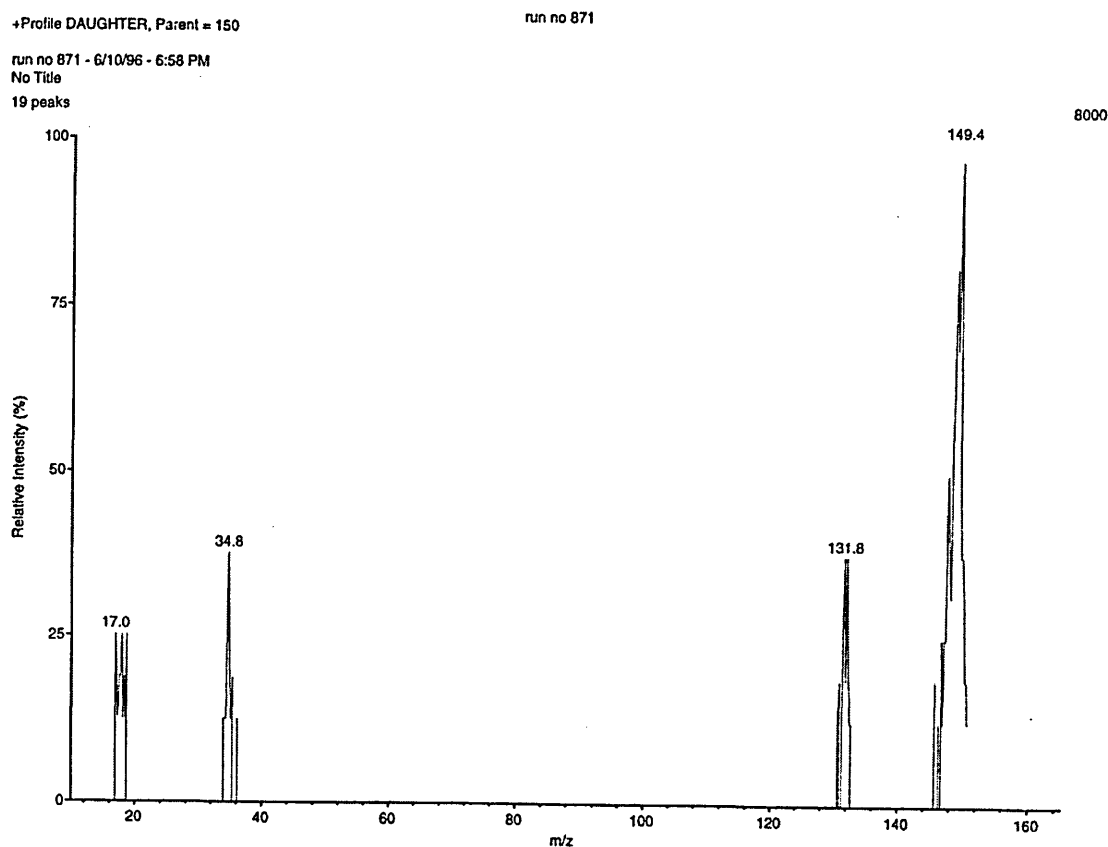
Figure 4.18: Product ion mass spectrum of the ammonia / 4-heptanone ion-molecule cluster at m/z 149

Table 4.13: Summary of ammonia / 4-heptanone ion chemistry; source doped region

Precursor Ion		MS-MS Product Ions					
149	$H^+(NH_3)_2(C_7H_{14}O)$	132	$NH_4^+(C_7H_{14}O)$	35	$H^+(NH_3)_2$	18	NH_4^+
246	$NH_4^+(C_7H_{14}O)_2$	132	$NH_4^+(C_7H_{14}O)$	18	NH_4^+		
132	$NH_4^+(C_7H_{14}O)$	18	NH_4^+				
229	$H^+(C_7H_{14}O)_2$	115	$H^+(C_7H_{14}O)$				
115	$H^+(C_7H_{14}O)$						
52	$H^+(NH_3)_3$	35	$H^+(NH_3)_2$	18	NH_4^+		
35	$H^+(NH_3)_2$	18	NH_4^+				
18	NH_4^+						

In Figure 4.15, 3-pentanone molecules dissociated from the ion cluster to leave protonated ammonia. The difference between the proton affinity of ammonia and 3-pentanone was 17.2 $kJ.mol^{-1}$. The difference in the 4-heptanone and ammonia system was only 8.5 $kJ.mol^{-1}$. However, the ketone molecule dissociated from the ion-molecule cluster to leave the dimer ion of ammonia, which further dissociated to form the analyte monomer.

The peaks at m/z values of 96, 143, 161, 178, 203, and 219 were assumed to have resulted from contamination. Not all of the peaks could be assigned a formula. The ion at m/z 143 was thought to be the protonated reaction product of 4-heptanone and MMH, and the cluster at m/z 161 an MMH / 4-heptanone ion cluster.

It was disconcerting to observe peaks at m/z values of 161, 219, and 247, in case the contaminants were carried over from the 3-pentanone / ammonia experiments. MS-MS analysis of the ion at m/z 247 confirmed the loss of 114 amu from a precursor ion of 246 amu, but as this was the molecular mass of both the 3-pentanone hydrazone and the 4-heptanone the identity of the ion-molecule could not be confirmed. It might have been

possible for the peak to comprise both $H^+(C_6H_{14}N_2)(N_2H_3CH_3)$ and

$H^+(N_2H_3CH_3)(C_7H_{14}O)$ clusters. On close inspection of Figure 4.17, a trace of the

3-pentanone was observed at m/z 87. However, the greater concentration and higher

proton affinity of 4-heptanone was an indication of the possible composition tending

towards the latter formula.

The ion at m/z 178 was assigned the formula $NH_4^+(N_2H_3CH_3)(C_7H_{14}O)$. The

TMH ion was present at m/z 89. Therefore, it was assumed that the peak at m/z 203 was

produced by the $H^+(N_2(CH_3)_4)(C_7H_{14}O)$ ion cluster. The peaks at m/z values 96 and 193

could not be explained.

Doping the IMS through the drift region formed the additional cluster at m/z 360

which was assumed to be $NH_4^+(C_7H_{14}O)_3$. A trace of $H^+(C_7H_{14}O)_3$ was recorded at m/z

343. The predominant ion cluster was $NH_4^+(C_7H_{14}O)_2$. The results are summarised in

Table 4.14. Contamination peaks similar to those in the source-doped tests were

recorded.

Table 4.14: Summary of ammonia / 4-heptanone ion chemistry; drift region doped

Precursor Ion		Product Ions					
246	$NH_4^+(C_7H_{14}O)_2$	132	$NH_4^+(C_7H_{14}O)$	18	NH_4^+		
132	$NH_4^+(C_7H_{14}O)$	18	NH_4^+				
229	$H^+(C_7H_{14}O)_2$	115	$H^+(C_7H_{14}O)$				
115	$H^+(C_7H_{14}O)$						
149	$H^+(NH_3)_2(C_7H_{14}O)$	132	$NH_4^+(C_7H_{14}O)$	35	$H^+(NH_3)_2$	18	NH_4^+
360	$NH_4^+(C_7H_{14}O)_3$	246	$NH_4^+(C_7H_{14}O)_2$				
343	$H^+(C_7H_{14}O)_3$	229	$H^+(C_7H_{14}O)_2$	115	$H^+(C_7H_{14}O)$		

The higher ketone concentration favoured the formation of ion-molecule clusters with one molecule of ammonia rather than two. There was evidence that ammonia formed ion-molecule clusters with three molecules of ketone but not four. The air flow rates forced across the analyte and dopant chemicals were not altered, and because of the decrease in vapour pressure ascending the homologous series of symmetrical ketones, it was probable that the ketone concentration decreased with each ketone through the series. The progressively lower concentrations would have led to the equilibrium not being forced so far to the right (see equations on page 45), and so would have favoured the formation of $NH_4^+(C_7H_{14}O)_n$ where n = 2 or 3 rather than 4. The formation of $NH_4^+(C_7H_{14}O)_5$ could not be tested as the m/z value of 586 was outside the mass spectrometer range.

4.12.4 5-Nonanone / ammonia ion chemistry

Doping of the source region with 5-nonanone in the presence of ammonia produced $NH_4^+(C_9H_{18}O)_2$, the predominant ion (see Figure 4.19 and Table 4.15) at more than four times the amplitude of any other peak in the spectrum. Two other ion peaks of lower intensity were assigned the formulae $NH_4^+(C_9H_{18}O)$ and $H^+(C_9H_{19}O)_2$. A peak at m/z 331 was attributed to $H^+(N_2H_3CH_3)(C_9H_{18}O)_2$ arising from contamination of the system with MMH from a prior experiment. It was also considered that the reaction of MMH with 5-nonanone resulted in the formation of 5-nonanone methylhydrazone, m/z 313, which clustered with MMH to form $H^+(C_{10}H_{22}N_2)(C_9H_{18}O)$, m/z 360.

There was a peak recorded at approximately m/z 187 which could have been attributed to either $H^+(N_2H_3CH_3)(C_9H_{18}O)$, m/z 189, or $NH_4^+(C_{10}H_{22}N_2)$, m/z 188. MS-MS analysis was not possible because of the low intensity of this and other contaminant peaks, so further postulation of their respective formulae was not attempted.
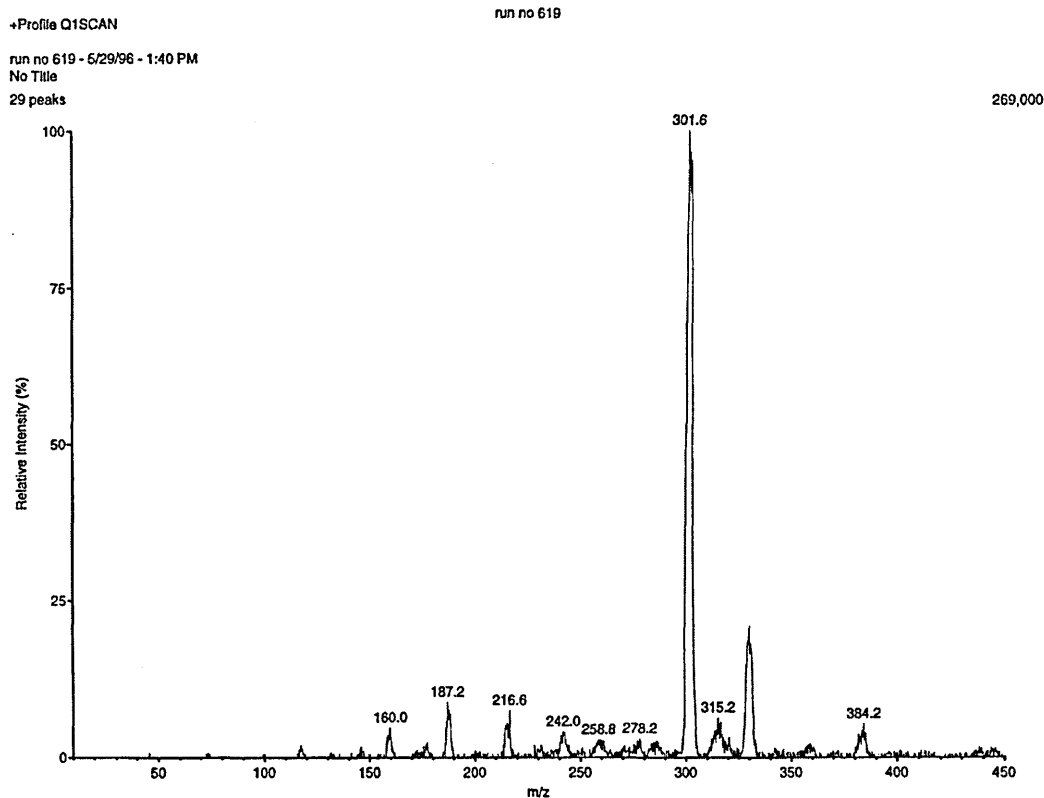
Figure 4.19: Mass spectrum of the ion clusters formed from ammonia with the 5-nonanone doped source region

Table 4.15: Summary of ammonia / 5-nonanone ion chemistry; source region doped

Precursor Ion		MS-MS Product Ions					
302	$NH_4^+(C_9H_{18}O)_2$	160	$NH_4^+(C_9H_{18}O)$	143	$H^+(C_9H_{18}O)$	18	NH_4^+
160	$NH_4^+(C_9H_{18}O)$	18	NH_4^+				
*285	$H^+(C_9H_{18}O)_2$						
177	$H^+(NH_3)_2(C_9H_{18}O)$	160	$NH_4^+(C_9H_{18}O)$	35	$H^+(NH_3)_2$	18	NH_4^+

*Confirmation of ion-molecule composition by MS-MS analysis was unavailable due to insufficient intensity of the precursor ion peak

During MS-MS analysis of the ion at m/z 160, the charge tended to stay preferentially with the ammonia rather than the ketone. This was an indication that ammonia had the greater proton affinity, but the difference was only 2.4 $kJ.mol^{-1}$.

Doping of the system via the drift region produced predominant ion clusters which corresponded to $H^+(C_9H_{18}O)_3$ and $NH_4^+(C_9H_{19}O)_3$ respectively (see Figure 4.20 and Table 4.16). The $H^+(C_9H_{18}O)_2$ cluster ion was also present.
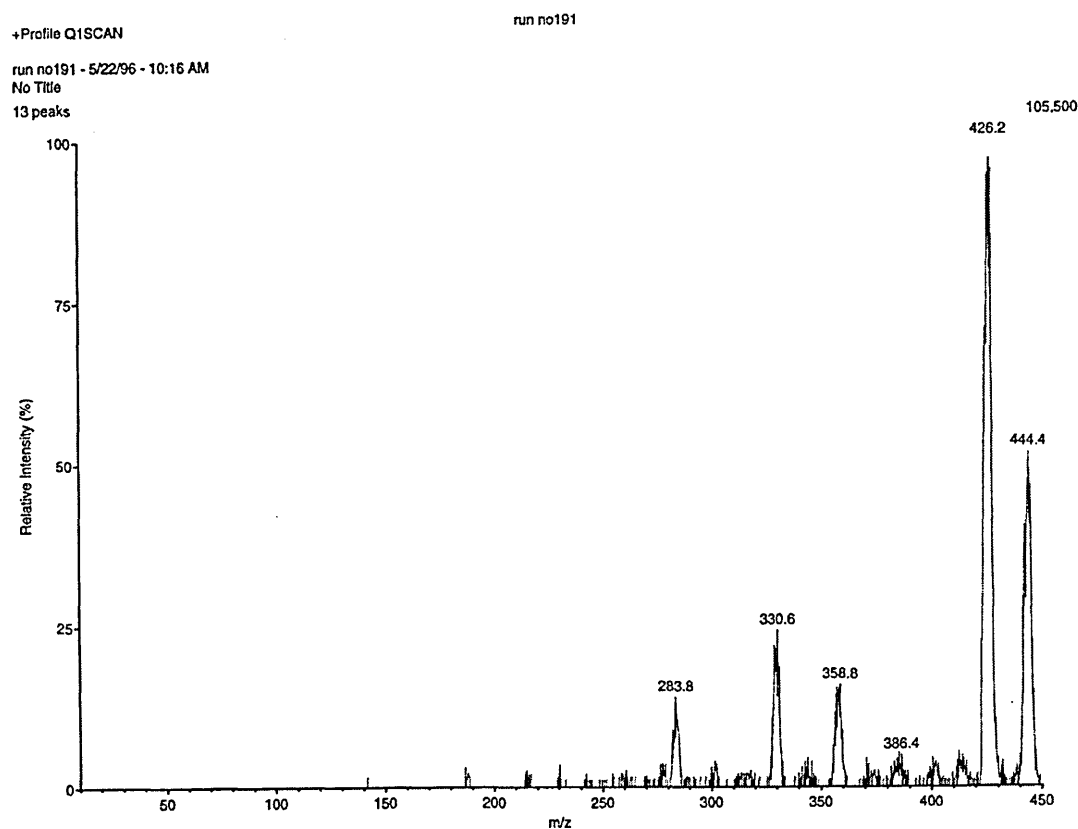
Figure 4.20: Mass spectrum of the ion clusters formed from ammonia with the 5-nonanone doped drift region

Table 4.16: Summary of ammonia / 5-nonanone ion chemistry; drift region doped

Precursor Ion		MS-MS Product Ions					
427	$H^+(C_9H_{18}O)_3$	285	$H^+(C_9H_{18}O)_2$	143	$H^+(C_9H_{18}O)$		
444	$NH_4^+(C_9H_{18}O)_3$	302	$NH_4^+(C_9H_{18}O)_2$				
*285	$H^+(C_9H_{18}O)_2$						
302	$NH_4^+(C_9H_{18}O)_2$	160	$NH_4^+(C_9H_{18}O)$	143	$H^+(C_9H_{18}O)$	18	NH_4^+

*Confirmation of ion-molecule composition by MS-MS analysis was unavailable

The MS-MS spectra for the ion-molecule clusters with m/z values 302 and 427 are

shown in Figures 4.21 and 4.22 respectively.

run no 612

12,000
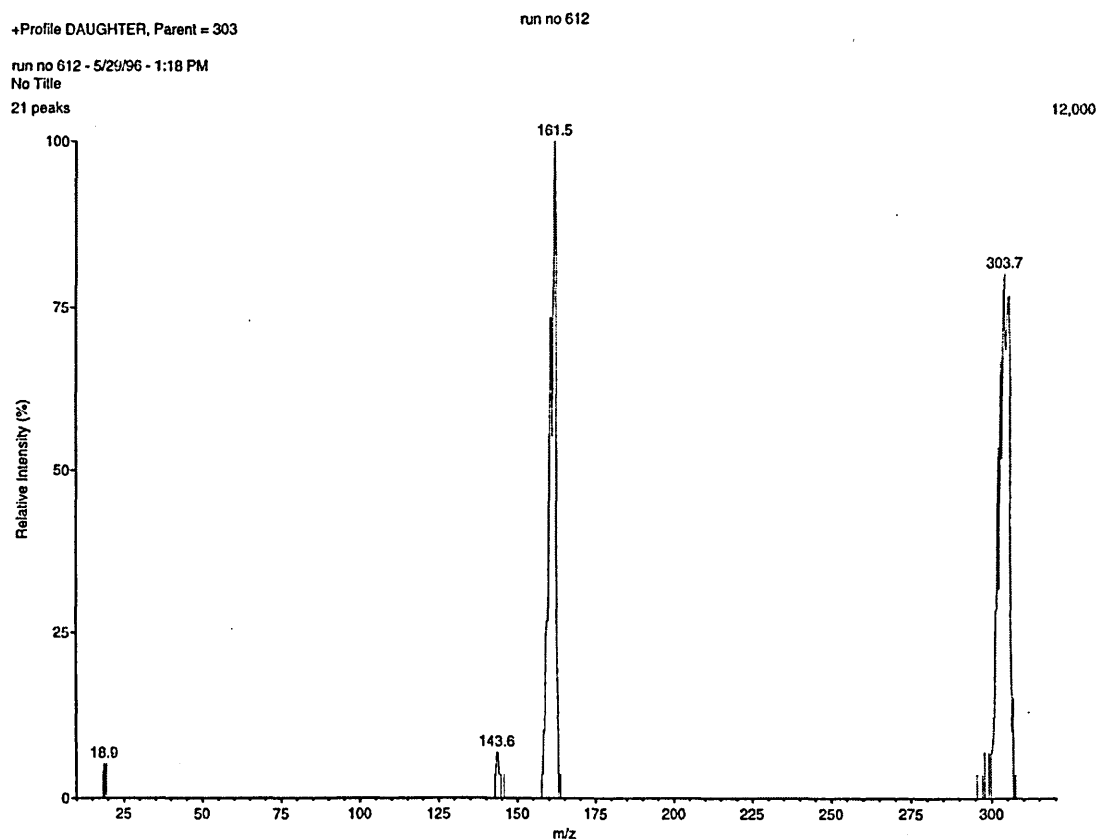
Figure 4.21: Product ion mass spectrum of the ammonia / 5-nonanone ion-molecule
cluster at m/z 302

As expected, there was a general shift to higher m/z values for the ion-molecule

clusters because of the heavier mass of the ketone (a progressive trend observed through

the series). However, the absence of ion peaks below m/z 285 indicated that the

equilibrium had been forced to the right, i.e. had favoured the formation of larger ion-

molecule clusters, where n = 2 or 3. It was possible that larger ion clusters were formed,

but these would not have been detected within the mass range available. The predicted

ion clusters of $H^+(C_9H_{18}O)_4$ and $NH_4^+(C_9H_{18}O)_4$ would have had m/z values of 569 and

586 amu respectively.
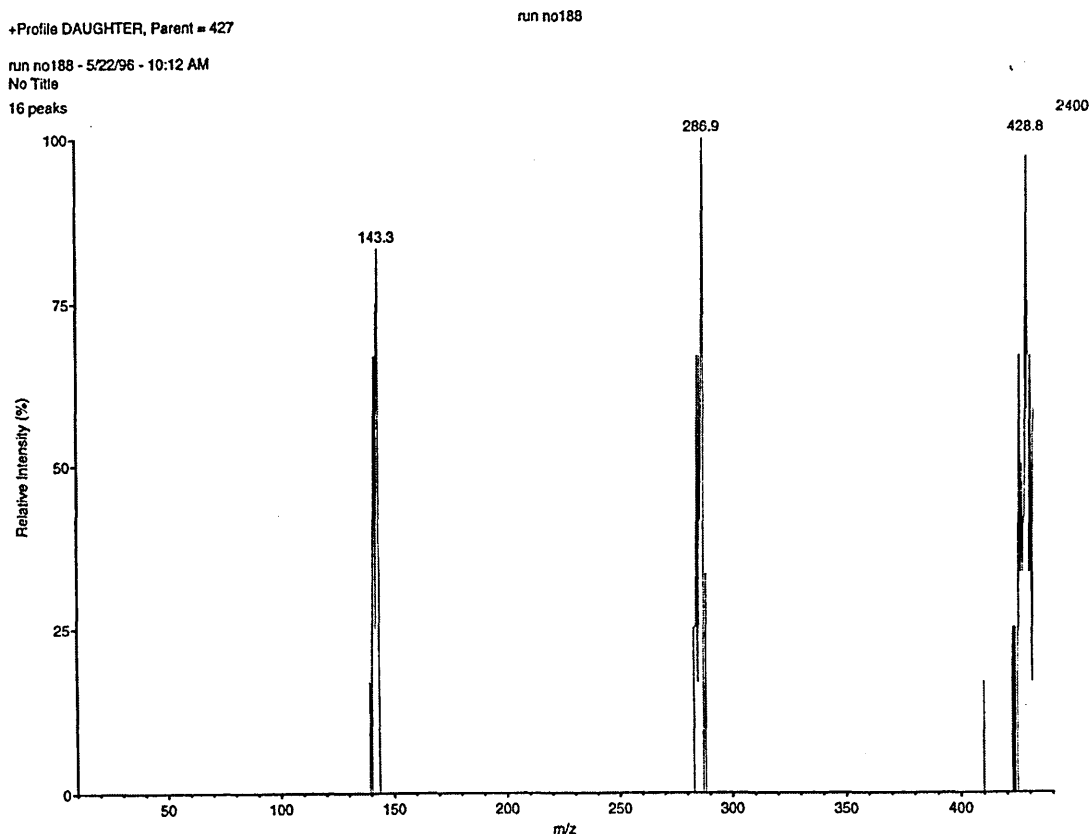
Figure 4.22:Product ion mass spectrum of the ammonia / 5-nonanone ion-molecule cluster at m/z 427

4.13.5 1,1,1-Trifluoroacetone / ammonia ion chemistry

The IMS-MS spectra obtained when ammonia was introduced into an IMS with the source region doped with 1,1,1-trifluoroacetone were distinctive for their lack of significant intensity of peaks for ion clusters involving the two compounds of interest. Traces of ammonia monomer, dimer, and trimer ions were evident with increased peak intensity through m/z values of 18, 35, and 52. The peaks in the region of m/z values 130 and 242 were too low for identification by MS-MS analysis but were assumed to be $NH_4^+(CH_3COCF_3)_n$, where n = 1 or 2. The spectra captured during the experiments with the drift region doped also lacked any ion clusters of significant intensity. However, it was assumed from the recorded peaks at m/z values of 147, 259, and 371 that ammonia / 1,1,1-trifluoroacetone ion clusters were present and corresponded to

$H^+(NH_3)_2(CH_3COCF_3)_n$ where n = 1, 2, and 3 respectively, and m/z 354 was attributed to $NH_4^+(CH_3COCF_3)_3$. The assigned peaks could not be attributed to contamination from previous experiments nor to decomposition products. There was no evidence of ion-molecule clusters with n = 4 with either one or two molecules of the analyte in the cluster. The presence of the fluorinated compound significantly decreased the intensity of the peaks observed in the mass spectra, and because the compound was so volatile it was difficult to maintain the required high concentration of the dopant in order to make a direct comparison between this and the previous experiments. Many of the peaks recorded could not be assigned.

4.13 Proton bound clusters of ketones and hydrazine

4.13.1 Acetone / hydrazine ion chemistry

When the source region was doped with a low concentration of acetone, the predominant ions were at m/z values of 117, 149, and 131. When a higher concentration of acetone was introduced into the source region the predominant ions were at m/z values of 149, 131, and 91 (see Figure 4.23), with a lower intensity of ions at m/z values of 113, 73, and 33. Although the ions at m/z 149, 117, 91, and 33 could be attributed to $H^+(N_2H_4)(C_3H_6O)_2$, $H^+(C_3H_6O)_2$, $H^+(N_2H_4)(C_3H_6O)$, and $H^+(N_2H_4)$ cluster ions respectively, and the $H^+(C_3H_6O)_3$ ion was observed at m/z 175, the other three ions did not correspond to any combination of protonated HZ / acetone / water clustering. These ions have been attributed to clusters involving reaction products of acetone and the protonated HZ. The dehydration reaction was assumed to take place in the vapour phase with the formation of the corresponding hydrazone, m/z 73 (protonated), which further reacted with the acetone to form an azine, m/z 113 (protonated). (Refer to Figure 4.24 for the mechanism of reaction.)
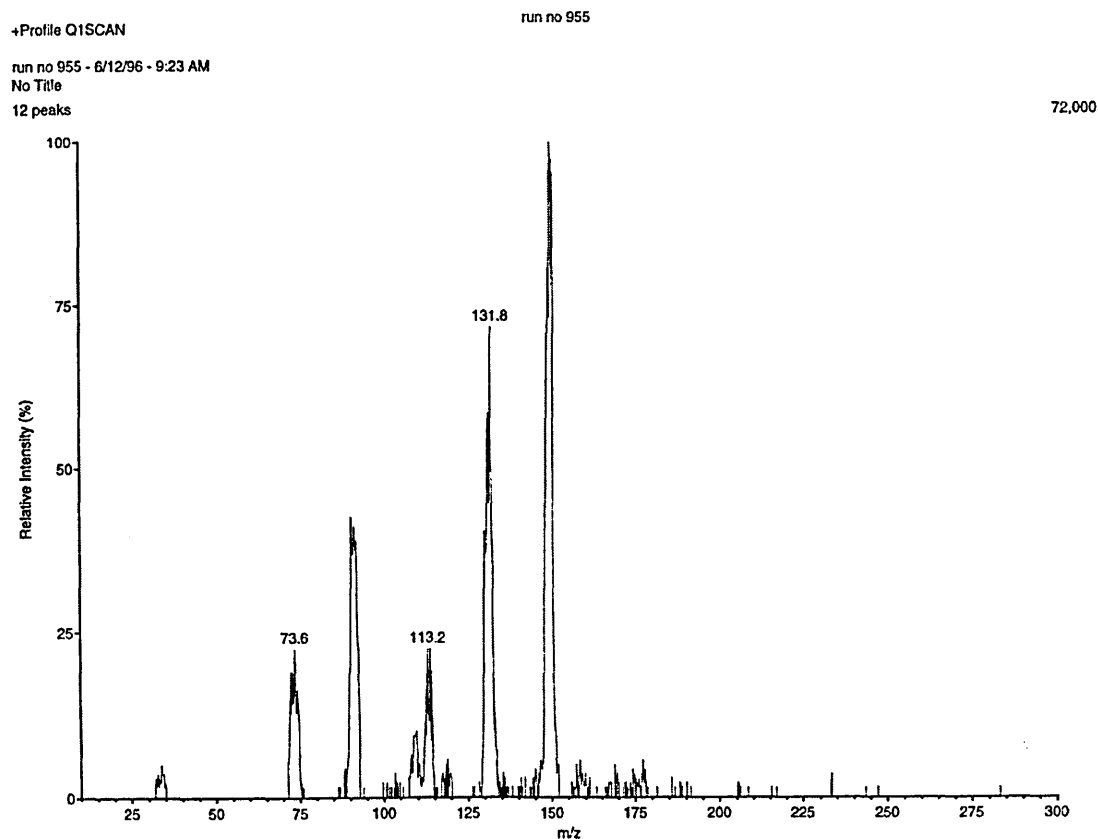
Figure 4.23: Mass spectrum of the ion clusters formed from hydrazine with the acetone doped source region

The clusters at m/z values of 145, 131, and 73 were then correct for $H^+(C_3H_8N_2)_2$, $H^+(C_3H_8N_2)(C_3H_6O)$, and $H^+(C_3H_8N_2)$ respectively. This theory was supported by MS-MS spectra. As the hydrazone and azine were products of reaction, rather than ion-molecule clustering, the ion species were extremely stable when subjected to MS-MS analysis, as indicated by a single peak of high intensity. The stable acetone azine ion peak is shown in Figure 4.25. The isolation of the hydrazone ion confirmed the two-stage reaction. The results are listed in Table 4.17.

(I) Formation of protonated hydrazone
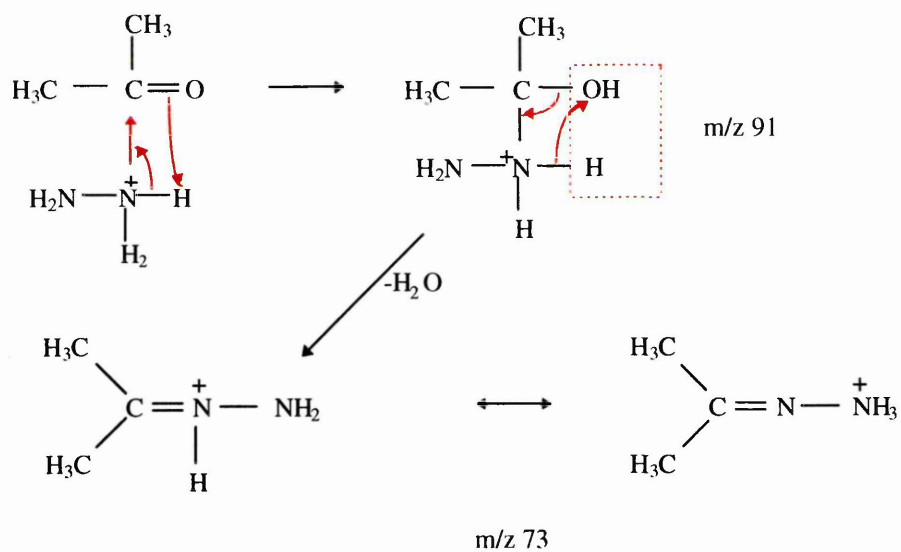
(ii) Formation of protonated azine from protonated hydrazone
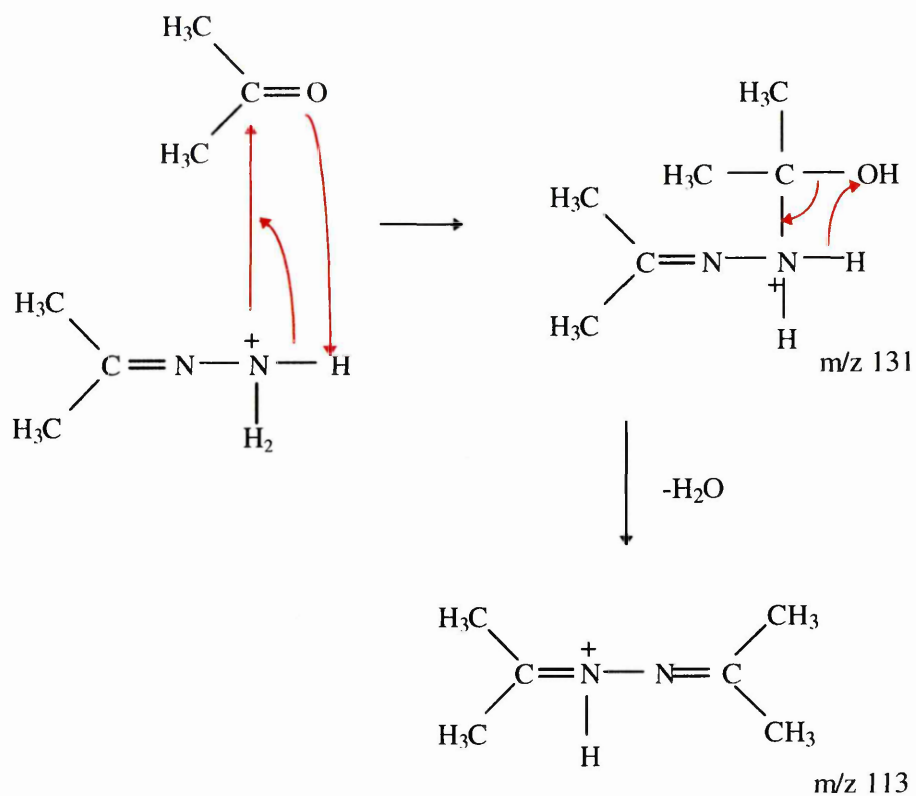
Figure 4.24: Mechanism for the reaction between acetone and protonated hydrazine

+Profile DAUGHTER, Parent = 113

run no 40 - 5/15/96 - 2:45 PM
No Title
1 peak   65,400
                                                                                               113.9
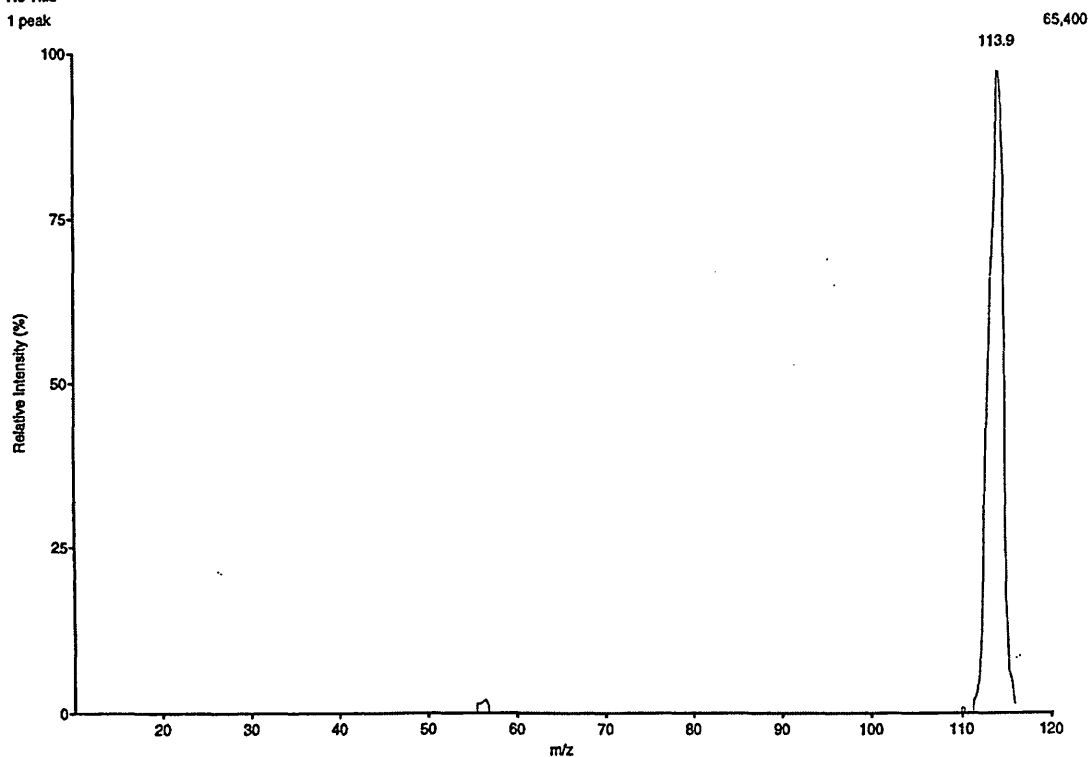
Figure 4.25: Product ion mass spectrum of the acetone azine ion at m/z 113

Table 4.17: Summary of the hydrazine / acetone ion chemistry; source region doped

Precursor Ion		MS-MS Product Ions			
149	$H^+(N_2H_4)(C_3H_6O)_2$	91	$H^+(N_2H_4)(C_3H_6O)$	33	$H^+(N_2H_4)$
131	$H^+(C_3H_8N_2)(C_3H_6O)$	73	$H^+(C_3H_8N_2)$		
91	$H^+(N_2H_4)(C_3H_6O)$	33	$H^+(N_2H_4)$		
73	$H^+(C_3H_8N_2)$				
113	$H^+(C_6H_{12}N_2)$				
33	$H^+(N_2H_4)$				
117	$H^+(C_3H_6O)_2$	59	$H^+(C_3H_6O)$		
175	$H^+(C_3H_6O)_3$	117	$H^+(C_3H_6O)_2$		
*233	$H^+(C_3H_6O)_4$				
145	$H^+(C_3H_8N_2)_2$	73	$H^+(C_3H_8N_2)$		

*Confirmation of ion-molecule composition by MS-MS analysis was unavailable

With the entire IMS doped from the drift region, lower intensity peaks (Figure 4.26) were observed for the protonated hydrazone clustered with one to three molecules of acetone at m/z values of 131, 189, and 247 respectively. The protonated acetone dimer, trimer, and tetramer species were also detected, at m/z values of 117, 175, and 233 respectively, possibly with $H^+(C_3H_6O)_5$ at m/z 291. There was evidence of larger clusters formed with unreacted HZ, viz. $H^+(N_2H_4)(C_3H_6O)$, $H^+(N_2H_4)(C_3H_6O)_2$, $H^+(N_2H_4)(C_3H_6O)_3$, and $H^+(N_2H_4)(C_3H_6O)_4$, at values of 91, 149, 207, and 265 respectively. The clusters involving HZ combined with the monomer through to the tetramer of the acetone series predominated in the ion chemistry, with peak intensity decreasing in the order $H^+(N_2H_4)(C_3H_6O)_2 > H^+(N_2H_4)(C_3H_6O)_3 > H^+(N_2H_4)(C_3H_6O) > H^+(N_2H_4)(C_3H_6O)_4$. The ion-molecule clusters are listed in Table 4.18.
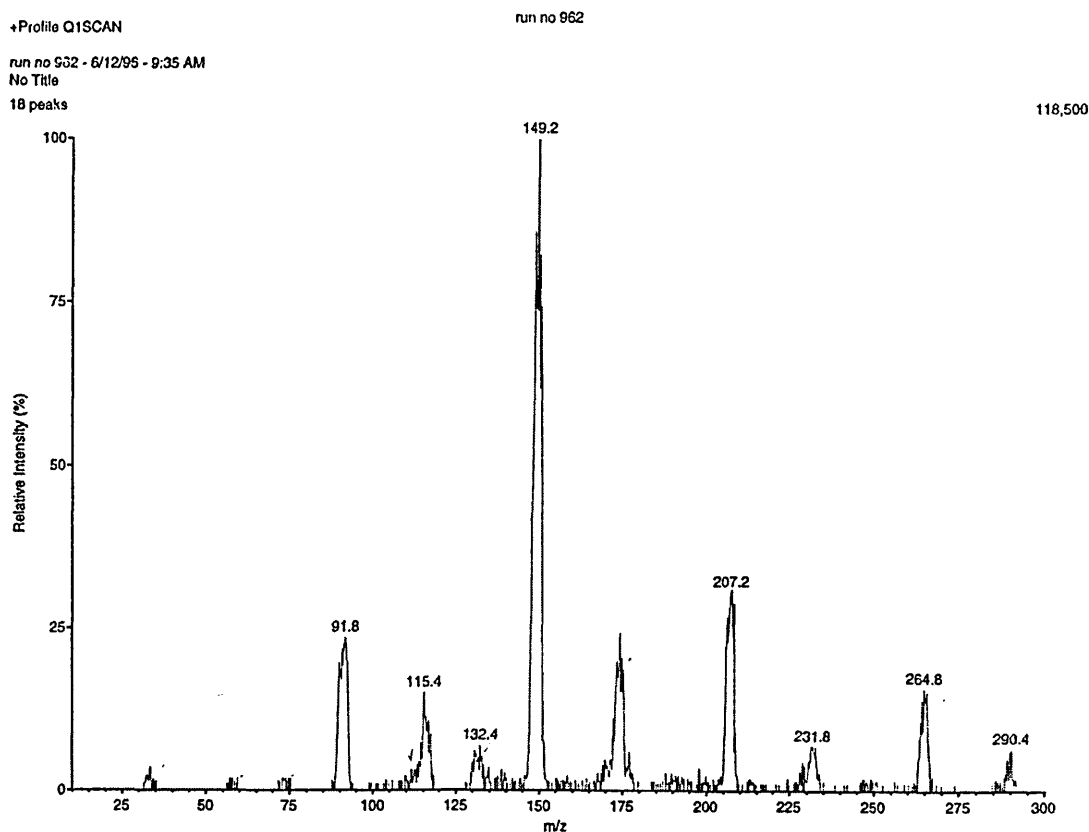
Figure 4.26: Mass spectrum of the ion clusters formed from hydrazine with the acetone doped drift region

Table 4.18: Summary of hydrazine / acetone ion chemistry; drift region doped

Precursor Ion		MS-MS Product Ions						
149	$H^+(N_2H_4)(C_3H_6O)_2$	91	$H^+(N_2H_4)(C_3H_6O)$	33	$H^+(N_2H_4)$			
207	$H^+(N_2H_4)(C_3H_6O)_3$	149	$H^+(N_2H_4)(C_3H_6O)_2$	91	$H^+(N_2H_4)(C_3H_6O)$	33	$H^+(N_2H_4)$	
91	$H^+(N_2H_4)(C_3H_6O)$	33	$H^+(N_2H_4)$					
175	$H^+(C_3H_6O)_3$	117	$H^+(C_3H_6O)_2$					
265	$H^+(N_2H_4)(C_3H_6O)_4$	207	$H^+(N_2H_4)(C_3H_6O)_3$	149	$H^+(N_2H_4)(C_3H_6O)_2$	91	$H^+(N_2H_4)(C_3H_6O)$	
117	$H^+(C_3H_6O)_2$	59	$H^+(C_3H_6O)$					
*233	$H^+(C_3H_6O)_4$	175	$H^+(C_3H_6O)_3$	117	$H^+(C_3H_6O)_2$	59	$H^+(C_3H_6O)$	
131	$H^+(C_3H_8N_2)(C_3H_6O)$	73	$H^+(C_3H_8N_2)$					
291	$H^+(C_3H_6O)_5$	233	$H^+(C_3H_6O)_4$	175	$H^+(C_3H_6O)_3$	117	$H^+(C_3H_6O)_2$	
171	$H^+(C_6H_{12}N_2)(C_3H_6O)$	113	$H^+(C_6H_{12}N_2)$					
113	$H^+(C_6H_{12}N_2)$							
33	$H^+(N_2H_4)$							
73	$H^+(C_3H_8N_2)$							
247	$H^+(C_3H_8N_2)(C_3H_6O)_3$	189	$H^+(C_3H_8N_2)(C_3H_6O)_2$	131	$H^+(C_3H_8N_2)(C_3H_6O)$	73	$H^+(C_3H_8N_2)$	
59	$H^+(C_3H_6O)$							
189	$H^+(C_3H_8N_2)(C_3H_6O)_2$	131	$H^+(C_3H_8N_2)(C_3H_6O)$	73	$H^+(C_3H_8N_2)$			

*Confirmation of ion-molecule composition by MS-MS analysis was unavailable

The formation of the $H^+(N_2H_4)(C_3H_6O)_4$ ion-molecule cluster had not been predicted in the model. Its formation could have been due to either to the attachment of acetone molecules at the hydrogens on the secondary core nitrogen or a second layer of dopant attachment through solvation.

4.13.2 3-pentanone / hydrazine ion chemistry

The introduction of HZ into an IMS system, having only the source region doped with 3-pentanone, produced the predominant ions $H^+(C_5H_{12}N_2)(C_5H_{10}O)$ and $H^+(C_{10}H_{20}N_2)$ at m/z values of 187 and 169 (see Figure 4.27). Also present were ions at m/z values of 101, 205, 273, 119, 255, and 173. The ion cluster with an m/z value of 173 was the protonated dimer ion of the 3-pentanone, whilst those ion clusters with m/z values of 119 and 205 were the result of HZ clustering directly with the 3-pentanone to form

$H^+(N_2H_4)(C_5H_{10}O)$ and $H^+(N_2H_4)(C_5H_{10}O)_2$. Only a trace of the $H^+(N_2H_4)(C_5H_{10}O)_3$ ion was observed at m/z 291. HZ reacted with the ketone, as described in the previous section, to produce the corresponding protonated 3-pentanone hydrazone $H^+(C_5H_{12}N_2)$, m/z 101. This product ion then also clustered with the 3-pentanone to form ion clusters with m/z values of 187 and 273 which were identified as $H^+(C_5H_{12}N_2)(C_5H_{10}O)_n$ where n = 1 and 2 respectively. It was assumed that very minor contamination with MMH again produced the peaks at m/z values of 161, 219, and 247.

Another scan, covering a wider range of amu, showed the presence of a peak at m/z 359 which was assigned the formula $H^+(C_5H_{12}N_2)(C_5H_{10}O)_3$. The ion at m/z 169 was the protonated 3-pentanone azine, $H^+(C_{10}H_{20}N_2)$, which when clustered with a molecule of 3-pentanone produced an ion at m/z 255, $H^+(C_{10}H_{20}N_2)(C_5H_{10}O)$. The results are summarised in Table 4.19.
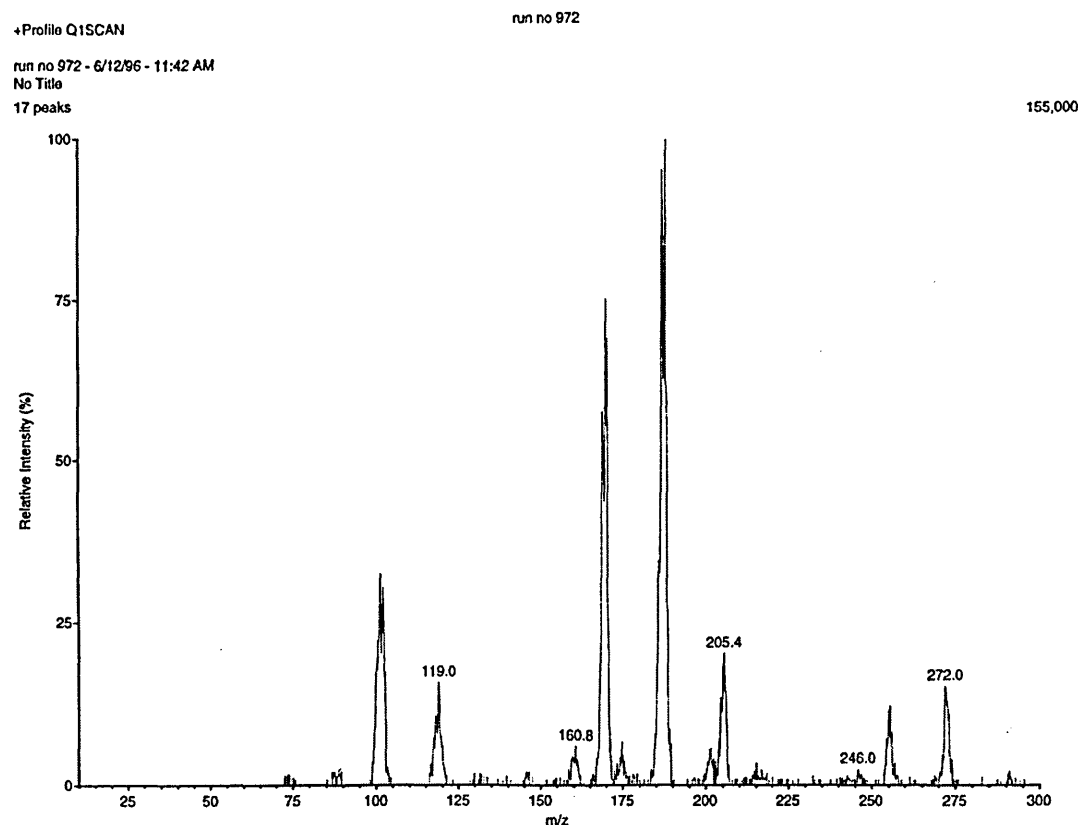
Figure 4.27: Mass spectrum of the ion clusters formed from hydrazine with the 3-pentanone doped source region

Table 4.19: Summary of hydrazine / 3-pentanone ion chemistry; source doped region

Precursor Ion		MS-MS Product Ions			
187	$H^+(C_5H_{12}N_2)(C_5H_{10}O)$	101	$H^+(C_5H_{12}N_2)$		
169	$H^+(C_{10}H_{20}N_2)$				
101	$H^+(C_5H_{12}N_2)$				
205	$H^+(N_2H_4)(C_5H_{10}O)_2$	119	$H^+(N_2H_4)(C_5H_{10}O)$	33	$H^+(N_2H_4)$
273	$H^+(C_5H_{12}N_2)(C_5H_{10}O)_2$	187	$H^+(C_5H_{12}N_2)(C_5H_{10}O)$	101	$H^+(C_5H_{12}N_2)$
119	$H^+(N_2H_4)(C_5H_{10}O)$	33	$H^+(N_2H_4)$		
255	$H^+(C_{10}H_{20}N_2)(C_5H_{10}O)$	169	$H^+(C_{10}H_{20}N_2)$		
*201	$H^+(C_5H_{12}N_2)_2$				
87	$H^+(C_5H_{10}O)$				
291	$H^+(N_2H_4)(C_5H_{10}O)_3$	205	$H^+(N_2H_4)(C_5H_{10}O)_2$	119	$H^+(N_2H_4)(C_5H_{10}O)$
359	$H^+(C_5H_{12}N_2)(C_5H_{10}O)_3$	273	$H^+(C_5H_{12}N_2)(C_5H_{10}O)_2$	187	$H^+(C_5H_{12}N_2)(C_5H_{10}O)$

*Confirmation of ion-molecule composition by MS-MS analysis was unavailable

Following doping of the system via the drift region, the predominant ions were at m/z values of 205 and 291 (Figure 4.28). Most of the other ions observed during the tests with only the source region doped survived the increase in dopant concentration, but the equilibrium favoured the existence of the unreacted HZ clustered with the ketone. Significantly, there was no azine formation, and only lower intensities of the protonated 3-pentanone hydrazone / ketone series $H^+(C_5H_{12}N_2)(C_5H_{10}O)_n$, where n = 0 to 2 molecules, were recorded.
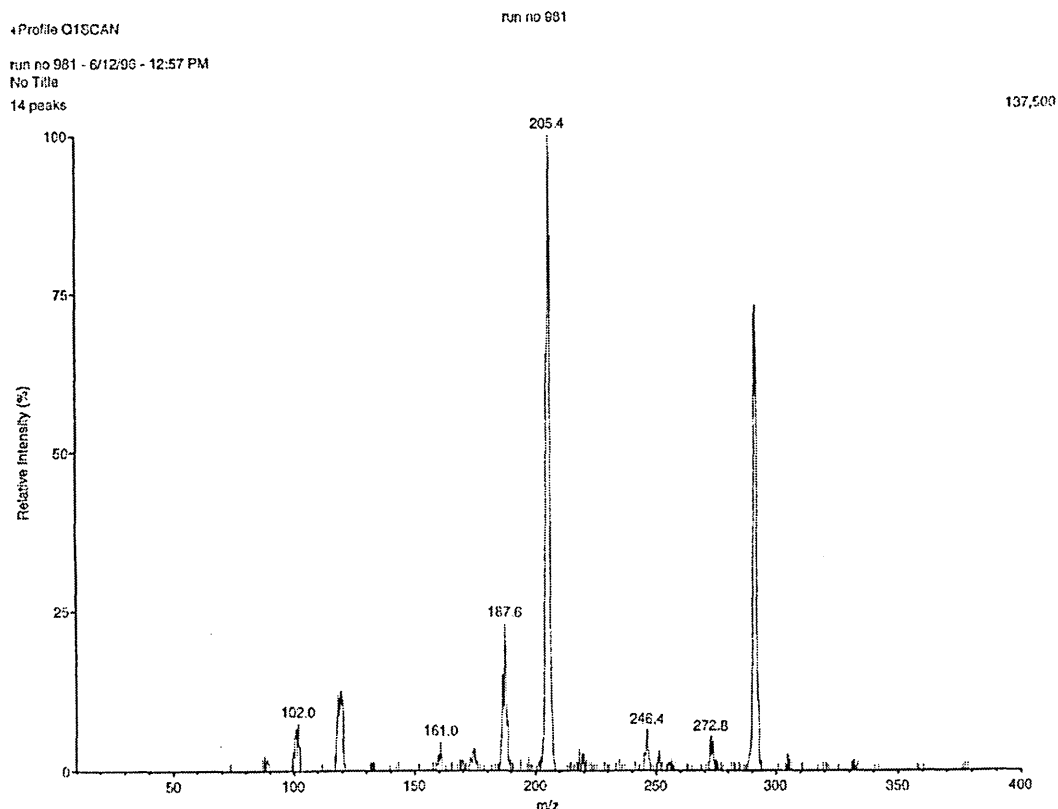
Figure 4.28: Mass spectrum of the ion clusters formed from hydrazine with the 3-pentanone doped drift region

The protonated HZ / ketone series $H^+(N_2H_4)(C_5H_{10}O)_n$ produced the predominant ion clusters, with $n = 2 > n = 3 >> n = 1$, and a short range scan indicated the existence of the cluster with $n = 4$ (m/z 377), as seen during the previous experiment with acetone. The product ion mass spectrum which confirmed the presence of the $H^+(N_2H_4)(C_5H_{10}O)_3$ cluster is shown in Figure 4.29. A previous experiment also produced this series, although the product ion mass spectrum (Figure 4.30) was out of calibration by +2 to +3 amu, and confirmed the existence of the $H^+(N_2H_4)(C_5H_{10}O)_4$ ion cluster. The results for the 3-pentanone doped drift region for analysis of HZ are shown in Table 4.20. At 853.2 kJ.mol^{-1}, HZ has a similar proton affinity value to ammonia, and loss of ketone molecules during MS-MS analysis resulted in the protonated analyte.

run no 982

7000
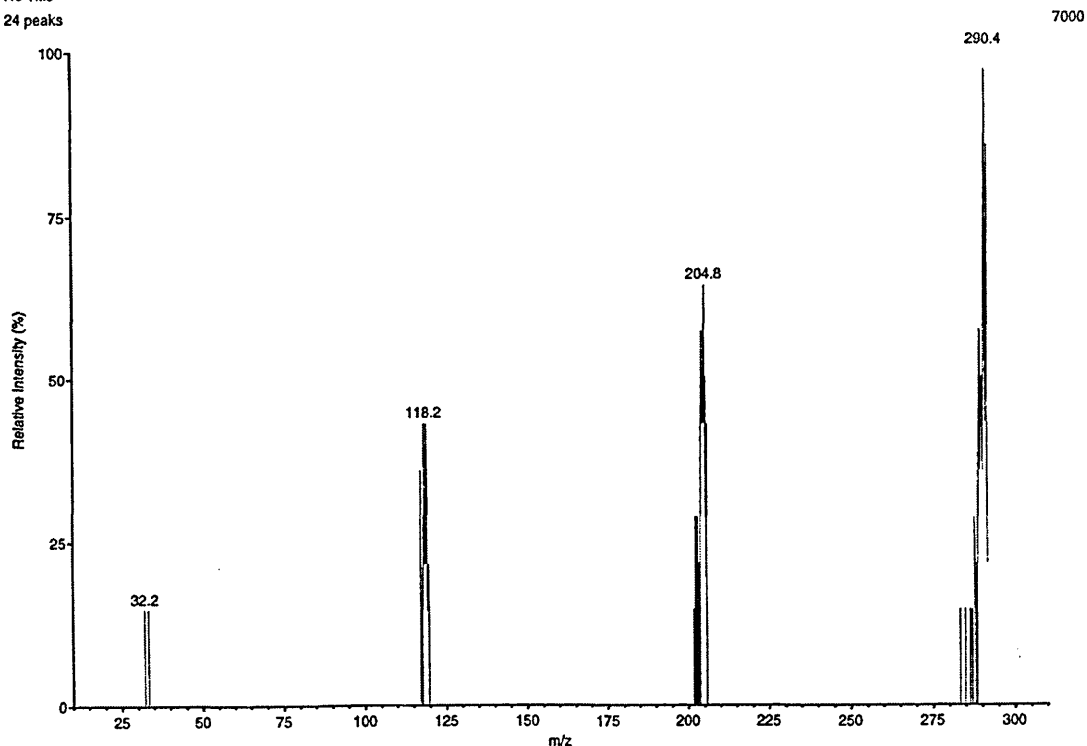
Figure 4.29: Product ion mass spectrum of the hydrazine / 3-pentanone ion-molecule cluster at m/z 291

run no 701

6200
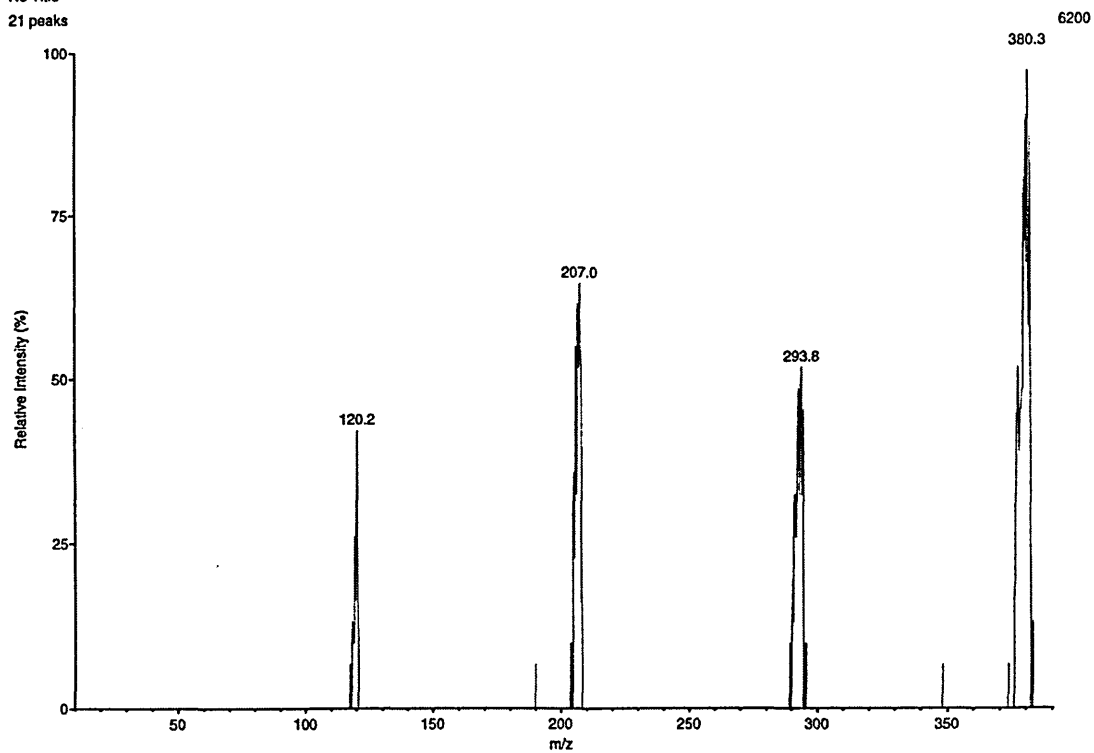
Figure 4.30: Product ion mass spectrum of the hydrazine / 3-pentanone ion-molecule cluster at m/z 377

Table 4.20: Summary of hydrazine / 3-pentanone ion chemistry; drift region doped

Precursor Ion		MS-MS Product Ions					
205	$H^+(N_2H_4)(C_5H_{10}O)_2$	119	$H^+(N_2H_4)(C_5H_{10}O)$	33	$H^+(N_2H_4)$		
291	$H^+(N_2H_4)(C_5H_{10}O)_3$	205	$H^+(N_2H_4)(C_5H_{10}O)_2$	119	$H^+(N_2H_4)(C_5H_{10}O)$	33	$H^+(N_2H_4)$
187	$H^+(C_5H_{12}N_2)(C_5H_{10}O)$	101	$H^+(C_5H_{12}N_2)$				
119	$H^+(N_2H_4)(C_5H_{10}O)$	33	$H^+(N_2H_4)$				
101	$H^+(C_5H_{12}N_2)$						
273	$H^+(C_5H_{12}N_2)(C_5H_{10}O)_2$	187	$H^+(C_5H_{12}N_2)(C_5H_{10}O)$	101	$H^+(C_5H_{12}N_2)$		
*173	$H^+(C_5H_{10}O)_2$						
169	$H^+(C_{10}H_{20}N_2)$						
255	$H^+(C_{10}H_{20}N_2)(C_5H_{10}O)$	169	$H^+(C_{10}H_{20}N_2)$				
87	$H^+(C_5H_{10}O)$						
377	$H^+(N_2H_4)(C_5H_{10}O)_4$	291	$H^+(N_2H_4)(C_5H_{10}O)_3$	205	$H^+(N_2H_4)(C_5H_{10}O)_2$	119	$H^+(N_2H_4)(C_5H_{10}O)$
133	$H^+(C_5H_{12}N_2)(N_2H_4)$	101	$H^+(C_5H_{12}N_2)$				
359	$H^+(C_5H_{12}N_2)(C_5H_{10}O)_3$	273	$H^+(C_5H_{12}N_2)(C_5H_{10}O)_2$	187	$H^+(C_5H_{12}N_2)(C_5H_{10}O)$		

*Confirmation of ion-molecule composition by MS-MS analysis was unavailable

4.13.4 4-Heptanone / hydrazine ion chemistry

The predominant ion clusters formed during the HZ experiments, with 4-heptanone used to dope the source region, were due to reaction products. Again, the equivalent protonated hydrazone ($H^+(C_7H_{16}N_2)$) and azine ($H^+(C_{14}H_{28}N_2)$) ions, with m/z values of 129 and 225, were formed (see Figure 4.31); the hydrazone then clustered with a single molecule of ketone to produce $H^+(C_7H_{16}N_2)(C_7H_{14}O)$ with an m/z value of 243. HZ also clustered with the ketone to form $H^+(N_2H_4)(C_7H_{14}O)$, m/z 147, without chemical reaction. The results are listed in Table 4.21.

The majority of the contamination could be assigned to the presence of MMH, TMH and / or 3-pentanone, for example, the peak nominally labelled m/z 89 appeared to be closer to m/z 88 and might even have been a mixture of both the TMH and 3-pentanone species. These two species may have combined to form a peak at m/z 175.
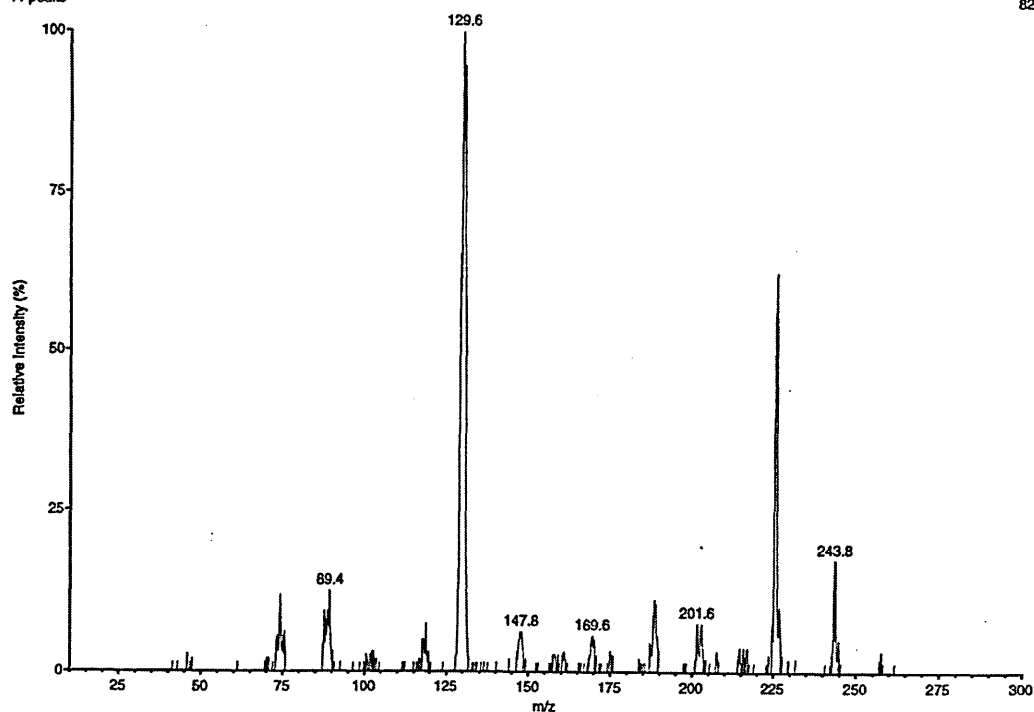
Figure 4.31: Mass spectrum of the ion clusters formed from hydrazine with the
4-heptanone doped source region

Table 4.21: Summary of hydrazine / 4-heptanone ion chemistry; source region doped

Precursor Ion		MS-MS Product Ions	
129	$H^+(C_7H_{16}N_2)$		
225	$H^+(C_{14}H_{28}N_2)$		
243	$H^+(C_7H_{16}N_2)(C_7H_{14}O)$	129	$H^+(C_7H_{16}N_2)$
147	$H^+(N_2H_4)(C_7H_{14}O)$	33	$H^+(N_2H_4)$
*161	$H^+(C_7H_{16}N_2)(N_2H_4)$		
*229	$H^+(C_7H_{14}O)_2$		

*Confirmation of ion-molecule composition by MS-MS analysis was unavailable due to
insufficient intensity of the precursor ion peak

If the peak around m/z 202 was due to the presence of 3-pentanone combined with 4-heptanone the ion would have occurred at m/z 201, but if 3-pentanone was substituted with TMH the value would have been m/z 203; either option appeared to be plausible.

The peaks at m/z values of 169 and 187 were attributed to ion-molecule clusters which involved HZ and 3-pentanone reaction products, namely 3-pentanone azine and 3-pentanone hydrazone($C_5H_{10}O$) respectively, and m/z 215 was assigned the formula $H^+(C_{10}H_{20}N_2)(N_2H_3CH_3)$. The only ready explanation for the peaks at m/z values 73 and 117 was minimal contamination by acetone, which led to the formation of acetone hydrazone and the dimer ion of acetone respectively.

Doping the detector with 4-heptanone through the drift region initially forced the equilibrium to favour the completion of the reaction to azine formation, but with increased time the predominant ion cluster comprised unreacted HZ combined with two molecules of ketone, $H^+(N_2H_4)(C_7H_{14}O)_2$, m/z 261. The monomer ketone / HZ ion cluster, m/z 147, also increased in intensity, although to a lesser degree. The HZ also combined with three molecules of 4-heptanone to produce $H^+(N_2H_4)(C_7H_{14}O)_3$, m/z 375. The protonated azine peak was still quite high in intensity, but the protonated hydrazone peak had nearly disappeared; the hydrazone / ketone peak increased but was still fairly low in intensity. The azine also clustered with 4-heptanone to form $H^+(C_{14}H_{28}N_2)(C_7H_{14}O)$, m/z 339 (see Figure 4.32 for the product ion spectrum providing confirmation of the identity of this cluster). There was no attempt to scan for the $H^+(N_2H_4)(C_7H_{14}O)_4$ ion at m/z 489 because of mass range was limited to 450 amu. The results are listed in Table 4.22.

Table 4.22: Summary of hydrazine / 4-heptanone ion chemistry; drift region doped

Precursor Ion		MS-MS Product Ions			
261	$H^+(N_2H_4)(C_7H_{14}O)_2$	147	$H^+(N_2H_4)(C_7H_{14}O)$		
225	$H^+(C_{14}H_{28}N_2)$				
147	$H^+(N_2H_4)(C_7H_{14}O)$	33	$H^+(N_2H_4)$		
375	$H^+(N_2H_4)(C_7H_{14}O)_3$	261	$H^+(N_2H_4)(C_7H_{14}O)_2$	147	$H^+(N_2H_4)(C_7H_{14}O)$
339	$H^+(C_{14}H_{28}N_2)(C_7H_{14}O)$	225	$H^+(C_{14}H_{28}N_2)$		
243	$H^+(C_7H_{16}N_2)(C_7H_{14}O)$	129	$H^+(C_7H_{16}N_2)$		
129	$H^+(C_7H_{16}N_2)$				
*161	$H^+(C_7H_{16}N_2)(N_2H_4)$				

*Confirmation of ion-molecule composition by MS-MS analysis was unavailable due to insufficient intensity of the precursor ion peak
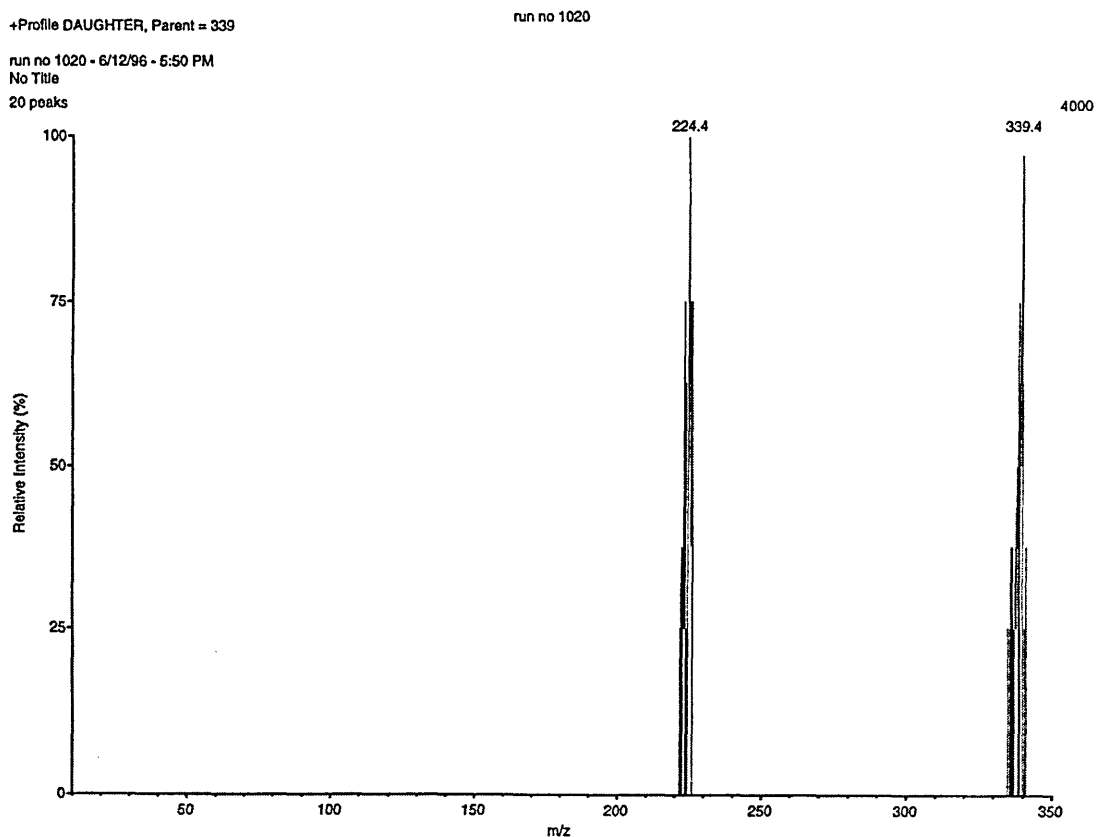
Figure 4.32: Product ion mass spectrum of the 4-heptanone azine / 4-heptanone ion cluster at m/z 339

4.13.4 5-Nonanone / hydrazine chemistry

The predominant ion chemistry observed during the determination of HZ, when the source region was doped with 5-nonanone (Figure 4.33), was the hydrazone reaction product series $H^+(C_9H_{20}N_2)(C_9H_{18}O)_n$ where the ion peak for the ketone bound hydrazone was of higher intensity than the peak for the free hydrazone; the m/z values were 299 and 157 respectively (see Figure 4.34 for the product ion mass spectrum). The intensity of the 5-nonanone azine peak, $H^+(C_{18}H_{36}N_2)$ at m/z 281, was comparable to that of the 5-nonanone hydrazone, m/z 157. The peak at m/z 313 could have been due to the clustering of HZ with the azine reaction product, $H^+(C_{18}H_{36}N_2)(N_2H_4)$ or the dimer ion of the hydrazone reaction product, $H^+(C_9H_{20}N_2)_2$. MS-MS analysis confirmed its composition to be the latter.

Figure 4.33: Mass spectrum of the ion clusters formed from hydrazine with the 5-nonanone doped source region

Table 4.23: Summary of hydrazine / 5-nonanone ion chemistry; source region doped

Precursor Ion		MS-MS Product Ions	
299	$H^+(C_9H_{20}N_2)(C_9H_{18}O)$	157	$H^+(C_9H_{20}N_2)$
157	$H^+(C_9H_{20}N_2)$		
281	$H^+(C_{18}H_{36}N_2)$		
313	$H^+(C_9H_{20}N_2)_2$	157	$H^+(C_9H_{20}N_2)$
317	$H^+(N_2H_4)(C_9H_{18}O)_2$	175	$H^+(N_2H_4)(C_9H_{18}O)$
*285	$H^+(C_9H_{18}O)_2$		
175	$H^+(N_2H_4)(C_9H_{18}O)$	33	$H^+(N_2H_4)$
143	$H^+(C_9H_{18}O)$		

*Confirmation of ion-molecule composition by MS-MS analysis was unavailable

+Profile DAUGHTER, Parent = 299

run no 1030 - 6/12/96 - 7:03 PM
No Title

19 peaks

run no 1030

11,500
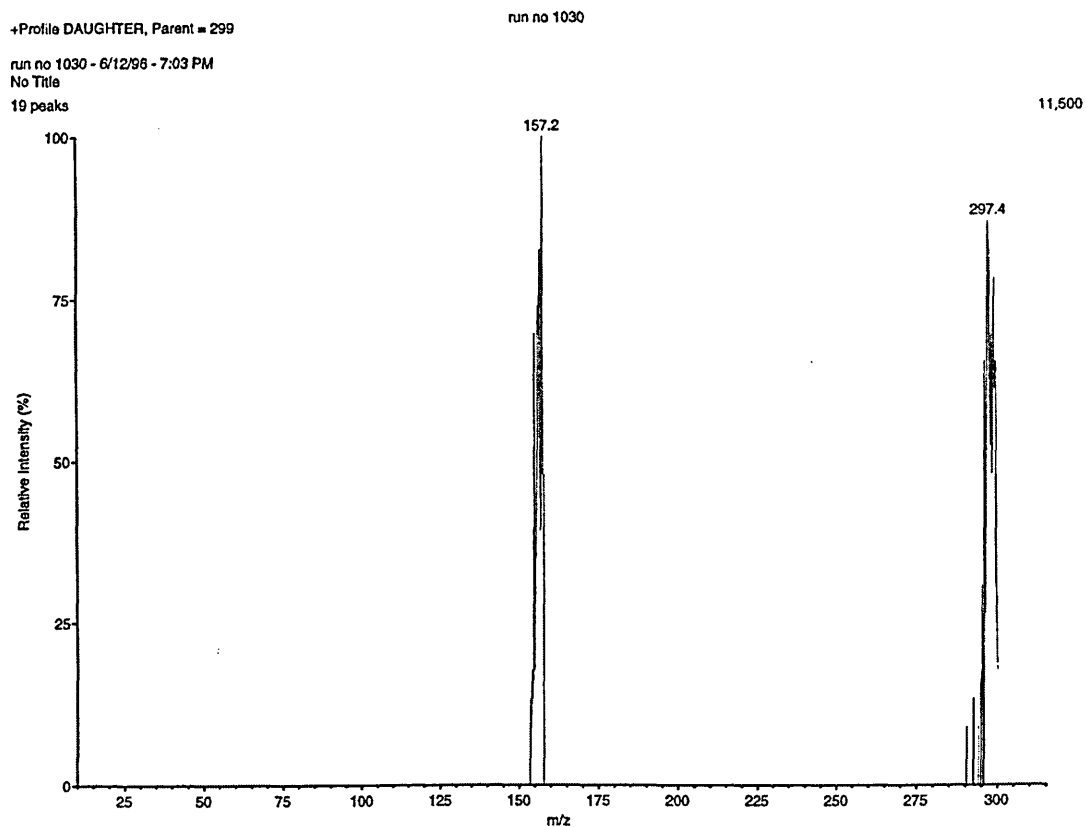
Figure 4.34: Product ion mass spectrum of the 5-nonanone hydrazone / 5-nonanone ion cluster at m/z 299

There was a minor amount of the dimer ion of 5-nonanone clustered with HZ at m/z 317, $H^+(N_2H_4)(C_9H_{18}O)_2$, and a trace of the monomer ketone / HZ ion cluster, $H^+(N_2H_4)(C_9H_{18}O)$, at m/z 175. The results are listed in Table 4.23.

The contamination peaks were assumed to have resulted from the presence of acetone, 3-pentanone, and 4-heptanone, possibly cumulative and residual through the sequence of experiments. The ion-molecule clusters thought to have formed from the contamination appeared to be very complicated. However, it was considered that because the range of proton affinities involved across these ketones was narrow (812.0 to 851.6 $kJ.mol^{-1}$ including 5-nonanone) then the clusters could co-exist. The identity of the contaminant ion clusters could not be proven as the peaks were too low in intensity for MS-MS analysis.

Forcing the dopant concentration higher, by its introduction through the drift region, increased the intensity of the predominant ion cluster observed at m/z 299 in the source region doped test. The intensity of the $H^+(N_2H_4)(C_9H_{18}O)$ ion at m/z 317 increased noticeably, whilst the intensity of the peak at m/z 313 decreased (see Figure 4.35). Whether the peak at m/z 313 was due to either the $H^+(C_{18}H_{36}N_2)(N_2H_4)$ or $H^+(C_9H_{20}N_2)_2$ ion-molecule clusters was uncertain. The implication was that at higher dopant concentration either the reaction between HZ and the ketone to form the hydrazone and azine was partially quenched, or that although there was reaction between HZ and 5-nonanone, the ketone clusters had a higher proton affinity than the resultant hydrazone and azine reaction products. The increased dopant concentration allowed for greater competition for the protons so that the reaction products might have been converted to neutral species through proton transfer. Their relative intensities were therefore reduced and thus the ion-molecule clusters which incorporated the protonated ketones were of greater intensity. The latter theory was the most probable.

Although the intensity of the ion clusters at m/z values of 423 and 459 were too low to capture MS-MS spectra, these were assumed to be the azine / ketone and the trimer ketone / HZ ion clusters, $H^+(C_{18}H_{36}N_2)(C_9H_{18}O)$ and $H^+(N_2H_4)(C_9H_{18}O)_3$ respectively. The results are listed in Table 4.24.
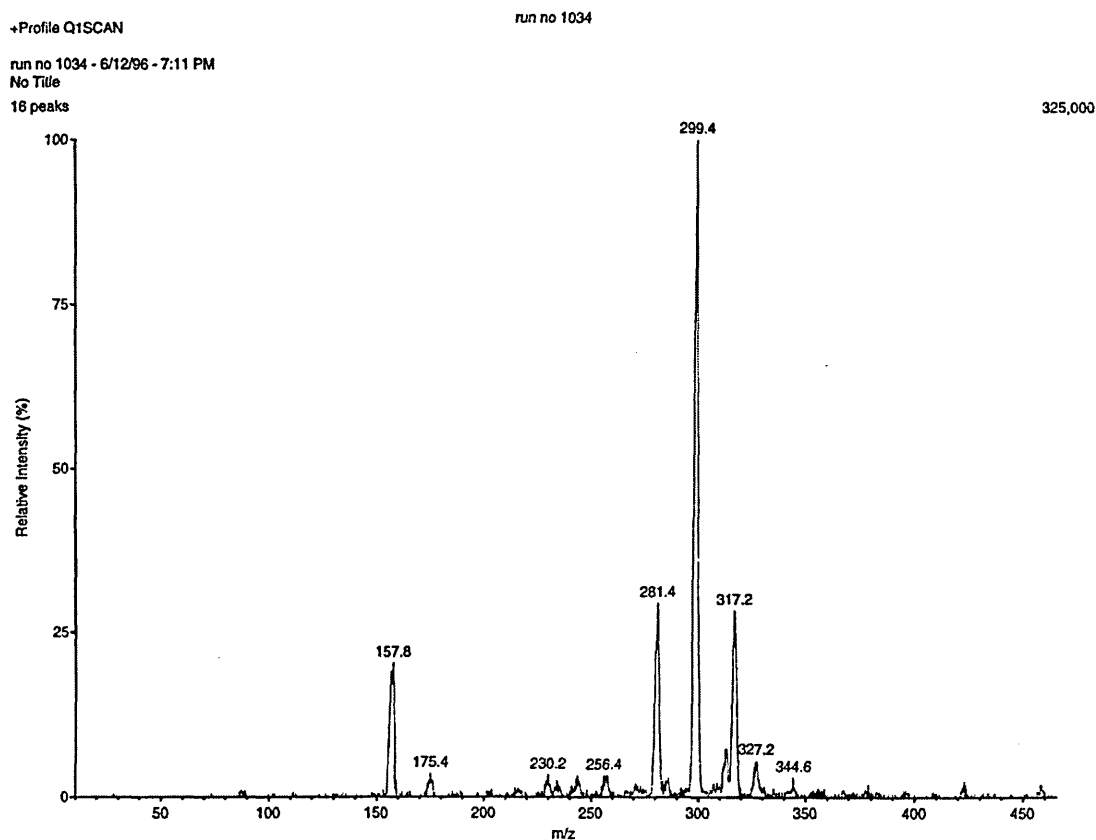
Figure 4.35: Mass spectrum of the ion clusters formed from hydrazine with the 5-nonanone doped drift region

Due to the scan range of the IMS it was not possible to detect the presence of the $H^+(N_2H_4)(C_9H_{18}O)_n$ ion clusters, where n = 4 or 5, which would have been observed at m/z 601 and 743 respectively.

Table 4.24: Summary of hydrazine / 5-nonanone ion chemistry; drift region doped

Precursor Ion		MS-MS Product Ions	
299	$H^+(C_9H_{20}N_2)(C_9H_{18}O)$	157	$H^+(C_9H_{20}N_2)$
317	$H^+(N_2H_4)(C_9H_{18}O)_2$	175	$H^+(N_2H_4)(C_9H_{18}O)$
281	$H^+(C_{18}H_{36}N_2)$		
157	$H^+(C_9H_{20}N_2)$		
313	$H^+(C_9H_{20}N_2)_2$	157	$H^+(C_9H_{20}N_2)$
175	$H^+(N_2H_4)(C_9H_{18}O)$	33	$H^+(N_2H_4)$
*423	$H^+(C_{18}H_{36}N_2)(C_9H_{18}O)$		
*459	$H^+(N_2H_4)(C_9H_{18}O)_3$		
*285	$H^+(C_9H_{18}O)_2$		

*Confirmation of ion-molecule composition by MS-MS analysis was unavailable

4.13.5 1,1,1-Trifluoroacetone / hydrazine ion chemistry

Doping of the source region with 1,1,1-trifluoroacetone did not produce any derivatised ion clusters. The predominant peaks were probably due to contaminant ion clusters. HZ monomer, dimer, and, possibly, trimer ions were observed at m/z values of 33, 65, and 97 respectively. Increasing the overall dopant concentration, through its addition into the system via the drift region, produced a predominant peak with an m/z value of 257. This was due to protonated HZ combining with two molecules of 1,1,1-trifluoroacetone. Also present was the HZ ion with one molecule of the fluorinated ketone. The HZ ion combined with three molecules of the dopant was also observed, but at lower intensity than the other two clusters.

The electron withdrawing effects of the fluorine atoms affected the formation of the hydrazone and azine products in the presence of HZ. The electron distribution of the

carbonyl bond meant that the carbonyl oxygen was less electronegative than that in the acetone molecule.

4.14 Proton bound clusters of ketones and methylhydrazine

4.14.1 Acetone / methylhydrazine ion chemistry

When the source region of the IMS was doped with acetone the predominant cluster ions formed in the presence of MMH were at m/z 105, $H^+(N_2H_3CH_3)(C_3H_6O)$, m/z 145, $H^+(C_4H_{10}N_2)(C_3H_6O)$, the protonated methylhydrazone reaction product clustered with a molecule of the ketone (see Figure 63), m/z 163, $H^+(N_2H_3CH_3)(C_3H_6O)_2$, and m/z 87, $H^+(C_4H_{10}N_2)$. Lower intensity ion clusters were recorded at m/z values of 133, $H^+(C_4H_{10}N_2)(N_2H_3CH_3)$, and m/z 173 $H^+(C_4H_{10}N_2)_2$, 117 $H^+(C_3H_6O)_2$, and 47 and 93 were assigned $H^+(N_2H_3CH_3)_n$, where n = 1 or 2.
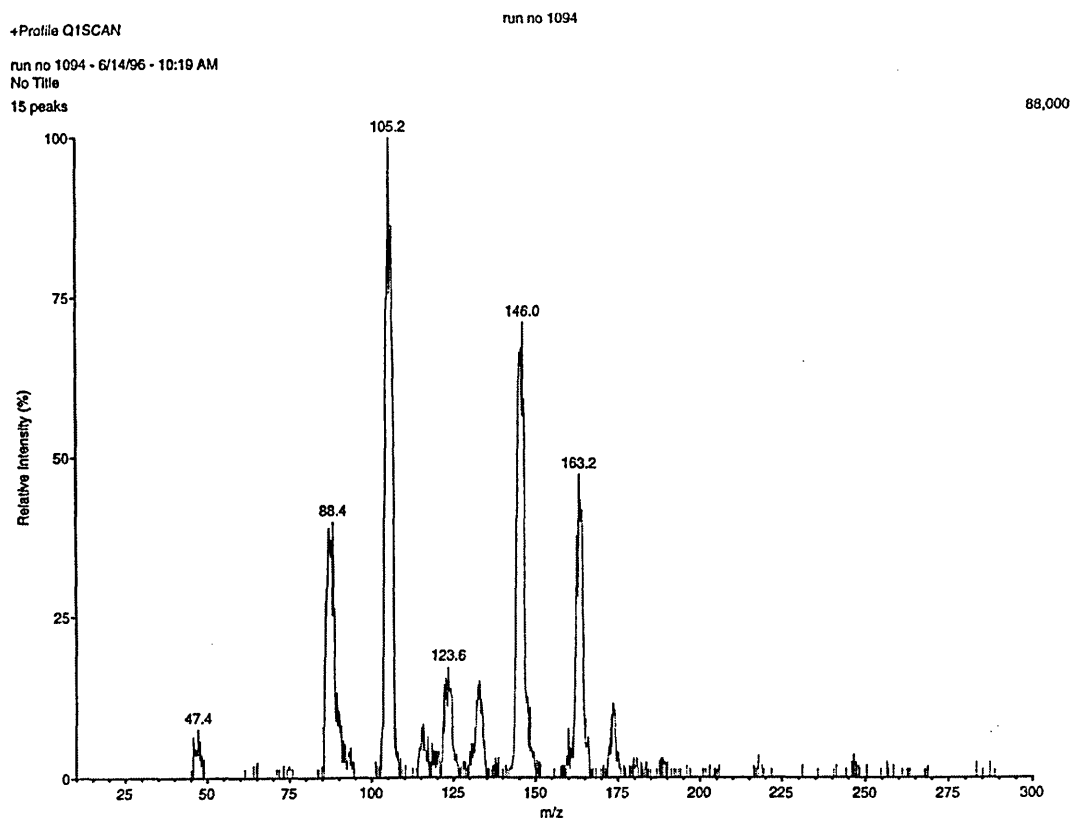
Figure 4.36: Mass spectrum of the ion clusters formed from methylhydrazine with the acetone doped source region

The peaks at m/z values of 76 and 122 may have arisen from contamination by ammonia, possibly as a breakdown product from MMH, and were assigned the structures $NH_4^+(C_3H_6O)$ and $NH_4^+(N_2H_3CH_3)(C_3H_6O)$, but the latter cluster seems improbable due to the much higher proton affinity of MMH compared with ammonia (895.7 and 854.0 $kJ.mol^{-1}$ respectively). The results are recorded in Table 4.25.

Table 4.25: Summary of methylhydrazine / acetone ion chemistry; source region doped

Precursor Ion		MS-MS Product Ions			
105	$H^+(N_2H_3CH_3)(C_3H_6O)$	59	$H^+(C_3H_6O)$	47	$H^+(N_2H_3CH_3)$
145	$H^+(C_4H_{10}N_2)(C_3H_6O)$	87	$H^+(C_4H_{10}N_2)$		
163	$H^+(N_2H_3CH_3)(C_3H_6O)_2$	105	$H^+(N_2H_3CH_3)(C_3H_6O)$	47	$H^+(N_2H_3CH_3)$
87	$H^+(C_4H_{10}N_2)$				
133	$H^+(C_4H_{10}N_2)(N_2H_3CH_3)$	87	$H^+(C_4H_{10}N_2)$		
173	$H^+(C_4H_{10}N_2)_2$	87	$H^+(C_4H_{10}N_2)$		
117	$H^+(C_3H_6O)_2$	59	$H^+(C_3H_6O)$		
47	$H^+(N_2H_3CH_3)$				
93	$H^+(N_2H_3CH_3)_2$	47	$H^+(N_2H_3CH_3)$		
*175	$H^+(C_3H_6O)_3$				
*151	$H^+(N_2H_3CH_3)_2(C_3H_6O)$				

*Confirmation of ion-molecule composition by MS-MS analysis was unavailable

The doping of the drift region with acetone shifted the equilibrium to make the ion at m/z 163 the predominant ion (Figure 4.37). The other major ions were at m/z values of 221, 133, 189, and 105, with a minor ion cluster observed at m/z 279 and possibly one at m/z 145. The ions at m/z values 221 and 279 had not been recorded in the source-only doped test. The MS-MS analysis showed the ion cluster at m/z 221 to comprise the protonated trimer ion of the ketone with one molecule of the analyte (see

Figure 4.38), not the dimer of the hydrazone with the analyte, as might have been expected from the results from the source doped test. Once again, the results indicated that the increased dopant concentration did not favour the existence of the protonated hydrazone product species. Due to insufficient intensity of the ion cluster peak at m/z 279, its identity could not be proven, although it has been assumed to be the tetramer ketone ion clustered with the analyte to form $H^+(N_2H_3CH_3)(C_3H_6O)_4$. The results are listed in Table 4.26.
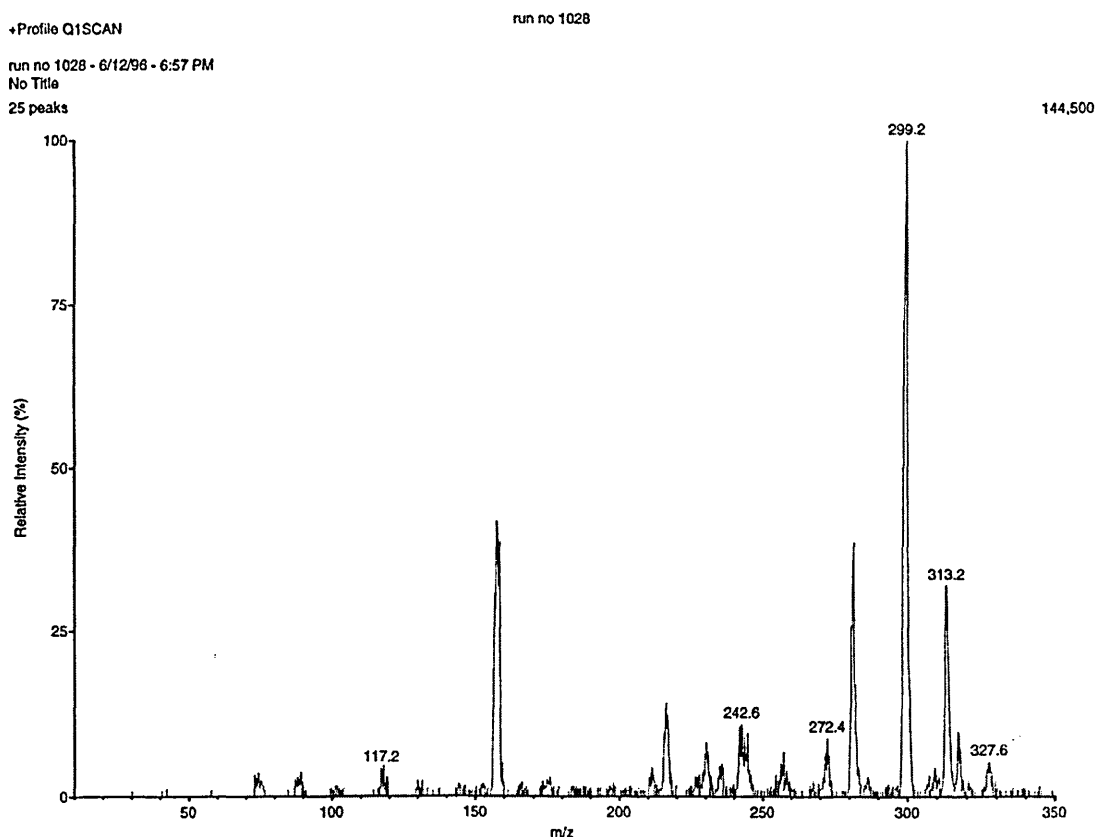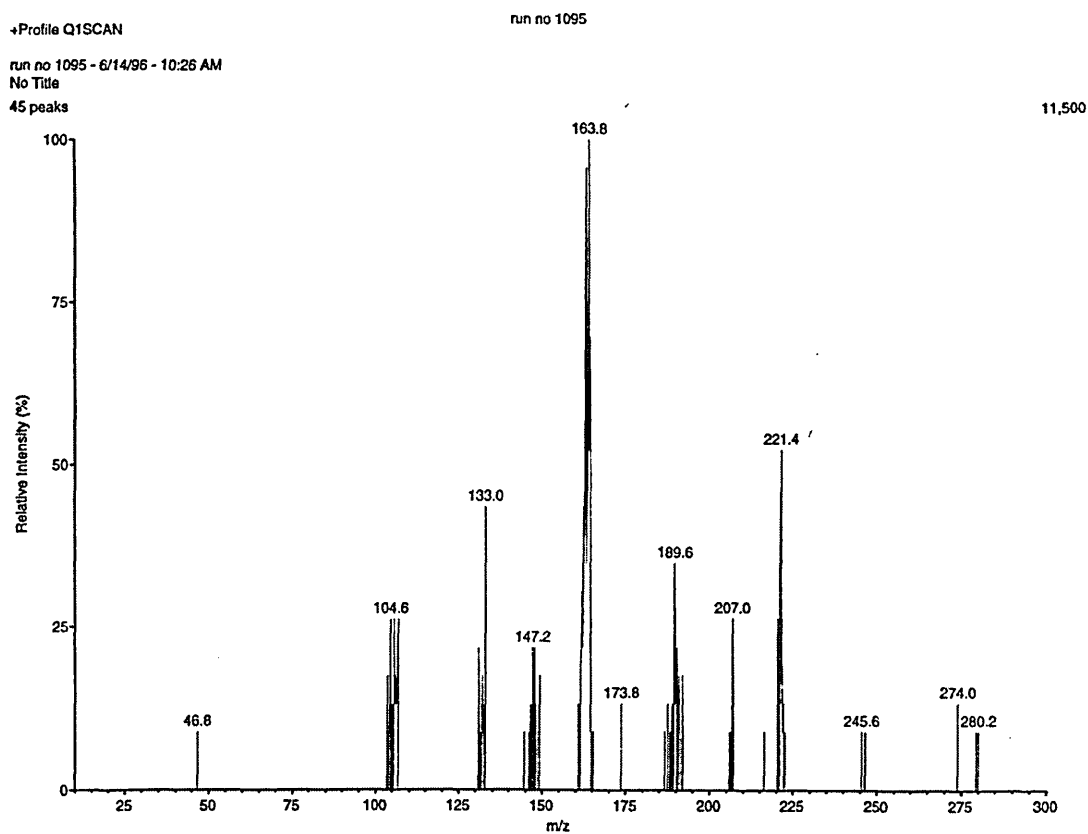

Figure 4.37: Mass spectrum of the ion clusters formed from methylhydrazine with the acetone doped drift region

Table 4.26: Summary of methylhydrazine / acetone ion chemistry; drift region doped

Precursor Ion			MS-MS Product Ions		
163	$H^+(N_2H_3CH_3)(C_3H_6O)_2$	105	$H^+(N_2H_3CH_3)(C_3H_6O)$	47	$H^+(N_2H_3CH_3)$
221	$H^+(N_2H_3CH_3)(C_3H_6O)_3$	163	$H^+(N_2H_3CH_3)(C_3H_6O)_2$	105	$H^+(N_2H_3CH_3)(C_3H_6O)$
133	$H^+(C_4H_{10}N_2)(N_2H_3CH_3)$	87	$H^+(C_4H_{10}N_2)$		
105	$H^+(N_2H_3CH_3)(C_3H_6O)$	59	$H^+(C_3H_6O)$	47	$H^+(N_2H_3CH_3)$
*279	$H^+(N_2H_3CH_3)(C_3H_6O)_4$				
173	$H^+(C_4H_{10}N_2)_2$	87	$H^+(C_4H_{10}N_2)$		
47	$H^+(N_2H_3CH_3)$				
145	$H^+(C_4H_{10}N_2)(C_3H_6O)$	87	$H^+(C_4H_{10}N_2)$		

*Confirmation of ion-molecule composition by MS-MS analysis was unavailable

+Profile DAUGHTER, Parent = 220

run no 74

run no 74 - 5/16/96 - 9:40 AM
No Title
5 peaks

1200
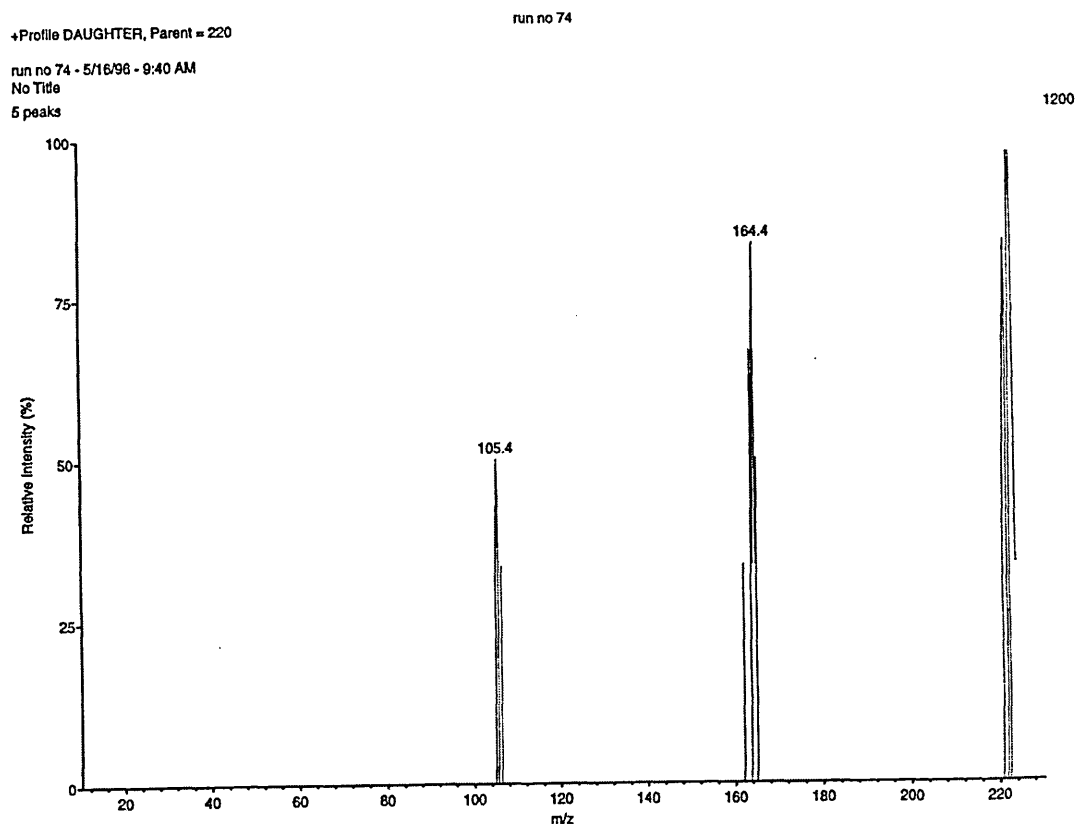
Figure 4.38: Product ion mass spectrum of the methylhydrazine / acetone ion-molecule cluster at m/z 221

During this experiment, the presence of the $H^+(N_2H_3CH_3)(C_3H_6O)_5$ ion cluster was not investigated, but the low intensity of the ion peak at m/z 279 was an indication that an ion-molecule cluster with a greater number of ketone molecules attached would have been improbable. Consideration of the relative peak intensities indicated that the cluster with the fourth ketone molecule was either not readily formed or was unstable, so that the fourth ketone molecule was only attracted weakly. However, the intensity of the $H^+(N_2H_3CH_3)(C_3H_6O)_3$ peak indicated that this cluster was readily formed. For MMH, the model had only predicted two molecules of ketone would be attracted to the most basic of the core nitrogens. Therefore, it must be assumed that the additional ketone molecules were attracted to the hydrogen atoms around the second nitrogen in MMH or formed a second layer of ketones through solvation.

4.14.2 3-Pentanone / methylhydrazine ion chemistry

Using the IMS-MS-MS system, with only the source region doped with 3-pentanone, for the determination of MMH (Figure 4.39), the predominant ion clusters were recorded at m/z 133, $H^+(N_2H_3CH_3)(C_5H_{10}O)$, m/z 179, $H^+(N_2H_3CH_3)_2(C_5H_{10}O)$, m/z 93, $H^+(N_2H_3CH_3)_2$ and m/z 219, $H^+(N_2H_3CH_3)(C_5H_{10}O)_2$. Low intensity peaks were recorded for the following ion-molecule clusters: $H^+(C_5H_{10}O)_2$, $H^+(C_5H_{10}O)$, $H^+(C_6H_{14}N_2)$, $H^+(N_2H_3CH_3)_3$ (see Figure 4.40 for the product ion mass spectrum), and $H^+(N_2H_3CH_3)$. The results are listed in Table 4.27. Some contamination was attributed to the presence of ammonia and, perhaps, hydrazine.

The presence of the ion-molecule cluster $H^+(N_2H_3CH_3)(C_5H_{10}O)_3$ was not investigated, but the $H^+(C_5H_{10}O)_3$ cluster was not recorded in the spectrum. The detection of ion-molecule clusters containing more than one molecule of the analyte in conjunction with the dopant was apparent in this experiment. This type of ion-molecule cluster had been seen previously, during the set of experiments involving ammonia.

+Profile Q1SCAN

run no 1098 - 6/14/96 - 11:41 AM
No Title
31 peaks

81,000
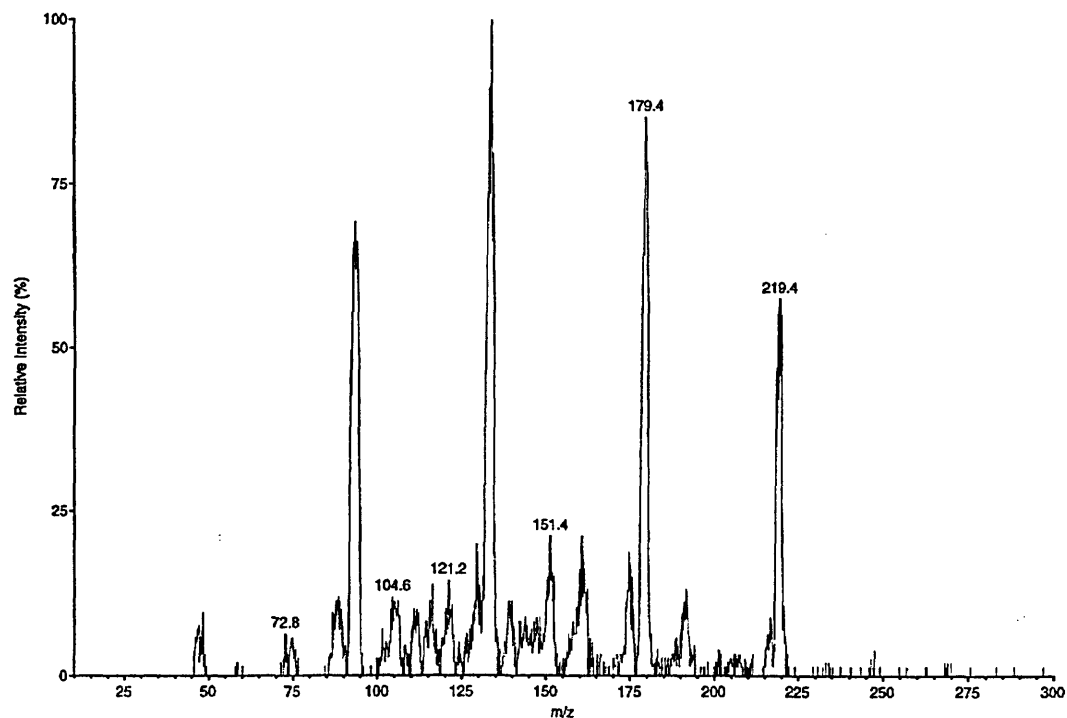
Figure 4.39: Mass spectrum of the ion clusters formed from methylhydrazine with the 3-pentanone doped source region

+Profile DAUGHTER, Parent = 138

run no 337 - 5/23/96 - 12:09 PM
No Title
13 peaks

16,400
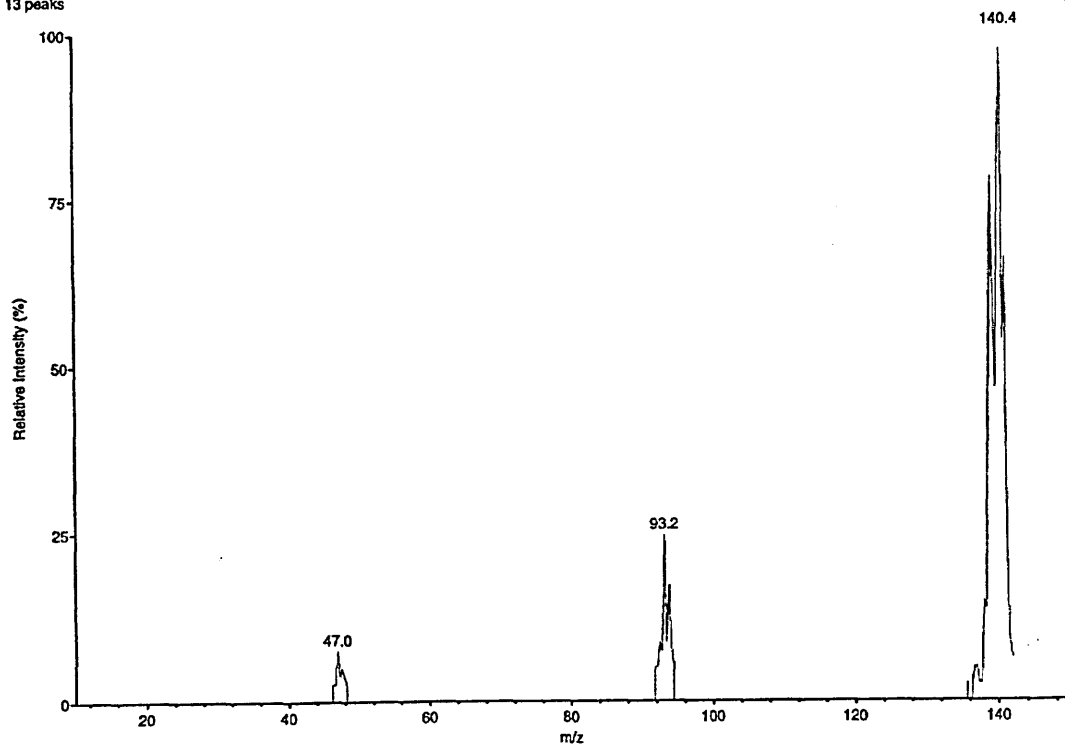
Figure 4.40: Product ion mass spectrum of the methylhydrazine ion-molecule cluster at m/z 139

Table 4.27: Summary of methylhydrazine / 3-pentanone ion chemistry; source region doped

Precursor Ion		MS-MS Product Ions			
133	$H^+(N_2H_3CH_3)(C_5H_{10}O)$	47	$H^+(N_2H_3CH_3)$		
*179	$H^+(N_2H_3CH_3)_2(C_5H_{10}O)$				
93	$H^+(N_2H_3CH_3)_2$	47	$H^+(N_2H_3CH_3)$		
219	$H^+(N_2H_3CH_3)(C_5H_{10}O)_2$	133	$H^+(N_2H_3CH_3)(C_5H_{10}O)$	47	$H^+(N_2H_3CH_3)$
*161	$H^+(C_6H_{14}N_2)(N_2H_3CH_3)$				
87	$H^+(C_5H_{10}O)$				
115	$H^+(C_6H_{14}N_2)$				
139	$H^+(N_2H_3CH_3)_3$	93	$H^+(N_2H_3CH_3)_2$	47	$H^+(N_2H_3CH_3)$
47	$H^+(N_2H_3CH_3)$				
173	$H^+(C_5H_{10}O)_2$	87	$H^+(C_5H_{10}O)$		
201	$H^+(C_6H_{14}N_2)(C_5H_{10}O)$	115	$H^+(C_6H_{14}N_2)$		

*Confirmation of ion-molecule composition by MS-MS analysis was unavailable

Increased dopant concentration, by its addition through the drift region, saw the equilibrium shift the predominance to the ion cluster at m/z 219 (Figure 4.41), with the ion cluster at m/z 133 much lower in intensity. The shift in equilibrium also produced low intensity peaks of the ion clusters $H^+(N_2H_3CH_3)(C_5H_{10}O)_3$ at m/z 305 and $H^+(C_6H_{14}N_2)(C_5H_{10}O)$ at m/z 201, which had not been confirmed at the lower dopant concentration. It was stated earlier in this section that the presence of the $H^+(N_2H_3CH_3)(C_5H_{10}O)_3$ ion at m/z 305 had not been investigated. However, due to the presence of only a low intensity peak for this ion at the higher dopant concentration it was assumed that this ion-molecule cluster did not exist during the source-only doped tests as the ketone concentration would have been insufficient to support its formation. This theory was supported by the presence of peaks for the monomer, dimer, and trimer

ion species of the analyte, without combination of the ketones. There was no indication

of the $H^+(N_2H_3CH_3)(C_5H_{10}O)_4$ cluster. The results are listed in Table 4.28.

+Profile Q1SCAN

run no 1100

run no 1100 - 6/14/96 - 11:45 AM
No Title

35 peaks

50,500
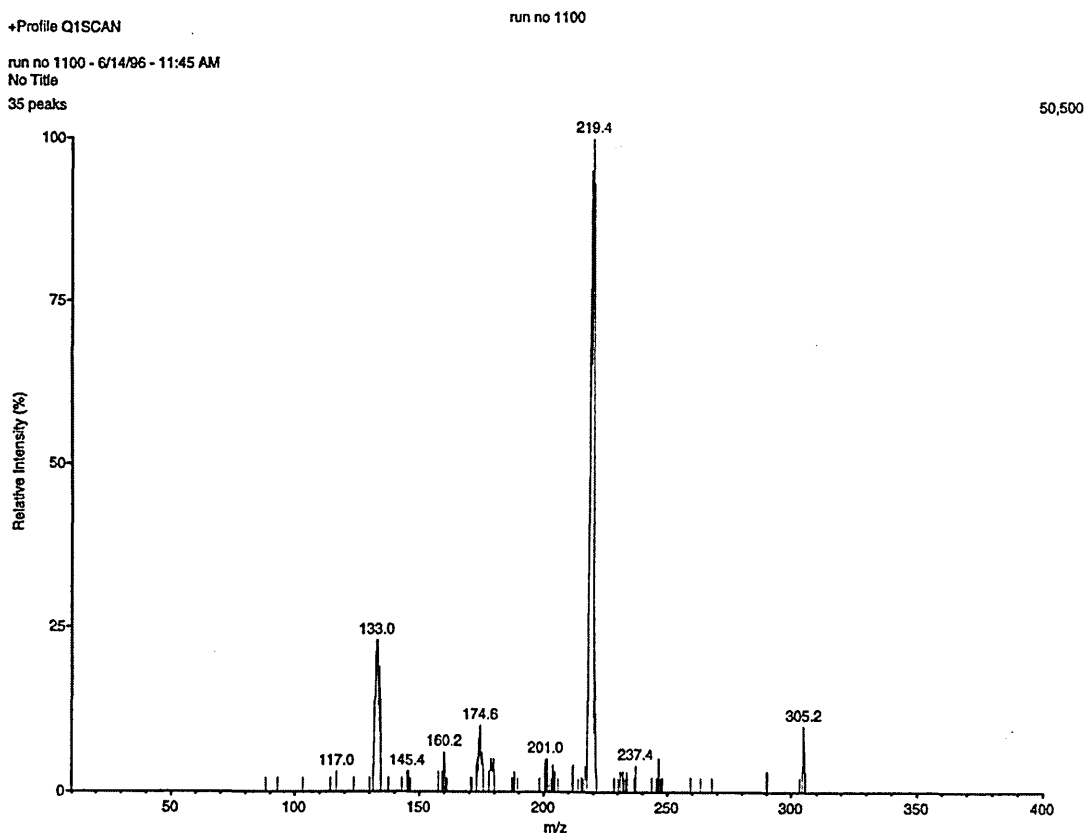
Figure 4.41: Mass spectrum of the ion clusters formed from methylhydrazine with the
3-pentanone doped drift region

Table 4.28: Summary of methylhydrazine / 3-pentanone ion chemistry; drift region
doped

Precursor Ion		MS-MS Product Ions			
219	$H^+(N_2H_3CH_3)(C_5H_{10}O)_2$	133	$H^+(N_2H_3CH_3)(C_5H_{10}O)$	47	$H^+(N_2H_3CH_3)$
133	$H^+(N_2H_3CH_3)(C_5H_{10}O)$	47	$H^+(N_2H_3CH_3)$		
*305	$H^+(N_2H_3CH_3)(C_5H_{10}O)_3$				
201	$H^+(C_6H_{14}N_2)(C_5H_{10}O)$	115	$H^+(C_6H_{14}N_2)$		
*179	$H^+(N_2H_3CH_3)_2(C_5H_{10}O)$				
*161	$H^+(C_6H_{14}N_2)(N_2H_3CH_3)$				

*Confirmation of ion-molecule composition by MS-MS analysis was unavailable

4.14.3 4-Heptanone / methylhydrazine ion chemistry

Two predominant ion clusters of comparable intensity were formed during the determination of MMH when the source region was doped with 4-heptanone (Figure 4.42). These ion clusters occurred at m/z values 275 and 161, corresponding to $H^+(N_2H_3CH_3)(C_7H_{14}O)_n$, where n = 2 and 1 respectively. Other significant ion clusters were recorded at m/z values of 143 and 257, $H^+(C_8H_{18}N_2)$ and $H^+(C_8H_{18}N_2)(C_7H_{14}O)$. Ion peaks observed at m/z values of 207, 93, 47, and 229, were assigned to the ion-molecule clusters of $H^+(N_2H_3CH_3)_2(C_7H_{14}O)$, the protonated dimer and monomer of MMH, and the dimer of 4-heptanone $H^+(C_7H_{14}O)_2$. The product ion mass spectrum of the ion-molecule cluster at m/z 207 is shown in Figure 4.43. The ion-molecule clusters are listed in Table 4.29. Again, m/z values for contaminant species were calculated as ion-molecule clusters which involved other ketones from the series and the presence of ammonia.

+Profile Q1SCAN

run no 1104

run no 1104 - 6/14/96 - 2:26 PM
No Title
33 peaks

108,000
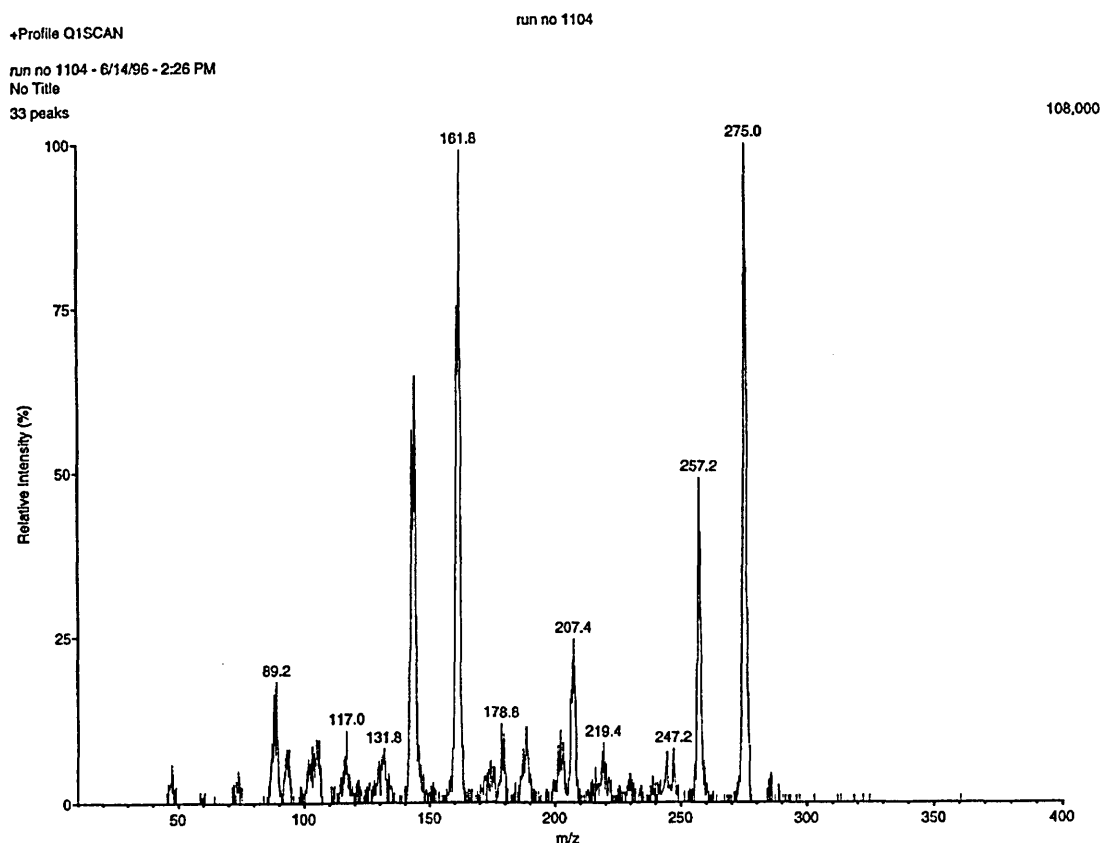
Figure 4.42: Mass spectrum of the ion clusters formed from methylhydrazine with the 4-heptanone doped source region

run no 336
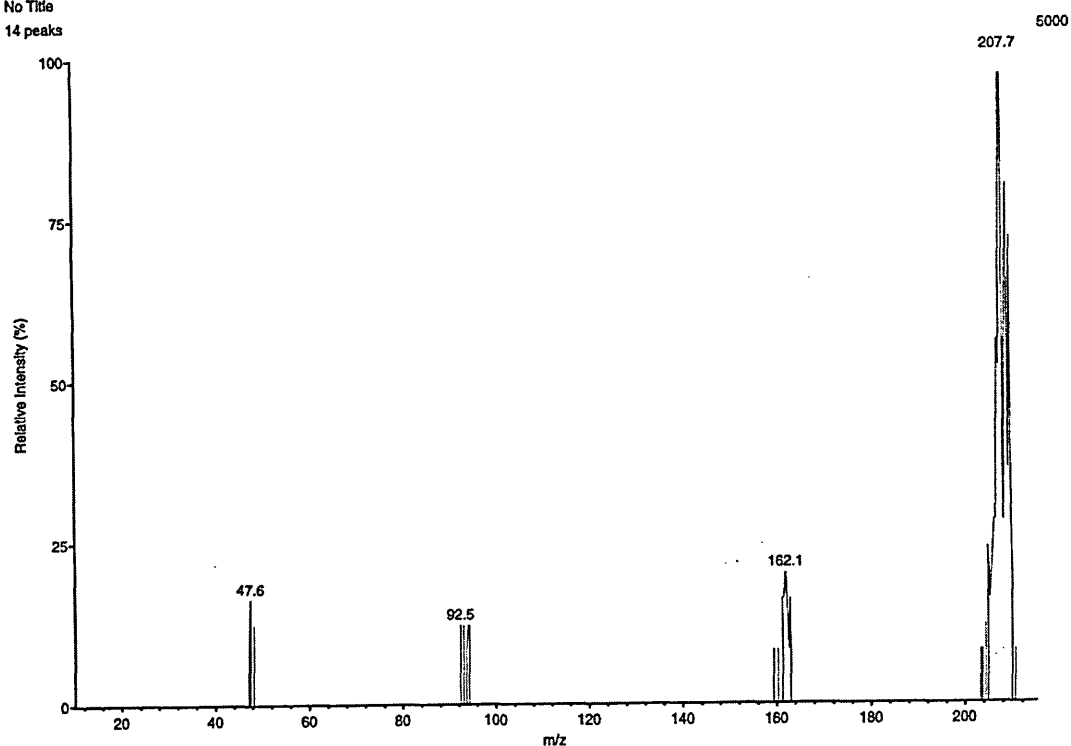
Figure 4.43: Product ion mass spectrum of the methylhydrazine ion-molecule cluster at m/z 207

Table 4.29: Summary of methylhydrazine / 4-heptanone ion chemistry; source region doped

Precursor Ion		MS-MS Product Ions					
275	$H^+(N_2H_3CH_3)(C_7H_{14}O)_2$	161	$H^+(N_2H_3CH_3)(C_7H_{14}O)$				
161	$H^+(N_2H_3CH_3)(C_7H_{14}O)$	47	$H^+(N_2H_3CH_3)$				
*143	$H^+(C_8H_{18}N_2)$						
257	$H^+(C_8H_{18}N_2)(C_7H_{14}O)$	143	$H^+(C_8H_{18}N_2)$				
207	$H^+(N_2H_3CH_3)_2(C_7H_{14}O)$	161	$H^+(N_2H_3CH_3)(C_7H_{14}O)$	93	$H^+(N_2H_3CH_3)_2$	47	$H^+(N_2H_3CH_3)$
93	$H^+(N_2H_3CH_3)_2$	47	$H^+(N_2H_3CH_3)$				
47	$H^+(N_2H_3CH_3)$						
*229	$H^+(C_7H_{14}O)_2$						
*189	$H^+(C_8H_{18}N_2)(N_2H_3CH_3)$						
285	$H^+(C_8H_{18}N_2)_2$	143	$H^+(C_8H_{18}N_2)$				
115	$H^+(C_7H_{14}O)$						

*Confirmation of ion-molecule composition by MS-MS analysis was unavailable

The higher concentration of dopant, achieved through doping of the system via the drift region, significantly increased the relative intensity of the ion cluster at m/z 275 (see Figure 4.44). Most of the other ions found with the lower concentration of dopant were reduced to trace quantities. The increased dopant concentration allowed the formation of an ion cluster recorded at m/z 389, in the short range scan of 250 to 460 amu, identified as $H^+(N_2H_3CH_3)(C_7H_{14}O)_3$ (Figure 4.45).

This result was significant because the peak was not recorded in the original spectrum range of 1 to 400 amu. Because the ion cluster was predicted, it was possible to determine its presence through the shorter range scan which led to a greater number of scans averaged. It would not have been possible to detect $H^+(N_2H_3CH_3)(C_7H_{14}O)_4$ at m/z 503. The ion clusters are listed in Table 4.30.

+Profile Q1SCAN

run no 1105

run no 1105 - 6/14/96 - 2:29 PM
No Title

11 peaks

238,000
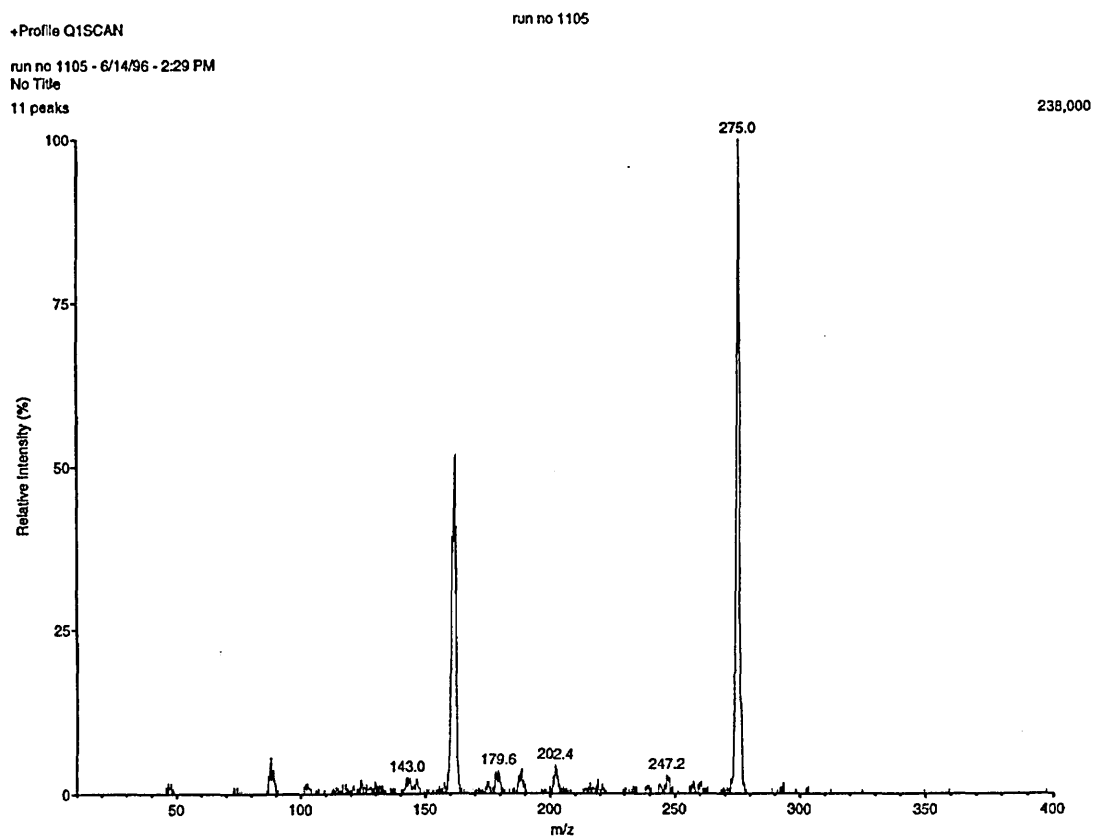
Figure 4.44: Mass spectrum of the ion clusters formed from methylhydrazine with the 4-heptanone doped drift region
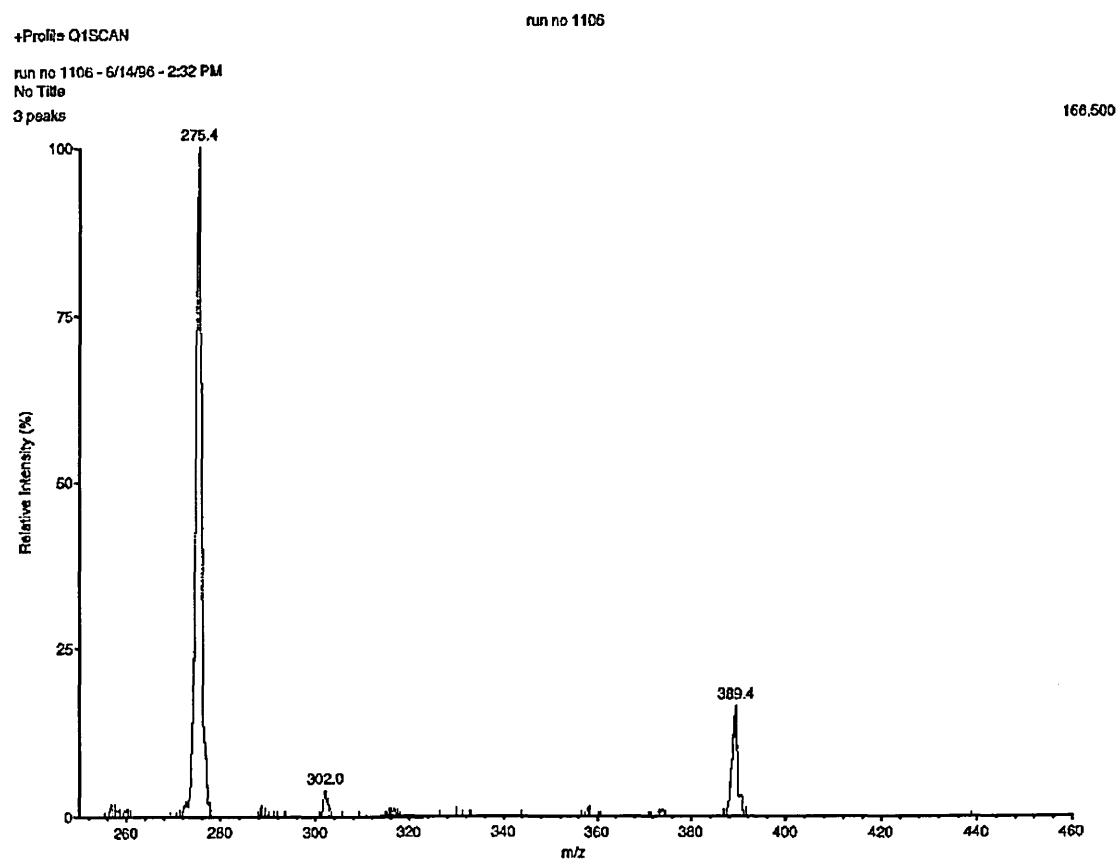
Figure 4.45: Mass spectrum of the ion clusters formed from methylhydrazine with the 4-heptanone doped drift region, in the range 250 to 460 amu

Table 4.30: Summary of methylhydrazine / 4-heptanone ion chemistry; drift region doped

Precursor Ion		MS-MS Product Ions			
275	$H^+(N_2H_3CH_3)(C_7H_{14}O)_2$	161	$H^+(N_2H_3CH_3)(C_7H_{14}O)$		
161	$H^+(N_2H_3CH_3)(C_7H_{14}O)$				
*143	$H^+(C_8H_{18}N_2)$				
*189	$H^+(C_8H_{18}N_2)(N_2H_3CH_3)$				
47	$H^+(N_2H_3CH_3)$	47	$H^+(N_2H_3CH_3)$		
389	$H^+(N_2H_3CH_3)(C_7H_{14}O)_3$	275	$H^+(N_2H_3CH_3)(C_7H_{14}O)_2$	161	$H^+(N_2H_3CH_3)(C_7H_{14}O)$

*Confirmation of ion-molecule composition by MS-MS analysis was unavailable

4.14.4 5-Nonanone / methylhydrazine ion chemistry

The precursor ion spectrum of MMH detection with a 5-nonanone doped source region appeared to be contaminated with acetone, which contributed to the major ions. However, there was a clear indication of the reaction of MMH with 5-nonanone through the formation of the corresponding protonated 5-nonanone hydrazone at m/z 171. This reaction product combined with MMH to produce $H^+(C_{10}H_{22}N_2)(N_2H_3CH_3)$ at m/z 217. 5-Nonanone also combined with unreacted MMH to form a cluster at m/z 189, $H^+(N_2H_3CH_3)(C_9H_{18}O)$. The hydrazone also combined with the ketone to produce $H^+(C_{10}H_{22}N_2)(C_9H_{18}O)$, m/z 313. The dimer ion of MMH was also present. The results are listed in Table 4.31. Again, contamination peaks were recognised as arising from clusters containing the other ketones, ammonia, and HZ.

Table 4.31: Summary of methylhydrazine / 5-nonanone ion chemistry; source region doped

Precursor Ion		MS-MS Product Ions						
171	$H^+(C_{10}H_{22}N_2)$							
217	$H^+(C_{10}H_{22}N_2)(N_2H_3CH_3)$	171	$H^+(C_{10}H_{22}N_2)$					
189	$H^+(N_2H_3CH_3)(C_9H_{18}O)$	47	$H^+(N_2H_3CH_3)$					
93	$H^+(N_2H_3CH_3)_2$	47	$H^+(N_2H_3CH_3)$					
235	$H^+(N_2H_3CH_3)_2(C_9H_{18}O)$	189	$H^+(N_2H_3CH_3)(C_9H_{18}O)$	93	$H^+(N_2H_3CH_3)_2$	47	$H^+(N_2H_3CH_3)$
313	$H^+(C_{10}H_{22}N_2)(C_9H_{18}O)$	171	$H^+(C_{10}H_{22}N_2)$					
47	$H^+(N_2H_3CH_3)$							
139	$H^+(N_2H_3CH_3)_3$	93	$H^+(N_2H_3CH_3)_2$	47	$H^+(N_2H_3CH_3)$		
143	$H^+(C_9H_{18}O)$							
*285	$H^+(C_9H_{18}O)_2$							

*Confirmation of ion-molecule composition by MS-MS analysis was unavailable

With the drift region of the spectrometer also doped with 5-nonanone the predominant ion cluster became the $H^+(N_2H_3CH_3)(C_9H_{18}O)_2$ cluster at m/z 331 (Figure 4.46). The ions of second highest intensity were those at m/z values 313 and 171, which were of comparable peak amplitude, followed by the ion clusters at m/z values of 189, and 217. The results are listed in Table 4.32. Due to a temporary malfunction of the MS-MS system, it was not possible to check for the presence of the $H^+(N_2H_3CH_3)(C_9H_{18}O)_3$ cluster at m/z 473.
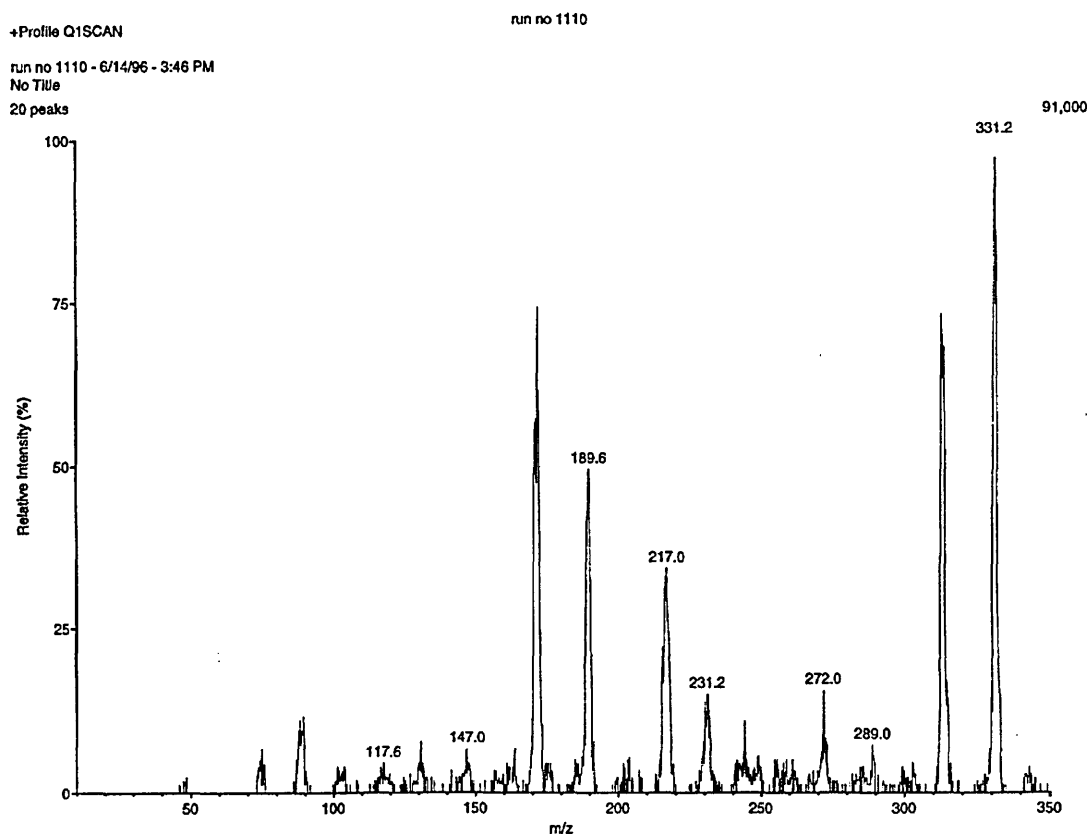
Figure 4.46: Mass spectrum of the ion clusters formed from methylhydrazine with the 5-nonanone doped drift region

Table 4.32: Summary of methylhydrazine / 5-nonanone ion chemistry; drift region doped

Precursor Ion		MS-MS Product Ions			
331	$H^+(N_2H_3CH_3)(C_9H_{18}O)_2$	189	$H^+(N_2H_3CH_3)(C_9H_{18}O)$	47	$H^+(N_2H_3CH_3)$
313	$H^+(C_{10}H_{22}N_2)(C_9H_{18}O)$	171	$H^+(C_{10}H_{22}N_2)$		
171	$H^+(C_{10}H_{22}N_2)$				
189	$H^+(N_2H_3CH_3)(C_9H_{18}O)$	47	$H^+(N_2H_3CH_3)$		
217	$H^+(C_{10}H_{22}N_2)(N_2H_3CH_3)$	171	$H^+(C_{10}H_{22}N_2)$		
*285	$H^+(C_9H_{18}O)_2$				
47	$H^+(N_2H_3CH_3)$				
*341	$H^+(C_{10}H_{22}N_2)_2$				

*Confirmation of ion-molecule composition by MS-MS analysis was unavailable

4.14.5 1,1,1-Trifluoroacetone / methylhydrazine ion chemistry

The predominant ion in the 1,1,1-trifluoroacetone doped detection of MMH (Figure 4.47) was the dimer ion of the analyte. Although a calculated m/z value of 139 for the hydrazone product of reaction of these two chemicals was recorded in the parent ion spectrum, MS-MS analysis showed this cluster to be the trimer ion of the MMH. Addition of the dopant through the drift region did not assist the formation / survival of any relevant ion clusters comprising analyte and dopant.

It was assumed that the electron withdrawing properties of the fluorine atoms decreased the activity of the normally reactive carbonyl group, through inductive effects, so that there were no reaction products. Also, MMH had a much higher proton affinity (895.7) kJ.mol^{-1}) than the 1,1,1-trifluoroacetone (725.5 kJ.mol^{-1}) which resulted in clusters of the analyte only.

+Profile Q1SCAN

run no 451

run no 451 - 5/24/96 - 2:37 PM
No Title
52 peaks

123,500
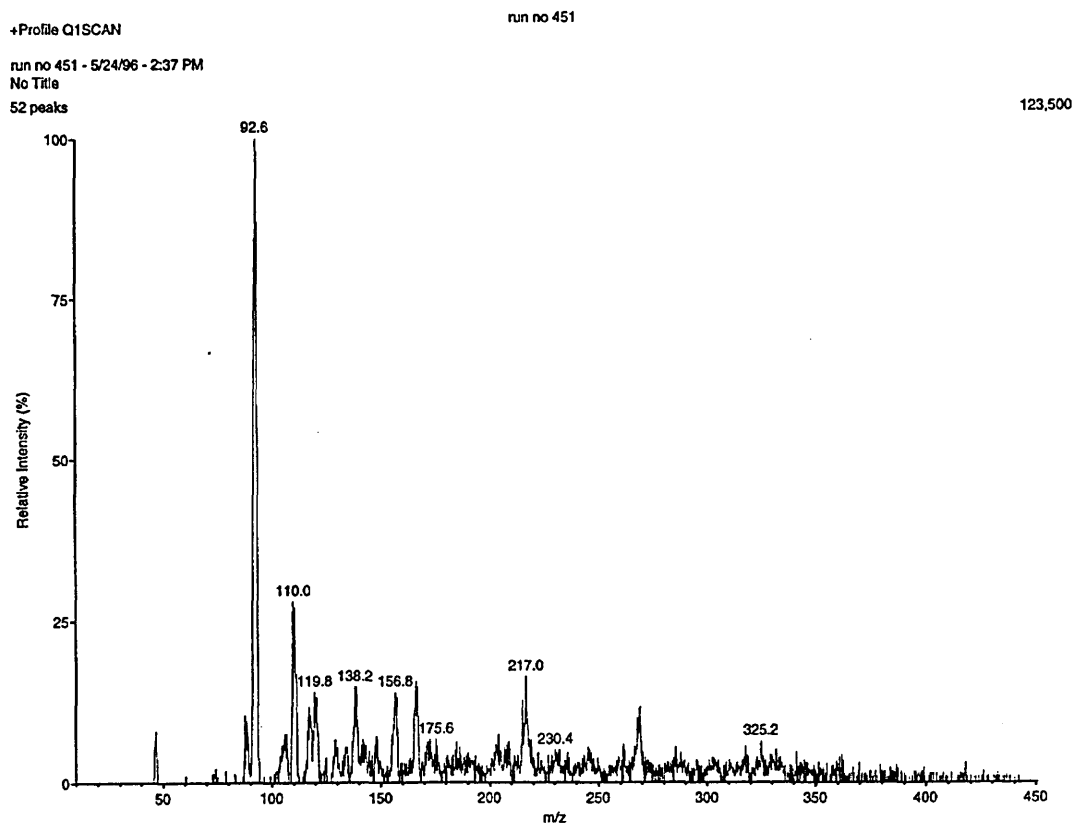
Figure 4.47: Mass spectrum of the ion clusters formed from methylhydrazine with the 1,1,1-trifluoroacetone doped source region

4.15 Proton bound clusters of ketones and 1,1-dimethylhydrazine

4.15.1 Acetone / 1,1-dimethylhydrazine ion chemistry

During the detection of UDMH with only the source region doped with acetone, the spectrometer was susceptible to the ion chemistry being controlled or predominated by what appeared to be contaminant species (Figure 4.48). The main contaminant species was MMH which, when combined with acetone, formed the $H^+(N_2H_3CH_3)(C_3H_6O)$ ion cluster at m/z 105. The preliminary experiments with UDMH also indicated MMH contamination in the system. Therefore, the experiments were repeated so that analyses involving MMH were performed last of all. Thus, there was no MMH in the system when UDMH was used as the analyte. Consequently, it was assumed that there was a

mechanism for the extraction of a methylene group, or perhaps a methyl group, from the

UDMH through primary single bond cleavage.
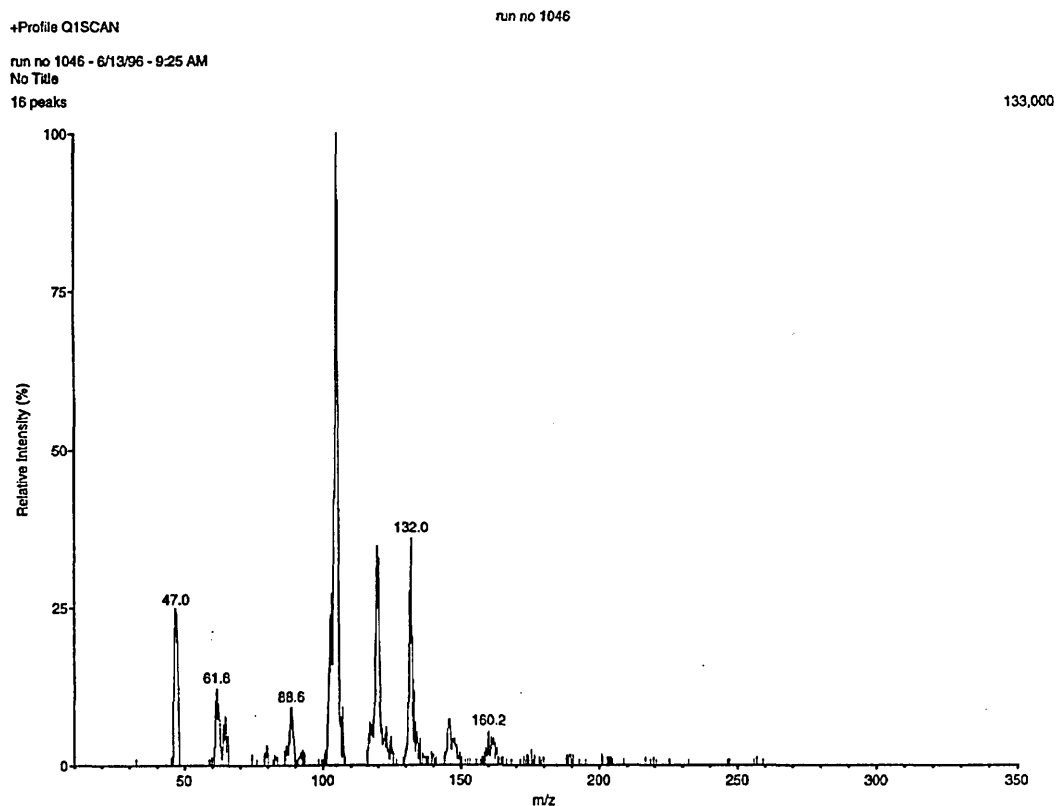
Figure 4.48: Mass spectrum of the ion clusters formed from 1,1-dimethylhydrazine with the acetone doped source region

The only evidence of clustering involving the ketone with UDMH was apparent in the $H^+(N_2(CH_3)_2H_2)(C_3H_6O)$ ion cluster at m/z 119. A peak at m/z 61 for the protonated UDMH was approximately one third of the intensity of the peak at m/z 119. The results are listed in Table 4.33. There appeared to be minor TMH contamination of the system.

Table 4.33: Summary of UDMH / acetone ion chemistry; source region doped

Precursor Ion		MS-MS Ions	
105	$H^+(N_2H_3CH_3)(C_3H_6O)$	47	$H^+(N_2H_3CH_3)$
119	$H^+(N_2(CH_3)_2H_2)(C_3H_6O)$	59	$H^+(C_3H_6O)$
*133	$H^+(C_4H_{10}N_2)(N_2H_3CH_3)$		
47	$H^+(N_2H_3CH_3)$		
61	$H^+(N_2(CH_3)_2H_2)$		
*147	$H^+(C_4H_{10}N_2)(N_2(CH_3)_2H_2)$		
117	$H^+(C_3H_6O)_2$	59	$H^+(C_3H_6O)$
121	$H^+(N_2(CH_3)_2H_2)_2$	61	$H^+(N_2(CH_3)_2H_2)$
*161	$H^+(C_5H_{12}N_2)(N_2(CH_3)_2H_2)$		
93	$H^+(N_2H_3CH_3)_2$	47	$H^+(N_2H_3CH_3)$
*159	$H^+(C_5H_{12}N_2)(C_3H_6O)$		
101	$H^+(C_5H_{12}N_2)$		

*Confirmation of ion-molecule composition by MS-MS analysis was unavailable

Acetone doping of the drift region produced ion clusters of higher m/z values during the detection of UDMH. The acetone series $H^+(C_3H_6O)_n$, where n = 2 to 4, produced peaks at m/z 117, 175, and 233 (Figure 4.49). There was no evidence of UDMH being present in the system (see Table 4.34). All of the contamination peaks recorded were for products of the ketone and / or MMH being present in the system.

Table 4.34: Summary of UDMH / acetone ion chemistry; drift region doped

Precursor Ion		MS-MS Product Ions			
175	$H^+(C_3H_6O)_3$	117	$H^+(C_3H_6O)_2$	59	$H^+(C_3H_6O)$
117	$H^+(C_3H_6O)_2$	59	$H^+(C_3H_6O)$		
233	$H^+(C_3H_6O)_4$	175	$H^+(C_3H_6O)_3$	117	$H^+(C_3H_6O)_2$
*133	$H^+(C_4H_{10}N_2)(N_2H_3CH_3)$				
105	$H^+(N_2H_3CH_3)(C_3H_6O)$	47	$H^+(N_2H_3CH_3)$		
*201	$H^+(C_5H_{12}N_2)_2$				
119	$H^+(N_2(CH_3)_2H_2)(C_3H_6O)$	61	$H^+(N_2(CH_3)_2H_2)$		
163	$H^+(N_2H_3CH_3)(C_3H_6O)_2$	105	$H^+(N_2H_3CH_3)(C_3H_6O)$	47	$H^+(N_2H_3CH_3)$

*Confirmation of ion-molecule composition by MS-MS analysis was unavailable
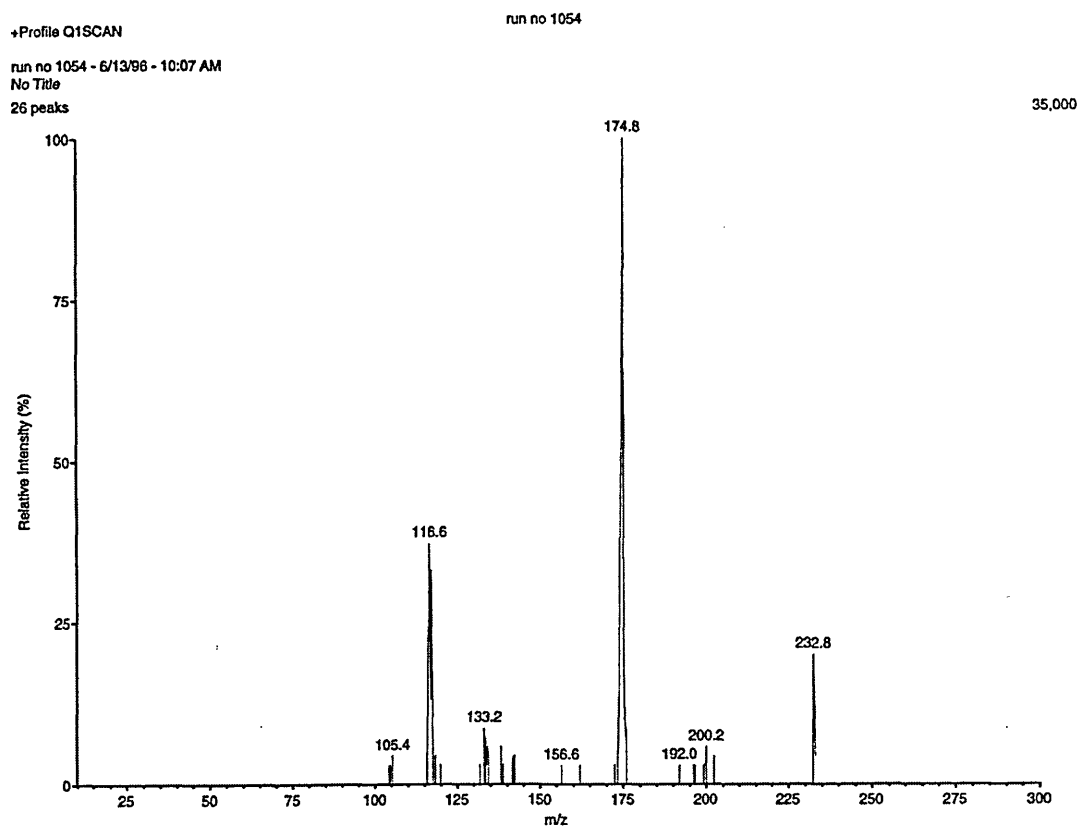
Figure 4.49: Mass spectrum of the ion clusters formed from 1,1-dimethylhydrazine with the acetone doped drift region

The results of the previous experiments, which had involved reaction between either HZ or MMH with the ketones, might be explained through their proton affinities. The proton affinity for acetone was 812.0 kJ.mol^{-1}. The symmetrical addition of methylene groups next to the carbonyl bond increased the proton affinity to 851.6 kJ.mol^{-1} for 5-nonanone. The proton affinity of HZ, at 853.2 kJ.mol^{-1}, was close to the 5-nonanone value, and as the proton affinity for the analyte and dopant were similar, either chemical would have been capable of competing for the proton leading, perhaps, to an even distribution of the positive charge between the two reactants.

The proton affinity of MMH was higher, at 895.7 kJ.mol^{-1} and would have been predominant in the competition for the protons. It was not until the greater concentration of ketone entered the system that there was sufficient distribution of protons between the analyte and dopant, so that reaction between them took place only when the drift region was doped.

The greater the methyl substitution of HZ the greater was the proton affinity. For the UDMH the proton affinity had increased to 926.6 kJ.mol^{-1}; this higher proton affinity meant that UDMH would have attracted protons preferentially and not favoured reaction with the ketone. The ion-molecule chemistry was simpler for UDMH than for either HZ or MMH.

Another explanation might have been the increased vapour pressure of the hydrazines, with greater methyl substitution leading to the relative concentrations of UDMH > MMH > HZ, so that the concentration difference between the ketone and a given hydrazine increased with progression up the homologous ketone series.

4.15.2 3-Pentanone / 1,1-dimethylhydrazine ion chemistry

The ion chemistry of the 3-pentanone doped source system in the presence of UDMH

was predominated by the unreacted analyte, present as the dimer and monomer at m/z

121 and 61 respectively (see Figure 4.50). Again, the ion chemistry was affected by the

presence of MMH (see section 4.14), the peak at m/z 133 being a combination of the

dopant and MMH, $H^+(N_2H_3CH_3)(C_5H_{10}O)$. However, in this experiment, with

3-pentanone as the dopant material, there was evidence of clustering with the UDMH

through the peak at m/z 147, $H^+(N_2(CH_3)_2H_2)(C_5H_{10}O)$ (see Figure 4.51). There was

only a trace of the monomer and dimer ketone ions. There were no significant quantities

of reaction products (see Table 4.35) due to the much higher proton affinity of UDMH

$(926.6 \text{ kJ.mol}^{-1})$.

+Profile Q1SCAN

run no 1059

run no 1059 - 6/13/96 - 11:24 AM
No Title

15 peaks

91,000
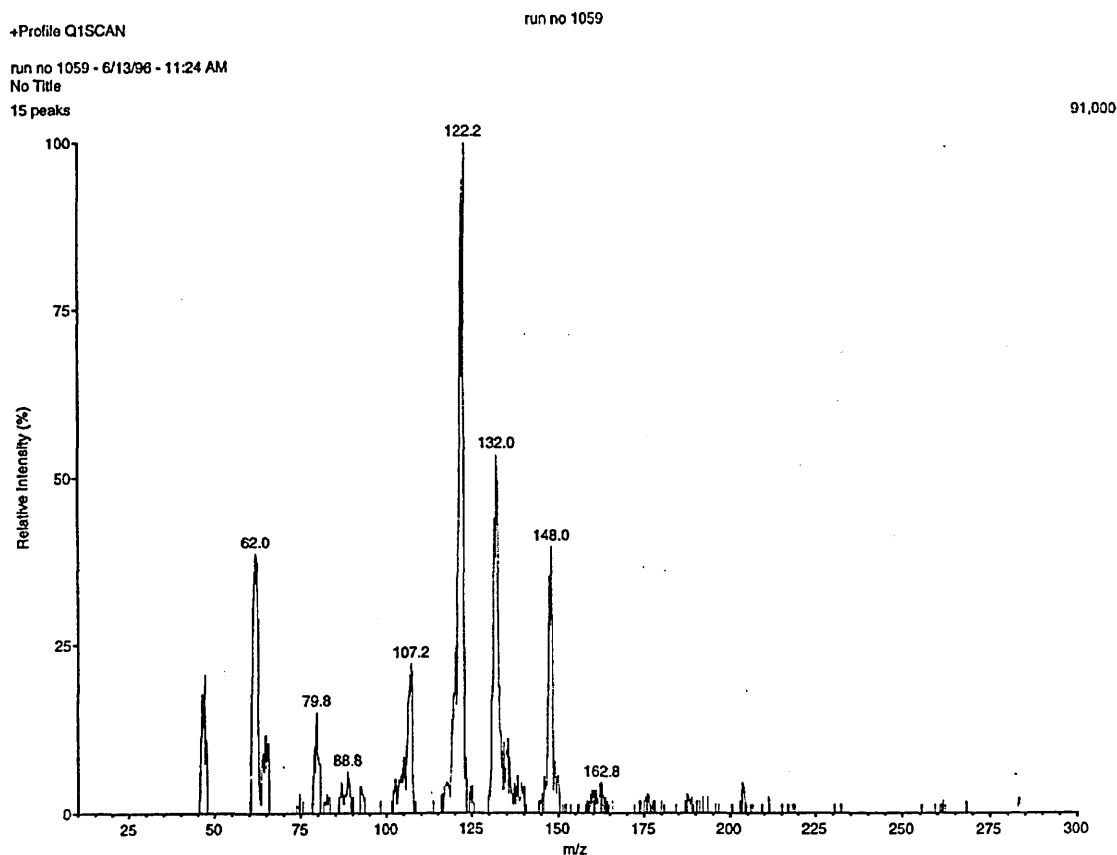
Figure 4.50: Mass spectrum of the ion clusters formed from 1,1-dimethylhydrazine with the 3-pentanone doped source region

run no 1060
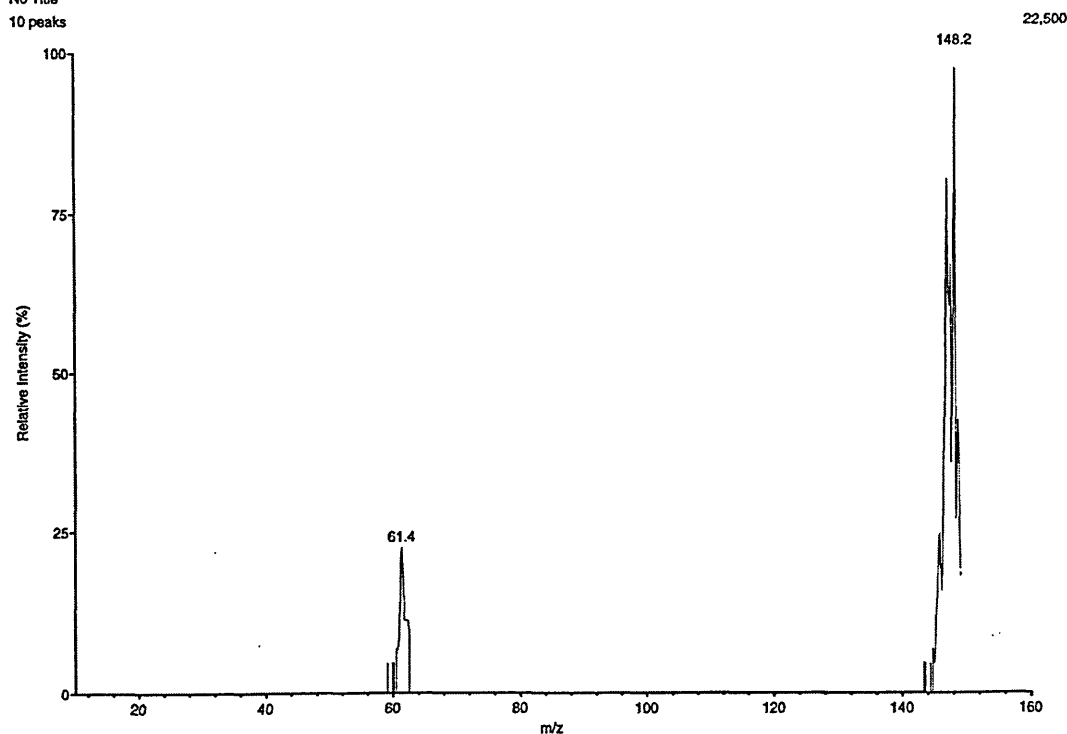
Figure 4.51: Product ion mass spectrum of the 1,1-dimethylhydrazine ion-molecule cluster at m/z 147

Table 4.35: Summary of UDMH / 3-pentanone ion chemistry; source region doped

Precursor Ion		MS-MS Product Ions			
121	$H^+(N_2(CH_3)_2H_2)_2$	61	$H^+(N_2(CH_3)_2H_2)$		
133	$H^+(N_2H_3CH_3)(C_5H_{10}O)$	87	$H^+(C_5H_{10}O)$	47	$H^+(N_2H_3CH_3)$
61	$H^+(N_2(CH_3)_2H_2)$				
147	$H^+(N_2(CH_3)_2H_2)(C_5H_{10}O)$	61	$H^+(N_2(CH_3)_2H_2)$		
107	$H^+(N_2H_3CH_3)(N_2(CH_3)_2H_2)$	61	$H^+(N_2(CH_3)_2H_2)$	47	$H^+(N_2H_3CH_3)$
47	$H^+(N_2H_3CH_3)$				
93	$H^+(N_2H_3CH_3)_2$	47	$H^+(N_2H_3CH_3)$		
*161	$H^+(C_6H_{14}N_2)(N_2H_3CH_3)$				
87	$H^+(C_5H_{10}O)$				
*187	$H^+(C_7H_{14}N_2)(N_2(CH_3)_2H_2)$				

*Confirmation of ion-molecule composition by MS-MS analysis was unavailable

It was also possible that the peaks at m/z 64 and 78 were due to ammonia combining with MMH and UDMH respectively. As in the previous section, there was an indication of TMH contamination.

Increased dopant concentration almost annihilated the dimer of the analyte although the monomer survived. The intensity of the $H^+(N_2(CH_3)_2H_2)(C_5H_{10}O)$ cluster ion at m/z 147 increased, as did the contaminant ion at m/z 133 (Figure 4.52). The larger clusters were not apparent. The peak at m/z 219 was assigned the formula $H^+(N_2H_3CH_3)(C_5H_{10}O)_2$. A trace of the ketone monomer was observed at m/z 87 (see Table 4.36). The peak at m/z 175 might have arisen from the combination of 3-pentanone with TMH.
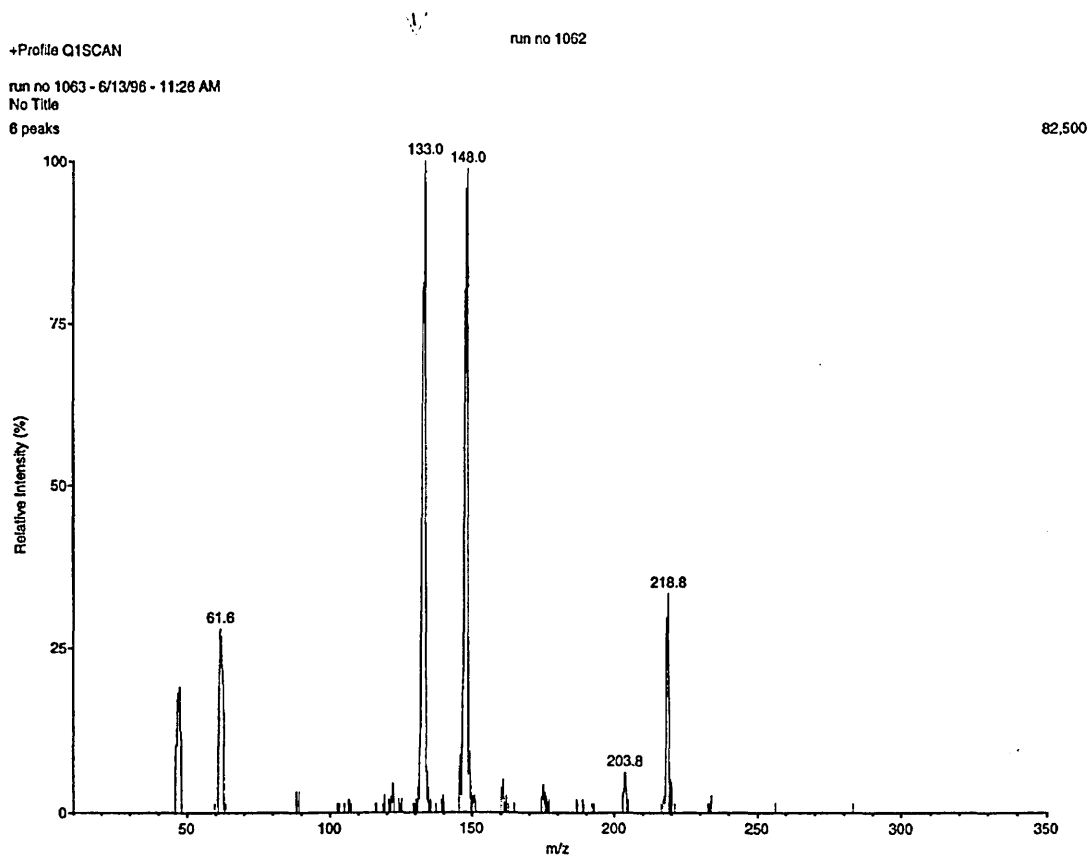
Figure 4.52: Mass spectrum of the ion clusters formed from 1,1-dimethylhydrazine with the 3-pentanone doped drift region

Table 4.36: Summary of UDMH / 3-pentanone ion chemistry; drift region doped

Precursor Ion		MS-MS Product Ions			
133	$H^+(N_2H_3CH_3)(C_5H_{10}O)$	47	$H^+(N_2H_3CH_3)$		
147	$H^+(N_2(CH_3)_2H_2)(C_5H_{10}O)$	61	$H^+(N_2(CH_3)_2H_2)$		
219	$H^+(N_2H_3CH_3)(C_5H_{10}O)_2$	133	$H^+(N_2H_3CH_3)(C_5H_{10}O)$	47	$H^+(N_2H_3CH_3)$
61	$H^+(N_2(CH_3)_2H_2)$				
47	$H^+(N_2H_3CH_3)$				
121	$H^+(N_2(CH_3)_2H_2)_2$	61	$H^+(N_2(CH_3)_2H_2)$		
*161	$H^+(C_6H_{14}N_2)(N_2H_3CH_3)$				
233	$H^+(N_2(CH_3)_2H_2)(C_5H_{10}O)_2$	147	$H^+(N_2(CH_3)_2H_2)(C_5H_{10}O)$	61	$H^+(N_2(CH_3)_2H_2)$
*187	$H^+(C_7H_{14}N_2)(N_2(CH_3)_2H_2)$				
107	$H^+(N_2H_3CH_3)(N_2(CH_3)_2H_2)$	61	$H^+(N_2(CH_3)_2H_2)$	47	$H^+(N_2H_3CH_3)$

*Confirmation of ion-molecule composition by MS-MS analysis was unavailable

4.15.3 4-Heptanone / 1,1-dimethylhydrazine ion chemistry

The 4-heptanone doped source system with UDMH analyte produced the $H^+(N_2(CH_3)_2H_2)(C_7H_{14}O)$ cluster at m/z 175 (Figure 4.53). The monomer and dimer analyte ions were recorded at m/z values of 61 and 121 (see Table 4.37). Again, significant contamination was also indicated, for example, the predominant ions at m/z values of 161 and 47 (refer to MMH ion chemistry) and so the majority of the contamination of the contamination peaks were attributed to decomposition products. Another predominant peak, at m/z 132, could have been assumed to be the combination of ammonia and 4-heptanone, but MS-MS analysis confirmed the m/z value was 133, and that the ion-molecule cluster comprised MMH combined with the contaminant 3-pentanone. The 3-pentanone could also have combined with ammonia to produce an ion peak at m/z 104, but this value appeared high; there was no obvious explanation for the peak at m/z 103. The peak at m/z 147 was probably 3-pentanone combined with UDMH. Again, UDMH and MMH combined to form an ion at m/z 107.

+Profile Q1SCAN

run no 1073 - 6/13/96 - 2:08 PM
No Title
13 peaks

59,000
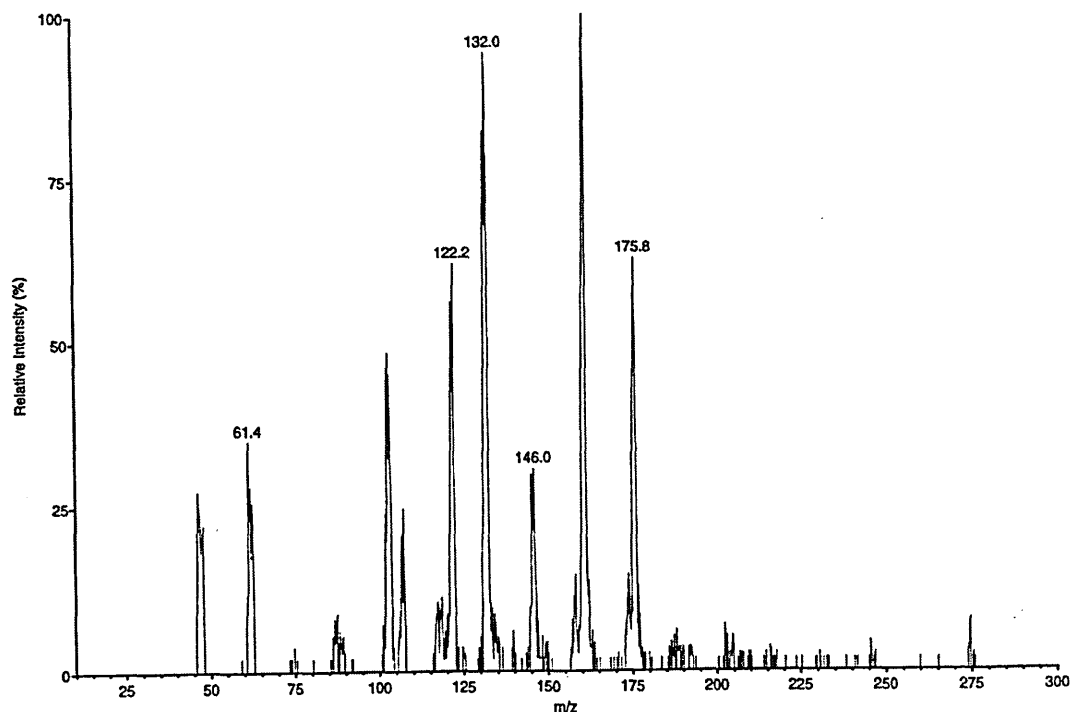
Figure 4.53: Mass spectrum of the ion clusters formed from 1,1-dimethylhydrazine with the 4-heptanone doped source region

Table 4.37: Summary of UDMH / 4-heptanone ion chemistry; source region doped

Precursor Ion		MS-MS Product Ions			
161	$H^+(N_2H_3CH_3)(C_7H_{14}O)$	47	$H^+(N_2H_3CH_3)$		
175	$H^+(N_2(CH_3)_2H_2)(C_7H_{14}O)$	61	$H^+(N_2(CH_3)_2H_2)$		
121	$H^+(N_2(CH_3)_2H_2)_2$	61	$H^+(N_2(CH_3)_2H_2)$		
61	$H^+(N_2(CH_3)_2H_2)$				
47	$H^+(N_2H_3CH_3)$				
107	$H^+(N_2H_3CH_3)(N_2(CH_3)_2H_2)$	61	$H^+(N_2(CH_3)_2H_2)$	47	$H^+(N_2H_3CH_3)$
157	$H^+(C_9H_{20}N_2)$				
275	$H^+(N_2H_3CH_3)(C_7H_{14}O)_2$	161	$H^+(N_2H_3CH_3)(C_7H_{14}O)$	47	$H^+(N_2H_3CH_3)$
*203	$H^+(C_8H_{18}N_2)(N_2(CH_3)_2H_2)$				
93	$H^+(N_2H_3CH_3)_2$	47	$H^+(N_2H_3CH_3)$		

*Confirmation of ion-molecule composition by MS-MS analysis was unavailable

The increased concentration of the 4-heptanone altered the ion chemistry to

encourage the reaction of the ketone and the analyte to produce 4-heptanone hydrazone

at m/z 157, the predominant ion (Figure 4.54). The monomer of the analyte survived,

due to the high proton affinity of UDMH. The peak at m/z 175 decreased in intensity.

There was also a trace peak indicating the combination of the hydrazone with the

ketone, at m/z 271 (see Table 4.38).
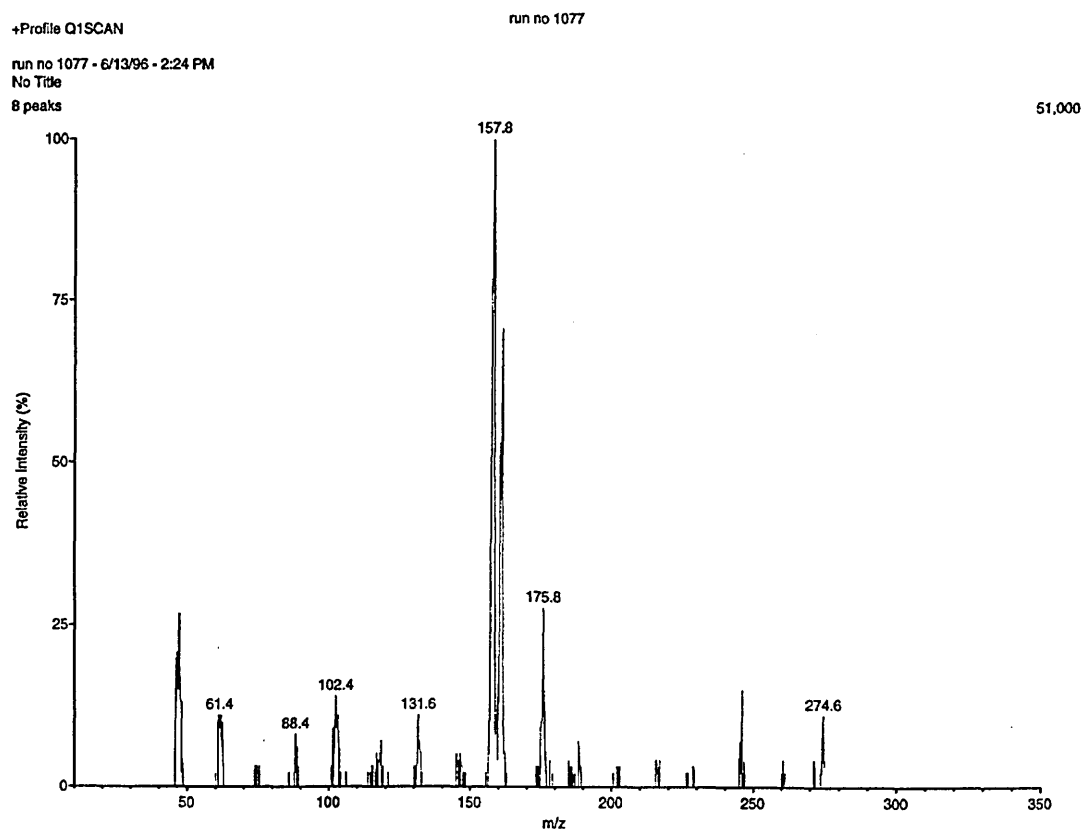
Figure 4.54: Mass spectrum of the ion clusters formed from 1,1-dimethylhydrazine with
the 4-heptanone doped drift region

Table 4.38: Summary of UDMH / 4-heptanone ion chemistry; drift region doped

Precursor Ion		MS-MS Product Ions			
157	$H^+(C_9H_{20}N_2)$				
161	$H^+(N_2H_3CH_3)(C_7H_{14}O)$	47	$H^+(N_2H_3CH_3)$		
175	$H^+(N_2(CH_3)_2H_2)(C_7H_{14}O)$	61	$H^+(N_2(CH_3)_2H_2)$		
47	$H^+(N_2H_3CH_3)$				
61	$H^+(N_2(CH_3)_2H_2)$				
*275	$H^+(N_2H_3CH_3)(C_7H_{14}O)_2$	161	$H^+(N_2H_3CH_3)(C_7H_{14}O)$	47	$H^+(N_2H_3CH_3)$
271	$H^+(C_9H_{20}N_2)(C_7H_{14}O)$				
*203	$H^+(C_8H_{18}N_2)(N_2(CH_3)_2H_2)$				
*189	$H^+(C_8H_{18}N_2)(N_2H_3CH_3)$				
115	$H^+(C_7H_{14}O)$				
229	$H^+(C_7H_{14}O)_2$	115	$H^+(C_7H_{14}O)$		
*217	$H^+(C_9H_{20}N_2)(N_2(CH_3)_2H_2)$				
121	$H^+(N_2(CH_3)_2H_2)_2$	61	$H^+(N_2(CH_3)_2H_2)$		

*Confirmation of ion-molecule composition by MS-MS analysis was unavailable

4.15.4 5-Nonanone / 1,1-dimethylhydrazine ion chemistry

With the source region doped with 5-nonanone (Figure 4.55), the introduction of UDMH produced relevant peaks at m/z values of 203, 121, 185, and 61 (see Table 4.39). The combined analyte / dopant peak of $H^+(N_2(CH_3)_2H_2)(C_9H_{18}O)$ was assigned to m/z 203; 121 and 61 were the analyte dimer and monomer ions, respectively. The peak at m/z 185 was the hydrazone reaction product $H^+(C_{11}H_{24}N_2)$. Again, contamination peaks due to the presence of MMH were recorded. The peak of highest intensity, at m/z 189, was due to the combination of MMH with 5-nonanone. Contamination peaks were similar to those in the previous section.

run no 1083

53,500
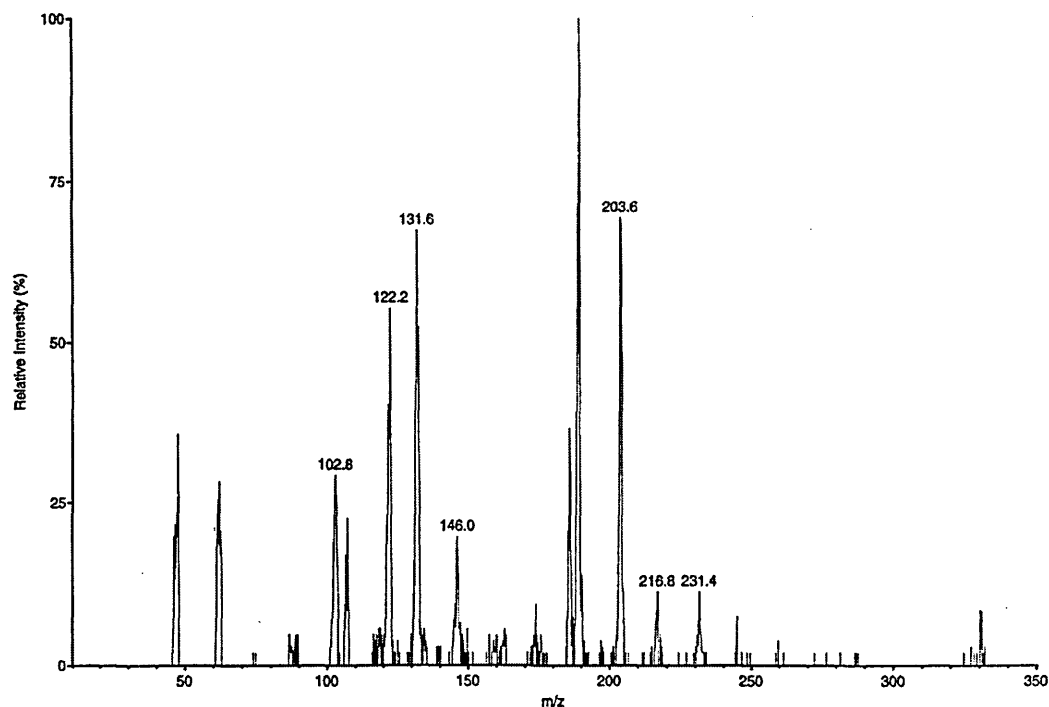
Figure 4.55: Mass spectrum of the ion clusters formed from 1,1-dimethylhydrazine with the 5-nonanone doped source region

Table 4.39: Summary of UDMH / 5-nonanone ion chemistry; source region doped

Precursor Ion		MS-MS Product Ions			
189	$H^+(N_2H_3CH_3)(C_9H_{18}O)$	47	$H^+(N_2H_3CH_3)$		
203	$H^+(N_2(CH_3)_2H_2)(C_9H_{18}O)$	61	$H^+(N_2(CH_3)_2H_2)$		
121	$H^+(N_2(CH_3)_2H_2)_2$	61	$H^+(N_2(CH_3)_2H_2)$		
185	$H^+(C_{11}H_{24}N_2)$				
47	$H^+(N_2H_3CH_3)$				
61	$H^+(N_2(CH_3)_2H_2)$				
107	$H^+(N_2H_3CH_3)(N_2(CH_3)_2H_2)$	61	$H^+(N_2(CH_3)_2H_2)$	47	$H^+(N_2H_3CH_3)$
*217	$H^+(C_{10}H_{22}N_2)(N_2H_3CH_3)$				
*231	$H^+(C_{10}H_{22}N_2)(N_2(CH_3)_2H_2)$				
331	$H^+(N_2H_3CH_3)(C_9H_{18}O)_2$	189	$H^+(N_2H_3CH_3)(C_9H_{18}O)$	47	$H^+(N_2H_3CH_3)$
245	$H^+(C_{11}H_{24}N_2)(N_2(CH_3)_2H_2)$	61	$H^+(N_2(CH_3)_2H_2)$		

*MS-MS analysis was inconclusive due to low ion population during analysis

Doping of the drift region with 5-nonanone had only a small effect upon the relative intensities of the two major peaks (see Figure 4.56 and Table 4.40). The relative intensities of the contaminant peaks at m/z values of 103 and 161 changed little. Neither peak could be identified.
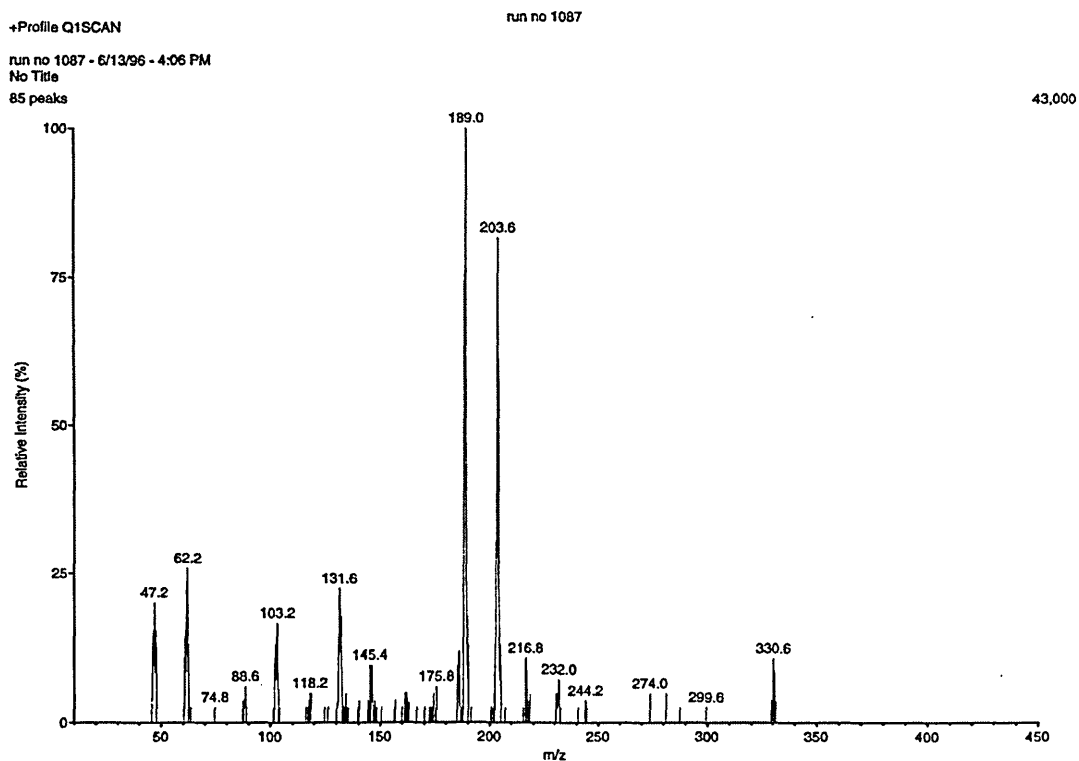
Figure 4.56: Mass spectrum of the ion clusters formed from 1,1-dimethylhydrazine with the 5-nonanone doped drift region

Table 4.40: Summary of UDMH / 5-nonanone ion chemistry; drift region doped

	Precursor Ion		MS-MS Product Ions		
189	$H^+(N_2H_3CH_3)(C_9H_{18}O)$	47	$H^+(N_2H_3CH_3)$		
203	$H^+(N_2(CH_3)_2H_2)(C_9H_{18}O)$	61	$H^+(N_2(CH_3)_2H_2)$		
61	$H^+(N_2(CH_3)_2H_2)$				
47	$H^+(N_2H_3CH_3)$				
185	$H^+(C_{11}H_{24}N_2)$				
331	$H^+(N_2H_3CH_3)(C_9H_{18}O)_2$	189	$H^+(N_2H_3CH_3)(C_9H_{18}O)$	47	$H^+(N_2H_3CH_3)$
*217	$H^+(C_{10}H_{22}N_2)(N_2H_3CH_3)$				
*231	$H^+(C_{10}H_{22}N_2)(N_2(CH_3)_2H_2)$				
245	$H^+(C_{11}H_{24}N_2)(N_2(CH_3)_2H_2)$	61	$H^+(N_2(CH_3)_2H_2)$		

*MS-MS analysis was inconclusive due to low ion population during analysis

4.15.5 1,1,1-Trifluoroacetone / 1,1-dimethylhydrazine ion chemistry

During the determination of UDMH with a 1,1,1-trifluoroacetone doped source region (Figure 4.57), there was an indication of the presence of the ion cluster $H^+(N_2(CH_3)_2H_2)(CH_3COCF_3)$ at m/z 173, although MS-MS analysis was inconclusive. This was probably because of a rapid change in the ion-molecule chemistry as a result of the volatility of the dopant, which led to the reservoir being emptied rapidly. The monomer and dimer ions of the analyte were present (see Table 4.41). The peaks at m/z values of 132, 103, and 146 were attributed to contamination and once again, MMH product ion peaks appeared to dominate.
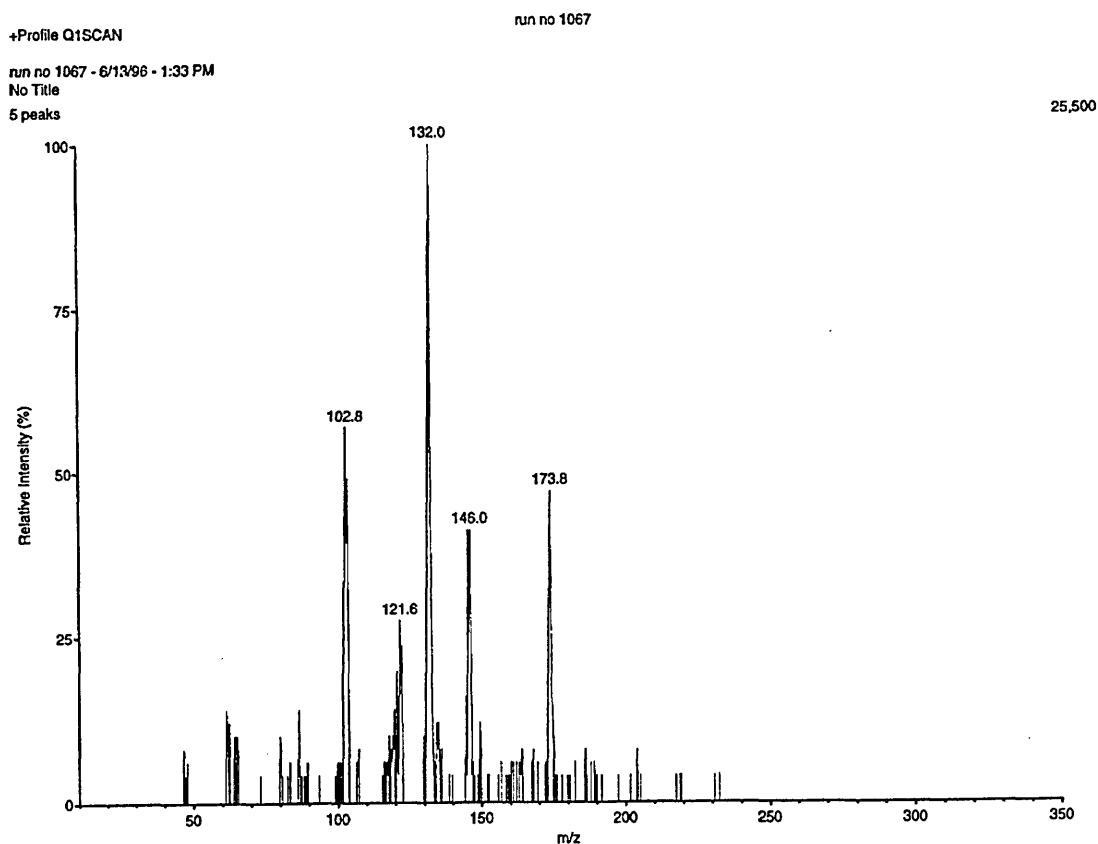
Figure 4.57: Mass spectrum of the ion clusters formed from 1,1-dimethylhydrazine with the 1,1,1-trifluoroacetone doped source region

Table 4.41: Summary of UDMH / 1,1,1-trifluoroacetone ion chemistry; source region doped

Precursor Ion		MS-MS Product Ions	
173	$H^+(N_2(CH_3)_2H_2)(CH_3COCF_3)$	61	$H^+(N_2(CH_3)_2H_2)$
121	$H^+(N_2(CH_3)_2H_2)_2$	61	$H^+(N_2(CH_3)_2H_2)$
61	$H^+(N_2(CH_3)_2H_2)$		
47	$H^+(N_2H_3CH_3)$		
159	$H^+(N_2H_3CH_3)(CH_3COCF_3)$	47	$H^+(N_2H_3CH_3)$
* 117	$H^+(C_3H_6O)_2$		
* 101	$H^+(C_5H_{12}N_2)$		

*Confirmation of ion-molecule composition by MS-MS analysis was unavailable due to insufficient intensity of the precursor ion peak

Doping the system via the drift region did little to alter the ion chemistry (see Table 4.42). Although there was an indication of the possible clustering of UDMH with one molecule of the dopant because of a peak at m/z 173, these results may be suspect due to the volatility of the dopant which may have evaporated before any significant amount of clustering could be recorded.

Table 4.42: Summary of UDMH / 1,1,1-trifluoroacetone ion chemistry; drift region doped

Precursor Ion		MS-MS Product Ions	
173	$H^+(N_2(CH_3)_2H_2)(CH_3COCF_3)$	61	$H^+(N_2(CH_3)_2H_2)$
121	$H^+(N_2(CH_3)_2H_2)_2$		
61	$H^+(N_2(CH_3)_2H_2)$		

4.16 Proton bound clusters of ketones and tetramethylhydrazine

4.16.1 Acetone / tetramethylhydrazine ion chemistry

With an acetone doped source region the introduction of TMH produced two predominant ion clusters at m/z values of 147 and 89 (Figure 4.58). These ion clusters have been identified as $H^+(C_3H_6O)(N_2(CH_3)_4)$ and $H^+(N_2(CH_3)_4)$. The dimer ion cluster of acetone was observed at m/z 117. A trace peak at m/z 176 might have been due to either the dimer ion of the dopant at m/z 175 or the dimer ion of the analyte at m/z 177, or a combination of the two species. When the table of results (Table 4.43) was compiled, the results from the experiment with the higher concentration of acetone were taken into account.
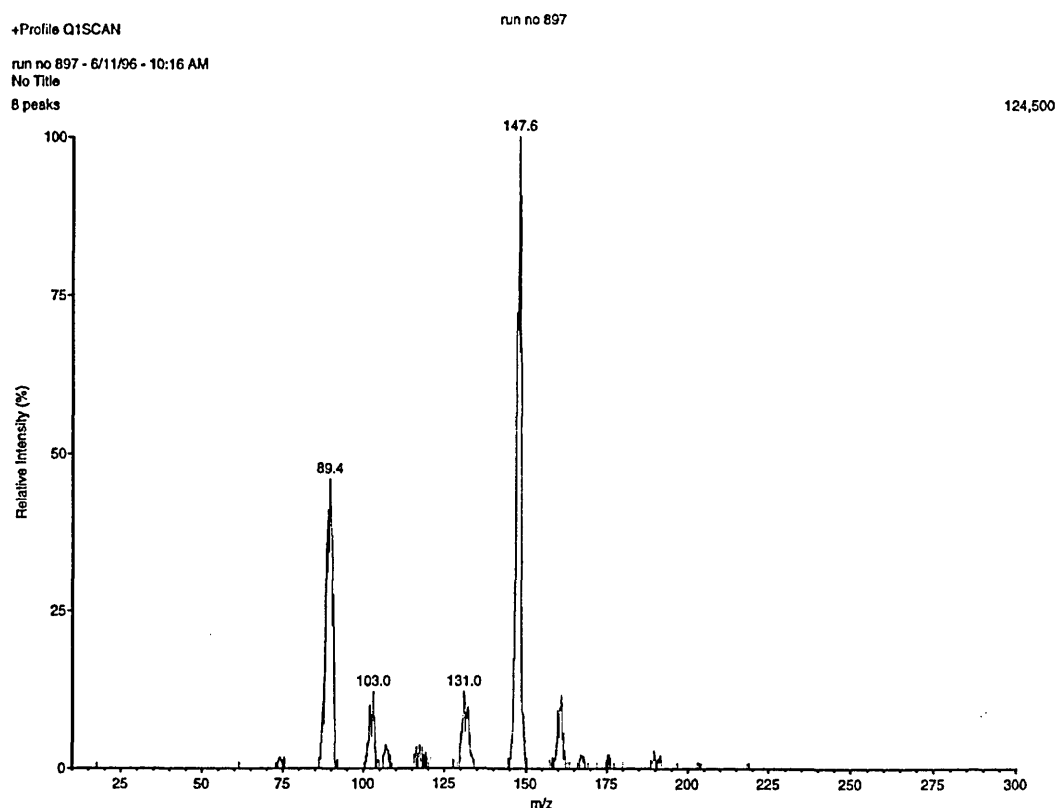
Figure 4.58: Mass spectrum of the ion clusters formed from tetramethylhydrazine with the acetone doped source region

Table 4.43: Summary of TMH / acetone chemistry; source region doped

Precursor Ion		MS-MS Product Ions	
147	$H^+(N_2(CH_3)_4)(C_3H_6O)$	89	$H^+(N_2(CH_3)_4)$
89	$H^+(N_2(CH_3)_4)$		
117	$H^+(C_3H_6O)_2$	59	$H^+(C_3H_6O)$
*175	$H^+(C_3H_6O)_3$		

*Confirmation of ion-molecule composition by MS-MS analysis was unavailable due to insufficient intensity of the precursor ion peak

Doping the complete system with acetone produced larger ion clusters of the dopant, with the trimer and tetramer predominating the ion chemistry at m/z values of 175 and 233 amu (see Figure 4.59). The indication from this experiment was that the ion peak in the region of m/z 176 was the m/z 175 ion-molecule cluster. However, the lower concentration of ketone may have allowed the existence of the dimer ion of the analyte, which has a much higher proton affinity (949.0 kJ.mol^{-1} compared with 812.0 kJ.mol^{-1}). The ion clusters of the dimer, protonated TMH, and $H^+(N_2(CH_3)_4)(C_3H_6O)$ were also present. The significant result from this experiment is that the number of dopant molecules per protonated TMH core did not exceed one. The results are listed in Table 4.44.

Table 4.44: Summary of TMH / acetone chemistry; drift region doped

Precursor Ion		MS-MS Product Ions			
175	$H^+(C_3H_6O)_3$	117	$H^+(C_3H_6O)_2$	59	$H^+(C_3H_6O)$
233	$H^+(C_3H_6O)_4$	175	$H^+(C_3H_6O)_3$	117	$H^+(C_3H_6O)_2$
117	$H^+(C_3H_6O)_2$	59	$H^+(C_3H_6O)$		
89	$H^+(N_2(CH_3)_4)$				
147	$H^+(N_2(CH_3)_4)(C_3H_6O)$	89	$H^+(N_2(CH_3)_4)$		
59	$H^+(C_3H_6O)$				
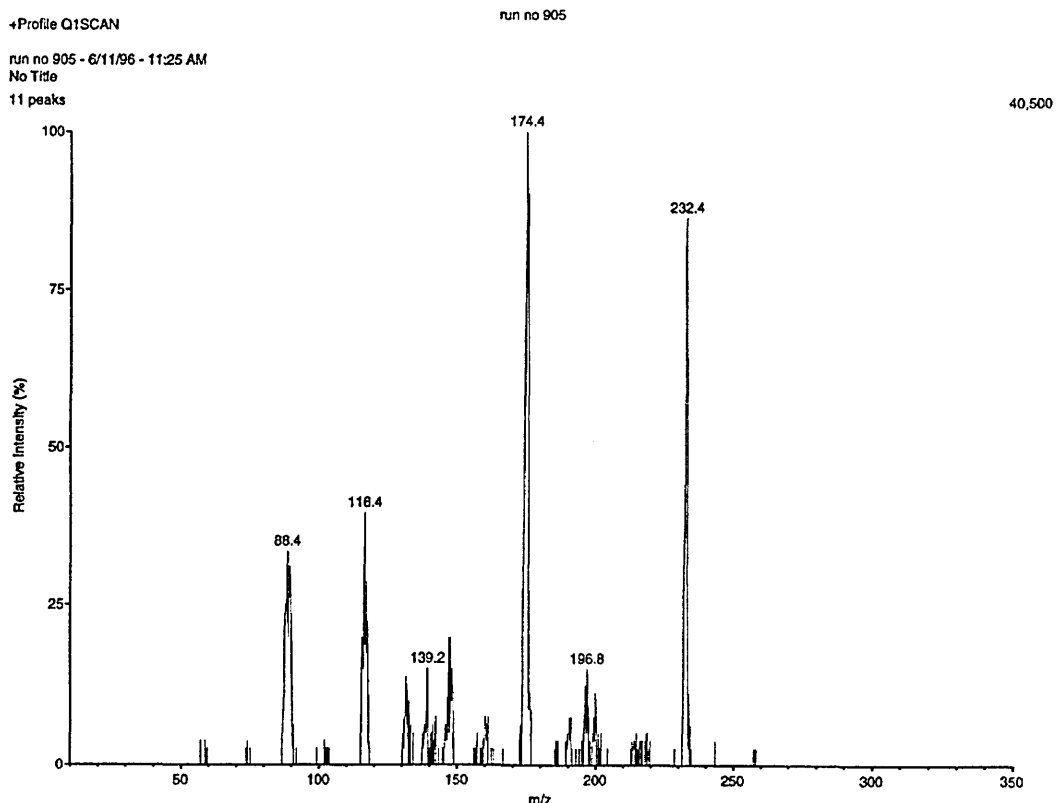
Figure 4.59: Mass spectrum of the ion clusters formed from tetramethylhydrazine with the acetone doped drift region

4.16.2 3-Pentanone / tetramethylhydrazine ion chemistry

The doping of the source region with 3-pentanone for the detection of tetramethylhydrazine produced an ion cluster with the ketone, $H^+(N_2(CH_3)_4)(C_5H_{10}O)$ at m/z 175 (Figure 4.60). Much care had to be taken in assigning the identities of the ion clusters due to the proximity of the relative masses of the ketone and the TMH. As the MS-MS product ion spectrum value of 91 was 2 amu high for TMH it was assumed that the ion cluster at 176 was most likely to be a majority of m/z 175 rather than 177, the dimer ion of TMH (Figure 4.61), even so, it was possible that the peak represented a mixture of the two species. Although this ion peak intensity was relatively high, the most abundant ion was the protonated tetramethylhydrazine, m/z 89. The ion cluster at m/z 147 might have been the previously described acetone-tetramethylhydrazine ion

cluster, formed due to the contamination of the system with acetone. Alternatively,

it could have been the mixed ketone (acetone / 3-pentanone) ion cluster at m/z 145. It

was considered that the former suggestion was the most probable, because of the higher

proton affinity of TMH, and the results of MS-MS analysis confirmed this (see Figure

4.61).
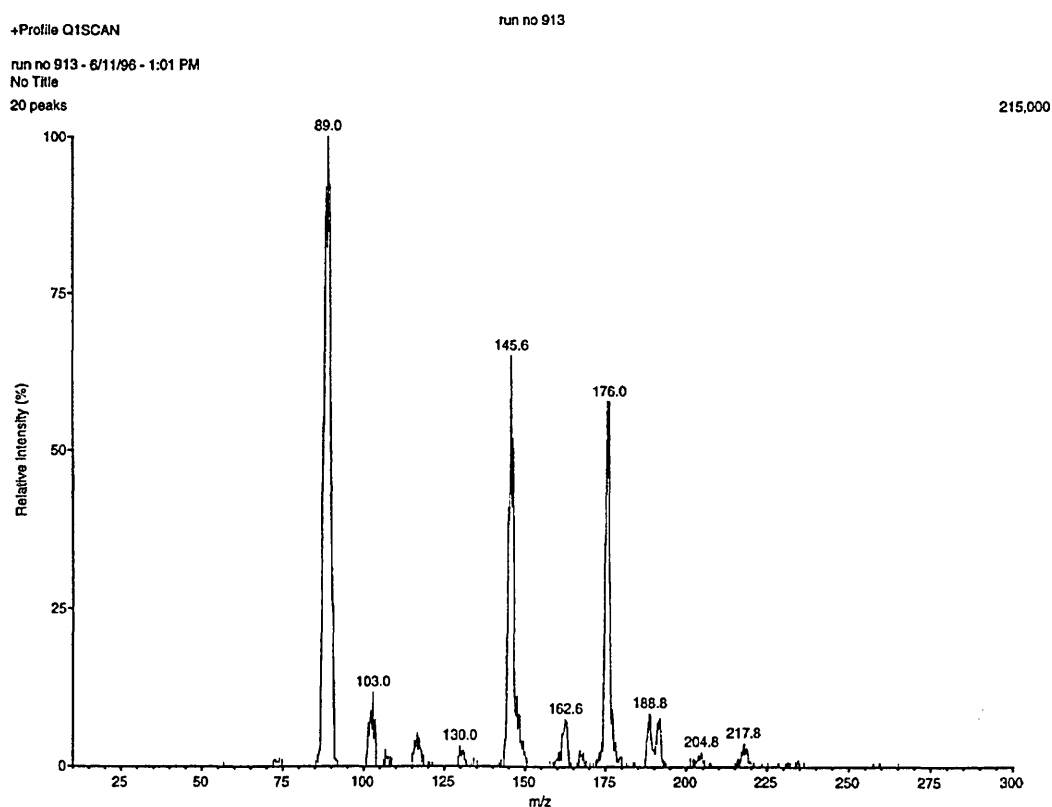
Figure 4.60: Mass spectrum of the ion clusters formed from tetramethylhydrazine with
the 3-pentanone doped source region

With the drift region also doped with 3-pentanone the predominant ion peak was

recorded at m/z 176, again, a possible mixture of the $H^+(N_2(CH_3)_4)(C_5H_{10}O)$ and

$H^+(N_2(CH_3)_4)_2$ ion-molecule clusters. The analyte ion peak was less than half the

intensity of the ketone bound TMH. The indication was that the mixed ketone ion

cluster may have present at m/z 145. Surprisingly, an ion cluster was observed at m/z

261, possibly the $H^+(N_2(CH_3)_4)(C_5H_{10}O)_2$ cluster.
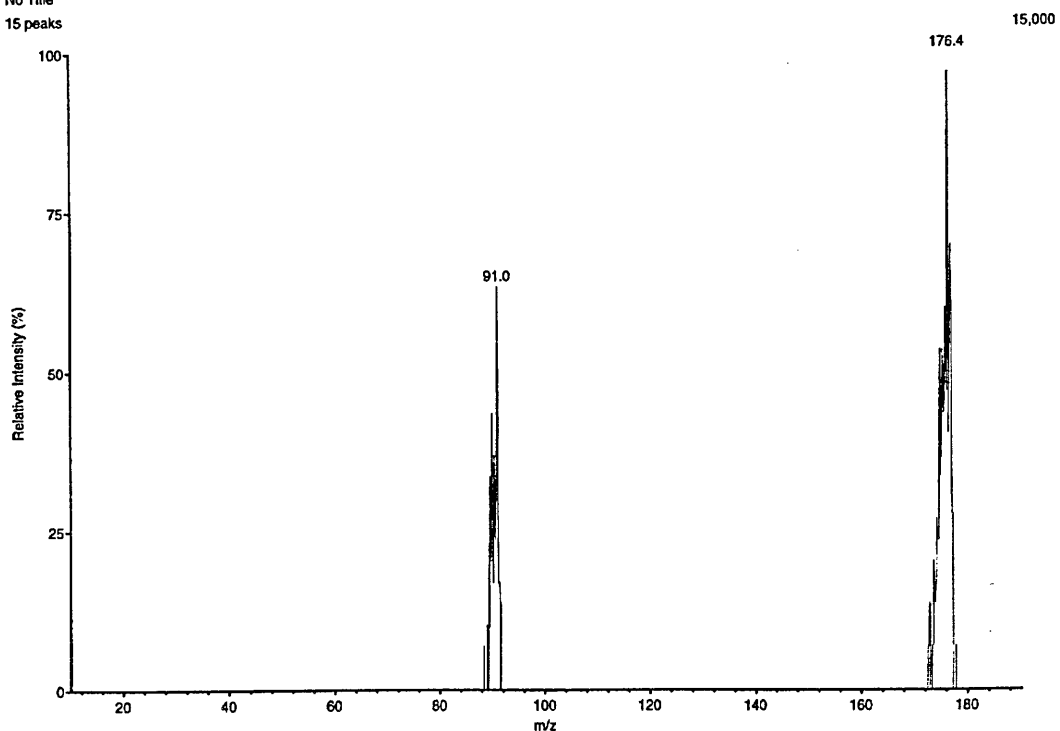
Figure 4.61: Product ion mass spectrum of the tetramethylhydrazine ion-molecule cluster at m/z 176
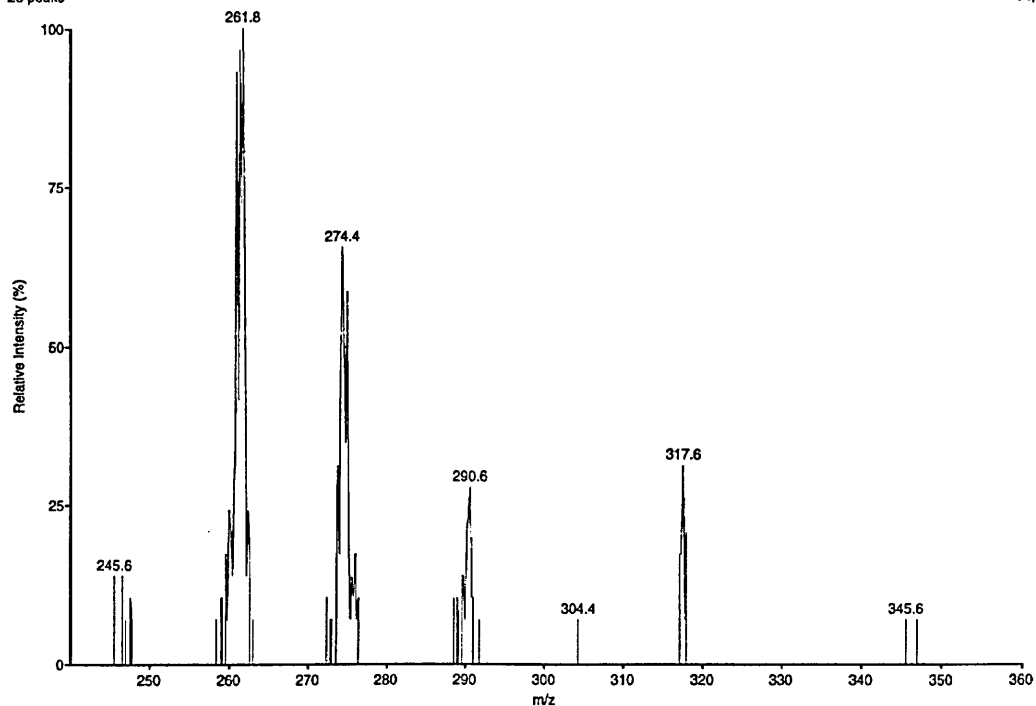
Figure 4.62: Mass spectrum of the ion clusters formed from tetramethylhydrazine with the 3-pentanone doped drift region, range 200 to 360 amu

A narrower mass range (200 to 360 amu) was scanned in order to confirm the presence

of the ion cluster at m/z 261. This was achieved as shown in Figure 4.62. The trimer ion

of TMH would have produced an m/z value of 265; the tetramer and

$H^+(N_2(CH_3)_4)(C_5H_{10}O)_3$ would have emerged at m/z values of 345 and 347 respectively,

both of which are adumbrated in the shorter scan range spectrum.

4.16.3 4-Heptanone / tetramethylhydrazine ion chemistry

During the detection of TMH with the source region doped with 4-heptanone, the

predominant ion clusters were observed at m/z values of 203 and 89 (Figure 4.63). As

with the 3-pentanone / TMH ion chemistry, the major ion cluster was that formed from

the single ketone and TMH molecules, $H^+(N_2(CH_3)_4)(C_7H_{14}O)$.
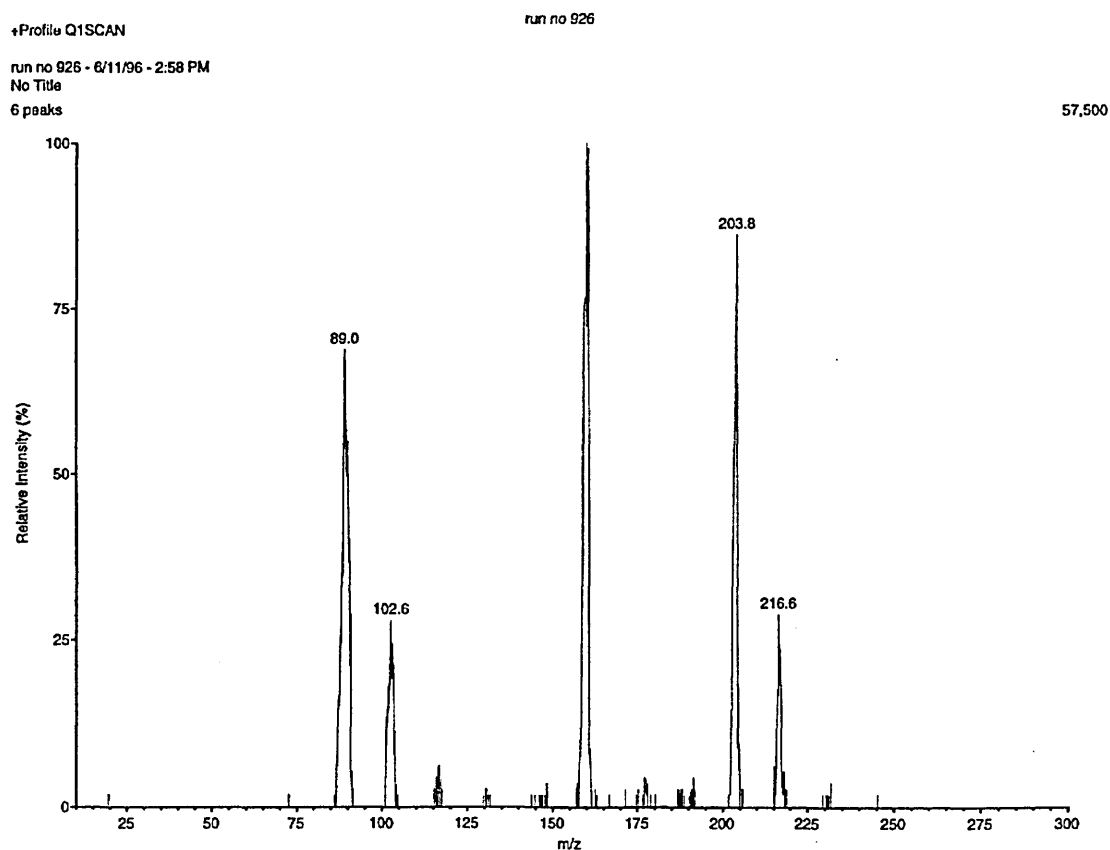
Figure 4.63: Mass spectrum of the ion clusters formed from tetramethylhydrazine with
the 4-heptanone doped source region

There was a minor indication of the presence of the protonated dimer of TMH at m/z 177. The ion clusters at m/z values of 161, 103, and 217 were considered to be the result of contamination in the system. It was unclear whether there was any breakdown of the TMH to form any compounds similar to MMH and UDMH.

When the drift region was doped with 4-heptanone the relative intensity ratio of the two major ions of interest changed only a little, with the predominance unchanged. The dimer ketone ion (m/z 229) and its TMH adduct cluster ion $H^+(N_2(CH_3)_4)(C_7H_{14}O)_2$ (m/z 317) were adumbrated, as shown in Figure 4.64. The shorter range scan (300 to 475 amu, shown in Figure 4.65) confirmed the presence of the latter ion cluster, and also repeated the pattern of hinting at the presence of the trimer ketone ion and its TMH adduct ion at m/z values of 343 and 431, respectively.

+Profile Q1SCAN

run no 932

run no 932 - 6/11/96 - 3:02 PM
No Title

29 peaks   22,000
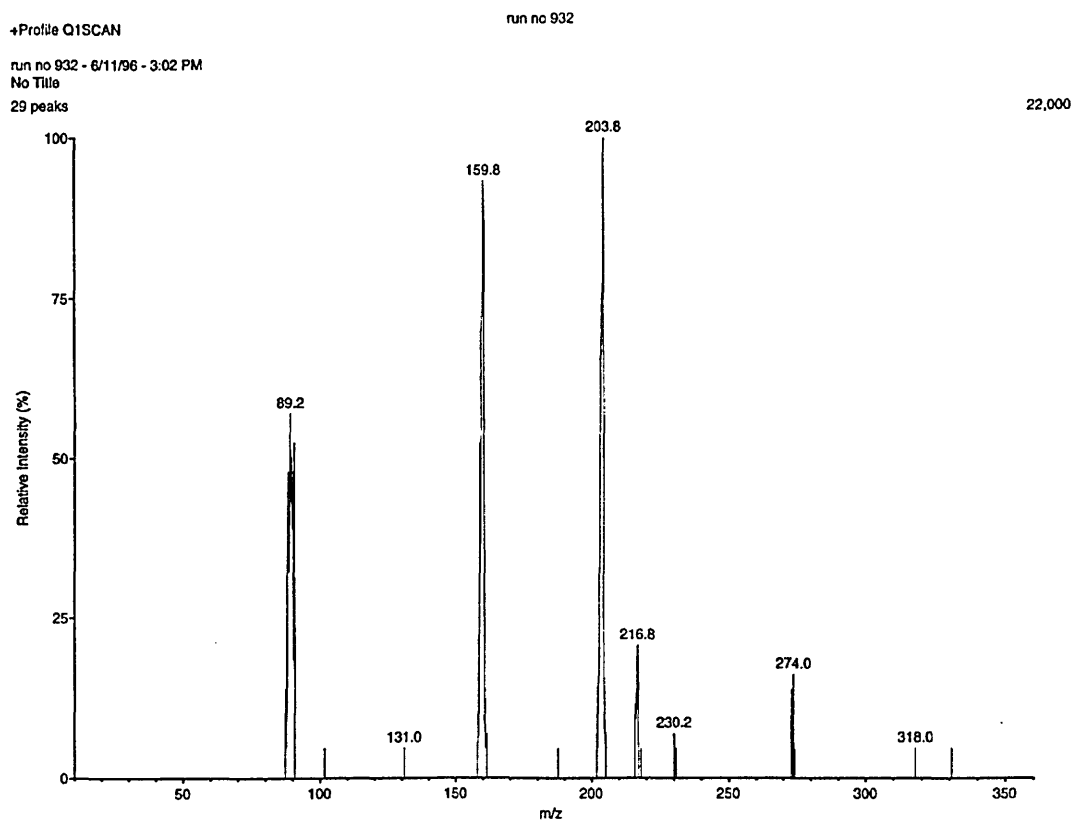
Figure 4.64: Mass spectrum of the ion clusters formed from tetramethylhydrazine with the 4-heptanone doped drift region
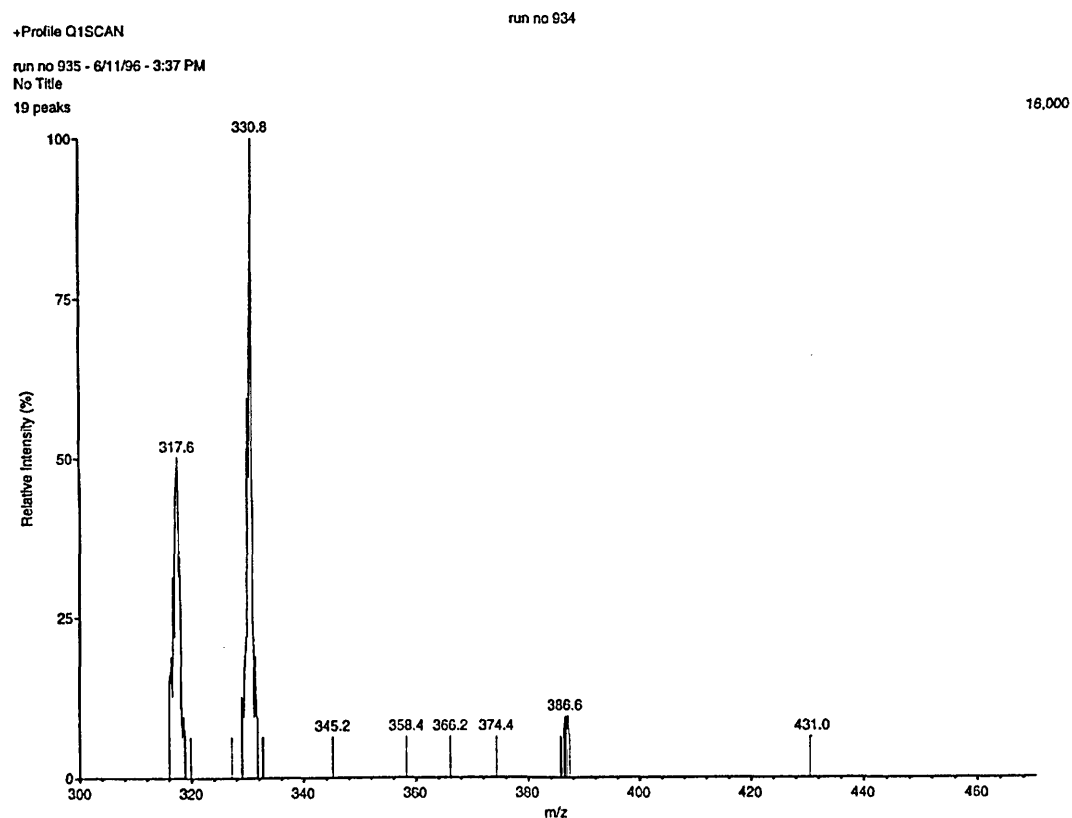
Figure 4.65: Mass spectrum of the ion clusters formed from tetramethylhydrazine with the 4-heptanone doped drift region, range 300 to 475 amu

4.16.4 5-Nonanone / tetramethylhydrazine ion chemistry

Yet again, there is evidence of the single ketone and TMH cluster ion present, with only the source region doped, this time with 5-nonanone used during the detection of TMH (Figure 4.66). The $H^+(N_2(CH_3)_4)(C_9H_{18}O)$ cluster has an m/z value of 231. A trace of the protonated ketone monomer was seen at m/z 143; the predominant ion was the protonated TMH molecule (m/z 89), with a small amount of the dimer present at m/z 177.
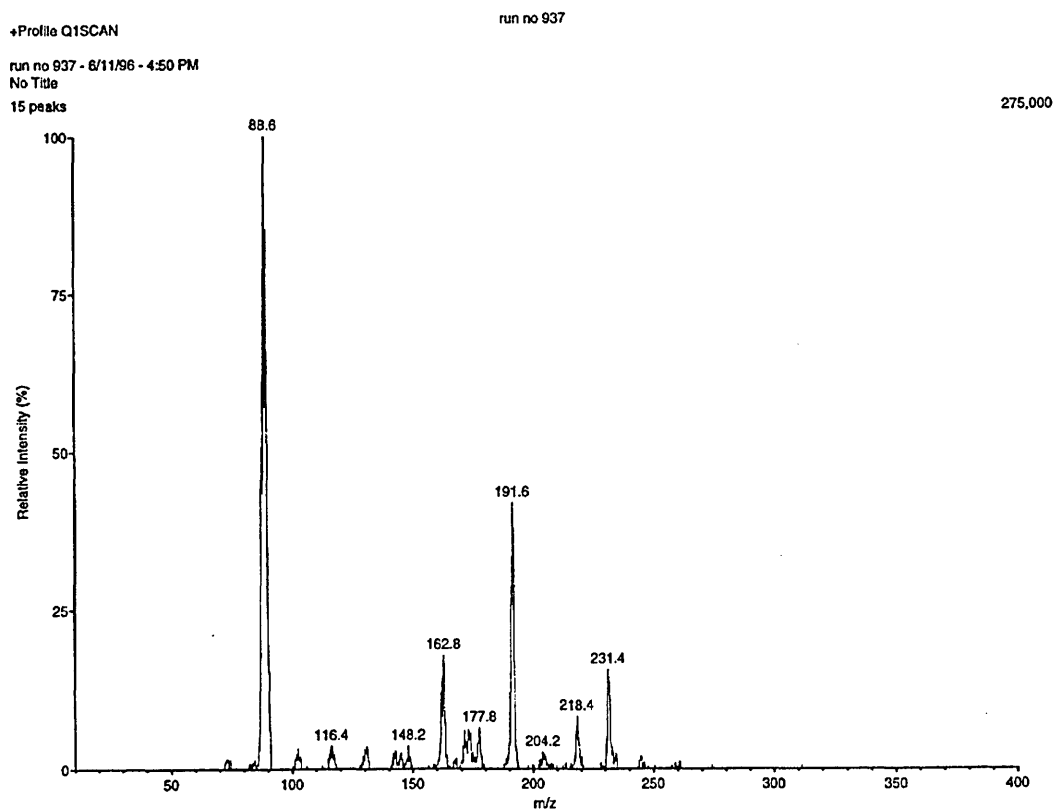
Figure 4.66: Mass spectrum of the ion clusters formed from tetramethylhydrazine with the 5-nonanone doped source region

When the drift region was also doped with 5-nonanone the $H^+(N_2(CH_3)_4)(C_9H_{18}O)$ and protonated tetramethylhydrazine clusters were of comparable intensity (see Figure 4.67). Again there was an indication of the formation of the dimer ketone / TMH adduct cluster ion, in this case $H^+(N_2(CH_3)_4)(C_9H_{18}O)_2$ at m/z 373. The peak was too low in intensity to obtain a meaningful MS-MS product ion mass spectrum. The peaks at m/z values of 235, 203, and 245 might have arisen from $H^+(N_2H_3CH_3)_2(C_9H_{18}O)$, $H^+(N_2(CH_3)_2H_2)(C_9H_{18}O)$, and $H^+(C_{11}H_{24}N_2)(N_2(CH_3)_2H_2)$ respectively if, as suspected in the source region doped experiment, there was decomposition of the TMH.

run no 939

47,000
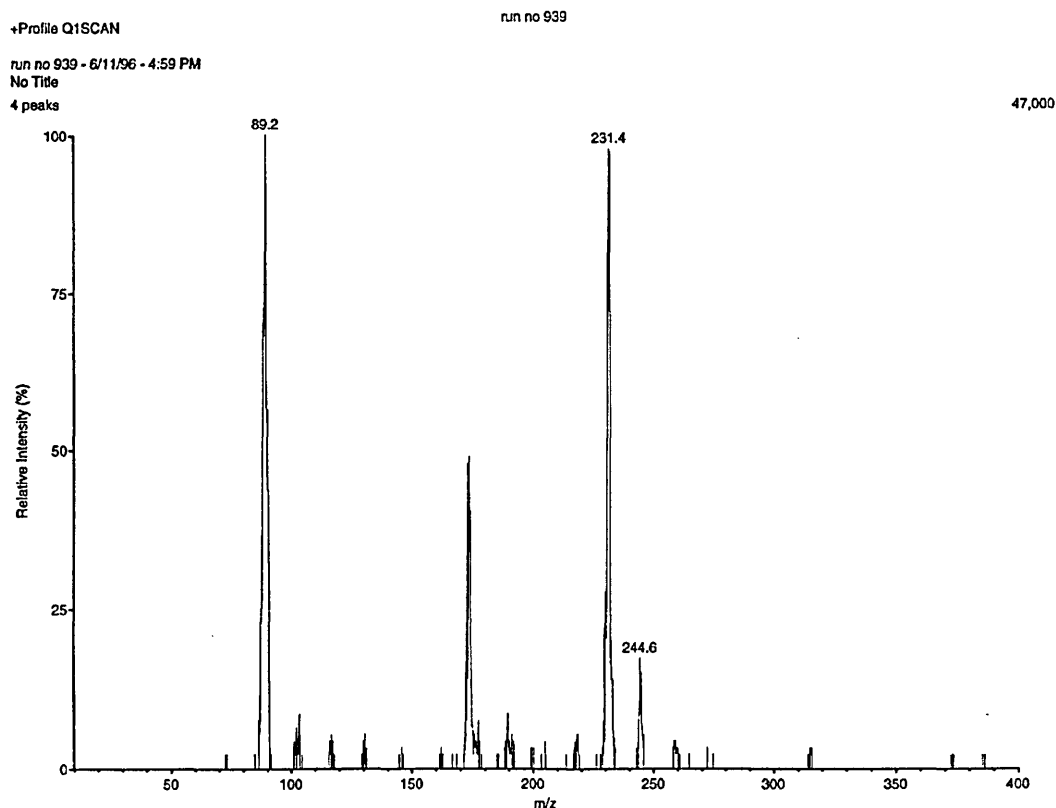
Figure 4.67: Mass spectrum of the ion clusters formed from tetramethylhydrazine with the 5-nonanone doped drift region

4.16.5 1,1,1-Trifluoroacetone / tetramethylhydrazine ion chemistry

The indications were that the system was contaminated during the experiment when the IMS source region was doped with 1,1,1-trifluoroacetone, but the protonated monomer of TMH did exist. It is possible that the single ketone and TMH cluster ion formed, with an m/z value of 201, but the intensity of the ion in this area was very low. There was no evidence of any other cluster ions forming, which may have involved the 5-nonanone and TMH molecules.

4.17 Summary of the ammonia, hydrazines, and ketones ion-molecule chemistry

The IMS-MS-MS studies were undertaken in order to determine the composition of the ion-molecule clusters and establish why the hydrazines and ammonia had mobility values in the reverse order to that expected, according to the relative size of the analyte molecules. With the IMS-MS-MS information, and the computed dimensions of the ion-molecule clusters, it was anticipated that it might be possible to determine if the size of the molecules could be controlled and used to effect resolution between the HZ and ammonia product ion peaks. The studies were used to investigate the Stone model, to ascertain whether the predicted structures of the ion-molecule clusters were correct.

Assignment of ion-molecule clusters to the ion peaks was difficult because the presence of contaminants made the chemistry more complicated and, therefore, the importance of MS-MS analysis was recognised. Even with knowledge of the analyte and ketone systems, commensurate with awareness of contamination, identification of low intensity peaks was problematic because of coincidental m/z values for different ion-molecule clusters. An example of this was observed during the HZ tests with 5-nonanone dopant, with the occurrence of a peak at m/z 313 representing both $H^+(C_{18}H_{36}N_2)(N_2H_4)$ and $H^+(C_9H_{20}N_2)_2$ ion-molecule clusters. The latter cluster was more probable because there was no evidence of the hydrazone combining with the analyte and therefore it was unlikely that the azine would combine with the analyte. There was also no evidence of azine formation from the reaction of HZ with any of the other ketones and then forming clusters through combination with HZ.

There was also a problem with the assignment of ion-molecules and ion clusters when the ion-molecules were of similar m/z values, for example TMH and 3-pentanone.

Even with calibration of the mass spectrometers the resolution could only be quoted to ±1 amu.

The variety and complexity of the ion-molecule chemistry became apparent as the IMS-MS-MS experiments progressed. The gas phase reactions of the hydrazines to form hydrazones was further complicated by the two-stage reaction of HZ to form azines with the various ketones. The product ion clusters became even more numerous because of the formation of mixed clusters involving the reaction products with the analyte or ketone. There was also the formation of ion-molecule clusters comprising two molecules of the analyte with one molecule of ketone. Although the proton affinity of UDMH is higher than for MMH, the set of UDMH experiments appeared to be dominated by the presence of MMH, formed by decomposition of UDMH, perhaps by primary single bond cleavage thus:

$$ \underset{H}{\overset{H}{\diagdown}}N - N\underset{CH_3}{\overset{CH_3}{\diagup}} \quad \xrightarrow{\;-CH_2\;} \quad \underset{H}{\overset{H}{\diagdown}}N - N\underset{H}{\overset{CH_3}{\diagup}} \qquad 30. $$
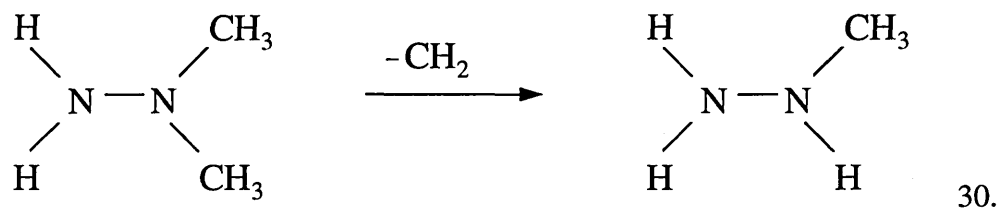
It is possible that the additional methyl group attached to the primary core nitrogen of UDMH provided steric hindrance, allowing the MMH to readily form ion-molecule clusters, or that the proton affinities were not sufficiently separated, and both had a high enough proton affinity to compete for the available positive charges.

Because the ion-molecule chemistry results were so complex, the m/z values and corresponding empirical formulae have been tabulated for quick reference in Tables 4.45 to 4.49, one table for each of the analytes, with increasing m/z values listed upwards. The results for 1,1,1-trifluoroacetone doped tests have not been included in

these summary tables because of the problems associated with trying to determine ion-molecule chemistry in an unstable environment. These tables have been colour coded to indicate the three most dominant ions for each experiment, in decreasing order of red > yellow > green; lower intensity peaks have not been shaded. This made the identification of ion-molecule clusters according to m/z values much easier, but the variety of the formulae does not allow easy recognition of the patterns of the ion-molecule chemistry of the hydrazines with ketones (twenty-eight different compositions have been recorded). To assist with interpretation, the resultant ion-molecule clusters have been summarised using simplified formulae in Tables 4.50 and 4.51, for the ion chemistry of the source and drift doped systems respectively. The abbreviations used in these latter tables are: A = analyte, K = ketone, P' = hydrazone, P'' = azine, and B = decomposition product, B' = hydrazone formed from a decomposition product. As protons are common to all of the ion-molecule clusters the H^+ symbol has been omitted from the simplified formulae in Tables 4.50 and 4.51. These two tables have been colour coded for approximate peak intensity so that the types of ions and their distribution could be identified easily. The tables have been printed on transparency film so that when the sheet of paper dividing them is removed the effect of change in dopant concentration may be observed. From the tables it is obvious that the concentration effect is more pronounced for bigger clusters, with higher levels of ketone present.

Concentration dependency of the ion-molecule chemistry was illustrated by the change in concentration through lowering of the vapour pressure with progression up the homologous series of ketones, and increased vapour pressure with increased methyl substitution of the hydrazines. Chemical reaction is less evident at lower ketone concentration i.e. with higher members of the homolgous series, or when the ketone is only present in the source region.

Table 4.45: Summary of ammonia / ketone ion-molecule chemistry

m/z (amu)	source acetone	drift acetone	source 3-pentanone	drift 3-pentanone	source 4-heptanone	drift 4-heptanone	source 5-nonanone	drift 5-nonanone
444								$NH_4^+(C_9H_{18}O)_3$
427								$H^+(C_9H_{18}O)_3$
362				$NH_4^+(C_5H_{10}O)_4$				
360						$NH_4^+(C_7H_{14}O)_3$		
343						$H^+(C_7H_{14}O)_3$		
302							$NH_4^+(C_9H_{18}O)_2$	$NH_4^+(C_9H_{18}O)_2$
285							$H^+(C_9H_{18}O)_2$	$H^+(C_9H_{18}O)_2$
276				$NH_4^+(C_5H_{10}O)_3$				
259				$H^+(C_5H_{10}O)_3$				
250		$NH_4^+(C_3H_6O)_4$						
246					$NH_4^+(C_7H_{14}O)_2$	$NH_4^+(C_7H_{14}O)_2$		
229					$H^+(C_7H_{14}O)_2$	$H^+(C_7H_{14}O)_2$		
192		$NH_4^+(C_3H_6O)_3$						
190			$NH_4^+(C_5H_{10}O)_2$	$NH_4^+(C_5H_{10}O)_2$				
177							$H^+(NH_3)_2(C_9H_{18}O)$	
175		$H^+(C_3H_6O)_3$						
173			$H^+(C_5H_{10}O)_2$	$H^+(C_5H_{10}O)_2$				
160							$NH_4^+(C_9H_{18}O)$	
149					$H^+(NH_3)_2(C_7H_{14}O)$	$H^+(NH_3)_2(C_7H_{14}O)$		
134	$NH_4^+(C_3H_6O)_2$	$NH_4^+(C_3H_6O)_2$						
132					$NH_4^+(C_7H_{14}O)$	$NH_4^+(C_7H_{14}O)$		
121			$H^+(NH_3)(C_5H_{10}O)$					
117	$H^+(C_3H_6O)_2$	$H^+(C_3H_6O)_2$						
115					$H^+(C_7H_{14}O)$	$H^+(C_7H_{14}O)$		
104			$NH_4^+(C_5H_{10}O)$	$NH_4^+(C_5H_{10}O)$				
93	$H^+(NH_3)_2(C_3H_6O)$							
87			$H^+(C_5H_{10}O)$	$H^+(C_5H_{10}O)$				
76	$NH_4^+(C_3H_6O)$	$NH_4^+(C_3H_6O)$						
59	$H^+(C_3H_6O)$	$H^+(C_3H_6O)$						
52					$H^+(NH_3)_3$			
35			$H^+(NH_3)_2$		$H^+(NH_3)_2$			
18	NH_4^+		NH_4^+	NH_4^+	NH_4^+			

Table 4.46: Summary of hydrazine / ketone ion-molecule chemistry

m/z (amu)	source acetone	drift acetone	source 3-pentanone	drift 3-pentanone	source 4-heptanone	drift 4-heptanone	source 5-nonanone	drift 5-nonanone
459								$H^+(N_2H_4)(C_9H_{18}O)_3$ $H^+(C_{18}H_{36}N_2)$
423								
375				$H^+(N_2H_4)(C_5H_{10}O)_4$				
359				$H^+(C_5H_{12}N_2)(C_5H_{10}O)_3$				
339						$H^+(N_2H_4)(C_7H_{14}O)_3$		
317			$H^+(C_5H_{12}N_2)(C_5H_{10}O)_3$			$H^+(C_{14}H_{28}N_2)(C_7H_{14}O)$	$H^+(N_2H_4)(C_9H_{18}O)_2$	$H^+(N_2H_4)(C_9H_{18}O)_2$
313							$H^+(C_9H_{20}N_2)_2$	$H^+(C_9H_{20}N_2)_2$
299							$H^+(C_9H_{20}N_2)(C_9H_{18}O)$	$H^+(C_9H_{20}N_2)(C_9H_{18}O)$
291			$H^+(N_2H_4)(C_5H_{10}O)_3$	$H^+(N_2H_4)(C_5H_{10}O)_3$				
285			$H^+(C_5H_{10}N_2)(C_5H_{10}O)_2$	$H^+(C_5H_{10}N_2)(C_5H_{10}O)_2$			$H^+(C_9H_{18}O)_2$	$H^+(C_9H_{18}O)_2$
281							$H^+(C_{18}H_{36}N_2)$	$H^+(C_{18}H_{36}N_2)$
273								
265								
261			$H^+(C_{10}H_{20}N_2)(C_5H_{10}O)$	$H^+(C_{10}H_{20}N_2)(C_5H_{10}O)$		$H^+(N_2H_4)(C_7H_{14}O)_2$		
255								
247		$H^+(C_3H_6O_4)$						
243								
233		$H^+(C_3H_6O_4)$				$H^+(C_{14}H_{30}N_2)(C_7H_{14}O)$		
229								
225		$H^+(N_2H_4)(C_3H_6O)_3$			$H^+(C_6H_{16}N_2)(C_7H_{14}O)$	$H^+(C_{14}H_{28}N_2)$		
207	$H^+(N_2H_4)(C_3H_6O)_3$		$H^+(N_2H_4)(C_5H_{10}O)_2$ $H^+(C_5H_{11}N_3)$		$H^+(C_7H_{14}O_2)$			
205		$H^+(C_3H_6N_2)(C_3H_6O)$		$H^+(N_2H_4)(C_5H_{10}O)_2$	$H^+(C_{14}H_{28}N_2)$			
201								
189		$H^+(C_3H_6O)_3$						
187	$H^+(C_3H_6O)_3$		$H^+(C_5H_{10}N_2)(C_5H_{10}O)$	$H^+(C_{10}H_{20}N_2)(C_5H_{10}O)$			$H^+(N_2H_4)(C_9H_{18}O)$	$H^+(N_2H_4)(C_9H_{18}O)$
175		$H^+(C_3H_6N_2)(C_3H_6O)$						
173				$H^+(C_5H_{10}O)_2$				
171								
169			$H^+(C_{10}H_{20}N_2)$				$H^+(C_9H_{20}N_2)$	$H^+(C_9H_{20}N_2)$
161				$H^+(C_{10}H_{20}N_2)$				
157	$H^+(N_2H_4)(C_3H_6O)_2$				$H^+(C_7H_{14}N_2)(N_2H_4)$	$H^+(C_7H_{14}N_2)(N_2H_4)$		
149		$H^+(N_2H_4)(C_3H_6O)_2$						
147						$H^+(N_2H_4)(C_7H_{14}O)$		
145					$H^+(N_2H_4)(C_7H_{14}O)$			
143							$H^+(C_9H_{18}O)$	
133		$H^+(C_3H_6N_2)(C_3H_6O)$		$H^+(C_5H_{10}N_2)(N_2H_4)$				
131	$H^+(C_3H_6N_2)(C_3H_6O)$							
129					$H^+(C_7H_{16}N_2)$	$H^+(C_7H_{16}N_2)$		
119								
117	$H^+(C_3H_6O)_2$	$H^+(C_3H_6O)_2$	$H^+(N_2H_4)(C_5H_{10}O)$	$H^+(N_2H_4)(C_5H_{10}O)$				
113	$H^+(C_6H_{12}N_2)$	$H^+(C_6H_{12}N_2)$						
101			$H^+(C_5H_{10}N_2)$	$H^+(C_5H_{10}N_2)$				
91	$H^+(N_2H_4)(C_3H_6O)$	$H^+(N_2H_4)(C_3H_6O)$						
87			$H^+(C_5H_{10}O)$	$H^+(C_5H_{10}O)$				
73	$H^+(C_3H_6N_2)$	$H^+(C_3H_6N_2)(C_3H_6O)_3$						
59	$H^+(C_3H_6O)$	$H^+(C_3H_6O)$						
33	$H^+(N_2H_4)$	$H^+(N_2H_4)$						

Table 4.47: Summary of methylhydrazine / ketone ion-molecule chemistry

m/z (amu)	source acetone	drift acetone	source 3-pentanone	drift 3-pentanone	source 4-heptanone	drift 4-heptanone	source 5-nonanone	drift 5-nonanone
389						$H^+(N_2H_3CH_3)(C_7H_{14}O)_3$		
341								$H^+(C_{10}H_{22}N_2)_2$
331								$H^+(N_2H_3CH_3)(C_9H_{18}O)_2$
313							$H^+(C_{10}H_{22}N_2)(C_9H_{18}O)$	$H^+(C_{10}H_{22}N_2)(C_9H_{18}O)$
305				$H^+(N_2H_3CH_3)(C_5H_{10}O)_3$				
285					$H^+(C_8H_{18}N_2)_2$		$H^+(C_9H_{18}O)_2$	$H^+(C_9H_{18}O)_2$
279		$H^+(N_2H_3CH_3)(C_3H_6O)_4$						
275					$H^+(N_2H_3CH_3)(C_7H_{14}O)_2$	$H^+(N_2H_3CH_3)(C_7H_{14}O)_2$		
257					$H^+(C_8H_{18}N_2)(C_7H_{14}O)$			
241								
235							$H^+(N_2H_3CH_3)_2(C_9H_{18}O)$	
229					$H^+(C_7H_{14}O)_2$			
221		$H^+(N_2H_3CH_3)(C_3H_6O)_3$						
219			$H^+(N_2H_3CH_3)(C_5H_{10}O)_2$	$H^+(N_2H_3CH_3)(C_5H_{10}O)_2$				
217							$H^+(C_{10}H_{22}N_2)(N_2H_3CH_3)$	$H^+(C_{10}H_{22}N_2)(N_2H_3CH_3)$
207								
201			$H^+(C_6H_{14}N_2)(C_5H_{10}O)$	$H^+(C_6H_{14}N_2)(C_5H_{10}O)$				
189					$H^+(C_8H_{18}N_2)(N_2H_3CH_3)$	$H^+(C_8H_{18}N_2)(N_2H_3CH_3)$	$H^+(N_2H_3CH_3)(C_9H_{18}O)$	$H^+(N_2H_3CH_3)(C_9H_{18}O)$
179			$H^+(N_2H_3CH_3)_2(C_5H_{10}O)$	$H^+(N_2H_3CH_3)_2(C_5H_{10}O)$				
175	$H^+(C_3H_6O)_3$							
173	$H^+(C_4H_{10}N_2)_2$	$H^+(C_4H_{10}N_2)_2$	$H^+(C_5H_{10}O)_2$					
171							$H^+(C_{10}H_{22}N_2)$	$H^+(C_{10}H_{22}N_2)$
163	$H^+(N_2H_3CH_3)(C_3H_6O)_2$							
161			$H^+(C_6H_{14}N_2)(N_2H_3CH_3)$	$H^+(C_6H_{14}N_2)(N_2H_3CH_3)$	$H^+(N_2H_3CH_3)(C_7H_{14}O)$	$H^+(N_2H_3CH_3)(C_7H_{14}O)$		
151	$H^+(N_2H_3CH_3)_2(C_3H_6O)$							
145	$H^+(C_4H_{10}N_2)(C_3H_6O)$							
143					$H^+(C_8H_{18}N_2)$	$H^+(C_8H_{18}N_2)$	$H^+(C_9H_{18}O)$	
139			$H^+(N_2H_3CH_3)_3$				$H^+(N_2H_3CH_3)_3$	
133	$H^+(C_4H_{10}N_2)(N_2H_3CH_3)$	$H^+(N_2H_3CH_3)(C_4H_{10}N_2)$	$H^+(N_2H_3CH_3)(C_5H_{10}O)$	$H^+(N_2H_3CH_3)(C_5H_{10}O)$				
117	$H^+(C_3H_6O)_2$							
115			$H^+(C_6H_{14}N_2)$	$H^+(C_6H_{14}N_2)$	$H^+(C_7H_{14}O)$			
105	$H^+(N_2H_3CH_3)(C_3H_6O)$							
93	$H^+(N_2H_3CH_3)_2$		$H^+(N_2H_3CH_3)_2$	$H^+(N_2H_3CH_3)_2$	$H^+(N_2H_3CH_3)_2$		$H^+(N_2H_3CH_3)_2$	
87	$H^+(C_4H_{10}N_2)$		$H^+(C_5H_{10}O)$					
47	$H^+(N_2H_3CH_3)$	$H^+(N_2H_3CH_3)$	$H^+(N_2H_3CH_3)$	$H^+(N_2H_3CH_3)$	$H^+(N_2H_3CH_3)$	$H^+(N_2H_3CH_3)$	$H^+(N_2H_3CH_3)$	$H^+(N_2H_3CH_3)$

Table 4.48: Summary of 1,1-dimethylhydrazine / ketone ion-molecule chemistry

m/z (amu)	source acetone	drift acetone	source 3-pentanone	drift 3-pentanone	source 4-heptanone	drift 4-heptanone	source 5-nonanone	drift 5-nonanone
331							$H^+(N_2H_3CH_3)(C_9H_{18}O)_2$	$H^+(N_2H_3CH_3)(C_9H_{18}O)_2$
275					$H^+(N_2H_3CH_3)(C_7H_{14}O)_2$	$H^+(N_2H_3CH_3)(C_7H_{14}O)_2$ $H^+(C_7H_{30}N_3)(C_7H_{14}O)$		
271								
245							$H^+(C_{11}H_{22}N_2)(N_2(CH_3)_2H_2)$	$H^+(C_{11}H_{22}N_2)(N_2(CH_3)_2H_2)$
233		$H^+C_4H_6O_4$		$H^+(N_2(CH_3)_2)(C_5H_{10}O)_2$				
231				$H^+(N_2H_3CH_3)(C_5H_{10}O)_2$		$H^+(C_7H_{30}N_2)(N_2(CH_3)_2H_2)$	$H^+(C_{10}H_{22}N_2)(N_2(CH_3)_2H_2)$	$H^+(C_{11}H_{34}N_2)(N_2(CH_3)_2H_2)$
219					$H^+(C_{10}H_{22}N_2)(N_2(CH_3)_2H_2)$			
217						$H^+(C_{10}H_{22}N_2)(N_2(CH_3)_2H_2)$	$H^+(C_{10}H_{22}N_2)(N_2H_3CH_3)$	$H^+(C_{10}H_{22}N2)(N_2H_3CH_3)$
203							$H^+(N_2(CH_3)_2H_2)(C_9H_{18}O)$	$H^+(N_2(CH_3)_2H_2)(C_9H_{18}O)$
201								
189						$H^+(C_8H_{18}N_2)(N_2H_3CH_3)$	$H^+(N_2H_3CH_3)(C_6H_{18}O)$	$H^+(N_2H_3CH_3)(C_6H_{18}O)$
187				$H^+(C_7H_{14}N_2)(N_2(CH_3)_2H_2)$				$H^+(C_{11}H_{24}N_2)$
185				$H^+(C_6H_{10}N_2)(N_2(CH_3)_2H)$				
175		$H^+C_6H_6O_4$			$H^+(N_2(CH_3)_2H_2)(C_7H_{14}O)$	$H^+(N_2(CH_3)_2H_2)(C_7H_{14}O)$		
173		$H^+(N_2H_3CH_3)(C_6H_6O_2)$					$H^+(C_{11}H_{24}N_2)$	
163								
161	$H^+(C_3H_{12}N_2)(N_2(CH_3)_2H_2)$		$H^+(C_7H_{14}N_2)(N_2(CH_3)_2H_2)$	$H^+(C_6H_{14}N_2)(N_2H_3CH_3)$	$H^+(N_2H_3CH_3)(C_7H_{14}O)$	$H^+(N_2H_3CH_3)(C_7H_{14}O)$		
159	$H^+(C_3H_{12}N_2)(C_3H_6O)$		$H^+(C_4H_{10}N_2)(N_2(CH_3)_2H)$					
157					$H^+(C_9H_{20}N_2)$	$H^+(C_9H_{20}N_2)$		
147	$H^+(C_4H_{10}N_2)(N_2(CH_3)_2H_2)$	$H^+(C_4H_{10}N_2)(N_2H_3CH_3)$	$H^+(C_6H_{14}N_2)(N_2H_3CH_3)$	$H^+(N_2(CH_3)_2H_2)(C_5H_{10}O)$ $H^+(N_2H_3CH_3)(C_5H_{10}O)$				
133			$H^+(N_2(CH_3)_2H_2)(C_5H_{10}O)$ $H^+(N_2H_3CH_3)(C_5H_{10}O)$					
129				$H^+(C_5H_{12}N_2)$ $H^+(N_2(CH_3)_2H_2)_2$			$H^+N_2(CH_3)_2H)_3$	
121	$H^+(N_2(CH_3)_2H_2)_2$		$H^+(N_2(CH_3)_2H)_4$		$H^+(N_2(CH_3)_2H_2)_2$	$H^+(N_2(CH_3)_2H_2)_2$		
119	$H^+(N_2(CH_3)_2H_2)(C_3H_6O)$	$H^+(N_2(CH_3)_2H_2)(C_3H_6O)$ $H^+(C_3H_6O_2)$						
117	$H^+(C_3H_6O)$					$H^+(C_7H_{14}O)$		
115								
107		$H^+(N_2H_3CH_3)(C_3H_6O)$	$H^+(N_2H_3CH_3)(N_2(CH_3)_2H_2)$	$H^+(N_2H_3CH_3)(N_2(CH_3)_2H_2)$	$H^+(N_2H_3CH_3)(N_2(CH_3)_2H_2)$		$H^+(N_2H_3CH_3)(N_2(CH_3)_2H_2)$	
105	$H^+(N_2H_3CH_3)(C_3H_6O)$							
101	$H^+(C_3H_{12}N_2)$							
93	$H^+(N_2H_3CH_3)_2$		$H^+(N_2H_3CH_3)_2$ $H^+(C_5H_6O)$		$H^+(N_2H_3CH_3)_2$			
87								
61	$H^+(N_2(CH_3)_2H_2)$		$H^+(N_2(CH_3)_2H_2)$	$H^+(N_2(CH_3)_2H_2)$	$H^+(N_2(CH_3)_2H_2)$	$H^+(N_2(CH_3)_2H_2)$	$H^+(N_2(CH_3)_2H_2)$	$H^+(N_2(CH_3)_2H_2)$
47	$H^+(N_2H_3CH_3)$		$H^+(N_2H_3CH_3)$	$H^+(N_2H_3CH_3)$	$H^+(N_2H_3CH_3)$	$H^+(N_2H_3CH_3)$	$H^+(N_2H_3CH_3)$	

Table 4.49: Summary of tetramethylhydrazine / ketone ion-molecule chemistry

m/z (amu)	source acetone	drift acetone	source 3-pentanone	drift 3-pentanone	source 4-heptanone	drift 4-heptanone	source 5-nonanone	drift 5-nonanone
373								$H^+(N_2(CH_3)_4)(C_9H_{18}O)_2$
347								
317							$H^+(N_2(CH_3)_4)(C_7H_{14}O)_2$	
265								
261				$H^+(N_2(CH_3)_4)(C_5H_{10}O)_2$				
233		$H^+(C_3H_6O)_4$						
231							$H^+(N_2(CH_3)_4)(C_9H_{18}O)$	$H^+(N_2(CH_3)_4)(C_9H_{18}O)$
229						$H^+(C_7H_{14}O)_2$		
203					$H^+(N_2(CH_3)_4)(C_7H_{14}O)$	$H^+(N_2(CH_3)_4)(C_7H_{14}O)$		
177			$H^+(N_2(CH_3)_4)_2$	$H^+(N_2(CH_3)_4)_2$	$H^+(N_2(CH_3)_4)_2$		$H^+(N_2(CH_3)_4)_2$	$H^+(N_2(CH_3)_4)_2$
175	$H^+(C_3H_6O)_3$	$H^+(C_3H_6O)_3$	$H^+(N_2(CH_3)_4)(C_5H_{10}O)$	$H^+(N_2(CH_3)_4)(C_5H_{10}O)$				
147	$H^+(N_2(CH_3)_4)(C_3H_6O)$	$H^+(N_2(CH_3)_4)(C_3H_6O)$						
143							$H^+(C_9H_{18}O)$	
117	$H^+(C_3H_6O)_2$	$H^+(C_3H_6O)_2$						
115					$H^+(C_7H_{14}O)$			
89	$H^+(N_2(CH_3)_4)$	$H^+(N_2(CH_3)_4)$	$H^+(N_2(CH_3)_4)$	$H^+(N_2(CH_3)_4)$	$H^+(N_2(CH_3)_4)$	$H^+(N_2(CH_3)_4)$	$H^+(N_2(CH_3)_4)$	$H^+(N_2(CH_3)_4)$
59		$H^+(C_3H_6O)$						

Table 4.50: Summary of ion-molecule cluster composition, source region doped

Chemical system										Ion-molecule cluster composition																					
Analyte	Dopant	A	A₂	A₃	K	K₂	K₃	K₁	K₅	AK	AK₂	AK₃	AK₄	A₂K	P'	P''	P'₂	P'A	P'K	P'K₂	P'K₃	P''K	B	B₂	BK	BK₂	BA	B'A
NH₃	Acetone																											
NH₃	3-P							NK					NK															
NH₃	4-H						NK	NK				NK	NK															
NH₃	5-N																											
HZ	Acetone																											
HZ	3-P											NK								NK	NK	NK						
HZ	4-H						NK	NK				NK	NK							NK	NK	NK						
HZ	5-N						NK	NK				NK	NK							NK	NK	NK						
MMH	Acetone																											
MMH	3-P																											
MMH	4-H											NK								NK								
MMH	5-N						NK	NK				NK	NK															
UDMH	Acetone																								BK			
UDMH	3-P																							B₂	BK			
UDMH	4-H																NK								BK		BA	B'A
UDMH	5-N																NK											
TMH	Acetone																											
TMH	3-P						NK	NK			AK₂	NK	NK															
TMH	4-H						NK	NK			NK	NK	NK															
TMH	5-N						NK	NK				NK	NK															

Colour   Approximate relative peak intensity
80 - 100%
60 - 80%
35-59%
21 - 34%
10 - 20%
low intensity peak
minor peak
adumbrated or trace peak

Abbreviation
A   Analyte
K   Ketone
P'   Hydrazone
P''   Azine
B   Decomposition product
B'   Decomposition product hydrazone
NK   Existence unknown ; outside mass spectrometer range
NH₃   Ammonia

Table 4.51: Summary of ion-molecule cluster composition, drift region doped

Chemical system		Ion-molecule cluster composition																												
Analyte	Dopant	A	A2	A3	K	K2	K3	K4	K5	AK	AK2	AK3	AK4	A2K	P'	P''	P'2	P'A	P'K	P''K2	P''K3	P''K	B	B2	BK	BK2	BA	B'A	B
NH3	Acetone																												
NH3	3-P							NK					NK																
NH3	4-H							NK																					
NH3	5-N																												
HZ	Acetone																												
HZ	3-P																												
HZ	4-H																												
HZ	5-N												NK																
MMH	Acetone																												
MMH	3-P																												
MMH	4-H					NK	NK						NK																
MMH	5-N						NK	NK				NK	NK							NK	NK	NK							
UDMH	Acetone																			NK	NK	NK							
UDMH	3-P																												
UDMH	4-H																			NK	NK								
UDMH	5-N																												
TMH	Acetone																												
TMH	3-P											NK	NK																
TMH	4-H											NK	NK																
TMH	5-N																												

Colour — Approximate relative peak intensity

- 80 - 100%
- 60 - 80%
- 35 - 59%
- 21 - 34%
- 10 - 20%
- low intensity peak
- minor peak
- adumbrated or trace peak

Abbreviation

A	Analyte
K	Ketone
P'	Hydrazone
P''	Azine
B	Decomposition product
B'	Decomposition product hydrazone
NK	Existence unknown ; outside mass spectrometer range
NH3	Ammonia

Table 4.50: Summary of ion-molecule cluster composition, source region doped

Chemical system		Ion-molecule cluster composition																														
Analyte	Dopant	A	A₂	A₃	K	K₂	K₃	K₄	K₅	AK	AK₂	AK₃	AK₄	A₂K	P'	P''	P'₂	P'A	P'K	P'K₂	P'K₃	P''K	B	B₂	BK	BK₂	BA	B'A	B'B
NH₃	Acetone																												
NH₃	3-P																												
NH₃	4-H							NK				NK	NK																
NH₃	5-N																												
HZ	Acetone											NK																	
HZ	3-P												NK							NK	NK	NK							
HZ	4-H						NK	NK				NK								NK	NK	NK							
HZ	5-N																												
MMH	Acetone																												
MMH	3-P											NK									NK								
MMH	4-H						NK	NK				NK																	
MMH	5-N						NK	NK																					
UDMH	Acetone																NK											
UDMH	3-P																NK											
UDMH	4-H																												
UDMH	5-N																												
TMH	Acetone																												
TMH	3-P					NK		NK			NK	NK																	
TMH	4-H						NK	NK			NK	NK																	
TMH	5-N																												

Colour — Approximate relative peak intensity
- 80 - 100%
- 60 - 80%
- 35 - 59%
- 21 - 34%
- 10 - 20%
- low intensity peak
- minor peak
- adumbrated or trace peak

Abbreviation	
A	Analyte
K	Ketone
P'	Hydrazone
P''	Azine
B	Decomposition product
B'	Decomposition product hydrazone
NK	Existence unknown ; outside mass spectrometer range
NH₃	Ammonia

Table 4.51: Summary of ion-molecule cluster composition, drift region doped

Chemical system			Ion-molecule cluster composition																												
Analyte	Dopant	A	A_2	A_3	K	K_2	K_3	K_4	K_5	AK	AK_2	AK_3	AK_4	A_2K	P'	P''	P_2	P'A	P'K	$P'K_2$	$P'K_3$	P''K	B	B_2	BK	BK_2	BA	B'A	B'B
NH_3	Acetone																												
NH_3	3-P												NK																
NH_3	4-H							NK																					
NH_3	5-N							NK																					
HZ	Acetone																												
HZ	3-P																												
HZ	4-H																												
HZ	5-N												NK																
MMH	Acetone																												
MMH	3-P																												
MMH	4-H						NK					NK	NK																
MMH	5-N							NK				NK	NK							NK	NK	NK							
UDMH	Acetone																												
UDMH	3-P																												
UDMH	4-H																			NK		NK							
UDMH	5-N																				NK								
TMH	Acetone																												
TMH	3-P											NK																	
TMH	4-H											NK	NK																
TMH	5-N											NK	NK																

Colour — Approximate relative peak intensity

- 80 - 100%
- 60 - 80%
- 35-59%
- 21 - 34%
- 10 - 20%
- low intensity peak
- minor peak
- adumbrated or trace peak

Abbreviation

A	Analyte
K	Ketone
P'	Hydrazone
P''	Azine
B	Decomposition product
B'	Decomposition product hydrazone
NK	Existence unknown ; outside mass spectrometer range
NH_3	Ammonia

The main effect of the increase in concentration can be seen in the shift in H^+(analyte)(ketone)$_n$ from n = 1 or 2 at lower dopant concentration to n = 2 and 3, with the presence of some H^+(analyte)(ketone)$_4$ for the ammonia and HZ ion chemistry. The effect on UDMH and TMH ion chemistry was to pass from the protonated analyte to the H^+(analyte)(ketone) cluster. These findings are in keeping with Stone's model.

In the experiments involving HZ and 5-nonanone, it was postulated that either the reaction between HZ and the ketone was quenched at higher dopant concentration, or that following the reaction between HZ and 5-nonanone to form the hydrazone and azine, the higher proton affinity of HZ and ketone clusters resulted in proton transfer from the hydrazone and azine reaction products, thus reducing their relative intensities. The latter explanation was felt to be more probable.

It is also obvious that the analytes follow, in principle, the model outlined by Stone. The dominance of clusters involving the protonated species does indicate the reduction of the number of ketones as the degree of methyl substitution on the primary core nitrogen is increased.

The maximum number of ketones attracted by the hydrazines exceeded the numbers predicted by the Stone model, but the intensity of the ion peaks recorded for the additional ketone molecules was very low, for example H^+(TMH)K$_2$, and possibly even H^+(TMH)K$_3$. These extra ketones would have been attracted either to the second core nitrogen of the hydrazine, or would have formed a second layer around the ion cluster through solvation. In either case the attraction of these ketones would have been much lower than the attraction to the primary, protonated core nitrogen. The typical number of ketones recorded per ion-molecule cluster was lower than the maximum (see Table 4.52) predicted for ammonia and HZ, presumably because the ketone concentration was too low to achieve the maximum ketone attachment. The number for

n in H^+(analyte)(ketone)$_n$ was generally two, occasionally three. Owing to the restrictions of the mass range of the mass spectrometer it was not possible to determine the maximum number of ketones per ion-molecule cluster for each of the hydrazines with the higher molecular weight ketones.

In some of the experiments shorter range scans were recorded in order to determine whether predicted peaks, particularly at higher m/z values, did actually exist or if they were merely electrical noise spikes in the baseline. These scans confirmed the presence of ions at higher m/z values, for example in the tests involving TMH and 4-heptanone, where the trimer ketone ion and its TMH adduct ion were postulated at m/z values of 343 and 431 respectively. The shorter range scans were not employed prior to the experiments with 3-pentanone. These indications throw doubt upon the previous results obtained in experiments involving the ketones lower down the homologous series ($C_nH_{2n}O$), symmetrical about the carbonyl group, and other hydrazines, and should be investigated further. Larger cluster ions might have been detected if shorter range scans had been used to improve the recorded intensity of the ions present.

Although theory predicts that chemicals with the highest proton affinity will form ion clusters, the difference in proton affinity alone did not always ensure that the highest proton affinity chemical won the competition for the charge. Where proton affinities were similar, or were covered by a narrow range, the protons were distributed between the analytes and / or ketones, provided an excess of protons allowed for the existence of the lower proton affinity species.

Table 4.52: Maximum n and distribution profiles for H^+AK_n

Dopant	Maximum number of n for AK_n					Order of intensity of $H^+AK_n(n)$				
	Ammonia	HZ	MMH	UDMH	TMH	Ammonia	HZ	MMH	UDMH	TMH
Acetone	4	4	4	1	1	3,2,1,4	2,3,1,4	2,3,1,4	1	1
3-Pentanone	4	4	3	2	≥2	2,3,1,4	2,3,1,4	2,1,3	1,2	1,2
4-Heptanone	≥3	≥3	≥3	1	≥2	2,1,3	2,1,3	2,1,3	1	1,2
5-Nonanone	≥3	≥3	≥2	1	≥2	3,2	2,1,3	2,1	1	1,2

A = analyte
K = ketone
n = number of ketone molecules per ion-molecule cluster

Where the proton affinity of the analyte is much higher than the ketone, for example TMH and acetone, and the drift region is dominated with H^+K_n where n = 1 to 3, the predominance of clusters of the lower proton affinity component is explained by an excess of the dopant due to its higher vapour pressure.

The electron withdrawing effect of fluorine in 1,1,1-trifluoroacetone is reflected in the lower proton affinity (725.5 kJ.mol^{-1}). It was expected that few ion clusters would be formed with the ketones, particularly at low dopant concentration. Protonated HZ clusters were formed (H^+HZ_n where n = 1 to 3) which had not been seen with dopants of similar proton affinity to HZ. There was also a significant decrease in the number of reaction products formed. The electron withdrawing effects of the fluorinated acetone reduced the number of ion-molecule clusters formed in conjunction with this ketone resulting in low intensity ion peaks. The inclusion of 1,1,1-trifluoroacetone was solely an exercise in manipulation of the ion chemistry, and not a view to its suitability as a dopant in any practical instrument.

There was no H^+AK_2 in the HZ / 4-heptanone source doped tests, which may have been a result of the contaminant MMH dominating the ion-molecule chemistry because of the higher proton affinity of MMH compared with HZ.

The amount of H^+A in the ammonia tests reduced from the acetone source doped system to the 5-nonanone system, and there was none recorded in the drift doped experiments. The HZ tests produced a similar pattern, not unexpected because of the similarity of the proton affinities of HZ and ammonia. Analytes with higher proton affinity did produce H^+A, and UDMH had a sufficiently high proton affinity to produce H^+A when the drift region was also doped. The breakdown products of UDMH formed primarily H^+BK and then combinations of derivatives of B and underivatised A.

The ionisation region acts as an ion-molecule reaction chamber in which the ketones and hydrazines react to form the hydrazones and azines. At higher dopant concentrations the population of ion-molecule clusters of the reaction products were fewer than observed at lower ketone concentration. Using the HyperChem programme, the charge on the primary nitrogen of HZ, the acetone hydrazone, and the corresponding azine were calculated as -0.074, -0.159, and -0.141. The charge on the acetone hydrazone and acetone azine primary nitrogens render them both more basic than the nitrogen in the parent HZ suggesting a higher proton affinity. The charge on the carbonyl oxygen in acetone was calculated as -0.314 which suggests that the ketone would win the competition for protons, if the dopant was present in sufficient quantity.

The higher dopant concentration of the higher molecular weight ketones produces azines in the presence of HZ. Formation of the hydrazone ion occurs at low ketone concentrations, while the azine ion is formed at a higher dopant concentration, and the H^+AK_n ion at still higher ketone concentrations.

During the tests with UDMH the tendency to form monomer, dimer, and trimer ions of acetone during the drift doped tests was surprising as the proton affinity of UDMH (926.6 $kJ.mol^{-1}$) is much higher than that of acetone (812.0 $kJ.mol^{-1}$) but it could be explained by an excess of available protons and a high concentration of the ketone.

In general, it was found that higher proton affinities of analytes led to simplified ion chemistry.

There were two peaks observed in the UDMH ion mobility spectra, one occurring exactly where the MMH product ion peak was recorded. During the initial IMS experiments the occurrence of this second peak was attributed to MMH contamination in the sampling line. The sampling lines were changed and individually

labelled sample lines were dedicated to separate analytes, and UDMH continued to produce the second peak, indicating that a reaction by-product was produced which had a similar mobility to MMH. The results from the IMS-MS-MS studies confirmed the formation of MMH from UDMH and its ion chemistry was similar to the patterns observed previously for MMH, for example, with increased ketone concentration the intensity of the protonated adduct with two ketone molecules increased.

The earlier work provided no explanation as to why the hydrazines did not form ion clusters and consequently were not observed in the ion mobility spectrum at higher detector temperatures. A small number of experiments were tried at 50°C; the ratio of reaction products to unreacted species increased with increase in temperature i.e. the higher temperature favoured reaction of the hydrazines and ketones as would be expected. Therefore, it may have been expected that the analytes in tests with the ion mobility cell at even higher temperatures would lead to the formation of bigger ion clusters, so big that they would have too low a mobility to be recorded in the normal spectrum. However, the RIP would have depleted with the formation of product ions, so the information from the IMS-MS-MS studies offered no explanation as to the lack of response to the hydrazines in higher temperature cells. Response to the hydrazines increased with decrease in temperature towards ambient. If the temperatures had been sufficient to decompose the hydrazines the most likely decomposition product would be ammonia which was also not detected at elevated temperature. Where ammonia was detected the response also increased with decrease in temperature.

Chapter 5

CONCLUSIONS

The aims of this research project were to investigate the factors affecting the IMS detection of hydrazines and ammonia in the positive mode, and nitrogen dioxide in the negative mode. The use of the ion mobility spectrometer breadboard, with choice of instrument configuration led to the optimisation of conditions for the real-time detection of these analytes. The initial thoughts had been to use one drift tube with a relay switch to change detection modes, or to integrate twin drift tubes into one instrument, to allow simultaneous monitoring of all the analytes of interest. This was dependent upon finding one suitable dopant which could be used to effect the ion mobility separation of the RIP and product ion peaks. However, because of the choice of a different dopant for the detection of nitrogen dioxide, there was little advantage to be gained from pursuing the development of one configuration for the detection of all the analytes. A miniaturised version of the ion mobility spectrometer breadboard was configured for the detection of ammonia and the hydrazines, capable of detecting low vpm and low vpb concentrations respectively.

Investigation into further miniaturisation could consider the possibility of a smaller power supply; replacement of the external carrier gas supply with a recirculating gas system, involving the integration of sieve packs and minimising sample inlet flow, in order to keep water vapour to a minimum and thereby prolonging sieve life; integration of software into the spectrometer, to negate the need for the external computer system (this would allow the unit to become truly hand-held portable); and intrinsic safety might also be a requirement for the final hand held instrument. Although possible in theory, due to the high electrical tension supply (at 1 kV) and the use of

numerous capacitors, a large proportion of encapsulation (potting) might be necessary, which could lead to the expensive replacement of existing parts.

There was still the unsolved problem of partial resolution of the ammonia and HZ peaks, and an order of mobility in reverse to that predicted from the relative sizes of ammonia and the hydrazines during experimental work. Attention was directed to determining how the resultant ion-molecule clusters affected the mobility, and molecular modelling was used to optimise ion clusters comprising the analytes and various straight chain and branched chain ketones. Maximum diameters were measured in an attempt to predict if one of the ketones would be more effective in the separation of the ammonia and HZ product ion peaks of the type predicted by the Stone model.

The measured diameters from the optimised ion-molecule clusters made sense of the experimentally determined order of mobility and partial resolution of the ammonia and HZ peaks. In future, it would be beneficial to model ion-molecule clusters to ascertain likely separation of any analytes as much time and effort could be saved in experimental work. The time and effort involved, in doping an ion mobility spectrometer to the correct concentration level for a satisfactory RIP, performing experiments, and then decontaminating the spectrometer before the next chemical system is tried, can be cost ineffective. Molecular modelling takes time to set up the calculation parameters but then requires little attention until the optimisations are complete. Experience from this project indicates some chemical systems can be excluded from practical evaluation based on the results of the computational chemistry.

To test the Stone model, chemical systems comprising combinations of either ammonia or one of the hydrazines (including TMH) with a symmetrical, straight chain ketone were subjected to IMS-MS-MS studies. The results indicated that provided the ketone concentration was high enough the maximum number of ketones readily attached

to the analytes would be four for ammonia, three for HZ, two for MMH, and one each for UDMH and TMH. The results of the studies were complicated because of the gas phase reactions of the HZ, MMH, and UDMH with the ketones, and the decomposition products of UDMH forming even more clusters. The results of these studies also emphasised the effect of concentrations in the chemical system. However, it was difficult to produce the concentration of dopant required to ensure the maximum ketone attachment. It was deemed necessary to continue with the HyperChem optimisations for the ammonia / ketone and hydrazine / ketone systems for ion-molecules of H^+(analyte)(ketone)$_n$ where n represented numbers ranging from one to the maximum predicted in the Stone model. The diameters measured from the computations are reproduced in Table 5.1, and this table may be used to estimate the likely mobility separation of various ketone / analyte ion-molecule clusters. Careful control of the dopant concentration would be required in any instrument in order to achieve the appropriate cluster formations.

Use of dopant materials with different inductive effects may be considered to improve selectivity. The studies which involved 1,1,1-trifluoroacetone indicated that the electron withdrawing effects of the fluorine atom hindered the formation of ion-molecule clusters and allowed ion-molecules of the analyte to pass unattached through the system. The affect upon resolution of the analytes, and their resolution from the RIP, would have to be investigated; the surface affinity of the analytes might also prove problematic.

Chemical systems favouring the detection of ammonia also favour detection of HZ. Separation of these two compounds by direct IMS may prove to be impossible. A means of separating the components, prior to IMS detection, may be necessary, for example, GC-IMS (a gas chromatograph coupled to an ion mobility spectrometer).

Table 5.1: Maximum diameters (Å) of ion-molecule clusters comprising ammonia, the hydrazines, and straight and branched chain ketones

	H^+AK_4	H^+AK_3	H^+AK_2	H^+AK	H^+HZK_3	H^+HZK_2	H^+HZK	H^+MK_2	H^+MK	H^+UK
Acetone	10.4478	10.5918	11.2284	6.4782	10.3399	10.4814	7.4749	9.6289	7.6453	7.7678
3-Pentanone	12.1015	12.1855	10.8679	6.9661	11.9349	10.8935	7.7958	10.7395	8.5226	8.3737
4-Heptanone	14.1747	13.2255	13.2377	9.3381	13.5557	13.4379	9.3956	12.5791	9.3987	9.3936
5-Nonanone	16.4678	15.2553	13.4044	11.8535	14.7810	14.4980	11.8700	13.3410	11.8445	11.8724
6-Undecanone	18.6819	17.5326	17.5310	14.4098	16.3980	16.2083	14.4061	15.6212	14.4101	14.4093
2,4-Dimethyl-3-pentanone	12.6728	12.5704	12.4164	7.5510	12.5194	12.7183	8.8632	12.7773	8.3021	8.8990
2,2,4,4-Tetramethyl-3-pentanone	13.6244	13.7471	13.6469	7.7497	12.5223	12.7549	9.0154	12.9903	8.2655	8.7559
2,2,6,6-Tetramethyl-4-heptanone	14.4496	16.4664	14.1881	9.3475	13.3539	13.5505	9.3673	14.1374	9.4022	9.4273
2,6-Dimethyl-4-heptanone	13.9506	12.9345	12.7100	8.8130	13.7382	13.8722	9.4247	12.8044	8.8448	9.3252
2,8-Dimethyl-5-nonanone	16.6692	16.6113	13.6469	11.8744	14.9967	14.5505	11.8620	15.1096	11.8838	11.8573

K = ketone; H^+ = proton; A = ammonia; HZ = hydrazine, M = methylhydrazine; U = 1,1-dimethylhydrazine

Future work should also include relating the ion mobility peaks to ion-molecule clusters determined by IMS-MS-MS studies, and the mass spectrometric analysis over a wider range of amu would be beneficial.

Appendix A

Table of proton affinities[210]

Chemical substance	Proton affinity (kJ.mol^{-1})
Tetramethylhydrazine	949.0
1,1-Dimethylhydrazine	926.6
Methylhydrazine	895.7
2,2,4,4-Tetramethyl-3-pentanone	861.7
Ammonia	854.0
Hydrazine	853.2
5-Nonanone	851.6
2,4-Dimethyl-3-pentanone	850.3
4-Heptanone	845.5
3-Pentanone	836.8
Acetone	812.0
1,1,1-Trifluoroacetone	725.5
Water	691.0

References

1. Schiessl H W. *Aldrichimica Acta* **13,** 33-40 (1980)

2. Gough D B, Heys S D, Eremin O. *Eur. J. Surg. Oncol.,* **22,** 286-297 (1996)

3. Gajda M A, Ahmed H, Shaw J E A, Putnis A. *Sens.Actuators, A,* **40,** 227-236 (1994)

4. Ueda S, Kuroda Y, Miyajima H, Kuwahara T. *J. Propulsion and Power,* **10,** 646-652 (Sept.-Oct. 1994)

5. Leakakos T, Shank R C. *Toxicol. Appl. Pharmacol.,* **126,** 295-300 (1994)

6. Douglas G R, Gingerich J D, Soper L M. *Carcinogenesis,* **16,** 801-4 (1995)

7. Jenner A M, Timbrell J A. *Arch. Toxicol.,* **68,** 349-357 (1994)

8. Jenner A M, Timbrell J A. *Arch. Toxicol.,* **68,** 240-5 (1994)

9. Ghantineh S, Timbrell J A. *Toxic. in Vitro,* **8,** 393-9 (1994)

10. Poso A, von Wright A, Gynther J. *Mutat. Res.,* **332,** 63-71 (1995)

11. Toth B. *Int. J. Oncol.,* **4,** 231-9 (1994)

12. OSHA *Method No 20.* Organic Methods Evaluation Branch, OSHA Analytical Laboratory (September 1980)

13. ACGIH *Documentation of the threshold limit values and biological exposure indices* (1989-90)

14. *Catalogue Handbook of Fine Chemicals.* Aldrich (1998-9)

15. Taffe P A, Rose-Pehrsson S L, Wyatt J R. *Material compatibility with threshold limit value levels of monomethyl hydrazine.* Naval Research Laboratory, Washington D C (May 1987)

16. Sax N I, Lewis R J Sr. *Dangerous properties of industrial materials 7th ed.,* **Vol II & III** van Nostrand Reinhold (1989)

17. Calabrese E J, Kenyon E M. *Air toxics and risk assessment.* Lewis Publishers (1991)

18. Schweisfurth H, Schöttes C. *Zentralbl. Hyg. Umweltmed,* **19591,** 46-54 (1993)

19. Morris J, Densem J W, Wald N J, Doll R. *Occupational and Environmental Medicine,* **52,** 43-5 (1995)

20. Runge-Morris M, Wu N, Novak R F. *Toxicol. Appl. Pharmacol.,***125,** 123-132 (1994)

21. Savill, Richard. *Cancer research doctor died after work on rats.* Daily Telegraph (26 September 1989)

22. OSHA *Limits for air pollutants* (1984)

23. OSHA *Air contaminants; Final rule* (1989)

24. NIOSH *Criteria for a recommended standard. Occupational exposure to hydrazines.* DHEW (NIOSH) 78-172 (1978)

25. NIOSH *Method S-237, Hydrazine* (April 1975) [replaced by 3503 (2/15/84)]

26. NIOSH *Method S-149, Monomethylhydrazine* (April 1975)

27. NIOSH *Method S-143, 1,1-Dimethylhydrazine* (April 1975)

28. *Environmental health criteria 68, Hydrazine.* International Programme on Chemical Safety, World Health Organisation, Geneva (1987)

29. Health and Safety Executive, *Occupational exposure limits,* Table 4: *Substances to be reviewed,* Guidance note EH40, HMSO (1994)

30. Health and Safety Executive, *Occupational exposure limits,* Guidance note EH40, HMSO (1997)

31. Collins G E, Latturner S, Rose-Pehrsson S L. *Talanta,* **42,** 543-551 (1995)

32. Young R. *A report on test results on ion mobility spectrometer detection of hydrazines.* **NASA, KSC DL-ESS-24** Toxic Vapour Detection Laboratory (June 26, 1989)

33. Audrieth L F, Ackerson Ogg B. *The chemistry of hydrazines,* 154-157. J Wiley & Sons (1951)

34. *Ammonia & hydrazine,* 708 (source unknown)

35. Safavi A, Ensafi A A. *Anal. Chim. Acta,* **300,** 307-311 (1995)

36. Pinkerton M K, Lauer J M, Diamond P, Tamas A A. *ASD Technical report 61-708* (March 1962)

37. Pesez M, Petit A. *Bull. Soc. Chim.* Fr., 122 (1947)

38. Pilz W, Stelzl E. *Z. Analyt. Chem.* **219,** 416-424 (1966)

39. Tsuboi T, Nakamura T, Matsukura A, Motomizu S. *Bunseki Kakgaku,* **45,** 993-8 (1996)

40. Agudo M, Rios A, Valcárcel M, Danet A. *J. Autom.Chem.,* **17,** 17-20 (Jan.-Feb. 1995)

41. Keen C, Pengelly M I. *Development of a method for measuring airborne hydrazine.* HSE Report No. IR/L/SP/95/07 (September 1995)

42. Kaveeshwar R., Gupta V k. *Fresenius' J. Anal. Chem.,* **344,** No 3, 114-117 (1992)

43. Collins G E, Rose-Pehrsson S L. *Anal. Chim. Acta,* **284,** No 1, 207-215 (1993)

44. Collins G E, Rose-Pehrsson S L. *Analyst* **119,** 1907-1913 (1994)

45. Gastec Precision gas data system Gastec hydrazine tube.

46. Leichnitz K. *Detector tube handbook.* p 91. Dräger. 7th edition (1989)

47. Dee L A. *Anal. Chem.* **43,** 1416-9 (September 1971)

48. Dee L A, Webb A K. *Anal. Chem.* **39,** 1165-7 (August 1967)

49. NIOSH *Method P & CAM 248* (November 1976)

50. Kirchherr H. *J. Chromatogr. B, Biomed. Appl.* **617,** 157-162 (1993)

51. Ueno K, Umeda T. *J. Chromatogr.,* **585,** 225-231 (1991)

52. Original reference unknown.

53. Holtzclaw J R, Rose S L, Wyatt J R, Rounbehler D P, Fine D H. *Anal. Chem.* **56,** 2952-6 (1984)

54. Vatsala S, Bansal V, Tuli D K, Rai M M, Jain S K, Srivastava S P, Bhatnager A K. *Chromatographia,* **38,** 456-460 (April 1994)

55. Olson, Edward C. *Anal. Chem.* **32,** 1545-7 (November 1960)

56. Buck R P, Eldridge R W. *Anal. Chem.* **37,** 1242-5 (September 1965)

57. Pastor T J, Vijgand V J, Antonijevic V V. *Mikrochim. Acta,* **II,** 131-9 (1978)

58. Lupea A Y, Oprescu D. *Rev. Chim. (Bucharest),* **45,** 433-436 (1994)

59. Wyatt J R, Rose-Pehrsson S L, Cecil T L, Crossman K P, Mehta N K, Young R. *Am. Ind. Hyg. Assoc. J.* **54,** 285-292 (1993)

60. Ikeda S, Satake H. *Anal. Lett.,* **(5),** 403-413 (1978)

61. Mallela S P, Khandelwal B L. *Mikrochim. Acta* **II,** 245-248 (1977)

62. Usvyatzov A A, Sudakov A R, Krylov Yu A, Agasyan P K, Lomonosov V. *Zh. Anal. Khim.,* **29,** 170-2 (1974)

63. Hou W, Ji H, Wang E. *Talanta* **39**, 45-50 (1992)

64. Pamidi P V A, Wang J. *Electroanalysis,* **8,** 244-7 (1996)

65. Wang J, Chen Q, Cepria G. *Talanta,* **43,** 1387-1391 (1996)

66. Zen J M, Tang J S. *Anal. Chem.* **67,** 208-211 (1995)

67. Peng Q Y, Guarr T F. *Electrochim. Acta* **39,** 2629-2632 (1994)

68. Wang J, Pamidi P V A. *Talanta* **42,** 463-467 (1995)

69. Zhou W H, Xu L J, Wu M J, Xu L J, Wang E K. *Chin. Sci. Bull.,* **41,** 34-7 (Jan. 1996)

70. Liu J, Zhou W, You T, Li F, Wang E, Dong S. *Anal. Chem.,* **68,** 3350-3 (1996)

71. Ohura H, Imato T, Yamasaki S. *Bunseki Kakgaku,* **45,** 689-695 (1996)

72. Stetter J R, Tellefsen K A, Saunders R A, DeCorpo J J. *Talanta* **26,** 799-804 (1979)

73. Hydrazine monitor Hyba-1000. *Bulletin HRE-1851A.* Horiba.

74. Santacesaria E, Giuffrè L. *Riv. Combust.* **23,** 490-5 (1969)

75. Stetter J R, Shi C-X, Maclay G J. *Anal. Chem.,* **63,** 1755-1759 (1991)

76. *Research proposal for the development of hydrazines sensors.* Cranfield Biotechnology Centre (October 1986)

77. Wang J, Chen L. *Anal. Chem.,* **67,** 3824-7 (1995)

78. Wang J, Chicharro M, Rivas G, Cai X, Dontha N, Farias P A M, Shiraishi H. *Anal. Chem.,* **68,** 2251-2254 (1996)

79. Rose-Pehrsson S L, Wyatt J R, Brenner K P, Carver P T, Brown S W, Thurow A R, Travis J C. *Am. Ind. Hyg. Assoc. J.,* **55,** 149-162 (Feb. 1994)

80. Wernlund R F, Cohen M J. *A brief demonstration study of ion molecule behaviour of selected agents and interferents made with the atmospheric ion mobility spectrometer coupled to a quadrupole mass spectrometer.* Report under Edgewood Arsenal contract No DAAK11-77-C-0015 (1977)

81. Rokushika S, Hatano H, Hill H H Jr. *Anal. Chem.* **58,** 361-5 (1986)

82. Kojiro D R, Cohen M J, Stimac R M, Wernlund R F, Humphrey D E, Takeuchi N. *Anal. Chem.,* **63,** 2295-2300 (1991)

83. Leasure C S, Eiceman G A. *Anal. Chem.* **57,** 1890-4 (1985)

84. Mathews R J. CDE Porton Down. Unpublished data (January 1983)

85. Brokenshire J L. GIL. Unpublished data.

86. Spangler G E, Cohen M J. *Plasma Chromatography*, (Ed. Carr T W) Plenum Press (1984)

87. Spangler G E, Campbell D N, Vora K N, Carrico J P. *ISA Trans.*, **23**, 17-28 (1984)

88. Spangler G E, Collins C I, Harrison J W. *Considerations on the sensitivity of plasma chromatography.* Paper 106, Pittsburgh Conference on Analytical Chemistry & Applied Spectroscopy (1975)

89. Watts P. *Use of ion mobility spectroscopy for the detection and analysis of vapours.* Paper presented at a symposium of the RSC Analytical Division, on gas and headspace vapour analysis, at the School of Chem. & Appl. Chem., Univ. of Wales, College of Cardiff (March 1991)

90. Ketkar S N, Dulak J G, Dheandhanoo S, Fite W L. *Anal. Chim. Acta*, **245**, 267-270 (1991)

91. Begley P, Corbin R, Foulger B E, Simmonds P G. *J. Chromatogr.*, **588**, 239-249 (1991)

92. Leasure C S, Fleischer M E, Anderson G K, Eiceman G A. *Anal. Chem.* **58**, 2142-7 (1986)

93. Baim M A, Eatherton R L, Hill H H Jr. *Anal. Chem.* **58**, 2142-7 (1986)

94. Connor J. *Atmospheric pressure ionisation for trace gas detection.* Private communication.

95. Hill H H Jr, Siems W F, St. Louis R H, McMinn D G. *Anal. Chem.* **62**, 1201A-1209A (Dec. 1990)

96. Brokenshire J L, Dharmarajan V, Coyne L B, Keller J. *J. of Cell. Plastics*, **26**, 123-142 (March 1990)

97. Brokenshire J, Pay N. *Int. Lab.*, (Oct. 1989)

98. Brokenshire J L. Personal communication.

99. Strathman H, Bell C-M, Kimmerle K. *Pure & Appl.Chemistry* **58**, 1663-8 (1986)

100. Eiceman G A. *Crit.Rev. Anal. Chem.*, **22**, 471-490 (1991)

101. Bollan H R. *Development of methods for the detection of hydrazines.* M.Phil. thesis, 92-103, 105-112. University of the West of England, Bristol (1993)

102. Spangler G E. *Anal. Chem.*, **65**, 3010-4 (1993)

103. Kim S H, Spangler G E. *Anal. Chem.* **57,** 567-569 (1985)

104. Preston J M, Karasek F W, Kim S H. *Plasma chromatography of phosphorus esters.* Report No 733. Canadian Department of National Defence, Ottawa (1975)

105. Hill H H Jr., Morrissey M. *Plasma chromatography,* Chapter 6, 96-113 (Ed. Carr T W). Plenum Press (1984)

106. Graseby Dynamics Limited. *Vapour detection techniques using ionic mobility principles.* Presentation at CDE Porton Down (May 1983)

107. Karpas Z, Eiceman G A, Ewing R G, Algom A, Avida R, Friedman M, Matmor A, Shahal O. *Int. J. Mass Spectrom.Ion Processes,* **127,** 95-104 (1993)

108. Karasek F W. *Industrial Research & Development.* (December 1978)

109. Baim M A, Hill H H Jr. *Anal. Chem.* **54,** 38-43 (1982)

110. Proctor C J, Todd J F J. *Anal. Chem.* **56,** 1794-7 (1984)

111. Witkiewicz Z, Stryszak E. *Chem. Anal. (Warsaw),* **30,** 683-697 (1985)

112. Kim S H, Karasek F W, Rokushika S. *Anal. Chem.* **50,** 152-5 (January 1978)

113. Karpas Z. *Anal. Chem.* **61,** 684-9 (1989)

114. Lawrence A H. *Anal. Chem.* **61,** 343-9 (1989)

115. Cohen M J. *Detecting a trace substance in a sample gas comprising reacting the sample with different species of reactant ions.* US patent 3,621,239 (Nov. 16, 1971)

116. Carr T W (Ed.). *Plasma Chromatography* Plenum Press (1984)

117. Karpas Z. Personal communication.

118. Eiceman G A, Karpas Z. *Ion Mobility Spectrometry,* CRC Press Inc. (1994)

119. Lubman D M. *Anal. Chem.,* **56,** 1298-1302 (1984)

120. Giles K, Grimsrud E P. *J. Phys. Chem.,* **96,** 6680-7 (1992)

121. Thuillard M. *J. Aerosol Sci. Technol.,* **26,** 219-225 (1995)

122. Stimac R M, Wernlund R F, Cohen M J, Lubman D M, Harden C S. *Initial studies on the operation and performance of the tandem ion mobility spectrometer.* Paper 234, Pittsburgh Conference and Exposition on Analytical Chemistry and Applied Spectroscopy (New Orleans, Louisiana. 25 Feb. 1985)

123. Kim S H, Spangler G E. *Anal. Chem.,* **57,** 569-571 (1985)

124. Spangler G E. *Anal. Chem.*, **64,** 1312 (1992)

125. Skullerud H R. *J. Phys. B: Atom. Molec. Phys.*, **9,** 535-546 (1976)

126. Buryakov I A, Krylov E V, Makas A L, Nazarov E G, Pervukhin V V, Rasulev U Kh. *J. Anal. Chem.*, **48,** 114-121 (1993)

127. Hill H H Jr., Shumate C, St. Louis R H. *J. Chromatogr.*, **373,** 141-173 (1986)

128. Leonhardt J W. *J. Radioanal. Nucl.Chem., Articles,* **206,** 333-9 (1996)

129. Baim M A, Eatherton R L, Hill H H Jr. *Anal. Chem.*, **55,** 1761-6 (1983)

130. Lubman D M, Kronik M N. *Anal. Chem.*, **54,** 1546-1551 (1982)

131. Shumate C B, Hill H H Jr. *ACS Symp. Ser.*, **508,** 192-206 (1992)

132. Shumate C B. *Trends Anal. Chem.*, **13,** No 3, 104-9 (1994)

133. Wittmer D, Chen Y H, Luckenbill B K, Hill H H Jr. *Anal. Chem.*, **66,** 2348-2355 (1994)

134. Chen Y H, Hill H H Jr., Wittmer D P. *Int. J. Mass Spectrom.Ion Processes,* **154,** 1-13 (1996)

135. Shumate C B, Hill H H Jr. *Anal. Chem.*, **61,** 601-6 (1989)

136. Chen Y H, Hill H H Jr., Wittmer D P. *J. Microcolumn Sep.*, **6,** 515-524 (1994)

137. Eiceman G A, Wang Y F, Garcia-Gonzalez L, Harden C S, Shoff D B. *Anal. Chim. Acta,* **306,** 21-33 (1995)

138. Karpas Z, Tironi C. *Struct. Chem.*, **2,** 655-9 (1991)

139. Karpas Z, Bell S E, Wang Y-F, Walsh M, Eiceman G A. *Struct. Chem.*, **5,** 135-140 (1994)

140. Watts P, Wilders A. *Int. J. Mass Spectrom. Ion Processes,* **112,** 179-190 (1992)

141. Siems W F, Wu C, Tarver E E, Hill H H Jr., Larsen P R, McMinn D G. *Anal. Chem.*, **66,** 4195-4201 (1994)

142. Davis D M, Harden C S, Shoff D B, Bell S E, Eiceman G A, Ewing R G. *Anal. Chim. Acta,* **289,** 263-272 (1994)

143. Bell S E, Wang Y F, Walsh M K, Du Q, Ewing R G, Eiceman G A. *Anal. Chim. Acta,* **303,** 163-174 (1995)

144. Simpson M, Anderson D R, McLeod C W, Cooke M, Saatchi R. *Analyst,* **118,** 1293-8 (October 1993)

145. Boger Z, Karpas Z. *J. Chem. Inf. Comput. Sci.*, **34,** 576-580 (1994)

146. Zheng P, de B. Harrington P, Davis D M. *Chemom. Intell. Lab. Syst.*, **33,** 121-132 (1996)

147. Bell S E, Mead W C, Jones R D, Eiceman G A, Ewing R G. *J. Chem. Inf. Comput. Sci.*, **33,** No 4, 609-615 (1993)

148. Boger Z, Karpas Z. *Anal. Chim. Acta,* **292,** No 3, 243-251 (1994)

149. Bird G M, Keller R A. *J. Chromatogr. Sci.*, **14,** 574-7 (Dec. 1976)

150. Dworzanski J P, Kim M-G, Snyder A P, Arnold N S, Meuzelaar H L C. *Anal. Chim. Acta,* **293,** 219-235 (1994)

151. Jones D, Brenton A G, Games D E, Brittain A H, Taylor S, Kennedy D, Smith P. *Rapid commun. Mass Spectrom.,* **7,** 561-6 (1993)

152. Hill H H Jr., Baim M A. *Plasma chromatography,* Chapter 5, 143-176 (Ed. Carr T W). Plenum Press (1984)

153. St. Louis R H, Siems W F, Hill H H Jr. *J. Chromatogr.,* **479,** 221-231 (1989)

154. Simpson G, Klasmeier M, Hill H, Atkinson D, Radolovich G, Lopez-Avila V, Jones T L. *J. High Resolut. Chromatogr.,* **19,** 301-312 (June 1996)

155. Rokushika S, Hatano H, Hill H H Jr. *Anal. Chem.,* **59,** 8-12 (1987)

156. Widmer H M. *LC-GC,* **10,** 251 (1992)

157. PCP Inc. *The IMS as an HPLC detector.* **Application note.**

158. Hill H H Jr., St. Louis R H, Morrissey M A, C B, Siems W F, McMinn D G. *J. High Resolut. Chromatogr.,* **15,** 417-422 (July 1992)

159. Simpson M, Anderson D R, McLeod C W, Cooke M. *Analyst,* **118,** 449-451 (April 1993)

160. Knorr F J, Eatherton R L, Siems W F, Hill H H Jr. *Anal. Chem.,* **57,** 402-6 (1985)

161. St. Louis R H, Siems W F, Hill H H Jr. *Anal. Chem.,* **64,** 171-7 (1992)

162. Chen Y H, Siems W F, Hill H H Jr. *Anal. Chim. Acta,* **334,** 75-84 (1996)

163. Baumbach J I, Berger D, Leonhardt J W, Klockow D. *Int. J. Environ. Anal. Chem.,* **52,** 189-193 (1993)

164. Preston J M. *Survey of the mobility of large ions in air with comments on the ions of chemical warfare agents.* (Unpublished report)

165. Bell A J, Watts P. *J. of Defence Science,* **1,** 236-241 (1996) (Unpublished journal)

166. PCP Inc. *Research into ion mobility spectrometry. Cyanide anion measurements using the Phemto-Chem® MMS-160 IMS/quadrupole MS.* (1981)

167. Eiceman G A, Sowa S, Lin S, Bell S E. *J. Hazard. Mater.,* **43,** 13-30 (1995)

168. Karasek F W. *Anal. Chem.,* **43,** 1982-6 (Dec. 1971)

169. Karpas Z, Pollevoy Y. *Anal. Chim. Acta,* **259,** 333-8 (1992)

170. Schecter I, Schroder H, Kompa K L. *Anal. Chem.,* **65,** 1928-1931 (1993)

171. Bell S E, Ewing R G, Eiceman G A, Karpas Z. *Am. Soc. Mass Spectrom.,* **5,** 177-185 (1994)

172. Bacon A T, Reategul J, Getz R C. *United States Patent* **5,032,721** (July 16, 1991)

173. Bell A J, Hayhurst C J, Mayhew C A, Watts P. *Int. J. Mass Spectrom. Ion Processes,* **140,** 133-147 (1994)

174. Benezra S A. *J. Chromatogr. Sci.,* **14,** 122-125 (March 1976)

175. Eiceman G A, Shoff D B, Harden A P, Martinez P M, Fleischer M E, Watkins M L. *Anal. Chem.,* **61,** 1093-9 (1989)

176. Holzapfel W, Budde K. *Fresenius' J. Anal. Chem.,* **343,** 769-770 (1992)

177. Meng Q, Karpas Z, Eiceman G A. *Int. J. Environ. Anal. Chem.,* **61,** 81-94 (1995)

178. Eiceman G A, Salazar M R, Rodriguez M R, Limero T F, Beck S W, Cross J H, Young R, James J T. *Anal. Chem.* **65,** 1696-1702 (1993)

179. Fetterolf D D, Clark T D. *J. Forensic Sci.,* **38,** No. 1, 28-39 (1993)

180. Garofolo F, Migliozzi V, Roio B. *Rapid Commun. Mass Spectrom.,* **8,** 527-532 (1994)

181. Garofolo F, Marziali F, Migliozzi V, Stama A. *Rapid Commun. Mass Spectrom,* **10,** 1321-1326 (1996)

182. Fytche L M, Hupe M, Kovar J B, Pilon P. *J. Forensic Sci.,* **37,** 1550-1566 (1992)

183. Eiceman G A, Garcia-Gonzalez L, Wang Y-F, Pittman B, Burroughs E G. *Talanta,* **39,** 459-467 (1992)

184. Poziomek E J, Eiceman G A. *Environ. Sci. Technol.,* **26,** 1313-8 (1992)

185. Przybylko A R M, Thomas C L P, Anstice P J, Fielden P R, Brokenshire J, Irons F. *Anal. Chim. Acta,* **311,** 77-83 (1995)

186. Snyder A P, Shoff D B, Eiceman G A, Blyth D A, Parsons J A. *Anal. Chem.,* **63,** 526-9 (1991)

187. Snyder A P, Blyth D A, Parsons J A. *J. Microbiol. Methods,* **27,** 81-8 (1996)

188. Kotiaho T, Lauritsen F R, Degn H, Paakkanen H. *Anal. Chim. Acta,* **309,** 317-325 (1995)

189. Atkinson D A, Hill H H Jr., Shultz T D. *J. Chromatogr. B, Biomed. Appl.,* **617,** 173-9 (1993)

190. Lawrence A H, Barbour R J, Sutcliffe R. *Anal. Chem.,* **63,** 1217-1221 (1991)

191. Pettersen R C, Ward J C, Lawrence A H. *Holzforschung,* **47,** 513-522 (1993)

192. Strachan N J C, Ogden I D. *Lett. Appl. Microbiol.,* **17,** 228-230 (1993)

193. Strachan N J C, Nicholson F J, Ogden I D. *Anal. Chim. Acta,* **313,** 63-7 (1995)

194. Milinkovic S A, Sadibasic A E, Milanko O S. *Anal. Chim. Acta,* **294,** 283-9 (1994)

195. Keenan F, Cooke M. *Anal. Proc.,* **31,** 27-29 (January 1994)

196. McClennen W H, Arnold N S, Muezelaar H L C. *Trends in Analytical Chemistry,* **13,** 286-293 (1994)

197. Snyder A P, Harden C S, Brittain A H, Kim M-G, Arnold N S, Meuzelaar H L C. *Anal. Chem.,* **65,** 299-306 (1993)

198. Snyder A P, Harden C S, Brittain A H, Kim M-G, Arnold N S, Meuzelaar H L C. *Am. Lab.,* 32B-32H (Oct. 1992)

199. Turner R B, Brokenshire J L. *Trends Anal. Chem.,* **13,** 275-280 (1994)

200. Brittain A H, Taylor S J. *Atmospheric trace monitoring using gas chromatography-ion mobility techniques.* **5th International Symposium on Protection Against Chemical and Biological Warfare Agents.** (Stockholm, Sweden, 11-16 June 1995)

201. Limero T, Brokenshire J, Cumming C, Overton E, Carney K, Cross J, Eiceman G, James J. *A volatile organic analyser for space station: description and evaluation of a gas chromatography / ion mobility spectrometer.* **SAE Technical paper series 921385,** 22nd International Conference on Environmental Systems (Seattle, Washington July 13-16, 1992)

202. McNair H M, Bonelli E J. *Basic gas chromatography,* 5th edition, 119. (Varian Aerograph 1969)

203. Stone J A. Queen's University, Ontario, Canada. Personal communication (May 1996)

204. Nelson G O. *Controlled test atmospheres.* Ann Arbor Publications (1976)

205. Bass P G. *Investigation and resolution of the problem in H mode CAM*. Graseby Research technical report (Unpublished report)

206. Ashworth A J, Brisdon B J, England R, Reddy B S R, Zafar I. *The permselectivity of polyorganosiloxanes containing specific functionalities*. Separation of gases 96-107.

207. Foley T. *Membrane gas separation - current status and future developments*. Paper presented to the London & Southern Gas Association (11 June 1987)

208. Fritzsche A K, Narayan R S. *Chem. Econ. & Eng. Review* **19,** (No 205) (Jan.-Feb.-Mar. 1987)

209. Hypercube Inc. *HyperChem™ Computational chemistry, Molecular visualisation and simulation*. Part 1, 19 (April 1994)

210. http://webbook.nist.gov/chemistry

LIST OF AUTHOR'S PUBLICATIONS

1.   The author has had 45 classified reports published, within the Ministry of Defence, covering a variety of projects.

2.   Bollan H R. *Development of methods for the detection of hydrazines.* M.Phil. thesis, University of the West of England, Bristol, UK (November 1993)

3.   Bollan H R. *Submarine atmosphere control and the role of ion mobility spectrometry.* Proceedings, 4th International Workshop on Ion Mobility Spectrometry Proceedings, Cambridge UK (August 1995)

4.   Bollan H R, West D J. *Quantitative assessment of ion mobility spectrometry and alternative technologies in monitoring hydrogen fluoride vapour in recycled atmospheres.* Proceedings, 5th International Workshop on Ion Mobility Spectrometry, Jackson Hole, Wyoming, USA (August 1996)

5.   Bollan H R, Brokenshire J L, Eiceman G A, Rodriguez R, Stone J A. *Ion-molecule chemistry of ketones with ammonia, hydrazine, and methyl-substituted hydrazines, as determined by IMS-MS.* Proceedings, 5th International Workshop on Ion Mobility Spectrometry, Jackson Hole, Wyoming, USA (August 1996)

6.   Bollan H R. *Ion mobility spectrometry, real-time monitoring for submarine atmospheres.* Proceedings, 2nd International Conference on Submarine Atmosphere Monitoring and Air Purification, Portsmouth, UK (July 1997)

7.   Bollan H R, Brokenshire J L, West D J. *Assessment of ion mobility spectrometry for monitoring monoethanolamine in recycled atmospheres.* Proceedings, 6th International Workshop on Ion Mobility Spectrometry, Bastei, Dresden, Germany (August 1997)

8.   Bollan H R, Brokenshire J L, Eiceman G A, Rodriguez R, Stone J A. *Ion-molecule chemistry of ketones with ammonia, hydrazine, and methyl-substituted hydrazines, as determined by IMS-MS.* In preparation for submission for journal publication.